





This is to certify that the
dissertation entitled

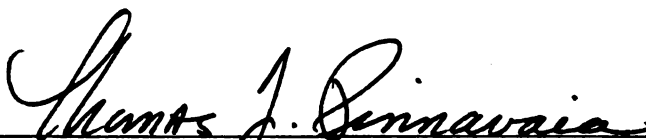
ENCAPSULATION OF POLYMERIC
COMPLEXANTS IN MESOSTRUCTURED
SILICA AND THE ENRICHMENT OF
PHOSPHORYLATED PEPTIDES ON GRID
SUPPORTED MESOPOROUS METAL OXIDE
THIN FILMS

presented by

Christian Paule Canlas

has been accepted towards fulfillment
of the requirements for the

Ph.D. degree in Chemistry



Major Professor's Signature


Date

**ENCAPSULATION OF POLYMERIC COMPLEXANTS IN
MESOSTRUCTURED SILICA AND THE ENRICHMENT OF
PHOSPHORYLATED PEPTIDES ON GRID SUPPORTED
MESOPOROUS METAL OXIDE THIN FILMS**

By

Christian Paule Canlas

A DISSERTATION

Submitted to
Michigan State University
In partial fulfillment of the requirements
for the degree of

DOCTOR OF PHILOSOPHY

Chemistry

2010

ABSTRACT

ENCAPSULATION OF POLYMERIC COMPLEXANTS IN MESOSTRUCTURED SILICA AND THE ENRICHMENT OF PHOSPHORYLATED PEPTIDES ON GRID SUPPORTED MESOPOROUS METAL OXIDE THIN FILMS

By

Christian Paule Canlas

The advent of mesoporous silicas has opened new fields of research. The inherent high surface area, chemical and mechanical stability, and tailorable pore size have made mesoporous silica as an ideal substrate in many applications such as catalysis, enzyme immobilization, drug delivery, chemical sensing and separation chemistry. Mesoporous silica by itself is not very useful even with the above mentioned properties. Functionalities must be introduced to make them suitable for each preferred application. Two of the most common techniques of introducing functionality onto mesoporous silica surface are thru post-synthesis grafting and direct-synthesis. In the first half of this study, an alternate approach was explored, that is the utilization of the surfactant template as an organic functionality. Oleyl amine surfactants were used to assemble wormhole silica products. The surfactant template was crosslinked using divinylbenzene to prevent leeching out of the framework pores. The cross-linked template in turn acts as a polymeric complexant which was later tested for trapping Pb(II). Moreover, the mesoporous silicas assembled using oleyl amine surfactants under varying solvent polarity and temperature were explored. Results revealed that it is possible to control pore size down to the supermicroporous range (1-2nm) using

oleyl amine surfactants with the proper solvent polarity and assembly temperature.

The second part of the study is the use of mesoporous metal oxide thin films for the enrichment of model phosphopeptides. Phosphorylation is one of several post-translational modifications and is very important as it is involved in the regulation of many cellular processes. In order to understand cellular regulation on a molecular level, post-translational modifications need to be identified and characterized. Despite recent advancements in mass spectrometry techniques, the characterization of protein phosphorylation sites is challenging due to the low abundance of phosphorylated proteins. Enrichment prior to mass spectrometry analysis will greatly facilitate the analysis of phosphorylated proteins. In this study, an alternative method to immobilized metal-ion affinity chromatography (IMAC) and metal oxide columns is introduced. Instead of columns packed with IMAC or metal oxide particles, transmission electron microscopy (TEM) grid supported mesoporous metal oxide thin films were used. These mesoporous metal oxide thin films were synthesized and characterized. These were tested by enriching β -casein and ovalbumin digests. Results revealed a successful enrichment of the phosphopeptides up to 50 fmol concentration.

Copyright by
Christian Paule Canlas
2010

for Pam...for inspiring me to pursue my dreams and for teaching me things that
the four corners of a classroom, and in this case, a lab could not

ACKNOWLEDGMENTS

First of all, I want to thank God Almighty, for giving me the gift of intellect and as my source of strength. For always guiding me in every endeavor I take.

Prof. Tom Pinnavaia for his unending patience and for taking me under his wing. I really appreciate how he stimulates me to think creatively and how he molded me into what I am today as chemist.

Dr. Fan for all his expertise in TEM.

Prof. Tepe for his expertise in the proteomics project and Prof. Reid for his mass spec expertise and for letting us use his MALDI-MS instrument.

I would also like to thank my parents and my siblings for their support and inspiration and for always believing in me.

The Pinnavaia group members, for their friendship, with special mentions to Kim, Joel, Susan, Noemi and Xin.

To my friends who kept me sane all through these years. Especially to Janir and Armando for all the help they have extended to me.

The MSU Filipino Club for serving as an avenue to do things other than chemistry, special mention to Ann, Maricris, Gizelle, and Charrise.

Jerry...for not giving up on our friendship, for always believing in me...for being a brother.

Matt for teaching me how to be a kid again and appreciate things I've forgotten because I grew up too fast. For being a best friend.

And lastly, Pam, for teaching me so much about life and for inspiring me to pursue my doctorate degree. You will always have a special place in my heart.

TABLE OF CONTENTS

LIST OF TABLES.....	ix
LIST OF FIGURES	x
ABBREVIATIONS	xvii
CHAPTER 1	
SYNTHESIS AND APPLICATIONS OF MESOPOROUS SILICA.....	1
1.1 Introduction	1
1.1.1 Synthesis of Mesoporous Silica	1
1.2 Mesoporous Silica Applications	6
1.2.1 As Stationary Phase for High Performance Liquid Chromatography.....	7
1.2.2 Immobilization of Biomolecules	10
1.2.3 Catalysis.....	15
1.2.3.1 Preparation of Mesoporous Catalysts.....	15
1.2.3.2 Applications of Mesoporous Silica Catalyst	19
1.2.4 Mesoporous Silica As Adsorbents	21
1.2.5 Polymer Reinforcement	23
1.3 Objectives	24
1.4 References	26
CHAPTER 2	
SUPRAMOLECULAR ASSEMBLY OF MESOSTRUCTURED SILICA FROM OLEYLAMINE SURFACTANTS.....	38
2.1 Introduction	38
2.1.1 Background on Supramolecular Assembly.....	38
2.1.2 Pore Size and Morphological Control of Mesoporous Silica.....	43
2.1.3 Tailoring the Pore Size Distribution Between the Microporous and Mesoporous Region	47
2.1.4 Objectives	48
2.2 Experimental.....	50
2.2.1 Reagents.....	50
2.2.2 Material Synthesis.....	50
2.2.2.1 Mesostructure Synthesis via the Electrostatic S ⁺ I ⁺ Pathway.....	51
2.2.2.2 Mesostructure Synthesis via the Electrically Neutral S ⁰ I ⁰ Pathway.....	52
2.2.2.3 Effect of Solvent Polarity and Assembly Temperature on Mesoporous Silica Assembled Using Oleyl Amine Surfactants	54

2.3 Physical Measurements	57
2.4 Results and Discussion.....	58
2.5 Conclusions	112
2.6 References.....	116

CHAPTER 3

ENCAPSULATION OF POLYMERIC NEUTRAL AMINE SURFACTANT ON MESOPOROUS SILICA	119
---	-----

3.1 Introduction to Mesoporous Silica Functionalization	119
3.1.1 Post-Synthesis Grafting Technique	120
3.1.2 Direct Assembly / Co-Condensation.....	121
3.1.3 Polymerization of Surfactants.....	125
3.1.4 Polymerization In Mesoporous Silica.....	128
3.1.5 Heavy Metal Trapping Using Mesoporous Silica.....	129
3.2 Objectives	130
3.3 Experimental	130
3.3.1 Co-Polymerization of the Templating Agent Inside HMS Wormhole Mesostructures with Divinylbenzene as the Cross-linker	130
3.3.2 Leaching Studies.....	134
3.3.3 Lead (II) Trapping by Batch Studies.....	135
3.3.4 Characterization	135
3.4 Results and Discussions.....	137
3.5 Conclusions	149
3.6 References.....	154

CHAPTER 4

PHOSPHOPROTEIN ENRICHMENT USING GRID SUPPORTED MESOPOROUS METAL OXIDE THIN FILMS	158
---	-----

4.1 Introduction to Post-translational Modification	158
4.1.1 Background on Protein Phosphorylation	161
4.1.2 Enrichment of Phosphoproteins	165
4.2 Objectives	175
4.3 Experimental	176
4.3.1 Materials.....	176
4.3.2 Precursor Solution Preparation	176
4.3.3 Preparation of Thin Films	177
4.3.4 Characterization of Mesoporous Metal Oxide Thin Films	178
4.3.5 Protein Digestion.....	179
4.3.6 Phosphoprotein Enrichment.....	179
4.4 Results and Discussions.....	184
4.4.1 Fabrication of Grid Supported Mesoporous Metal Oxide Thin Films.....	190
4.4.2 Phosphoprotein Enrichment	196
4.5 Conclusions	213
4.6 References.....	215

LIST OF TABLES

Table 1.1 Classification of mesoporous silica based on the interaction of inorganic species and organic template.	3
Table 1.2 Mesoporous silica used as stationary phases for HPLC.	9
Table 1.3 Examples of fine chemical reactions catalyzed over mesoporous catalysts.	20
Table 2.1 The different packing parameter range corresponding to different micellar aggregates.	42
Table 2.2 Structures and quantities of S ⁰ surfactants used for the synthesis of mesoporous silica.	55
Table 2.3 Reaction Temperature and Solvent Compositions Used for the Mesostructure Templating by Armeen OLD (oleyl-NH ₂) and Duomeen O (oleyl-NH(CH ₂) ₃ NH ₂) Surfactants	56
Table 2.4 Structural properties of calcined wormhole silica materials.....	67
Table 2.5 Summary of the pore properties of mesoporous silica products assembled using Duomeen O as a templating agent under varying assembly temperature and varying water composition.	102
Table 2.6 Summary of the pore properties of mesoporous silica products assembled using Armeen OLD as a templating agent under varying assembly temperature and varying water composition.	103
Table 3.1. Wormhole Silica Products Synthesized in 60 volume % Ethanol Media.	133
Table 3.2 Summary of pore properties of calcined and extracted silica products assembled with crosslinked surfactant templates.	144
Table 3.3 Pb(II) uptake of mesoporous materials by crosslinked oleylamine surfactant encapsulated in mesoporous silica	152
Table 4.1. Phosphorylated peptides from tryptic digests of β -casein and ovalbumin	198

LIST OF FIGURES

Figure 1.1 Functionalization techniques of mesoporous silica for catalytic applications	17
Figure 2.1 Schematic representation of MCM-41 synthesis	39
Figure 2.2 Structure of CTAB and Ethoquad	51
Figure 2.3 Powder x-ray diffraction of calcined silica products synthesized using (A) Ethoquad (oleyl-N ⁺ (CH ₃)(CH ₂ CH ₂ OH) ₂ Cl ⁻) and (B) cetyl trimethyl ammonium bromide (CTAB) as the templating surfactants.....	62
Figure 2.4 Low angle powder x-ray diffraction of calcined wormhole silicas synthesized from different electrically neutral oleyl amine surfactants (60/40 ethanol water by volume). The structure of the oleylamine surfactants are given in Table 2.1. The pattern for the wormhole mesostructure made from dodecylamin is included for comparison. Each product was synthesized at a reaction temperature of 25°C.....	63
Figure 2.5 Low angle powder x-ray diffraction calcined wormhole silicas synthesized from oleyl amine surfactants in water rich media (30/70 ethanol/water by volume).The structure of the oleyl surfactants are given in Table 2.1. The pattern for the silica template by DDA is included for comparison. The reaction temperature was 25°C.	64
Figure 2.6 Nitrogen isotherms for the wormhole silicas synthesized at 25°C under ethanol rich media (60 vol %) in the presence of oleyl amine surfactants. The isotherm for the silica template by dodecylamine (DDA) is included for comparison.	65
Figure 2.7 Nitrogen isotherms for the wormhole silicas synthesized at 25°C under water rich media (70 vol %) in the presence of oleyl amine surfactants. The isotherm for the silica template by dodecylamine (DDA) is included for comparison.	66
Figure 2.8 Powder x-ray diffraction of mesostructured silica products synthesized from Duomeen O (oleyl-NH(CH ₂) ₃ NH ₂) at 25, 45, and 60°C. The labeling scheme is described in the text.....	71

Figure 2.9 Powder x-ray diffraction of mesostructured silica products synthesized from Armeen OLD (oleyl-NH ₂) in reaction medium containing 10% to 100% H ₂ O at 25, 45, and 60 °C. The labeling scheme for each sample is described in the text.	72
Figure 2.10 Nitrogen adsorption isotherms of mesostructured silica synthesized from Duomeen O at 25 °C with varying water fraction (Top) 10-50%, (Bottom) 60-100%.	74
Figure 2.11 BJH pore size distribution of mesostructured silica synthesized from Duomeen O at 25 °C with varying water fraction (Top) 10-50% (Bottom) 60-100%.....	75
Figure 2.12 TEM images of mesostructured silica synthesized from Duomeen O at 25 °C with varying solvent polarity a liquid.	76
Figure 2.12 (cont'd).....	77
Figure 2.13 Nitrogen adsorption isotherms of mesostructured silica synthesized from Duomeen O at 45 °C with varying water fraction (Top) 10-50% (Bottom) 60-100%.....	80
Figure 2.14 Nitrogen adsorption isotherms of mesostructured silica synthesized from Duomeen O at 60 °C with varying water fraction (Top) 10-50% (Bottom) 60-100%.....	81
Figure 2.15 BJH pore size distribution of mesostructured silica synthesized from Duomeen O at 45 °C with varying water fraction (Top) 10-50% (Bottom) 60-100%.....	82
Figure 2.16 BJH pore size distribution of mesostructured silica synthesized from Duomeen O at 60 °C with varying water fractions of (Top) 10-50% and (Bottom) 60-100%.	83
Figure 2.17 TEM images of mesostructured silica synthesized from Duomeen O at 45 °C with varying solvent polarity.....	84
Figure 2.17 (cont'd).....	85
Figure 2.18 TEM images of mesostructured materials synthesized from Duomeen O at 60 °C with varying solvent polarity.....	86
Figure 2.18 (cont'd).....	87

Figure 2.19 Nitrogen adsorption isotherms of mesostructured silica synthesized from Armeen OLD at 25 °C with varying water fraction (Top) 10-50% (Bottom) 60-100%.	89
Figure 2.20 BJH pore size distribution of mesostructured silica synthesized from Armeen OLD at 25°C with varying water fraction (Top) 10-50% (Bottom) 60-100%.....	90
Figure 2.21 TEM images of mesostructured materials synthesized from Armeen OLD at 25 °C with varying solvent polarity.	91
Figure 2.21 (cont'd).....	92
Figure 2.22 Nitrogen adsorption isotherms of mesostructured silica synthesized from Armeen OLD at 25 °C with varying water fraction (Top) 10-50% (Bottom) 60-100%.	93
Figure 2.23 BJH pore size distribution of mesostructured silica synthesized from Duomeen O at 25 °C with varying water fraction (Top) 10-50% (Bottom) 60-100%.....	94
Figure 2.24 TEM images of mesostructured materials synthesized from Armeen OLD at 45 °C with varying solvent polarity.	95
Figure 2.24 (cont'd).....	96
Figure 2.25 Nitrogen adsorption isotherms of mesostructured silica synthesized from Armeen OLD at 25 °C with varying water fraction (Top) 10-50% (Bottom) 60-100%.	97
Figure 2.26 BJH pore size distribution of mesostructured silica synthesized from Duomeen O at 25 °C with varying water fraction (Top) 10-50% (Bottom) 60-100%.....	98
Figure 2.27 TEM images of mesostructured materials synthesized from Armeen OLD at 60 °C with varying solvent polarity.	99
Figure 2.27 (cont'd).....	100
Figure 2.28 Schematic illustration on how the oleyl surfactant decreases their hydrophobe chain length.....	108
Figure 2.29 Nitrogen isotherms (top) and BJH pore size distributions (bottom) of mesostructured silicas synthesized from tallow amine (TA) at 25 °C under varying water fractions (10-100%).	109

Figure 2.30 Pore size variations of mesoporous silicas assembled under varying water fractions using Armeen OLD (oleyl-NH ₂) with respect to temperature variations. (Note: A10-60 (10 volume % water) was not included in the plot since it did not produced a mesostructured silica.).....	110
Figure 2.31 Pore size variations of mesoporous silicas assembled under varying water fractions using Duomeen O (oleyl-NH(CH ₂) ₃ NH ₂) with respect to temperature variations.	111
Figure 3.1 Schematic representation of the post-synthesis grafting technique for introducing organic functionality in the pore walls of mesoporous silica.	122
Figure 3.2 Schematic representation of direct assembly or co-condensation technique of introducing organic functionality in mesoporous silica.....	123
Figure 3.3 Two dimensional, highly idealized polymeric micelle with polymerizable group on the hydrophobic tail (A) and on the hydrophilic head (B); C-D: Sherrington's concept of a polymerized micelle with polymerizable group on the hydrophobic tail (C) and on the hydrophilic head (D).....	127
Figure 3.4 Two possible schemes on incorporating a polymeric complexant inside mesoporous silica materials.	132
Figure 3.5 Low angle powder x-ray diffraction pattern of crosslinked oleyl surfactant in mesostructured silicas made by pre-assembly and post-assembly crosslinking of the surfactant progen.	138
Figure 3.6 Representative TEM images mesostructured silica assembled in the presence of oleyl surfactant cross-linked by divinylbenzene prior to the addition of TEOS (pre-assembly crosslinking).....	139
Figure 3.7 Representative TEM images calcined mesostructured silica assembled in the presence of oleylamine surfactant followed by crosslinking of the surfactant by divinylbenzene.....	140
Figure 3.8 (Top) Nitrogen adsorption isotherms and (Bottom) BJH pore size distributions for non-crosslinked, calcined and ethanol extracted silicas made by pre-assembly DVB crosslinking of the surfactant.....	142
Figure 3.9 (Top) Nitrogen adsorption isotherms and (Bottom) BJH pore size distributions for non-crosslinked, calcined and ethanol extracted silicas made by post-assembly DVB crosslinking of the surfactant.	143

Figure 3.10 Thermal gravimetric analysis plots for: Left panel: A. As-made mesostructured silica templated with unpolymerized oleyl amine surfactant, B. Mesostructured silica from A after water extraction; Central Panel: C. Mesostructured silica whose surfactant template was crosslinked with DVB before supramolecular assembly(post-assembly crosslinking), D. Mesostructured silica C after water extraction; Right panel: E. Water extracted mesostructured silica material whose surfactant template was crosslinked after supramolecular assembly, F. Material E after water extraction.	147
Figure 3.11 Distribution of Pb(II) species as a function of pH based on the equilibrium constants.	151
Figure 3.12 Pb(II) uptake by mesoporous silica with encapsulated crosslinked oleylamine surfactant as a complexant. The amount of Pb(II) added varied from 0.22 to 4.73 mmole Pb(II) per gram as-made material. The ratio of N : Pb for pre- and post-assembly polymerization are 3.63 and 3.73 respectively.	153
Figure 4.1 The two general schemes for post-translational modification: covalent modification and covalent cleavage.	159
Figure 4.2 The five major types of covalent additions to protein side chains	160
Figure 4.3 The phosphorylated amine residues	162
Figure 4.4 General scheme for the modification for phosphoserine by β -elimination.....	167
Figure 4.5 Enrichment of a modified phosphopeptide coupled with a biotin affinity tag.....	168
Figure 4.6 Modified phosphopeptide enrichment via direct attachment to a solid support.....	169
Figure 4.7 Structures of A. Fe(III) iminodiacetic acid complex B. Fe(III) nitrilotriacetic acid complex C. phos-tag.....	171
Figure 4.8 Schematic illustration of the phosphopeptide enrichment process using grid supported mesoporous metal oxide thin films. Washing solution 1 is 2,5-dihydroxybenzoic acid in acetonitrile. Washing solution 2 is trifluoroacetic acid in acetonitrile.	182
Figure 4.9 Schematic representation of grid-supported mesoporous metal oxide thin film containing bound phosphopeptide being mounted on a MALDI plate and the subsequent release of the bound phosphopeptide for MALDI mass spec analysis.....	183

Figure 4.10 Different types of grids. A square mesh B. hexagonal mesh C. slots D. parallel E. combination of parallel and mesh F. folding and G. tabbed.	184
Figure 4.11 A. Bar B. Hole C. Pitch.....	185
Figure 4.12 Wide angle x-ray diffraction of calcined alumina, titania and zirconia powders.	187
Figure 4.13 Electron diffraction of grid supported mesoporous zirconia thin films taken from TEM selected area diffraction mode showing several rings indicating a polycrystalline structure.	188
Figure 4.14 Electron diffraction of grid supported mesoporous titania thin film taken from TEM selected area diffraction mode showing several rings indicating a polycrystalline structure.	189
Figure 4.15 TEM images of mesoporous titania thin film supported on a gold TEM grid (400 mesh). (Left) The lighter shades on the image represent the mesopores. (Right) Variable orientations of lattice fringes indicate the polycrystalline nature of the film.....	190
Figure 4.16 TEM images of mesoporous zirconia thin film supported on a gold TEM grid (400 mesh). (Left) The lighter shades on the image represent the pores. (Right) Lattice fringes on different directions indicate the polycrystalline nature of the material.	191
Figure 4.17 TEM image of mesoporous alumina thin film supported on a gold grid. The image shows the mesopores that arises from the stacking of lath-like nanocrystals of alumina.	192
Figure 4.18 SEM images of bare gold grid. The left image was taken from the matted side of the grid and the right image was taken from the glossy side of the grid.....	193
Figure 4.19 SEM image of a calcined mesoporous titania thin film supported on a gold grid. The crystalline anatase coats the bars of the grid and extends into the holes of the grid. The crystallization of the anatase phase during calcinations causes shrinkage which fragments the films.....	194
Figure 4.20 SEM image of a calcined mesoporous alumina thin film showing completely filled holes on the TEM grid as well as the coated bars of the grid.	195
Figure 4.21 Schematic illustration of phosphopeptide binding to a metal oxide surface and the release of the protein by reaction with ammonium hydroxide..	196

Figure 4.22 MALDI spectrum of un-enriched β -casein. The specimen was supported on a stainless steel MALDI plate.....	199
Figure 4.23 Incubation studies of 100 fmol β -casein on grid supported mesoporous titania (TiO_2) thin film.	200
Figure 4.24 Incubation studies of 100 fmol β -casein on grid supported mesoporous alumina (Al_2O_3) thin film.....	201
Figure 4.25 Enrichment of the monophosphorylated and tetraphosphorylated peptides in a tryptic digest of 50 fmol β -casein on TEM grid supported mesoporous zirconia (top), alumina (middle), and titania (bottom). A three-hour incubation time was used in obtaining each spectrum.	204
Figure 4.26 Enrichment of 50 fmol β -casein on gold TEM grid showing high selectivity towards tetraphosphorylated peptides – 4P ₂₉₆₆ and 4P ₃₁₂₂	205
Figure 4.27 Enrichment of 50 fmol of β -casein tryptic digest on bare gold (bottom) and bare titanium (top) TEM grids.....	207
Figure 4.28 Enrichment of a 50 fmol tryptic digest ovalbumin on grid supported mesoporous zirconia, alumina, and titania.....	210
Figure 4.29 MALDI spectrum of 100 fmol ovalbumin tryptic digest enriched on grid supported mesoporous zirconia, alumina and titania thin films. Note the weak or absence of enrichment for 1P ₂₅₁₁ and 1P ₂₉₀₁ fragments.	211
Figure 4.30 MALDI spectrum of the 50 fmol ovalbumin phosphorylated peptide enriched using titanium metal grid.....	212

ABBREVIATIONS

AIBN	Azobisisobutyronitrile
BET	Brunauer-Emmett-Teller
BJH	Barrett-Joyner-Halenda
DDA	Dodecylamine
DVD	Divinylbenzene
EtOH	Ethanol
fmol	Femtomoles
H-bonding	Hydrogen bonding
HK	Horvath and Kawazoe
HMS	wormhole mesostructured silica synthesized with a neutral amine surfactant using hydrogen bonding interactions
I ⁻	Anionic inorganic precursor
I ⁺	Cationic inorganic precursor
I ⁰	Neutral inorganic precursor
IUPAC	International Union of Pure and Applied Chemistry
MCM-41	Mobil Composition of Matter No. 41
mmol	Millimoles
nm	Nanometer (10 ⁻⁹ m)
No	Non-ionic amphiphilic PEO based surfactant
P/P ₀	Relative Pressure P = pressure, P ₀ = saturation pressure
PEO	Polyethylene oxide

pmol	Picomoles
S ⁻	Anionic amphiphilic surfactant
S ⁺	Cationic amphiphilic surfactant
S ⁺ I ⁻	Electrostatic Assembly between cationic surfactant and anionic silica precursor
S ⁺ X ⁻ I ⁺	Electrostatic assembly between cationic surfactant and cationic silica precursors with halogen ions as mediating counter ions
SBA-15	Mesostructure silica assembled under high acid conditions with TEOS and triblock copolymer PEO based surfactant
S ⁰	Neutral amphiphilic amine surfactant
S ⁰ I ⁰	Neutral assembly pathway between neutral amine surfactant and TEOS
TEOS	Tetraethylorthosilicate
XRD	X-ray Diffraction

Chapter 1 Synthesis and Applications of Mesoporous Silica

1. Introduction

The International Union of Pure and Applied Chemistry (IUPAC) has classified porous materials into three classes: microporous (pore size <2 nm), mesoporous (2-50 nm) and macroporous (>50 nm) materials.¹ Other porous materials such as pillared clays, anodic alumina, carbon nanotubes and related porous carbons also have been extensively described in literature.² Among the best known microporous materials are the zeolites. Zeolites have narrow and uniform pore size distributions due to their crystallographically defined structures. The ability of zeolites to act as solid acids and in some cases as bases, has attracted strong attention. However, zeolites applications are severely limited for applications involving large molecules. This limitation is most evident in the synthesis of fine chemicals where mass transfer is very difficult to achieve in zeolite micropores. Efforts have been made to improve the diffusion of reactants to the catalytic sites of zeolites by increasing framework pore sizes,³ decreasing the zeolites crystal size,⁴ or providing an additional mesopore system within the microporous crystals.^{5,6} A very important line of research has focused on the enlargement of the pore sizes.

1.1 Synthesis of Mesoporous Silica

The first synthesis of an ordered mesoporous silica was described in the patent literature of 1969. However, due in part to the lack of analysis and analytical knowhow, this product was not recognized.^{7,8} In 1992, a similar

material was reported by Mobil Oil Corporation scientists.⁹ This material was denoted Mobil Composition of Matter No. 41 (MCM-41). MCM-41 opened up a whole field of research. This mesoporous silica has highly ordered hexagonal array of unidimensional pores with a very narrow pore size distribution.^{10,11} The walls of MCM-41 resembles that of amorphous silica. Along with MCM-41, MCM-48 and MCM-50 having cubic and lamellar structures, respectively, also were reported. Depending on the assembly conditions, the silica source and the surfactant template used in the assembly process, mesoporous silica can be synthesized following co-operative assembly based on electrostatic interactions or electrically neutral hydrogen bonding.¹²⁻¹⁴ In addition, ordered mesoporous silica can also be synthesized using liquid crystalline templates¹⁵ and by nanocasting.^{16,17} Table 1.1 presents the classification of mesoporous forms of silica based on the interaction of the inorganic species and organic template molecule. The first ordered mesoporous silicas were prepared from ionic surfactants (quaternary ammonium salts) as the structure directing agent. The formation of the inorganic-organic composite is based on the electrostatic interactions between the positively charged surfactants (denoted S^+) and the negatively charged silicate species in solution (denoted I^-).

Table 1.1 Classification of mesoporous silica based on the interaction of inorganic species and organic template ^a

Template	Interaction		Synthesis Conditions	Examples
Ionic surfactant	Direct Interaction (Electrostatic)	S ⁺ I ⁻	Basic	MCM-41, MCM-48, MCM-50, ⁹⁻¹¹ FSM-16 ¹⁸⁻¹⁹
		S ⁻ I ⁺	Neutral-Basic	(Aluminum, iron, lead oxides, etc. ^{13,14}) AMS ²⁰⁻²¹
	Intermediated Interaction (Electrostatic)	S ⁺ X ⁻ I ⁺	Acidic	SBA-1, SBA-2, SBA-3 ²² TLCT ¹⁵
		S ⁻ X ⁺ I ⁻	Basic	(Aluminum, zinc oxide etc ^{14,15})
Non-Ionic Surfactant / Co-polymer	H-bonding	S ⁰ I ⁰		HMS ^{23,24}
		N ⁰ I ⁰	Acidic	MSU ^{25,26} , SBA-15 ^{27,28} , TLCT ¹⁵
(Ligand Assisted)	Covalent Bonding	S-I		Nb-TMS ^{29,30} , Ta-TMS ³¹
Nanocasting				CMK-n ^{16,32}

^aS⁺ and S⁰ denote cationic and electrically neutral surfactant templates, respectively; I⁻, I⁺ and I⁰ denote anionic and electrically neutral inorganic precursor; X⁻ and X⁺ denote inorganic ions participating in triple ion formation.

The prediction of surfactant aggregates (micelles) and the corresponding mesophases in surfactant-water systems (liquid crystals) was made possible by Israelachvili and co-workers^{33,34} through the development of a model that describes the packing parameter *g*. Briefly, *g* is the ratio of the molecular volume of the surfactant molecule to the volume the molecule would occupy if it were enclosed in a cylinder. It is important to note that the value the packing parameter, which is typically between 0.3 and 1.0, is not constant as it is affected

by solution conditions such as ionic strength, pH, co-surfactant concentration or temperature.³⁴

The synthesis-space diagram for a ternary system composed of NaOH, cetyltrimethylammonium bromide (CTAB) as a surfactant porogen, and tetraethylorthosilicate (TEOS) as the inorganic reagent has been described previously.^{35,36} It was shown that the surfactant to silica ratio has a substantial effect on the composite structure obtained.³⁷ Also, the mesopore size was found to be controlled by the length of the hydrophilic segment of the surfactant and the corresponding diameter of the surfactant micelle. However, the addition of auxiliary organic molecules such as aromatics,^{11,38} n-alkanes,³⁹ or fatty acid⁴⁰ can act as micelle swelling agents and lead to expansion of the mesopore size.

Pinnavaia et al. developed non-electrostatic pathways for the synthesis of mesoporous silica, denoted the $S^{0/0}$ pathway (see Table 1.1). This approach utilizes the H-bonding interactions between the silica precursor (silicic acid formed by tetraethylorthosilicate hydrolysis) and the electrically neutral amine surfactant or poly(ethylene oxides) to prepare wormhole HMS and MSU silicas. This approach is advantageous in both economical and ecological points of view for as much as 90% of the surfactant template can be recovered by simple extraction with ethanol²³ or aqueous acids.⁴¹ Compared to MCM-41, HMS and MSU silicas have very similar surface areas and pore volumes but the pore size distributions are broader. Also, many of the modifications that can be applied to MCM-41 are applicable to HMS wormhole silicas such as the tailoring of the pore

size by changing the alkyl chain length of the surfactant or by the addition of mesitylene to the reaction mixture in order to swell the templating micelles.^{42,43}

In the ligand assisted assembly approach (denoted S-I in Table 1.1), covalent bonds are formed between the organic precursors and the organic surfactant molecule prior to assembly. The approach was first developed by Antonelli and Ying for the preparation of mesoporous niobium oxide²⁹ and tantalum oxide.³¹ The assembly of Nb-TMS (Transition Metal oxides mesoporous molecular Sieve) and Ta-TMS involves the hydrolysis of long-chain amine complexes of niobium or tantalum. The removal of the template by extraction afforded open porous structures with surface areas of up to 500 m²/g. Mesostructured niobia with 3D hexagonal symmetry, as well as a cubic phase and a layered structure, was obtained.³⁰

The true liquid crystal templating (TLCT) had already been suggested as one possible mechanism for the formation of MCM-41. The first example of this approach was reported by Attard and co-workers¹⁵ for the hydrolysis of tetramethylorthosilicate (TMOS) in a liquid crystalline phase. The liquid crystalline phase is destroyed upon the formation of methanol as the reaction product but reforms when methanol evaporates. This method was later found to be useful in the synthesis of mesoporous metals⁴⁴⁻⁴⁷ and mesostructured assemblies of chalcogenide nanoparticles.⁴⁸

Another distinct method for producing mesostructure phases is the nanocasting method that was first reported by Ryoo and co-workers in 1999.³⁶ In this approach, no surfactant was utilized as a porogen. Instead an ordered

mesoporous silica was used as a hard template. The method involves infiltrating the mesoporous silica (eg. MCM-41) with a carbon precursor such as sucrose or furfuryl alcohol which is subsequently converted to carbon at high temperature under inert atmosphere. The mesoporous silica is removed by treatment with HF or NaOH leaving the carbon negative of the original mold (denoted as CMK-n). While this method is already established to produce carbon base materials,^{49,50} the use of silica as hard template was only recently reported for some examples such as CeO₂,⁵¹ Cr₂O₃,⁵² NiO,⁵³ OsO₄,⁵⁴ In₂O₃,^{55,56} and CoO₂.⁵⁶ The limited applicability of the method most likely is due to the incompatibility of many oxide materials with the conditions needed for leaching away the hard silica template.

1.2 Mesoporous Silica Applications

Although there are many reviews regarding the synthesis, formation mechanism, modification and control of their characteristics⁵⁷⁻⁶⁴, there are relatively few reviews of the material applications of mesoporous metal oxides. This introduction will provide a summary of recent studies and applications of mesoporous silica in liquid chromatography, the immobilization of biomolecules, catalysts, trapping agents and agents for polymer reinforcement.

1.2.1 As Stationary Phase for High Performance Liquid Chromatography

One major area of application for mesoporous silica is in liquid chromatography as a column packing material for the stationary phase. Mesoporous silicas are of interest as stationary phase materials for HPLC

because of their inherent high surface area and their organized pore structure. The silanol group density and the mechanical stability of the mesophase under chromatographic operating conditions are similar to those of the precipitated silica. Table 1.2 identifies several studies of mesoporous silica for use as stationary phases for HPLC.

In liquid chromatography, the efficiency (N, number of theoretical plates) of a column (length L) is given by the equation:

$$N = L^2/\sigma^2 = 16t_R / t_W \quad 1$$

$$H = \sigma^2/L = L/N \quad 2$$

where H is the plate height and σ^2 is a variance of a Gaussian-shaped band the solute acquire during migration through the column. N is calculated from retention time of a solute (t_R) and the base peak width ($t_W = 4\sigma$, σ is the standard deviation)

H is dependent on the particle size (d_p) and mobile phase linear velocity (u) as shown in equation 3 where C_E , C_D , C_S are the coefficients indicating the contributions of the eddy diffusion, molecular diffusion and slow mass transfer to band broadening, respectively. The smaller d_p gives a higher efficiency by the faster mass transfer based on the shorter diffusion path length inside and outside the particles, whereas a small d_p causes a large pressure drop due to small interstitial flow paths (η , solvent viscosity), where ϕ (a flow resistance factor) is commonly 700-1000 for a particle packed column.⁷⁷

$$H = C_E d_p + C_D / u + C_S d_p u \quad 3$$

$$\Delta P = \phi \eta u L / d_p^2 \quad 4$$

For high resolution and high speed it is desirable to have high efficiency (large N) and low pressure (small ΔP). Separation time is dictated by L, and the smaller d_p allows the use of shorter column. Actually, H is approximately $2d_p$ at optimum linear velocity. Recently, 1.7-2 μm particles, have started to provide greatly enhanced N per unit time^{78,79} compared to 3-5 μm particles, although accompanied by high pressure in proportion to $1/d_p^2$. Their optimum performance can be obtained with a specially designed instrument. Common HPLC equipment possesses a 35-40 MPa pressure limit. Monolithic silica columns having continuous structures can simultaneously provide higher efficiency and lower pressure than a particle packed column.⁸⁰⁻⁸² Prouzet and co-workers summarized the chromatographic application of MSU-X silica particles with controlled morphology.⁸³

Table 1.2 Mesoporous silica used as stationary phases for HPLC

Mesoporous Material	Chromatographic Applications	Ref
MCM-41 constituted by loose particles agglomerates	NP-HPLC (aromatic polycyclic hydrocarbons)	64
Solid obtained in acidic medium by using cationic surfactant and TMOS. It was grinded and separated in aggregates of 15 μ m	NP-HPLC (phthalic esters and aromatic compounds)	65
SBA-3 type spherical particles	NP-HPLC (ferrocene and acetylferrocene) y RP HPLC (aromatic hydrocarbon and racemic mixtures)	66
MSU-X type spherical particles (diameter \sim 7.6 μ m)	NP-HPLC and RP-HPLC (aromatic hydrocarbon)	67
SBA-15 or SBA-16 type spherical or polyhedral particles (diamter 3–10 μ m)	NP-HPLC and RP-HPLC (aromatic hydrocarbon)	68-70
MSU-X type silica agglomerates of nanometric particles	NP-HPLC (hydrocarbon)	71
MCM-41 type spherical particles (diameter 5 mm) obtained by pseudomorphic synthesis from macroporous silica gel	RP-HPLC (alkylbenzenes)	72
SBA-15 type spheroidal particles (diameter \sim 1 μ m)	Capillary RP-HPLC (biomolecules)	73
MCM-41 type silica with pore diameter \sim 3.38 nm	Exclusion size HPLC (low molecular weight polystyrene compounds)	74
MCM-41 type silica with pore diameter \sim 2.5 nm	Separation of three aluminum species (cationic, tridecameric and polynuclear)	75
Chiral stationary phases supported on MCM-48 or SBA-3 type silica	α -methylbenzylamine enantiomers	66
Bifunctionalized mesoporous organosilica spheres (diameter 5 μ m) with trans-(1R,2R)-diaminocyclohexane	Resolution of DL-valine by chiral HPLC	76

1.2.2 Immobilization of Biomolecules

Biomolecules are frequently immobilized on silica supports through a sol gel process. Mesoporous silica molecular sieves and related materials have received much attention as inorganic supports for biomolecules. Aside from the fact that they have very high surface area and large pore volume, they are chemically and mechanically stable and resistant to microbial attack. The mesostructured materials can be reliable in the accommodation or immobilization of biomolecules.

One of the current trends in material research is innovation in the fields of intelligent or smart materials. Smart materials are materials that display functionalities capable of detecting changes in the near environment and store, transfer or convert a signal in way analogous to a living cell.⁸⁴⁻⁸⁶ The design of smart materials focuses on the concept of biomimetic materials in order to reproduce specific and selective properties not deliverable by standard chemical or physical processes. The engineering of biohybrid enzyme based materials and their applications is limited by the intrinsic fragility of enzymes toward various environmental stresses and their narrow range of working conditions. A suitable inorganic host should allow high levels of enzyme uptake with minimum enzyme degradation or inactivation. In general, the support must have a high capacity to bind enzyme. The available surface area, chemical inertness and mechanical stability are usually the decisive factors. Moreover, other factors that must be considered are charge of the surface and hydrophilicity as well as diffusion ability in bulk. There are several immobilization approaches available but the most

common of which are sol-gel encapsulation and covalent grafting. The sol-gel encapsulation method has attracted much attention due to its potential for creating a high concentration of encapsulated enzyme. This approach is used mainly for immobilizing an enzyme in a silica matrix. In comparison with other methods, the sol-gel method generally exhibits simplicity, and versatility in composition and physio-chemical properties. However, since enzymes are weakly bound, leakage of entrapped enzyme is often observed through diffusion out of the matrix. Another hurdle is that the matrix acts as a mass transfer barrier that can limit or hamper the diffusion of large substrate molecules to the embedded enzyme. The covalent binding of the enzyme to a solid support appears to be the most appropriate treatment when enzymes must be used in drastic environments where high stability is required or leakage must be prevented. Proteins that display side chains with reactive groups able to undergo condensation reaction with various organic functions or complexation reactions with metallic cations can be used to fix biomolecules onto inorganic supports.

The immobilization of proteins in mesoporous MCM-41 was first attempted by Diaz and Balkus.⁸⁷ Several research groups then investigated the influence of various physical factors such as pore size, ambient pH, and ionic strength on the adsorption efficiency of proteins.⁸⁸⁻¹⁰⁴ Vinu and co-workers did an extensive study on the immobilization of hen egg white lysozyme into MCM-41. Based on their results they tried to explain the adsorption behavior of lysozyme inside the pores of mesopore.¹⁰⁵ The effect of pH changes and incorporated heteroatoms into a mesoporous framework (Al-substituted MCM-41) were also studied.

Immobilization of proteins also can be done through direct addition of the protein during the mesoporous silica assembly. Blin and co-workers¹⁰⁶ also demonstrated that hexagonally arranged pore structures can be synthesized using a fluorinated surfactant, $\text{CF}_3(\text{CF}_2)_7\text{C}_2\text{H}_4(\text{OC}_2\text{H}_4)_9\text{OH}$ in the presence of glucose oxidase as long as the protein concentration was below 3.2 mg/mL. Galarneau and co-workers¹⁰⁷ proposed the use of lecithin and cationic dodecyl amine as the structure directing agent in the presence of lactose for direct protein immobilization. In this study, the lecithin is thought to protect the enzyme and prevent the direct interaction between the silica and the enzyme. Ying and co-workers¹⁰⁸ reported a pressure driven method for entrapping lipase into siliceous mesocellular foam. A high pressure (3000-5000 psi) was used to achieve a high enzyme loading within the silica support. The immobilized lipase demonstrated high activity and enhanced thermal stability and the enzyme leaching was not significant.

Post treatment of adsorbed proteins in mesoporous silica is often beneficial for the stability of the immobilize protein. The use of gluteraldehyde for the immobilization of α -chymotrypsin in hierarchically ordered mesocellular mesoporous silica materials (HMMS) enables the crosslinking of the enzyme that resulted to an impressive stability with very high loadings with 10 times the activity.¹⁰⁹ Polymers have also been used for the stable entrapment of proteins inside mesoporous silica. Poly(methacrylate)-type polymers has been used to reduce the pore openings SBA-15 support that is loaded with porcine pancreatic lipase.¹¹⁰ This prevents the lipase from leaching out of the support. Wang and

Caruso¹¹¹ proposed a unique method to prepare a porous protein assembly using mesoporous silica as a hard template. In this approach, proteins such as lysozyme, cytochrome c and catalase were adsorbed in the channels of a mesoporous silica sphere. Next, a polyelectrolyte was infiltrated into the pore channels to bridge the proteins. The silica template is then removed leaving a nanoporous protein particle. Such materials are seen to find applications in the field of biosensing, catalysis, separations and controlled drug delivery.

Hudson and co-workers¹¹² discussed the driving forces for protein adsorption on mesoporous materials using SBA-15 silica and MSE, a periodic mesoporous organosilica. Cytochrome c and xylanase were adsorbed onto the two mesoporous materials. Electrostatic attraction dominated the protein interactions with SBA-15 silica, while weaker hydrophobic interactions were more prominent with MSE for both proteins. Moreover, their study also revealed that cytochrome c immobilized on SBA-15 through electrostatic interaction showed resistance to leaching with an enhance activity compared to the free protein.

Nucleic acids, RNA and DNA are attractive biopolymers that can be used for biomedical applications,^{113,114} nanostructure application,^{115,116} computing^{117,118} and materials for electron conduction.¹¹⁹⁻¹²⁰ The immobilization of DNA and RNA in a well defined structure would be one of the most unique subjects in current nanotechnology. Unfortunately, the silica surface cannot adsorb duplex DNA in aqueous solution due to electrostatic repulsions between the silica surface and polyanionic DNA. Recently a method was devised for adsorption of duplex DNA in protonated phosphoric acid form.¹²¹

Mesoporous silica alone adsorbs a negligible amount of DNA but the exchange of divalent cations such as Mg^{2+} and Ca^{2+} into the pores of mesoporous silica prior to DNA uptake was found to cause a significant amount of DNA to be adsorbed.¹²² Post synthetic treatment with aminopropyl groups further increased the adsorption capacity that 2-3 times higher in comparison to that observed for metal ion-exchanged mesoporous silica.¹²³

There are several potential applications for the immobilization of biomolecules in mesoporous materials. One is the production of microscopic reactors. Galarneau et al. have shown that lipase immobilized in mesoporous silica produce higher activity.¹²⁴ Cytochrome c immobilized on mesoporous silica has high specific activity toward the oxidation of polycyclic aromatic hydrocarbons. Immobilized aldolase antibody 84G3 in mesoporous silica with 15-25 nm pores exhibit highly accelerated aldol reactions and stability as compared to a free antibody.¹²⁵ The enhanced activity is attributed to a favorable microenvironment that results in higher efficiency due to size exclusion. A mesoporous nanospace can also provide an environment where molecular motions and orientations are highly constrained. This situation is similar to that in the confined spaces found in enzyme pockets.

Another application is selective binding and separation of biomolecules. Brennan and co-workers¹²⁶ reported the application of protein doped monolithic silica columns for immobilized enzyme reactor chromatography. This allowed the screening of enzyme inhibitors in mixtures using mass spectrometry for detection. The mesoporous materials also possess highly reliable and

controllable pore geometries that regulate the release of drugs from mesopores. Photo controlled regulation of drug storage and release using functionalized mesoporous silica has been reported as well as colloid capped mesoporous materials for controlled release and delivery. Biomolecules and mesoporous silica hybrids are very promising for biosensor applications.¹²⁷⁻¹²⁸

1.2.3 Catalysis

1.2.3.1 Preparation of Mesoporous Catalysts

The advantages of using mesoporous silica in catalysis include the relatively large pores which facilitate mass transfer and the very high surface areas which allows a high concentration of active sites per mass of material. There are several ways to modify mesoporous silica to provide the desired catalytic function. These include the introduction of highly dispersed heteroatoms in the framework walls, occlusion of metal, metal oxide or metal sulfide nanoparticles in the pores, and anchoring of molecular catalyst to the framework walls. Figure 1.1 shows these different approaches.

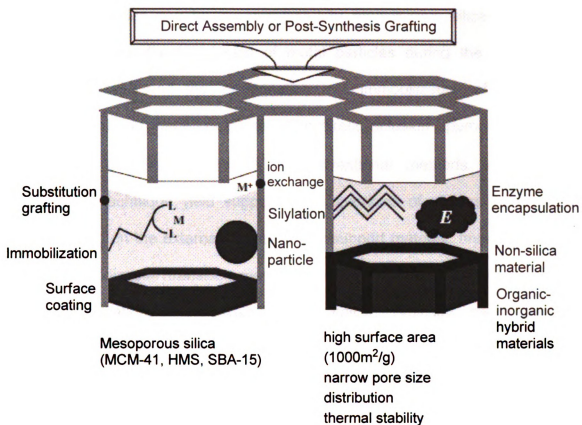
Incorporation of Heteroatoms

Much effort has been made on the introduction of heteroatoms such as B, Fe, Ga, Ti, V, Sn, and Al in siliceous frameworks to modify the composition of the inorganic walls. It should be noted that the walls of mesoporous silica resembles that of amorphous silica. The incorporation of heteroatoms allows the fine tuning of the acidity or redox properties, as observed in amorphous aluminosilicates or zeolites. The incorporation of Al into the walls affords enhanced hydrothermal

stability¹²⁹ and broader pore size distributions than the pure silica analogues^{10,130}. This also creates Bronsted acidity and ion exchange sites. The effect of the aluminum source such as $\text{Al}(\text{OH})_3$, aluminum isopropoxide or NaAlO_2 on the degree of aluminum incorporation has also been studied.¹³¹ Al-MCM-41 prepared using NaAlO_2 as the aluminum source gave the strongest Bronsted acidity. A comparison of Al-, Ga- and Fe- functionalized silicas, showed that the Bronsted acidity decreased in the order of $\text{Al} > \text{Ga} > \text{Fe}$ but for Lewis acidity the sequence was $\text{Ga} \approx \text{Al} \gg \text{Fe}$.¹³²

Zeolitization of the walls of mesoporous silica is another interesting development that can be achieved either through the conversion of the silica walls into zeolitic units or through the use of precursors that originally contain zeolitic structural elements.¹³⁸⁻¹⁴⁰ The cations can also be exchanged with Cs^+ , Zn^{2+} , or Fe^{3+} and to achieve catalytic activity as in the Diels-Alder reaction of cyclopentadiene and methyl methacrylate¹⁴¹ or in the selective catalytic reduction of NO .¹⁴² Not only inorganic cations but also cationic organometallic compounds such as $[\text{Fe}(\text{phen})_3\text{Cl}_2]$,¹⁴³ $[\text{Fe}(\text{8-quinolinol})_3\text{Cl}_2]$,¹⁴⁴ $[\text{Mn}(\text{2,2'-bipyridine})_2\text{NO}_3]$,¹⁴⁵ $[\text{Mn}(\text{porphyrin})\text{Cl}]$,¹⁴⁶ or $[\text{Mn}(\text{salen})\text{Cl}]$ ^{147,148} are also exchangeable. Titanium is incorporated by either grafting¹⁴⁹⁻¹⁵⁴ or direct assembly.^{155,156}

Figure 1.1 Functionalization techniques of mesoporous silica for catalytic applications



Incorporation of Metal, Metal Oxide and Metal Sulfide Nanoparticles

The deposition of catalytically active nanoparticles on support materials with high dispersion is an important and effective strategy for the design of mesoporous silica catalysts with very high surface areas. Mesoporous silicas have the advantage of confining nanoparticles and preventing their growth to a size larger than the framework pore size. Metal nanoparticles have been used in catalysis for many decades. These materials have great potential as catalyst

because of the large surface area and high fraction of atoms present at the surface.¹⁵⁷

Nanoparticles can be incorporated into mesoporous silica by different methods such as direct inclusion of metal particles during the mesoporous assembly process and the impregnation and immobilization of polynuclear molecular transition metal complexes. The direct inclusion approach has been reported for the Pt and Rh.^{158,159} Conventional methods such as the impregnation technique yield supported nanoparticles of various sizes in the mesopore and on the external surface of the support material. Immobilization of polynuclear molecular transition metal complexes is another promising method for the preparation of supported metal catalyst. Typically, metal carbonyl complexes are used to react with the surface silanol groups at elevated temperature. This approach has been used for immobilization of platinum and ruthenium nanoparticles.¹⁶⁰⁻¹⁶²

Anchoring of Molecular Catalyst to the Surface

The immobilization of homogeneous catalysts on solid supports is of high commercial interest since the heterogenized catalyst becomes easier to handle, retrieve and recycle. However, the immobilized catalyst often suffers from reduced activity upon immobilization. But occasionally, the catalytic performance can be improved as compared to the homogeneous counterpart.¹⁶³⁻¹⁶⁴ Immobilization of $\text{Mn}(\text{bipy})_2^{2+}$, for example exhibits a higher catalytic activity in terms of peroxide oxidation and selectivity for styrene oxidation than the

corresponding homogeneous catalyst.¹⁴⁵ This is explained by the fact the $\text{Mn}(\text{bipy})_2^{2+}$ easily forms a dimer and in this state preferentially decomposes peroxide rather than oxidize any substrate. The isolation of the catalytic metal centers prevents this dimerization.

1.2.3.2 Applications of Mesoporous Silica Catalyst

Among the most common uses for mesoporous silica catalysts are hydrocarbon cracking and other petrochemical conversions, acid/base catalyst for reactions in fine chemical synthesis and redox catalysis.

The patent literature contains many examples of the use of mesoporous silica catalyst for cracking and petrochemical conversions.¹⁶⁵ The low acid strength and low hydrothermal stability is an unfortunate disadvantage for MCM-41 but this is countered by the advantage of having a material with accessible pores even for larger molecules. Nevertheless, MCM-41 catalyst show substantial cracking activity for bulky substances such as palm oil and asphaltene.¹⁶⁶⁻¹⁶⁷ For small molecules, such as 1-butene, n-hexane, n-heptane or small cyclic hydrocarbons such as tetralin and decalin, the cracking activity of MCM-41 is much lower than that of USY or Beta Zeolites, and similar to that amorphous silica-alumina.¹⁶⁸⁻¹⁷²

Although the inherent weakness of the acid sites in mesoporous silica limits its applicability in many petrochemical reactions, it still can be used in reactions requiring weaker acidity such as reactions for synthesizing fine chemicals. Table 1.3 summarizes some of the reactions catalyzed by mesoporous catalyst.

Table 1.3 Examples of fine chemical reactions catalyzed over mesoporous catalysts

Reaction	Mesoporous catalysts	Substrates	Ref
Friedel–Crafts alkylation	Al(OPri) ₃ grafted	Phenol + methanol	220
	Ga-substituted / impregnated	Benzene + benzyl chloride	221
	Al-substituted	2,4-Di-tert-butylphenol + cinnamyl alcohol	209
	Fe-impregnated	Benzene + benzyl chloride	210
Acetalization	Siliceous/Al-substituted	Heptanal, 2-phenylpropanal, diphenylacetaldehyde + trimethyl orthoformate	211
	Al-substituted	Heptanal + methanol	212
	siliceous	Cyclohexanone + methanol	213
Diels–Alder	Al(OPri) ₃ grafted	Cyclopentadiene + crotonaldehyde	214
	Zn ²⁺ -ion exchanged	Cyclopentadiene + methylacrylate	141
Beckmann rearrangement	Al-substituted	Cyclohexanone oxime	215
Aldol condensation	Al- substituted	Heptanal + benzaldehyde (!jasminaldehyde)	212
Prins condensation	Sn-substituted	β-Pinene + paraformaldehyde	216
MPV-reduction	Zr(OPr), Al(OPri) ₃ -grafted	4-tert-butylcyclohexanone + 2-propanol	219
Metathesis	Siliceous	Propene	217
(Esterification)	Cs ⁺ -ion exchanged	Triolein + glycerol	218
(Etherification)	Cs-impregnated	Glycerol	222

Redox reactions also can be catalyzed using of mesoporous metal oxide. Titanium containing mesoporous materials as well as those modified with early transition metals, such as Zr, V, Cr, Mn, or Fe, are promising oxidation catalysts. Titanium modified MCM-41 allows relatively bulky peroxides to be used as oxidants for sterically demanding substrates. It also widens the range of catalysts

available for selective oxidation reactions with hydrogen peroxide or organic peroxides as oxidants.¹⁷³

1.2.4 Mesoporous Silica As Adsorbents

The high surface area and large pore of mesoporous silica makes them very suitable for adsorbing or trapping metal ions, acidic gases and organics. Heavy metals, particularly lead and mercury are important environmental pollutants, threatening the health of human populations and natural ecosystems. There are several methods for metal ion removal which include precipitation, coagulation/flocculation, ion exchange, reverse osmosis, complexation /sequestration, electrochemical operation and biological treatment. Some limitations of these are high operating and energy cost and relatively low and variable loading capacities.^{174,175} Functionalization of the framework walls with thiol groups tunes the mesoporous silica for mercury trapping while the introduction of amino group makes it suitable for Pb and As trapping. The functionalization of with thiol groups can be achieved either by post synthesis grafting or by direct assembly. Various mesostructures with thiol groups have been synthesized through direct assembly including MCM-41,¹⁷⁶⁻¹⁷⁸ MCM-48,¹⁷⁸ SBA-15,¹⁷⁹⁻¹⁸¹ SBA-16, and KIT-6,¹⁸²⁻¹⁸³ HMS,¹⁸³ MSU,¹⁸⁴⁻¹⁸⁵ SBA-1186-187. The aminopropyl functionalization has been used on trapping metal ions such as Ni,¹⁸⁸ Cr,¹⁸⁸ Mn¹⁸⁸ , Fe¹⁸⁸, As¹⁸⁹, Cu,¹⁹⁰ Co,¹⁹⁰ and Zn¹⁹⁰. Amine modified mesoporous silica has also been used to trap acidic gases such as CO₂ and H₂S. The chemistry of amine and CO₂ has been employed for

selectively removing CO₂ from gas streams. The idea of combining amines with solid supports to adsorb CO₂ has been examined by several groups.¹⁹¹⁻¹⁹⁸ The most common problems encountered when developing amine loaded solids supports are low capacity for CO₂ due to the limited quantity of amine retained on the support, operation in a narrow temperature range and poor thermal stability. Yang and co-workers¹⁹⁹ investigated the selective adsorption of CO₂ and H₂S from natural gases using silica xerogel and MCM-48. The trapping of organic molecules on mesoporous silica has also been studied. It has been reported that calcined and phenyl modified MCM-41 show great affinity for benzene²⁰⁰ and cyclohexane in the gas phase.²⁰¹ Both calcined pure silica and aluminosilicate MCM-41 have a high sorption capacity for cyclohexane (>0.4 g /g dry solid).²⁰¹ Vance and co-workers²⁰² reported the use of as-made MCM-41 for the removal of trichloroethylene and tetrachloroethylene in waste water.

1.2.5 Polymer Reinforcement

Inorganic particles with domain size less than 100 nm in at least one dimension can enhance the tensile properties of the polymer through beneficial interaction at the polymer-particle interface.²⁰² Layered silicate clays in exfoliated form has been widely investigated as reinforcing agents as well as barrier and flame retardation agents for a variety of organic polymer systems.²⁰³ Mesostructure silica and other metal oxides were also considered for polymer composite formation. MCM-41 has been used to direct polymerization of conjugated polymers such as polydiacetylene,²⁰⁴ polyvinylene,^{205,206} and

polythiophene.²⁰⁷ The alignment of the polymers within the pores resulted in unusual chromatic changes, polarized luminescence and stability. Pinnavaia and co-workers²⁰³ have improved the tensile modulus, strength, and toughness of mesocomposites formed from as-made and calcined MSU-J silica in comparison to pure rubbery epoxy polymer. These reinforcement benefits were achieved without the need for organic modification of the silica surface. Mark et al.²⁰⁸ reported the preparation of poly(ethylene oxide)/MCM-41 mesoporous silica composites and they found that after pressing the physical blend at 100 °C the polymer melting transition vanished. That effect was more clearly seen for polymers with low molecular weight.

1.3 Objectives

This thesis research effort has two general objectives. The main objective of the first half of the study was to synthesize mesoporous silica from biologically derived oleyl amine surfactants. All of the applications described in the foregoing introduction involve the use of mesophases for which the structure-directing porogens has been removed by ion exchange, solvent extraction or calcinations. There are no examples of the use of as-made surfactant-intercalated mesophases for a materials application. This is understandable because the organic surfactant occupies the pores of the inorganic framework. Nevertheless, the intercalated surfactant bears organic functionality that could be useful for the adsorption of organic and inorganic species from aqueous solution. The

limitation, however, is the leaching of the surfactant phase to solution and the eventual loss of the functionality provided by the surfactant.

Being renewable plant derived molecules, oleyl amines are attractive templating agents in their own right for the synthesis of "green" mesophases. Oleyl surfactants have not yet been reported as structure-directing agents for silica mesophases. Additionally, owing to the presence of the polar amine head group and the olefinic bond in the hydrophobic segment, these surfactants offer unique opportunities for the design of functional as-made mesophases adsorbents. For instance, the amine group may serve as a complexing agent for removing metal ions from aqueous solution. This approach may make it possible to circumvent the need for cost-intensive use of organosilanes as grafting agents for the introduction of ligand functionality in the framework walls. Also, the presence of the *cis* double at the 9-position of the hydrophobic group offers the possibility of cross linking of the surfactant, thus avoiding, or at least, minimizing surfactant leaching. The plausibility of these concepts is demonstrated through synthesis and oleyl amine surfactant/silica mesostructures and their ability to adsorb Pb(II) from aqueous solution.

The second general objective concerns the development of thin-film forms of mesoporous alumina, titania, and zirconia for the enrichment of phosphorylated protein fragments from protein digests. These oxides are recognized as selective media for the phosphoproteins enrichment by a chemisorption mechanisms. But the use of the oxides in packed column form requires the use undesirably large quantities of protein digest and cumbersome

procedures for the release of the enriched protein for identification by mass spectroscopy. Thin film forms of the mesophases represent a promising approach to circumventing these unattractive aspects of this chemistry. More specifically, we show that by supporting the oxide films on metal grids normally used to host specimens for transmission electron microscopy it is possible to reduce the amount of digest for the enrichment and MALDI mass spectroscopic analysis for two model phosphoproteins (namely, β -casein and ovalbumin) to 50 femtomoles or less. Moreover, the processing of the specimens can be achieved using 10-microliter volumes of reagents and this greatly facilitates through put of samples for analysis.

1.4 References

1. Sing, K.S.W., Everett, D.H. Haul, R.A.W. Moscou, L. Pierotti, R.A. Rouquerol, J. Siemieniewska, T. *Pure Appl. Chem.* **1985**, 57, 603.
2. Schuth, F., Sing, K., Weitkamp, J. *Handbook of Porous Solids*, vol. I–V, Wiley-VCH, Weinheim, **2002**.
3. Davis, M.E. Saldarriaga, C., Montes, J. Garces, C. Crowder, *Nature*, **1988** 331, 698.
4. Schoeman, B.J., Sterte, J., Otterstedt, J.E., *J. Chem. Soc. Chem. Commun.* **1993** 994.
5. Janssen, A.H., Koster, A.J., de Jong, K.P., *Angew. Chem. Int. Ed.* **2001** 40 1102.
6. Schmidt, I., Boisen, A., Gustavsson, E., Stahl, K., Pehrson, S., Dahl, S., Carlsson, A., Jacobsen, C.J.H., *Chem. Mater.* **2001**, 13, 4416.
7. Chiola, V., Ritsko, J.E., Vanderpool, C.D., *US Patent No.* 3 556725, **1971**.
8. Di Renzo, F., Cambon, H., Dutartre, R., *Micropor. Mater.* **1997** 10, 283.
9. Beck, J.S., Chu, C.T.-W., Johnson, I.D., Kresge, C.T., Leonowicz, M.E., Roth, W.J., Vartuli, J.W. WO Patent 91/11390, **1991**.
10. Kresge, C.T., Leonowicz, M.E., Roth, W.J., Vartuli, J.C., Beck, J.S., *Nature*, **1992**, 359, 710.
11. Beck, J.S.; Vartuli, J.C.; Roth, W.J.; Leonowicz, M.E.; Kresge, C.T., Schmitt, K.D.; Chu, C.T.W.; Olson, D.H.; Sheppard, E.W.; McCullen, S.B.; Higgins, J.B.; Schlenker, J.L.; *J. Am. Chem. Soc.* **1992**, 114, 10834.
12. Monnier, A.; Schuth, F.; Huo, Q.; Kumar, D.; Margolese, D.; Maxwell, R.S.; Stucky, G.; Krishnamurty, M.; Petroff, P.; Firouzi, A.; Janicke, M.; Chmelka, B.; *Science* **1993**, 261, 1299.
13. Huo, Q.; Margolese, D.; Ciesla, U.; Feng, P.; Gier, T.; Sieger, P.; Leon, R.; Petroff, P.M.; Ciesla, U.; Schuth, F.; Stucky, G., *Nature*. **1994**, 368, 317.
14. Huo, Q.; Margolese, D.; Ciesla, U.; Demuth, D.; Feng, P.; Gier, T.; Sieger, P.; Firouzi, A.; Chmelka, B.; Schuth, F.; Stucky, G.D., *Chem. Mater.* **1994**, 6, 1176.
15. Attard, G.S.; Glyde, J.C.; Goltner, C.G., *Nature*, **1995**, 378, 366.
16. Ryoo, R.; Joo, S.H.; Jun, S.; *J. Phys. Chem. B* **1999**, 103, 7743.
17. Lu, A.H.; Schmidt, W.; Taguchi, A.; Spliethoff, B.; Tesche, B.; Schuth, F.; *Angew. Chem. Int. Ed.* **2002**, 41, 3489.

18. Inagaki, S.; Fukushima, Y.; Kuroda, K.; *J. Chem. Soc. Chem. Commun.* **1993**, 680.
19. Inagaki, S.; Koiwai, A.; Suzuki, N.; Fukushima, Y.; Kuroda, K.; *Bull. Chem. Soc. Jpn.* **1996**, 69, 1449.
20. Che, S.; Garcia-Bennett, A.E.; Yokoi, T.; Sakamoto, K.; Kunieda, H.; Terasaki, O.; Tatsumi, T. *Nature Mater.* **2003**, 2, 801.
21. Garcia-Bennett, A.E.; Terasaki, O.; Che, S.; Tatsumi, T.; *Chem. Mater.* **2004** 16813.
22. Huo, Q.; Leon, R.; Petroff, P.M; Stucky, G.D.; *Science*, **1995**, 268, 1324.
23. Tanev, P.T.; Pinnavaia, T.J., *Science*, **1995**, 267, 865.
24. Tanev, P.T.; Chibwe, M.; Pinnavaia, T.J., *Nature*, **1994**, 368, 321.
25. Bagshaw, S.A.; Prouzet, E.; Pinnavaia, T.J. *Science*, **1995** 269, 1242.
26. Prouzet, E.; Pinnavaia, T.J. *Angew. Chem. Int. Ed.* **1997**, 36, 516.
27. Zhao, D.; Huo, Q.; Feng, J.; Chmelka, B.F.; Stucky, G.D.; *J. Am. Chem. Soc.* **1998**, 120, 6024.
28. Zhao, D.; Feng, J.; Huo, Q.; Melosh, N.; Fredrickson, G.H.; Chmelka, B.F.; Stucky, G.D. *Science*, **1998** 279, 548.
29. Antonelli, D.M.; Ying, J.Y., *Angew. Chem. Int. Ed.* **1996**, 35, 426.
30. Antonelli, D.M. Nakahira, A. Ying, J.Y. *Inorg. Chem.* **1996**, 35, 3126.
31. Antonelli, D.M. Ying, J.Y. *Chem. Mater.* **1996**, 8, 874.
32. Joo, S.H. Choi, S.J. Oh, I. Kwak, J. Liu, Z. Terasaki, O. Ryoo, R. *Nature* **2001**, 412, 169.
33. Israelachvili, J.N. Mitchell, D.J. Ninham, B.W. *J. Chem. Soc. Faraday Trans.* **1976**, 72, 2, 1525.
34. Israelachvili, J.N. *Intermolecular and Surface Forces*, Academic Press, London, **1991**.
35. Stucky, G.D. Monnier, A. Schuth, F. Huo, Q. Margolese, D. Kumar, D. Krishnamurty, M. Petroff, P. Firouzi, A. Janicke, M. Chmelka, B.F. *Mol. Cryst. Liq. Cryst.* **1994** 240, 187.
36. Firouzi, A. Kumar, D. Bull, L.M. Besier, T. Sieger, P. Huo, Q. Walker, S.A. Zasadzinski, J.A. Glinka, C. Nicol, J. Margolese, D.I. Stucky, G.D. Chmelka, B.F. *Science*, **1995**, 267, 1138.

37. Vartuli, J.C. Schmitt, K.D. Kresge, C.T. Roth, W.J. Leonowicz, M.E. McCullen, S.B. Hellring, S.D. Beck, J.S. Schlenker, J.L. Olson, D.H. Sheppard, E.W. *Chem. Mater.* **1994**, 6, 2317.
38. Linden, M. Agren, P. Karlsson, S. Bussian, P. Amenitsch, H. *Langmuir* **2000**, 16, 5831.
39. Ulagappan, N. Rao, C.N.R. *Chem. Commun.* **1996**, 2759.
40. Lind, A. Andersson, J. Karlsson, S. Agren, P. Bussian, P. Amenitsch, H. Linden, M. *Langmuir* **2002**, 18, 1380.
41. Cassiers, K. Van Der Voort, P. Vansant, E.F. *Chem. Commun.* **2000** 2489.
42. Tanev, P.T. Pinnavaia, T.J. *Chem. Mater.* **1996**, 8, 2068.
43. Zhang, W. Pauly, T.R. Pinnavaia, T.J. *Chem. Mater.* **1997**, 9, 2491.
44. Attard, G.S. Goltner, C.G. Corker, J.M. Henke, S. Templer, R.H. *Angew. Chem. Int. Ed.* **1997**, 36, 1315.
45. Goltner, C.G. Antonietti, M. *Adv. Mater.* **1997**, 9, 431.
46. Attard, G.S. Bartlett, P.N. Coleman, N.R.B. Elliott, J.M. Owen, J.R. Wang, J.H. *Science*, **1997**, 278, 838.
47. Whitehead, A.H. Elliott, J.M. Owen, J.R. Attard, G.S. *Chem. Commun.* **1999** 331.
48. Braun, P.V. Osenar, P. Stupp, S.I. *Nature* **1996**, 380, 325.
49. Johnson, S.A. Khushalani, D. Coombs, N. Mallouk, T.E. Ozin, G.A. *J. Mater. Chem.* **1998** 8, 13.
50. Kim, J.Y. Yoon, S.B. Kooli, F. Yu, J.-S. *J. Mater. Chem.* **2001**, 11, 2912.
51. Laha, S.C. Ryoo, R. *Chem. Commun.* **2003** 2138.
52. Zhu, K. Yue, B. Zhou, W. He, H. *Chem. Commun.* **2003** 98.
53. Tian, B. Liu, X. Yang, H. Xie, S. Yu, C. Tu, B. Zhao, D. *Adv. Mater.* **2003**, 15, 1370.
54. Lee, K. Kim, Y.-H. Han, S.B. Kang, H. Park, S. Seo, W.S. Park, J.T. Kim, B. Chang, S. *J. Am. Chem. Soc.* **2003** 125, 6844.
55. Yang, H. Shi, Q. Tian, B. Lu, Q. Gao, F. Xie, S. Fan, J. Yu, C. Tu, B. Zhao, D. *J. Am. Chem. Soc.* 125 **2003**, 4724.
56. Tian, B. Liu, X. Solovyov, L.A. Liu, Z. Yang, H. Zhang, Z. Xie, S. Zhang, F. Tu, B. Yu, C. Terasaki, O. Zhao, D. *J. Am. Chem. Soc.* **2004**, 126, 865.

57. Ying, J. Y. Mehnert, C. P. Wong, M. S. *Angew. Chem. Int. Ed.* **1999**, 38, 57.
58. David M Ford, D. F. S. *Nanotechnol.* **2005**, 16, S458.
59. Goltner-Spickermann, C. *Curr. Opin. Colloid Interface Sci.* **2002**, 7, 173.
60. Sayari, A. Hamoudi, S. *Chem. Mater.* **2001**, 13, 3151.
61. Soler-Illia, G. J. d. A. A. Crepaldi, E. L. Grosso, D. Sanchez, C. *Curr. Opin. Colloid Interface Sci.* **2003**, 8, 109.
62. Soler-Illia, G. J. D. A. A. Sanchez, C. Lebeau, B. Patarin, J. *Chem. Rev.* **2002**, 102, 4093.
63. Zhao, X. S. Lu, G. Q. Millar, G. J. *Ind. Eng. Chem. Res.* **1996**, 35, 2075.
64. Grun, M. Kurganov, A. A. Schacht, S. Schuth, F. Unger, K. K. *J. Chromatogr. A* **1996**, 740, 1.
65. Inagaki, S. O. Goto, S. Fukushima, Y. *Stud. Surf. Sci. Catal. Y.* **1998**, 65.
66. Gallis, K. W. Eklund, A. G. Jull, S. T. Araujo, J. T. Moore, J. G. Landry, C. C. *Stud. Surf. Sci. Catal.* **2000**, 129, 747.
67. C. Boissiere, A. Larbot, E. Prouzet, **2001**, 135, CD 08-O-01.
68. Sierra, L. Lopez, B. Ramirez, A. *Stud. Surf. Sci. Catal.* **2001**, 135, CD: A18PO6.
69. Mesa, M. Sierra, L. Lopez, B. Ramirez, A. Guth, J.-L. *Solid State Sci.* **2003**, 5, 1303.
70. Sierra, L. Mesa, M. Ramirez, A. Lopez, B. Guth, J.-L. *Stud. Surf. Sci. Catal.* **2004**, 154, 573.
71. Martines, M. U. Yeong, E. Persin, M. Larbot, A. Voorhout, W. F. Kubel, C. K. U. Kooyman, P. Prouzet, E. *Chimie* **2005**, 8, 627.
72. Martin, T. Galarneau, A. DiRenzo, F. Brunel, D. Fajula, F. Heinisch, S. Cretier, G. Rocca, J. L. *Chem. Mater.* **2004**, 16, 1725.
73. Zhao, J. Gao, F. Fu, Y. Jin, W. Yang, P. Zhao, D. *Chem. Commun.* **2002**, 752.
74. Nassivera, T. Eklund, A. G. Landry, C. C. *J. Chromatogr. A* **2002**, 973, 97.
75. Shindo, T. Kudo, H. Kitabayashi, S. Ozawa, S. *Micropor. Mesopor. Mater.* **2003**, 63, 97.
76. Zhu, G. Jiang, D. Yang, Q. Yang, J. Li, C. *J. Chromatogr. A* **2007**, 1149, 219.

77. Bristow, P. A.; Knox, J. H. *Chromatographia* **1977**, *10*, 279–289.
78. Gilar, M.; Daly, A. E.; Kele, M.; Neue, U. D.; Gebler, J. C. *J. Chromatogr., A* **2004**, *1061*, 183–192.
79. Mellors, J. S.; Jorgenson, J. W.; *Anal. Chem.* **2004**, *76*, 5441–5450.
80. Tanaka, N.; Kobayashi, H.; Nakanishi, K.; Minakuchi, H.; Ishizuka, N. Monolithic LC Columns. *Anal. Chem.* **2001**, *73*, 420A–429A.
81. Cabrera, K. Applications of silica-based monolithic HPLC columns. *J. Sep. Sci.* **2004**, *27*, 843–852.
82. Kobayashi, H.; Ikegami, T.; Kimura, H.; Hara, T.; Tokuda, D.; Tanaka, N. *Anal. Sci.* **2006**, *22*, 491–501.
83. Prouzet, E. Boissiere, C. *Chimie* **2005**, *8*, 579.
84. Crowson, A. (ed) *Smart Structures and Materials 1996: Smart Materials Technologies and Biomimetics*, Proceedings of SPIE, Vol.2716
85. Liming, D. *Intelligent Macromolecules for Smart Devices: From Material Synthesis to Device Applications 2004* Springer-Verlag, Berlin pp 496
86. Buchholz, K., Kasche, V. Bornscheuer, U.T. (eds) *Biocatalyst and Enzyme Technology*, **2005** Wiley-VCH, Weinheim
87. Diaz, J.F., Balkus, J.K. Jr. *J. Molec. Catal. B. Enzymatic* **1996**, *2*, 115
88. Washmon-Kriel, L. Jimenez, V.L. and Balkus, K.J. Jr. *J. Molec. Catal. B. Enzymatic* **2000**, *10*, 453
89. Takahashi, H., Li, B., Sasaki, T., Miyazaki, C., Kajino, T. and Inagaki, S. *Chem. Mat.* **2000** *12*, 3301
90. Wei, Y., Xu, J., Feng, Q., Lin, M., Dong, H., Zhang, W.J., Wang, C. J. *NanoSci Nanotech*, **2001** *1*, 83
91. Yiu, H.H.P., Botting, C.H., Botting, N.P. and Wright, P.A. *Physical Chemistry Chemical Physics* **2001** *3*, 2983
92. Yiu, H.H.P., Wright, P.A., Botting, N.P. *Microporous and Mesoporous Materials*, **2001**, 44–45, 763
93. Takahashi, H. Li, B., Sasaki, T., Miyazaki, C., Kajino, T. Inagaki, S. *Microporous and Mesoporous Materials* **2001**, 44–45, 755
94. Sasaki, T. Kajino, T., Li, B., Sugiyama, H. and Takahashi, H. *2001 Appl. Environ. Microbio.* **2001** *67*, 2208

95. Deere, J., Magner, E., Wall, J.G. and Hodnett, B.K. *Chem Commun.* **2001** 465
96. Deere, J., Magner, E., Wall, J.G. and HOdnett, B.K. *J. Phy Chem B.* **2002** 106,7340
97. Han, Y.J. Watson, J.T., Stucky, G.D. and Buttler, A. *J. Molec. Catal. B Enzymatic* **2002**, 17, 1
98. Deere, J., Magner, E., Wall, J.G. and Hodnett, B.K. *Catal Lett* 85, 19
99. Chong, A.S.M., Zhao, X.S. *Appl. Surf. Sci.* **2004** 237, 398
100. Goradia, D., Cooney, J., Hodnett, B.K., Magner, E. *J. Molec. Catal. B. Enzymatics* **2005**, 32, 231
101. Hartmann, M. *Chem Mater* **2005**, 17, 4577
102. Moelans, D., Cool, P., Baeyens, J., Vansant, E.F., *Catal Commun* **2005**, 6, 307
103. Diaz,, J.F., Balkus, K.J. Jr. *J. Molec Catal B – Enzymatics*, **2006**, 2, 115
104. Han, Y., Lee, S.S., and Ying, J.Y. *Chem Mater* **2006**, 18, 46
105. Vinu, A, Murugesan, V. Hatmann, M. *J Phy Chem B*, **2004**, 108 7323
106. Blin, J.L., Gerardin, C., Carteret, C., Selve, R.C. and Stebe, M.J. *Chem Mater*, **2005**, 17, 1479
107. Mureseanu, M., Galarneau, A. Renard, G. and Fahula, F. *Langmuir* 2005, 21, 4648
108. Han, Y., Lee, S.S., Ying, J.Y. *Chem Mater*, **2006**, 18, 643
109. Lee, J., Kim, J., Jia, H., Kim, M.I, Kwak, J.H., Jin, S. Dohnalkova, A., Park, H.G., Chang, H.N., Wang, P., Grate, J.W., Hyeon, T., *Small*, **2005**, 1, 744
110. He, J., Song, Z., Ma, H., Yang, L., Guo, C. *J. Mater Chem* **2006**, 16, 4307
111. Wang, Y., Caruso, F. *Adv Mater.* **2006**, 18, 795
112. Hudson, S. Magner, E., Cooney, J., Hodnett, B.K. *J. Phy Chem B.* **2005**, 109, 19496
113. Zakian, V.A., *Science*, **1995**, 270, 1601
114. Gurunathan, S., Klinman, D.M., Seder, R.A. *Annual Review of Immunology*, **2000**, 18, 927
115. Winfree, E., Liu, F.R., Wenzler, L.A. , Seeman, N.C. *Nature*, **2003**, 394, 539

116. Seeman, N.C., *Nature*, **2003**, 421, 427
117. Adleman, L.M. *Science*, **1994**, 266, 1021
118. Sakamoto, K., Gousu, H., Komiya, K., Kiga, D., Yokoyama, S., Yokomori, T., Hagiya, M. *Science*, **2000**, 288, 1223
119. Fink, H.W., Schonberger, C. *Nature*, **1999**, 398, 407
120. Kasumov, A.Y. Kociak, M., Gueron, S., Reulet, B., Volkov, V.T., Klinov, D.V., Bouchiat, H. *Science*, **2001**, 191, 280
121. Fujiwara, M., Yamamoto, F., Okamoto, K., Shiokawa, K. and Nomura, R. *Analytical Chemistry*, **2005**, 77, 8138
122. Solberg, S.M., Landry, C.C. *J. Phy. Chem B*. **2006**, 110, 15261
123. Zhang, X., Guan, R.F., Zhang, F., Chan, K.Y. *Scripta Materialia*, **2006**, 54, 1651
124. Galarnau, A., Muresanu, M., Atger, S. Renard, G., Fajula, F. *New Journal of Chemistry*, **2006**, 30, 562
125. Seelan, S., Sinha, A.K., Kato, K., Yokogawa, Y., *Adv. Mater.*, **2006**, 18, 3001
126. Besanger, T.R. Hodgson, R.J., Green, J.R.A., Brennan, J.D. *Analytica Chimica Acta* **2006**, 564, 106
127. Mal, N.K., Fujiwara, M., Tanaka, Y., *Nature*, **2003**, 421, 350
128. Mal, N.K., Fujiwara, M., Tanaka, Y., Taguchi, T., Matsukata, M. *Chem Mater*, **2003**, 15, 3385
129. Mokaya, R. *Angew. Chem. Int. Ed.* **1999**, 38, 2930.
130. Chen, C.Y. Li, H.X. Davis, M.E. *Micropor. Mater.* **1993**, 2, 17.
131. Chakraborty, B. Viswanathan, B. *Catal. Today* **1999**, 49, 253.
132. Schmidt, R. Akporiaye, D. Stocker, M. Ellestad, O.H. *Chem. Commun.* **1994** 1493.
133. Luan, Z. Cheng, C.-F. He, H. Klinowski, J. *J. Phys. Chem.* **1995**, 99, 10590.
134. Borade, R.B. Clearfield, A. *Catal. Lett.* **1995**, 31, 267.
135. Occelli, M.L. Biz, S. Auroux, A. Ray, G.J. *Micropor. Mesopor. Mater.* **1998**, 26, 193.
136. Meng, X. Li, D. Yang, X. Yu, Y. Wu, S. Han, Y. Yang, Q. Jiang, D. Xiao, F.-S. *J. Phys. Chem. B* **2003**, 107, 8972.

137. Kremer, S.P.B. Kirschhock, C.E.A. Aerts, A. Villani, K. Martens, J.A. Lebedev, O.I. Van Tendeloo, G. *Adv. Mater.* **2003**, 15, 1705.
138. Zhang, Z. Han, Y. Zhu, L. Wang, R. Yu, Y. Qiu, S. Zhao, D. Xiao, F.-S. *Angew. Chem. Int. Ed.* **2001**, 40, 1258.
139. Liu, Y. Zhang, W. Pinnavaia, T.J. *Angew. Chem. Int. Ed.* **2001**, 40, 1255.
140. Guo, W. Huang, L. Deng, P. Xue, Z. Li, Q. *Micropor. Mesopor.Mater.* **2001** 44–45, 427.
141. Onaka, M. Yamazaki, R. *Chem. Lett.* **1998** 259.
142. Yang, R.T. Pinnavaia, T.J. Li, W. Zhang, W. *J. Catal.* **1997**, 172, 488.
143. Liu, C. Ye, X. Wu, Y. *Catal. Lett.* **1996**, 36, 263.
144. Liu, C. Shan, Y. Yang, X. Ye, X. Wu, Y. *J. Catal.* **1997** 168, 35.
145. Kim, S.S. Zhang, W.Z. Pinnavaia, T.J. *Catal. Lett.* **1997** 43, 149.
146. Połtowicz, J. Serwicka, E.M. Bastardo-Gonzalez, E. Jones, W. Mokaya, R. *Appl. Catal. A: Gen.* **2001**, 218, 211.
147. Frunza, L. Kosslick, H. Landmesser, H. Hoft, E. Fricke, R. *J.Mol. Catal. A: Chem.* **1997**, 123, 179.
148. Kim, G.J. Kim, S.H. *Catal. Lett.* **1999**, 57, 139.
149. Maschmeyer, T. Rey, F. Sankar, G. Thomas, J.M. *Nature* **1995**, 378, 159.
150. Aronson, B.J. Blanford, C.F. Stein, A. *Chem. Mater.* **1997**, 9, 2842.
151. Wu, P. Iwamoto, M. *J. Chem. Soc. Faraday Trans.* **1998**, 94, 2871.
152. Hagen, A. Wei, D. Haller, G.L. in: Bonneviot, L. Beland, F. Danuhma, C. Giasson, S. Kaliaguine S. (Eds.), *Mesoporous Molecular Sieves 1998*, Studies in Surface Science Catalysis, vol. 117, Elsevier, Amsterdam, p. 191.
153. Widenmeyer, M. Grasser, S. Kohler, K. Anwander, R. *Micropor.Mesopor. Mater.* **2001** 44–45, 327.
154. Luan, Z. Maes, E.M. van der Heide, P.A.W. Zhao, D. Czernuszewicz, R.S. Kevan, L. *Chem. Mater.* **1999**, 11, 3680.
155. Alba, M.D. Luan, Z. Klinowski, J. *J. Phys. Chem.* **1996**, 100, 2178.
156. Corma, A. Navarro, M.T. Perez Pariente, J. *J. Chem. Soc.Chem. Commun.* **1994**, 147.
157. Roucoux, A. Schulz, J. Patin, H. *Chem. Rev.* **2002**, 102, 3757.

158. Junges, U. Jacobs, W. Voigt-Martin, I. Krutzsch, B. Schuth, F. *J. Chem. Soc. Chem. Commun.* **1995**, 2283.
159. Aramendia, M.A. Borau, V. Jimenez, C. Marinas, J.M. Romero, F.J. *Chem. Commun.* **1999**, 873.
160. Yamamoto, T. Shido, T. Inagaki, S. Fukushima, Y. Ichikawa, M. *J. Am. Chem. Soc.* **1996**, 118, 5810.
161. Yamamoto, T. Shido, T. Inagaki, S. Fukushima, Y. Ichikawa, M. *J. Phys. Chem. B* **1998**, 102, 3866.
162. Zhou, W. Thomas, J.M. Shephard, D.S. Johnson, B.F.G. Ozkaya, D. Maschmeyer, T. Bell, R.G. Ge, Q. *Science*, **1998**, 280 705.
163. Knops-Gerrits, P.P. De Vos, D. Thibault-Starzyk, F. Jacobs, P.A. *Nature* **1994**, 369, 543.
164. Pugin, B. *J. Mol. Catal. A: Chem.* **1996**, 107, 273.
165. Corma, A. *Chem. Rev.* **1997**, 97, 2373.
166. Twaiq, F.A. Mohamed, A.R. Bhatia, S. *Micropor. Mesopor. Mater.* **2003**, 64 95.
167. Byambajav, E. Ohtuska, Y. *Fuel* **2003**, 82, 1571.
168. Corma, A. Grande, M.S. Gonzalez-Alfaro, V. Orchilles, A.V. *J. Catal.* **1996** 159, 375.
169. Pater, J.P.G. Jacobs, P.A. Martens, J.A. *J. Catal.* **1999**, 184, 262.
170. Seo, G. Kim, N.H. Lee, Y.H. Kim, J.H. *Catal. Lett.* **1999**, 57, 209.
171. Corma, A. Gonzalez-Alfaro, V. Orchilles, A.V. *J. Catal.* **2001**, 200, 34.
172. Eliche-Quesada, D. Merida-Robles, J. Maireles-Torres, P. Rodriguez-Castellon, E. Jimenez-Lopez, A. *Langmuir* **2003** 19, 4985.
173. Franke, O. Rathousky, J. Schulz-Ekloff, G. Starek, J. Zukal, A. in: Weitkamp, J. Karge, H.G. Pfeifer, H. Holderich, W. (Eds.), *Zeolites and Related Microporous Materials: State of the Art 1994*, Studies in Surface Science Catalysis, vol. 84, Elsevier, Amsterdam, **1994**, p. 77.
174. Namasivayam C., Ranganathan, K. *Environ. Technol.* **1995**, 16, 851–860.
175. Kiffs, R.J. Barnes, D. Forster, C.F. Hrudey, S.E. *Surveys in industrial wastewater treatment, Manufacturing and Chemical Industries*, **1987**, 3, 377–399.
176. Etienne, M. Lebeau B., Walcarius, A. *New J. Chem.* **2002**, 26, 384.

177. Walcarius, A., Delacote, C. *Chem. Mater.* **2003**, 15, 4181.
178. Gaslain, F. Delacote, C. Lebeau, B. and Walcarius, A. *J. Sol-Gel Sci. Technol.* **2009**, 49, 112.
179. Wei, Q.; Nie, Z.; Hao, Y.; Chen, Z.; Zou, J.; Wang, W. *Mater. Lett.* **2005**, 59, 3611.
180. Grudzien, R.M.; Pikus S.; Jaroniec, M., *J. Phys. Chem. C* **2009**, 113, 4875.
181. Aguado, J. Arsuaga J.M., Arencibia, A. *Microporous Mesoporous Mater.* 109 (**2008**), p. 513.
182. Nohair, B. MacQuarrie, S. Crudden, C.M., Kaliaguine, S. *J. Phys. Chem. C* **2008**, 112, 6065.
183. Mercier L., Pinnavaia, T.J. *Chem. Mater.* **2000**, 12, 188.
184. Brown, J.; Richer R., Mercier, L. *Microporous Mesoporous Mater.* **2000**, 37, 41.
185. Bibby A.; Mercier, L., *Chem. Mater.* **2002**, 14, 1591.
186. Kao, H.M. Lee L.P. Palani, A. *Anal. Chem.* **2008**, 80, 3016.
187. Walcarius A. Delacote, C. *Anal. Chim. Acta*, **2005**, 547, 3.
188. Aoife M., Burke, A.M., Hanrahan, J.P., Healy,D.A., Sodeau, J.R., Holmes,J.D. and Morris, M.A., *Journal of hazardous Materials* **2009** 164 229-234
189. McKimmy, E.J. *Supramolecular Assembly of Organofunctional Mesostructures: Synthesis, Characterization, and Applications in Environmental Remediation.* **2005**. A Dissertation. Department of Chemistry. Michigan State University.
190. Park, D.H., Park, S.S., Choe, S.J., *Bull. Korean Chem. Soc.* **1999**, 20 291
191. Satyapal, S.; Filburn, T.; Trela, J.; Strange, J. *Performance and Properties of a Solid Amine Sorbent for Carbon Dioxide Removal in Space Life Support Applications.* *Energy Fuels* **2001**,15, 250
192. Birbara, P. J.; Filburn, T. P.; Michels, H.; Nalette, T. A. *Sorbent System and Method for Absorbing Carbon Dioxide (CO₂) from the Atmosphere of a Closed Habitable Environment.* U.S.Patent **2002** 6, 364, 938.
193. Huang, H.; Yang, R.; Chinn, D.; Munson, C. L. Amine-Grafted MCM-48 and Silica Xerogel as Superior Sorbents for Acidic Gas Removal from Natural Gas. *Ind. Eng. Chem. Res.* **2003**, 42, 2427.

194. Chang, A. C. C.; Chuang, S. S. C.; Gray, M.; Soong, Y. In Situ Infrared Study of CO₂ Adsorption on SBA-15 Grafted with ζ -(Aminopropyl)triethoxysilane. *Energy Fuels* **2003**, 17, 468.
195. Leal, O.; Bolivar, C.; Ovalles, C.; Garcia, J. J.; Espidel, Y. Reversible Adsorption of Carbon Dioxide on Amine Surface-bonded Silica Gel. *Inorg. Chim. Acta* **1995**, 240, 183.
196. Nalette, T. A.; Papale, W.; Filburn, T. Carbon Dioxide Scrubber for Fuel and Gas Emissions. U.S. Patent 6,755,892, 2004.
197. Xu, X.; Song, C.; Andresen, J. M.; Miller, B. G.; Scaroni, A. W. Novel Polyethylenimine-Modified Mesoporous Molecular Sieve of MCM 41 Type as High-Capacity Adsorbent for CO₂ Capture. *Energy Fuels* **2002**, 16, 1463.
198. Contarini, S.; Barbini, M.; Del Piero, G.; Gambarotta, E.; Mazzamurro, G.; Riocci, M.; Zappelli, P. In *Greenhouse Gas Control Technologies-6th International Conference*; Gale, J., Kaya, Y., Eds.; Tribology Series Vol. 41; Elsevier: New York, **2003**; Vol. 1, pp 169-175.
199. Huang, H.Y., Chinn, D., Munson, C.L., Yang, R.T. *Ind. Eng. Chem. Res.* **2003**, 42, 2427-2433
200. Bambrough, C. M.; Slade, R. T. C.; Williams, R. T.; Burkett, S.L.; Sims, S. D.; Mann, S. *J. Colloid Interface Sci.* **1998**, 201, 220-222.
201. Chen, C.-Y.; Li, H.-X.; Davis, M. E. *Microporous Mater.* **1993**, 2, 17-26.
202. Novak, B. M. *Adv. Mater.* **1993**, 5, 422.
203. Park, I., Peng, H., Gidley, D.W., Xue, S., Pinnavaia, T.J. *Chem. Mater.* **2006**, 18, 650-656
204. Lu, Y. F.; Yang, Y.; Sellinger, A.; Lu, M. C.; Huang, J. M.; Fan, H. Y.; Haddad, R.; Lopez, G.; Burns, A. R.; Sasaki, D. Y.; Shelnutt, J.; Brinker, C. J. *Nature* **2001**, 411, 617.
205. Nguyen, T. Q.; Wu, J. J.; Doan, V.; Schwartz, B. J.; Tolbert, S. H. *Science* **2000**, 288, 652.
206. Molenkamp, W. C.; Watanabe, M.; Miyata, H.; Tolbert, S. H. *J. Am. Chem. Soc.* **2004**, 126, 4476.
207. Li, G. T.; Bhosale, S.; Wang, T. Y.; Zhang, Y.; Zhu, H. S.; Fuhrhop, K. H. *Angew. Chem., Int. Ed.* **2003**, 42, 3818.
208. Vantomme, A. Surahy, L. Su, B. L. *Colloids Surf., A: Physicochem. Eng. Asp.* **2007**, 300, 65.
209. Armengol, E. M.L. Cano, A. Corma, H. Garcia, M.T. Navarro, *J. Chem. Soc. Chem. Commun.* **1995** 519.

210. He, N. Bao, S. Xu, Q. *Appl. Catal. A: Gen.* **1998**, 169, 29.
211. Climent, M.J. Corma, A. Iborra, S. Navarro, M.C. Primo, J. *J. Catal.* **1996** 161, 783.
212. Climent, M.J. Corma, A. Guil-Lopez, R. Iborra, S. Primo, J. *J. Catal.* **1998** 175, 70.
213. Iwamoto, M. Tanaka, Y. Sawamura, N. Namba, S. *J. Am. Chem. Soc.* **2003**, 125, 13032.
214. Kugita, T. Jana, S.K. Owada, T. Hashimoto, N. Onaka, M. Namba, S. *Appl. Catal. A: Gen.* **2003** 245, 353.
215. Dai, L.X. Koyama, K. Tatsumi, T. *Catal. Lett.* **1998** 53, 211.
216. Villade, A.L. Alarcon, P.E. de Correa, C.M. *Chem. Commun.* **2002** 2654.
217. Yoshida, H.; Kimura, K.; Inaki, Y.; Hattori, T., *Chem. Commun.* **1997** 129.
218. Corma, A. Iborra, S. Miquel, S. Primo, J. *J. Catal.* **1998**, 173, 315.
219. Zhu, Y. Jaenicke, S. Chuah, G.K. *J. Catal.* **2003**, 218, 396.
220. Landau, M.V. Dafa, E. Kaliya, M.L. Sen, T. Herskowitz, M. *Micropor. Mesopor. Mater.* **2001** 49, 65.
221. Okumura, K. Nishigaki, K. Niwa, M. *Micropor. Mesopor. Mater.* **2001** 44–45, 509.
222. Clacens, J.-M. Pouilloux, Y. Barrault, J. *Appl. Catal. A: Gen.* **2002**, 227, 181.

Chapter 2. Supramolecular Assembly of Mesostructured Silica from Oleylamine Surfactants

2.1 Introduction

2.1.1 Background on Supramolecular Assembly

The supramolecular synthesis of mesoporous silica generally follows two pathways – the electrostatic assembly pathway and the electrically neutral pathway. The electrostatic S^+I^- pathway utilizes charge matching interactions between the cationic surfactant (S^+) and the anionic inorganic silica precursor (I^-). This type of interaction was used by Mobil Corporation researchers in the synthesis of MCM-41 (hexagonal), MCM-48 (cubic) and MCM-50 (lamellar)¹. Figure 2.1 shows the synthetic scheme proposed for the assembly of hexagonal MCM-41 silica in the presence of surfactant micelle formed from quaternary ammonium ion. For the synthesis of MCM-41, a surfactant with long hydrophobic alkyl chain and a hydrophilic group in the form of a quaternary ammonium ion was used. When dispersed in solution, these surfactant molecules associate themselves into micelles. These micelles then serve as templates from which the silica precursor can condense. One such phase consists of cylindrical rod-like surfactant micelles. The addition of basic silicate anions to the micelle dispersion, under suitable hydrothermal conditions results in the formation of a surfactant silica composite^{1,2}.

Moreover, surfactants can form different mesophases depending on certain factors such as concentration, temperature and packing parameter. Concentration is an important parameter because for mesophase tailoring, the surfactant concentration should be at the critical micelle concentration (CMC).

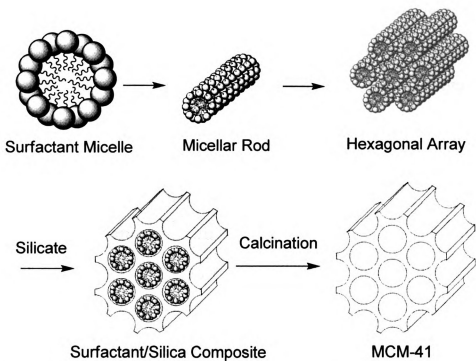


Figure 2.1 Schematic representation of MCM-41 synthesis

The CMC is the minimum concentration for surfactant molecules to aggregate to form micelles. This process happens to minimize energy and is entropy driven. It has also been noted that a surfactant with low CMC value is an important criterion toward increasing the regularity of a mesostructure³. Temperature is also an important factor as it affects the solubility of the surfactant in the reaction media thus affecting the CMC. The packing parameter (g) is also an important parameter in predicting and explaining the final mesostructure. The packing parameter, $g = V / (a_0 l)$ where V is the total volume of the surfactant hydrophobic chains plus any co-solvent between chains, a_0 is the effective hydrophilic head group area at the aqueous-micelle surface and l is the kinetic surfactant tail length. For a g value that is $<1/3$, the surfactant forms spherical micelles. For g

values of $1/3$ to $<1/2$ would give rise to cylindrical micelles, values $1/2$ to $< 2/3$ would give rise to 3D cylindrical micelles, a value of 1 would mean a lamellar structure and >1 would give rise to a reverse micelle. Table 2.1 provides the approximate ranges for the packing parameter and the type of micellar aggregates formed⁴.

MCM-41 and related silicas are characterized by long range ordered mesopores with uniform pore size distributions that can be tailored through variation in surfactant chain length, addition of auxiliary co-surfactant agents and by post-synthesis treatment. Powder x-ray diffraction of MCM-41 characteristically show 3 peaks that can be indexed to the hexagonal unit cell with the unit cell parameter $a_0 = 2d_{100} / \sqrt{3}$.¹ The nitrogen adsorption isotherm of MCM 41 is characterized by a sharp step that is due to capillary condensation. Capillary condensation is a phenomenon on porous materials when multilayer adsorption from the vapor phase proceeds to a point where the pores are filled with the condensed vapor. This usually occurs below the saturation pressure of the liquid phase. Brunauer-Emmett-Teller (BET) surface areas of MCM-41 materials are estimated to be $1000 \text{ m}^2/\text{g}$ for MCM-41 and pore sizes can be tuned to a range of 3.0 to $\sim 10\text{nm}$ by adding trimethyl benzene (TMB) as a co-surfactant or by varying the alkyl chain length of the surfactant.⁵

The electrostatic $\text{S}^+\text{X}^-\text{I}^+$ pathway on the other hand involves assembly using the interactions between a cationic surfactant (S^+) and a cationic silica precursor (I^+) as mediated by a counter ion (X^-). Stucky and co-workers produced SBA-15 through this pathway^{6,7}. By balancing the charge interactions

with charge matching interactions in aqueous synthesis enhances the long range periodic order of the mesoporous silica. The formation of the mesostructures occurs below the isoelectric point of silica (pH ~ 2). The solubilization of nonionic poly(alkylene oxide) surfactants and block copolymers in aqueous media is due to the association of water molecules with the alkylene oxide moieties through hydrogen bonding and is enhanced in strongly acidic media through association with hydronium ions instead of water molecules.⁸ SBA-15 also has hexagonal pores like MCM-41 but these mesopores are interconnected by micropores. SBA-15 has much thicker walls than MCM-41 giving it greater hydrothermal stability but as a result of the thicker walls, the surface area is decreased. A typical SBA-15 surface area is ~800 m²/g. Moreover, the pore diameter of SBA-15 can be tailored to range from 5-30 nm.⁶

The neutral assembly pathway, denoted S⁰|I⁰, utilizes hydrogen bonding interactions between a neutral surfactant (S⁰) and an uncharged silica precursor (I⁰). Tanev and Pinnavaia⁹ synthesized wormhole silica materials using this pathway. As opposed to MCM-41 and SBA-15 that utilize electrostatic interactions which results to long range order of hexagonal pores of MCM-41 and SBA-15, wormhole silica materials make use of hydrogen bonding interaction

Table 2.1 The different packing parameter range corresponding to different micellar aggregates

		$g = V/a_0d$				
		$< 1/3$	$1/3 < 1/2$	$1/2 < 2/3$	1	> 1
Micellar morphology	Surfactant description	Spherical micelles	Cylindrical micelles	3D cylindrical micelles	Lamellar micelles	Reversed micelles
		Single chain surfactant with large head groups e.g. $C_nH_{2n+1}N(C_2H_5)_3X$ (n = 12-18)	Single chain surfactant with small head groups e.g. $C_nH_{2n+1}N(CH_3)_3X$	Single chain surfactants with small head groups, e.g. CTAB, special surfactants with large hydrophobic polar head and double chain surfactants with large flexible chains	Double chain surfactants with small head groups or rigid, immobile chains e.g. $C_nH_{2n+1}N(CH_3)_3X$ (n=20,22), C16-2-16	Double chain surfactants with small groups
Mesoporous Silica		SBA-6, SBA-1, SBA-7, SBA-2	MCM-41, SBA-3	MCM-48	MCM-50, SBA-4	

that is relatively weaker thus resulting to short disordered channels. The pore motif of HMS materials has been termed “wormhole-like”. The surface area of a wormhole silica is typically $\sim 1000 \text{ m}^2/\text{g}$ and pore diameters range from 3-5nm.¹⁰ Moreover, the synthesis of wormhole silica materials afford milder conditions and does not require the addition of acids. The surfactant template is also easily recovered through solvent extraction and can be reused instead of the destructive calcination used to remove the quaternary ammonium template.

Another electrically neutral pathway is the N^0I^0 pathway. Like the S^0I^0 pathways used for synthesizing HMS wormhole type materials, N^0I^0 pathway utilizes amphiphilic PEO-based surfactants that have hydrophilic polyethylene oxide $(-\text{CH}_2\text{CH}_2\text{O})_n-$ segments connected to hydrophobic R groups of varying lengths and functionality. The R group can be an alkyl group as in the case of Brij and Tergitol surfactants an alkylated aromatic group as in the case of IGEPAL-RC and TRITON-X surfactants or a polypropylene oxide segment as in the Pluronic family of block co-polymer surfactants. The resulting materials have disordered pore wormhole structure with BET surface area of up to $1200 \text{ m}^2/\text{g}$ with framework pore diameters of up to 5.8 nm.^{11,12}

2.1.2 Pore Size and Morphological Control of Mesoporous Silica

The quest for mesoporous silica with larger pores has pushed researchers to develop methods of increasing the framework pore diameter. There are several known approaches on controlling the size of the framework pores, including the nature of the hydrophobic tail of the surfactant template¹, the

incorporation of an auxiliary organic solvent or swelling agent⁷, varying the assembly temperature¹³⁻¹⁸ and various post-synthesis treatment.³

Whether synthesized through the electrostatic pathway using quaternary ammonium surfactants or the neutral templating pathways using neutral amine surfactants, the mesopore framework diameter can be controlled by varying the hydrophobic chain length of the surfactant template. The original work of the Mobil group who developed MCM-41 has demonstrated that the pore size is dependent on the length of the hydrophobic tail of the quaternary ammonium surfactant.¹ Also, Tanev and Pinnavaia achieved pore size control for HMS wormhole by using a family of surfactants with different hydrophobic chain lengths.⁹

The addition of auxiliary organic solvent or swelling agents is also a significant way to expand mesopore diameter. The principle behind this method is that hydrophobic organic species can be solubilized inside the hydrophobic regions of the surfactant micelles which lead to the swelling of the micelles. The solubility of the auxiliary solvent in aqueous media should also be considered for their swelling roles. Examples of successful swelling agents include dodecane, trimethyl benzene (TMB), triisopropylbenzene, tertiary amines and poly(propylene glycol).¹⁹⁻²³ With the aid of TMB, pore sizes can be expanded to as much as 40nm for acidic triblock copolymer systems or to 10 nm in basic CTAB surfactant systems though the resulting materials are disordered. The pore size of ordered mesostructures can only be increased to 13 nm and 6 nm for SBA-15 and MCM-41, respectively, by the addition of TMB. The addition of large

amounts of TMB to a synthesis system of SBA-15 results in the formation of mesocellular foams (MCF).²⁰ Hanrahan and co-workers²⁴ also reported the use of super critical CO₂ in tailoring the pore size of hexagonal mesoporous silica.

Assembly temperature also plays a role in tailoring the mesopore diameter. Studies have shown that increase in the assembly temperature can be used to increase the framework pore size. It has been suggested that increases in assembly temperature can lead to the decomposition of the quaternary ammonium ion surfactant through reaction with surface –OH groups to yield the formation of neutral amines or by Hoffman degradation to yield alkenes.¹³ Either way both products are efficient swelling agents and can act as auxiliary co-surfactants for increasing framework pore size. For the case of MSU-X silicas formed under electrically neutral assembly conditions, pore size expansions up to 2.4 nm can be achieved using a single PEO surfactant simply by increasing the assembly temperature over the range of 25-65°C.²⁵ In this case, the mechanism leading to the increase in framework pore size with increasing assembly temperature has been attributed to temperature-dependent changes in the polarity of the S⁰/O interface and consequently, a decrease in H-bonding at the interface. As the assembly temperature is increase, the framework cross-linking is enhanced through further condensation of the silanol groups, leading to the reduction in the framework polarity. The degree of H-bonding, along with the hydration of the amine headgroup, decreases as the polarity of the interface decreases. This leads to an increase in the surfactant packing parameter (g) with

decreasing effective head group area (a_0) and therefore an increase in the framework diameter as the interfacial curvature decreases.²⁶

Post-synthesis treatment of as-made assembly products is used to improve not only the pore diameter of the mesostructure but also to improve the thermal stability of the mesoporous structure. For example, hydrothermal treatment of as-made mesostructures is one of the most efficient methods to improve the mesoscopic regularity of the products.^{3,27} After the initial assembly reaction, the mesostructure undergoes reorganization, growth, and crystallization during hydrothermal treatment. The post-synthesis treatment temperature is usually low, between 80 and 150°C, but more typically the range of 95-100°C because higher temperatures usually leads to the degradation of the surfactant template.²⁸ The post-synthesis treatment of wormhole silica provides an example of the effectiveness of post-synthesis hydrothermal treatment in mediating the pore structure of the mesophase. As-made HMS wormhole materials assembled at 25°C with $V_0/S_0 = 4$ was washed free of the mother liquor and then was digested in distilled water at 65°C for 1-5 days. A substantial increase in pore-pore correlation distance (d-spacing) from 3.8 to 4.6 nm was observed after 1 day of digestion, followed by a more gradual increase to 5.3 nm after 5 days. It was also observed that this method afforded a d-spacing increase of 1.5 nm, which is somewhat larger than the 1.2 nm expansion achieved through direct assembly at 65°C after a reaction time of one day.²⁹

2.1.3 Tailoring the Pore Size Distribution Between the Microporous and Mesoporous Region

Over the past decade a considerable number of studies have focused on the synthesis of mesoporous materials with pore diameters >2 nm and on making the framework pores even larger.³⁰ However, much less attention has been devoted in the synthesis of materials with pores in the super-microporous region. Super-microporous silicas have framework pore diameters between 1 and 2 nm. It is said that these materials bridge the gap between the microporous zeolites (pore diameters ≤ 1.2 nm) and the mesoporous silica (2-50 nm).³¹⁻³⁵ It has also been suggested that microporous materials are important materials for catalytic applications since they exhibit the potential for size and shape selectivity for organic molecules that are too large for to have access to the pores of the microporous zeolites.³⁶ Moreover, size-selectivity seldom is seldom observed for mesoporous materials because the sizes of the reagent and products involved in the catalytic reaction is smaller than the mesopores of the catalyst. There have been very few reports on the synthesis of super-microporous silicas. Most reports utilize specialized surfactants such as bolaform amines^{37,38}, adamantanamine³⁹, short double chain alkylammonium halides⁴⁰ and ionic liquids⁴¹ as templating agents. Moreover, these surfactant templates produce materials with only one super-microporous diameter. Changing the diameter of the super-micropores requires a change in the size of the templating surfactant. As the hydrophobic chain length is decreased, the pore diameter also decreases but only to an extent. As the hydrophobe becomes shorter, the amphiphilic property of the molecule also decreases and at a certain chain length, the

molecule loses its amphiphilic property and no longer forms a micelle. Instead, it becomes soluble in the reaction media. The challenge for synthesizing silicas with super-micropores with diameters less than 2 nm diameter is in finding a suitable temperature dependent surfactant template.

2.1.4 Objectives

This chapter describes the exploratory studies of the use of five oleyl amine surfactants as template for the supramolecular assembly of mesoporous assembly of mesoporous silica via the S^{010} pathway. These oleyl surfactant were first tested for their ability to template a mesostructure. The best surfactant templates then were chosen for further study. To the best of our knowledge, these oleyl surfactants have not been reported as templating agents for mesoporous silica. Thus, a profile of mesoporous silica synthesized under different reaction conditions was carried out. The effect of varying the polarity of the reaction medium was investigated as well as the effect of assembly temperature.

Our interest in using oleyl surfactants as mesostructure templates also is centered on the possible use of the as-made mesostructure as complexants for the trapping of heavy metal ions from aqueous solution. The amine head groups of the templating amine surfactant have been recognized as potential trapping agents for mercury, arsenic, lead and even carbon dioxide. However, a serious drawback prevents the use of as-made amine template mesostructures as trapping agents is the tendency of the intercalated surfactant to desorb in

aqueous suspension. One possible solution to this limitation is to cross-link the surfactant in-situ. The introduction of the organic functionality needed for the templating of this approach will require a great deal from the surfactant. First, the surfactant must be able to form a mesostructure. For the synthesis of a mesostructured silica, it is preferred that the surfactant be either cationic or electrically neutral. It is also important to consider the chain length of the hydrophobe and hydrophilic head because these two factors determine the packing parameter from which the types of micellar aggregates arise. Second, the surfactant must have functional groups that can act as a ligand for metal binding. Eventually, the synthesized materials will be used for metal trapping. Third, the surfactant must have a polymerizable group preferably a double bond so that it can form a polymer network inside the mesostructure. Fourth, the polymerized template should not be soluble in solvents like water or ethanol. And lastly, it would be preferred if the surfactant to be used are commercially available.

Finding the surfactant that fits all these requirements can be a daunting task. After reviewing the fundamentals of the synthesis pathways for mesostructured silica, I concluded that the oleylamine surfactants are the best candidates for the preparation of functional as-made mesostructures. The presence of a double bond in the hydrophobic tails should make it possible to immobilize the structure directing template in the pores of the mesostructure.

2.2 Experimental

2.2.1 Reagents

Oleymethylbis(2-hydroxyethyl)ammonium chloride (Ethoquad), bis(2-hydroxyethyl)oleylamine (Ethomeen), oleylamine (Armeen OLD), oleyldimethylamine (Armeen DMOD), N-oleyl-1,3-diaminopropane (Duomeen O) were provided by Akzo Nobel (www.surface.akzonobel.com) and were used without further purification. Tetraethyl orthosilicate (TEOS), dodecylamine (DDA), and cetyl trimethylammonium bromide (CTAB) were purchased from Aldrich. Absolute ethanol was purchased in-house. The water used in the experiments was double exchanged using a Millipore filter apparatus to remove cations and anions.

2.2.2 Material Synthesis

To the best of our knowledge, there have not been reports describing the synthesis of mesoporous silica using oleylamine surfactants. In this regard, the five surfactants were evaluated based on their ability to template mesostructure silica via the electrostatic S^{+1+} assembly pathway as well as the electrically neutral $S^{0|0}$ pathway

2.2.2.1 Mesostructure Synthesis via the Electrostatic S⁺I⁻ Pathway

The cationic surfactant, oleylmethylbis(2-hydroxyethyl)ammonium chloride (Ethoquad) was used as the template for the attempted S⁺I⁻ synthesis of a mesostructured silica by the S⁺I⁻ pathway according to the method of Edler and White.⁴² A control experiment for the S⁺I⁻ synthesis of MCM-41 also was carried out using CTAB as the S⁺ surfactant. The structures of the two surfactants used for this synthesis are shown below in Figure 2.2.

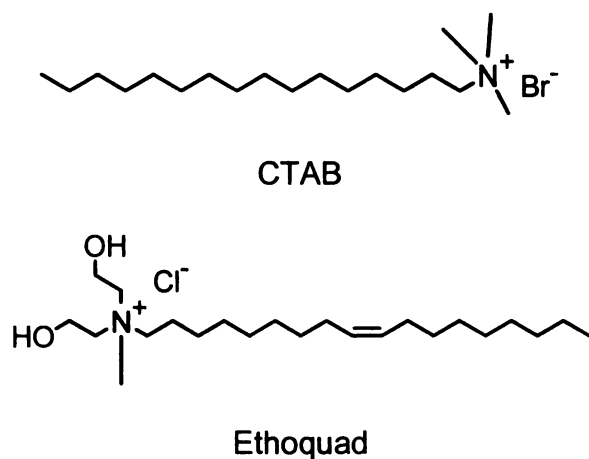


Figure 2.2 Structure of CTAB and Ethoquad

For the synthesis of the MCM-41 reference compound, CTAB (6.08g 0.0167mol) was dissolved in H₂O (45g, 2.5mol), then 7.014g, 0.0315mol of sodium silicate (14 wt% NaOH, 27 wt% SiO₂) was added and the mixture was stirred for 10 minutes. The pH was then adjusted to around pH 11 by adding 1M

sulfuric acid solution and was heated to 100°C for 3 days. Over the 3-day reaction period the pH was periodically checked and maintained at pH 11 through the addition of sulfuric acid. The product was filtered and was washed 3 times with deionized water. The product was allowed to air dry. The surfactant template was removed by calcination at 600°C for 4 hours with a heating rate of 2°C per minute.

In place of CTAB, the same procedures were used in an attempt to synthesize MCM-41 type material from oleylmethylbis(2-hydroxyethyl)ammonium chloride (12.79g, 0.0315mol) as structure director. At the end of the three day synthesis the product was recovered by filtration and was washed with deionized water 3 times. The material was air-dried and the surfactant template was removed by calcination at 600°C for 4 hours at a heating rate of 2°C per minute.

2.2.2.2 Mesostructure Synthesis via the Electrically Neutral S⁰I⁰ Pathway

. The method used for the synthesis of mesoporous silica via the S⁰I⁰ pathway was based on the paper of Pauly and Pinnavaia.⁴³ Table 2.1 provides the structures and quantities of surfactant used for the assembly of mesoporous silica based on the recipe that uses 10 g of TEOS as the silica source. Included for comparison purposes is a reaction mixture in which a non oleyl surfactant was used as structure director, namely dodecyl amine (DDA). As described below, the assembly reactions were carried out in an ethanol-rich and water rich solvent medium corresponding to 60% and 30% ethanol volume, respectively.

Mesostructures Prepared in 60 volume % Ethanol

The desired electrically neutral amine surfactant (0.013mol) was added to a mixture of ethanol (33.6mL) and water (22.4mL) in polypropylene bottles and the mixture was stirred for 30 minutes at room temperature. TEOS (10g, 0.048mol) was then added to the reaction mixture and the resulting mixture was stirred for 20 hours. The products were recovered by filtration and were air dried. The surfactant template was removed by calcination at 600°C for 4 hours at a heating rate of 2°C per minute

Mesostructures Prepared in 30 volume % Ethanol Rich Media



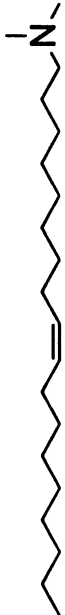

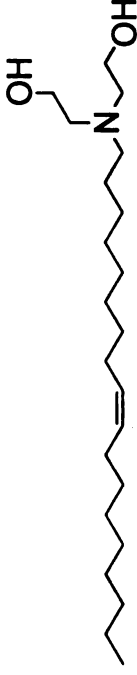
The desired electrically neutral (S⁰) amine surfactant (0.013mol) was added into a mixture of ethanol (16.8mL) and water (39.2mL) in polypropylene bottles and stirred for 30 minutes at room temperature. TEOS (10g, 0.048mol) was then added to the reaction mixture and was stirred for 20 hours at room temperature. The products were recovered by filtration and were washed at least 3 times. The surfactant template was removed by calcination at 600°C for four hours with a heating rate of 2°C per minute. The surfactant template was removed by calcination at 600°C for 4 hours at a heating rate of 2°C per minute.

2.2.2.3 Effect of Solvent Polarity and Assembly Temperature on Mesostructured Silica Assembled Using Oleyl Amine Surfactants

Mesostructures were synthesized under different conditions of solvent polarity through variation in the volume ratio of ethanol and water over the range of 10:90 to 100:0 v/v. Assembly reactions were done at room temperature, 45°C and 60°C. The details of the syntheses conditions are shown in Table 2.2.

In all of the syntheses, the ratio of silica to surfactant was maintained at 1.0 : 0.27, in accordance with the optimum ratio found in previous studies of amine template silicas by Pauly⁴³. For a typical reaction 0.013 mol surfactant template was weighed into a 250 mL polypropylene bottle and was dispersed in an appropriate amount of water/ethanol solution. The mixture was then either stirred (for room temperature synthesis) or shaken in a hot water bath. TEOS was added after 30 mins of stirring or shaking. The reaction was then aged for 20 hours with continuous stirring or shaking. The products were recovered by centrifugation and were washed with copious amount of water. The surfactant was removed by calcination at 600 °C for 4 hours in air with a heating rate of 2°C/min.

Table 2.2 Structures and quantities of S^o surfactants used for the synthesis of mesoporous silica.

Surfactant	Structure	Mass	Mole a
DDA		2.40g	0.013mol
Armeen OLD Oleyl-NH ₂		3.58g	0.013mol
Armeen DMOD Oleyl-N(CH ₃) ₂		3.95g	0.013mol
Duomeen O Oleyl-NH(CH ₂) ₃ NH ₂		4.34g	0.013mol
Ethomeen Oleyl-N(CH ₂ CH ₂ OH) ₂		4.76g	0.013mol

a. The amount of TEOS used in each synthesis was 0.048 mole providing for a surfactant : silica molar ratio of 0.27 : 1

Table 2.3 Reaction Temperature and Solvent Compositions Used for the Mesopore Templating by Armeen OLD (oleyl-NH₂) and Duomeen O (oleyl-NH(CH₂)₃NH₂) Surfactants^a

Product Designation ^b	Synthesis Temperature, °C	H ₂ O:EtOH solvent (v/v)	H ₂ O, mL	EtOH, mL	Mass TEOS ^c , g
X10-Z	25, 45, 60	10:90	5.6	50.4	10
X20-Z	25, 45, 60	20:80	11.2	44.8	10
X30-Z	25, 45, 60	30:70	16.8	39.2	10
X40-Z	25, 45, 60	40:60	22.4	33.6	10
X50-Z	25, 45, 60	50:50	28.0	28.0	10
X60-Z	25, 45, 60	60:40	33.6	22.4	10
X70-Z	25, 45, 60	70:30	39.2	16.8	10
X80-Z	25, 45, 60	80:20	44.8	11.2	10
X90-Z	25, 45, 60	90:10	50.4	5.6	10
X100-Z	25, 45, 60	100:0	56	0	10

- a. The mole ratio of reagents in each case was 1 SiO₂ : 0.3-1.0 H₂O : 0.9-1.1 EtOH
- b. For the X-Y-Z designation of the reaction products, the value of X is assigned an "A" if the surfactant is Armeen OLD or "D" if the surfactant is Duomeen O. the value of Y provides the volume % H₂O in the reaction medium and the Z provides the assembly temperature in °C.
- c. The mass of the surfactant used per 10 g aliquot of TEOS was 3.48 g (0.13 mol) for Armeen OLD and 4.12 g (0.013 mol) for Duomeen O

2.3 Physical Measurements

The physical properties of the mesostructured silica reaction products were determined by nitrogen adsorption isotherms, powder x-ray diffraction, transmission electron microscopy and scanning electron microscopy.

Nitrogen adsorption and desorption isotherms were obtained at -196 °C on a Micromeritics Tristar 3000 sorptometer. The calcined samples were outgased overnight at 150 °C and 10^{-3} torr.

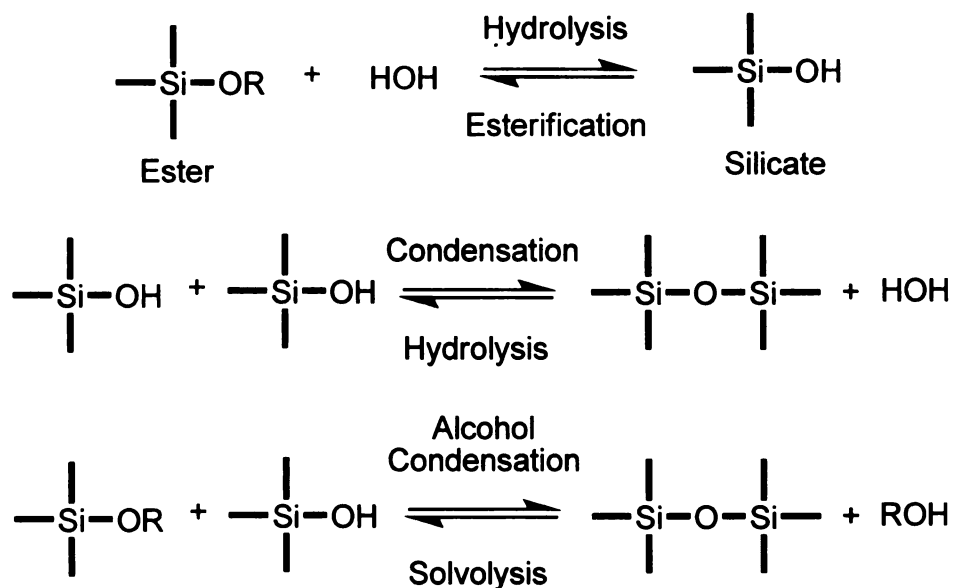
Powder x-ray diffraction patterns were obtained using Cu K α radiation ($\lambda = 1.542 \text{ \AA}$) and a Rigaku Rotaflex diffractometer equipped with a rotating anode operated at 45 kV and 100 mA. Counts were accumulated every 0.02 degree two theta at a scan speed of 0.5 degree per minute.

Transmission electron microscopy (TEM) images were obtained on a JEOL 2200FS with an accelerating voltage of 200kV. Samples were prepared by sonicating powdered samples in ethanol for 15 minutes and evaporation two drops of the suspension onto a carbon coated film supported on a 3 mm, 300 mesh copper grid.

Scanning electron microscopy (SEM) images were obtained on a 6400 SEM with an accelerating voltage of 220 kV. Samples were coated with gold prior to taking images.

2.4 Results and Discussion

According to Iler⁶¹, the condensation-polymerization of silicate ions in aqueous solution to form silica occur in three general stages: polymerization of monomers to form particles, growth of particles by Ostwald ripening and the linking of the particles into chains that form networks. The initial polymerization can be described by the following reaction equilibria starting with a silica ester as the silica source:



This incorporation of a polymeric complexant inside the framework pores of a mesostructured silica formed by condensation polymerization requires a suitably functionalized surfactant. As noted above the choice of an appropriate surfactant is critical.

First of all, the surfactant must be capable of templating a mesostructure. For the synthesis of a well-ordered mesoporous structure, it is preferred that the

surfactant be either cationic or neutral. Anionic surfactants have not afforded derivatives of comparable pore size regularity. It is also important to consider the chain length of the hydrophobic tail and the size of the hydrophilic head group because these two factors determine the packing parameter which determines the type of micellar aggregate and the final structure of the pore network. Most importantly, the surfactant must have functional groups that can act as a ligand for metal binding. This second requirement favors neutral surfactant over a cationic quaternary ammonium ions because the latter cannot function as a ligand. Third, the surfactant must have a polymerizable group, preferably a double bond, so that it can form a polymer network inside the mesostructure. And lastly, the polymerized template should not be soluble in solvents like water or ethanol. For these reasons, commercially available oleyl amine surfactants were investigated as templating agents for mesoporous silica.

Attempted Synthesis of Silica Using a Cationic Oleyl Quaternary Ammonium Ion Surfactant

It was of interest for comparison purpose to attempt the synthesis of silica mesostructure using a cationic oleyl surfactant. However, the commercial cationic surfactant oleyl- $N^+(\text{CH}_3)(\text{CH}_2\text{CH}_2\text{OH})_2 \text{Cl}^-$ (Ethoquad) failed to template a mesostructure form of silica under the reaction conditions where CTAB is known to template MCM-41 silica. Based on the x-ray patterns obtained, no mesostructure was formed in the presence of the ethoxylated oleyl surfactant. Figure 2.3 compares the powder x-ray diffraction patterns for the reaction

products obtained from oleyl-N⁺(CH₃)(CH₂CH₂OH)₂ Cl⁻ and CTAB under equivalent reaction conditions. CTAB forms a well ordered structure as evidence by the presence of four Bragg reflections indexed as d₁₀₀, d₁₁₀, d₂₀₀ and d₂₁₀. However, oleyl-N⁺(CH₃)(CH₂CH₂OH)₂ Cl⁻ exhibit no Bragg reflections indicating the absence of an ordered framework. A possible explanation for the lack of a template structure in the presence of oleyl-N⁺(CH₃)(CH₂CH₂OH)₂ Cl⁻ is the presence of the hydroxyethyl groups. In the S⁺I⁻ pathway, the electrostatic interaction between the cationic surfactant and the anionic silica precursor is very important. In the case of oleyl-N⁺(CH₃)(CH₂CH₂OH)₂ Cl⁻, the cationic N center is shielded by the relatively bulky hydroxyethyl groups. The large head group may have favor ion pairing of the onium ion center with the chloride rather than the larger silicate anions.

Synthesis of Mesostructured Silica with an Electrically Neutral Oleyl Amine Surfactant

The S⁰I⁰ assembly of mesoporous silicas with wormhole framework structures was accomplished using different commercially available oleyl amine surfactants. All the polymerizable surfactants have a double bond in the C-9 position of the hydrophobic tail. For initial survey experiments, reactions were carried out both in ethanol rich media (60 volume %) and in water rich reaction media (70 volume %). Varying the solvent polarity makes it possible to form amine template products with the same wormhole framework structure but with different hierarchical textural porosity. The importance of solvent polarity was

previously demonstrated for silica templated by DDA where a high textural porosity was obtained at low ethanol fractions and low textural porosity formed at low water fractions.⁴³

Figures 2.4 and 2.5 provide the powder x-ray diffraction patterns for the products in ethanol-rich and water-rich media respectively. Wormhole structures are known to exhibit a single low angle reflection that indicates an average pore-pore correlation distance. The wormhole product made using DDA as a structure-directing template serves as reference structure. Based on the x-ray diffraction patterns, we see that for products synthesized under ethanol-rich conditions (60 volume % ethanol), only Ethomeen (oleyl-N(CH₂CH₂OH)₂) produced a poorly ordered material. On the other hand, for the silicas synthesized under water-rich conditions (70 volume % water), Ethomeen again provided the most poorly ordered wormhole structure. As judged on the basis of the half widths of the diffraction peaks, Armeen OLD (oleyl-NH₂) and Duomeen O (oleyl-NH(CH₂)₃NH₂), afforded the most ordered wormhole structure in both reaction media.

Nitrogen adsorption isotherms were obtained to confirm the mesostructured assignments based on x-ray diffraction. Figure 2.6 and 2.7 show the nitrogen adsorption isotherms for each of the reaction products.

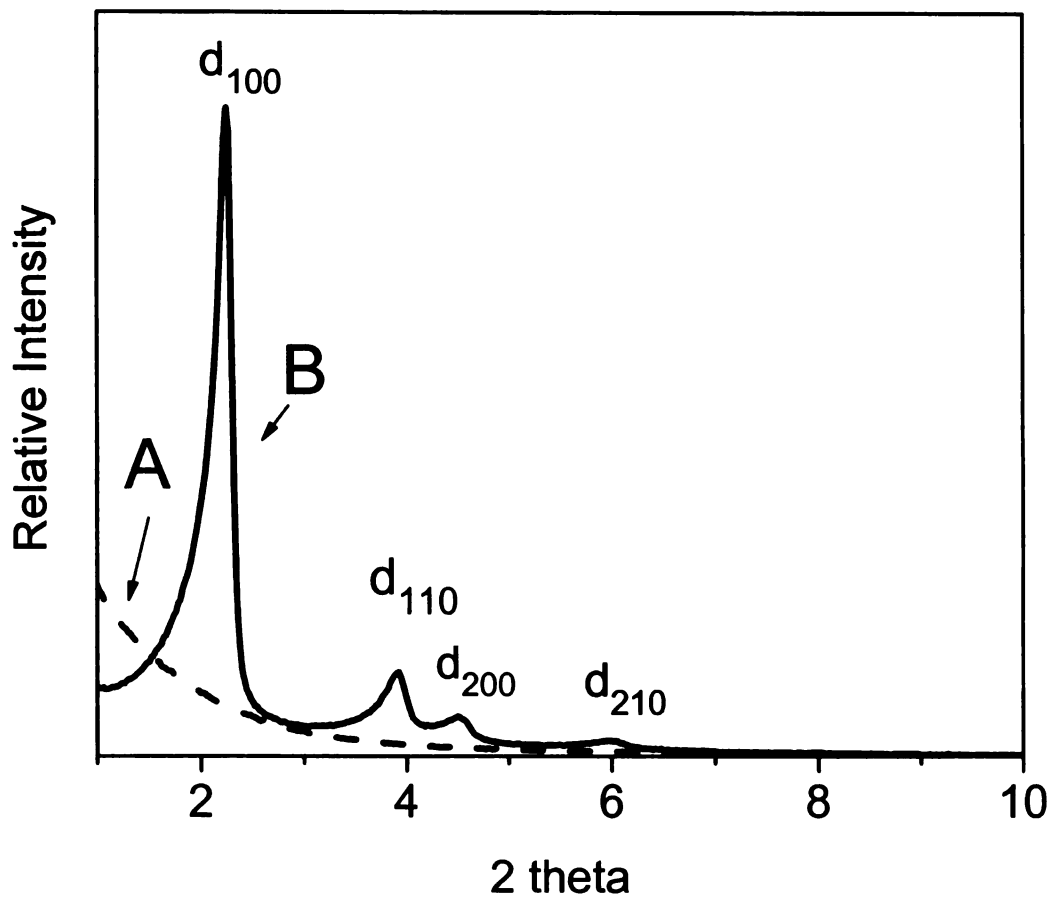


Figure 2.3 Powder x-ray diffraction of calcined silica products synthesized using (A) Ethoquad (oleyl- $N^+(\text{CH}_3)(\text{CH}_2\text{CH}_2\text{OH})_2 \text{Cl}^-$) and (B) cetyl trimethyl ammonium bromide (CTAB) as the templating surfactants.

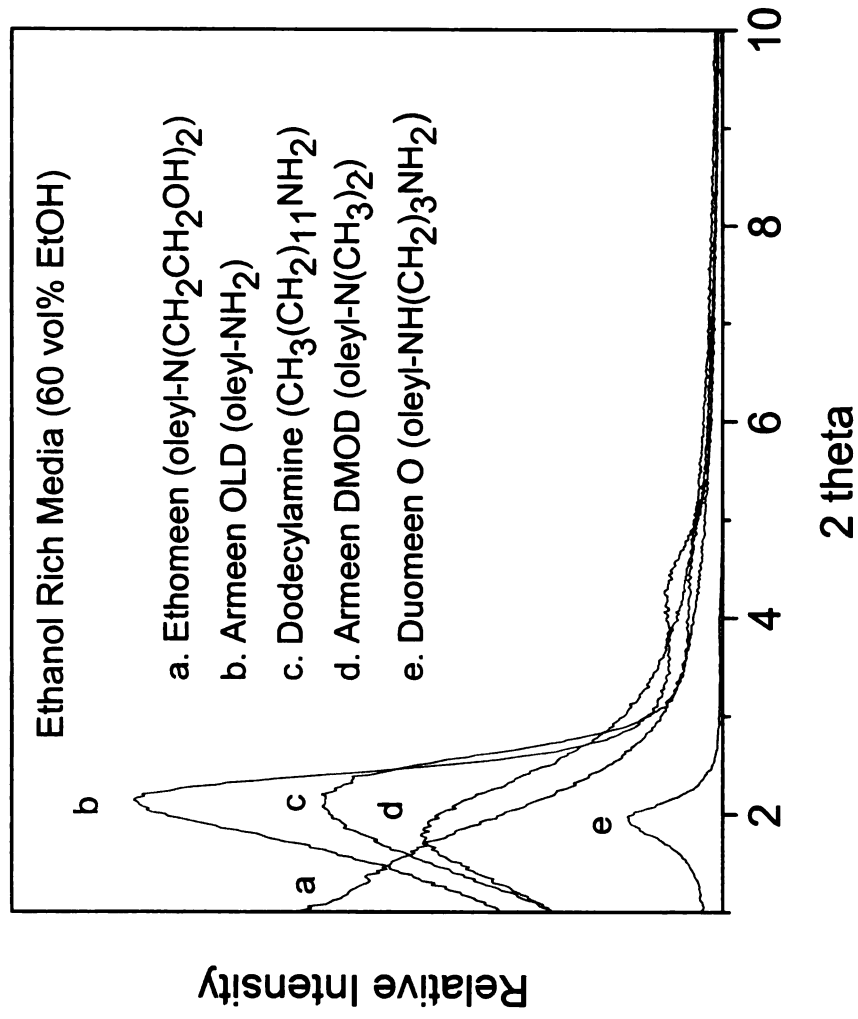


Figure 2.4 Low angle powder x-ray diffraction of calcined wormhole silicas synthesized from different electrically neutral oleyl amine surfactants (60/40 ethanol water by volume). The structure of the oleylamine surfactants are given in Table 2.1. The pattern for the wormhole mesostructure made from dodecylamine is included for comparison. Each product was synthesized at a reaction temperature of 25°C.

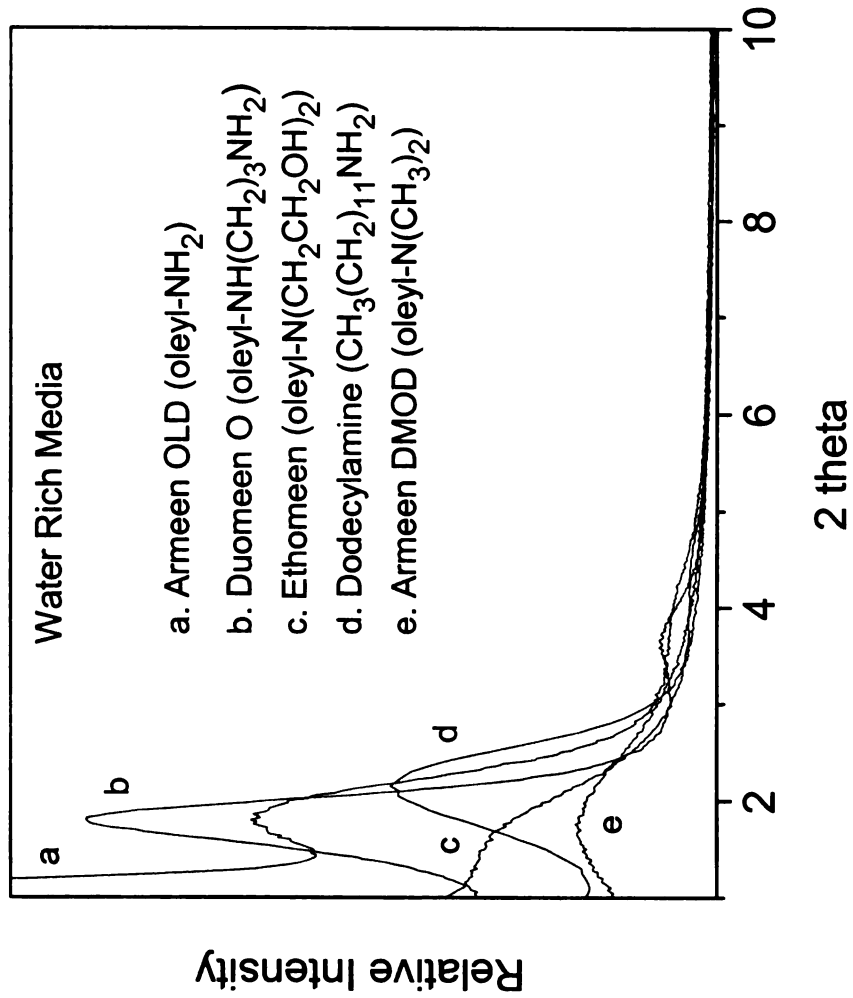


Figure 2.5 Low angle powder x-ray diffraction calcined wormhole silicas synthesized from oleyl amine surfactants in water rich media (30/70 ethanol/water by volume). The structure of the oleyl surfactants are given in Table 2.1. The pattern for the silica template by DDA is included for comparison. The reaction temperature was 25°C.

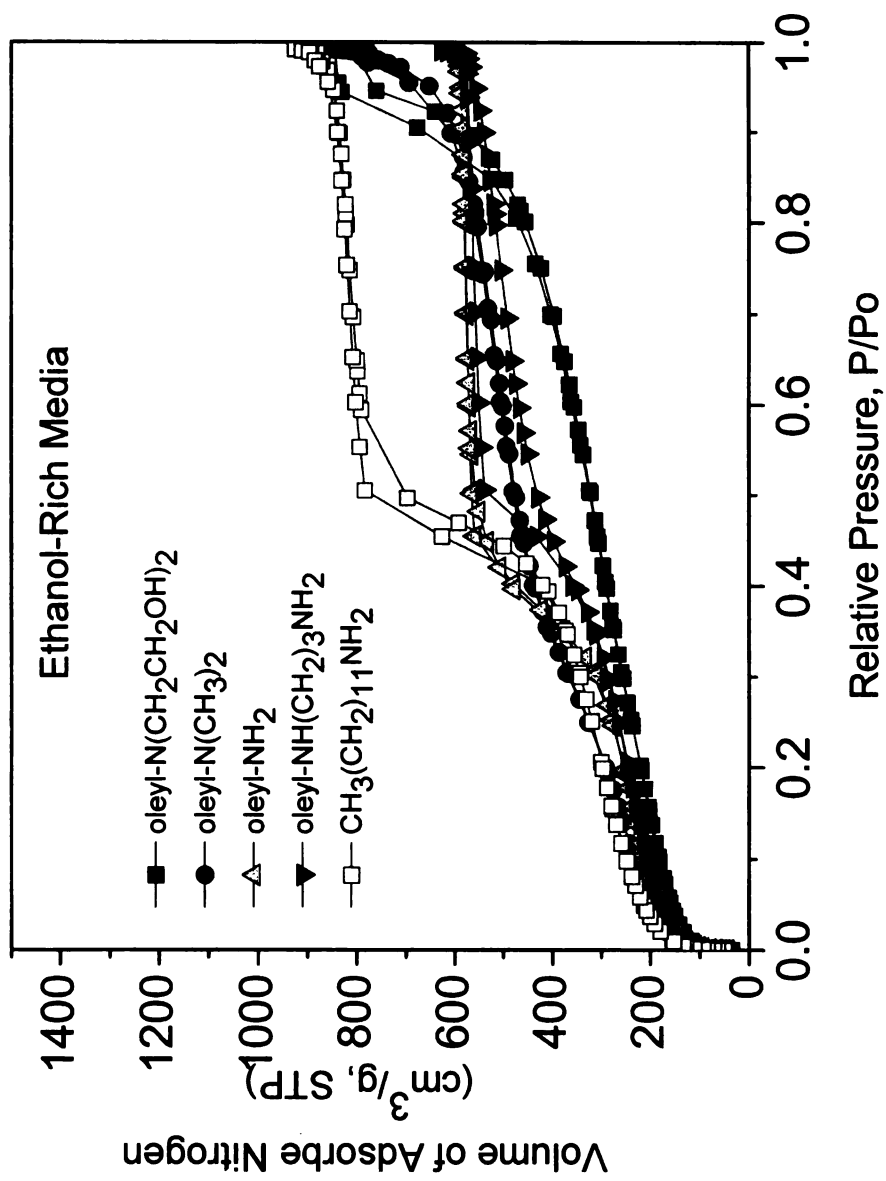


Figure 2.6 Nitrogen isotherms for the wormhole silicas synthesized at 25°C under ethanol rich media (60 vol %) in the presence of oleyl amine surfactants. The isotherm for the silica template by dodecylamine (DDA) is included for comparison.

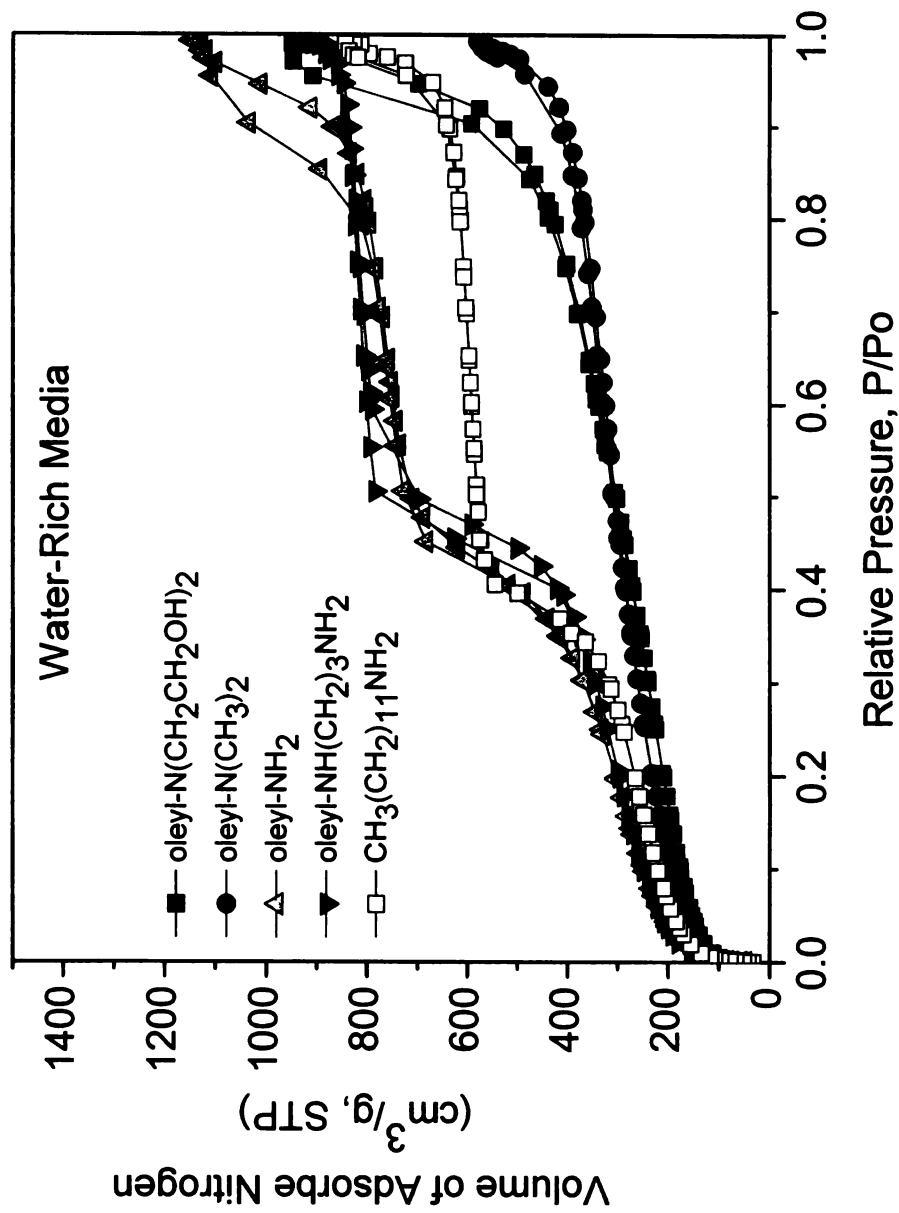


Figure 2.7 Nitrogen isotherms for the wormhole silicas synthesized at 25°C under water rich media (70 vol %) in the presence of oleyl amine surfactants. The isotherm for the silica template by dodecylamine (DDA) is included for comparison.

Table 2.4 Structural properties of calcined wormhole silica materials

Surfactant	Reaction Medium	d spacing (nm)	Pore size ^a BJH (nm)	Wall thickness ^b (nm)	Surface Area (m ² /g)	Framework pore volume ^c (cm ³ /g)	Total pore volume ^c (cm ³ /g)
Armeen OLD Oleyl-NH ₂	70% water	4.70	3.0	1.70	1165	1.28	1.71
Armeen DMOD Oleyl-N(CH ₃) ₂	70% water	5.32	-	-	801	-	0.93
Ethomeen Oleyl-N(CH ₂ CH ₂ OH) ₂	70% water	5.26	-	-	795	-	1.47
Duomeen O Oleyl-NH(CH ₂) ₃ NH ₂	70% water	4.46	3.1	1.36	1196	1.24	1.47
DDA	70% water	4.13	2.6	1.53	1012	0.95	1.32
Armeen OLD Oleyl-NH ₂	60% EtOH	4.17	2.5	1.67	1008	0.89	0.93
Armeen DMOD Oleyl-N(CH ₃) ₂	60% EtOH	4.46	2.1	2.36	1151	0.85	1.24
Ethomeen Oleyl-N(CH ₂ CH ₂ OH) ₂	60% EtOH	5.45	-	-	740	-	1.32
Duomeen O Oleyl-NH(CH ₂) ₃ NH ₂	60% EtOH	4.42	2.8	1.62	889	0.82	1.01
DDA	60% EtOH	4.02	2.5	1.52	984	1.28	1.47

a. Obtained from the adsorption leg of the nitrogen isotherm

b. Obtained from the difference between the d-spacing and pore diameter

c. The framework pore was determined at a partial pressure of 0.80

d. The total pore volume was obtained at a partial pressure of 0.95

The nitrogen isotherms revealed more information regarding the pore structure, morphology and most importantly, the mesoporosity of the materials. From the isotherms, it can be seen clearly that among the tested surfactants, oleyl- $\text{N}(\text{CH}_2\text{CH}_2\text{OH})_2$ does not provide products with well expressed mesostructured pores in either reaction medium as evidenced by the absence of the adsorption step in the region of $P/P_0 = \sim 0.35$. Also, oleyl- $\text{N}(\text{CH}_3)_2$ does not template well ordered mesopore in water rich medium but it performs better in ethanol rich conditions. This adsorption step found in the nitrogen isotherm is due to the filling of ordered mesopores template by the surfactant.

Table 2.3 summarizes the structural properties of the materials synthesized in the presence of oleyl surfactants. Note that the ordered products made from the polymerizable surfactants have larger d-spacings and pore diameters in comparison to the silica template by DDA. This observation was readily explained by the longer chain length of the polymerizable surfactant. On the basis of the surface area and framework pore volumes, two surfactants namely oleyl- NH_2 (Armeen OLD) and oleyl- $\text{NH}(\text{CH}_2)_3\text{NH}_2$ (Duomeen O), stand out as being the best oleyl surfactants for templating a wormhole mesostructure under ethanol-rich and water-rich reaction conditions. In ethanol rich media, however, neither surfactant is as effective as dodecylamine (DDA) in templating a mesostructure, but in water-rich conditions, these two surfactants are superior to DDA.

Detailed Study of the Effect of Solvent Polarity and Assembly Temperature on the Fidelity of the Oleylamine Templated Mesostructures

In order to better elucidate the effect of solvent polarity and assembly temperature on the pore structures of mesoporous silica template by oleylamine surfactants, oleyl-NH₂ and oleyl-NH(CH₂)₃NH₂ were selected as templating agents and the reaction medium was varied over the composition range 90/10 to 100/0 EtOH/H₂O v/v. Also, the assembly reactions were carried out at three temperatures, namely 25°, 45° and 60°C. The polarity of the reaction medium and the reaction temperature both mediate the H-bonding interactions between the amine head group and the walls of the mesostructure and thereby affect the properties of the mesostructures.

The following labeling scheme was adopted in order to identify the 60 reaction products. X-Y-Z where X identifies the templating surfactant ("A" for Armeen OLD, "D" for Duomeen O), Y provides the volume % of water in the reaction medium and Z is the reaction temperature in °C.

The XRD powder patterns for the products obtained in the presence of Duomeen O and Armeen OLD are provided in Figure 2.8 and 2.9, respectively. The products template by Armeen OLD over the temperature range 25°-60°C all with the exception of the product made in 10% water at 60°C, are mesostructured as evidenced by the presence of at least one low angle diffraction peak. The room temperature products assembled in 20-70% water exhibit a very weak second order peak, suggesting the presence of a major

lamellar phase. The presence of a single low angle reflection is characteristic of a wormhole framework structure.

With the exception of the silica template in 100% water at 25°C, all of the products made with Duomeen O over the range of 25-60 °C are mesostructured. Moreover, the products assembled in the 10-80 vol % water exhibit a clear second order diffraction peak indicative of the presence of a lamellar structure. This structural feature is retained for products made at 45o and 60 °C when the reaction medium contains 30-80 vol % water. The products made outside the range of solvent composition exhibit a single diffraction peak characteristic of a wormhole framework. The dependence of mesostructure formation as assembly temperature and the polarity of the solvent medium attest to the importance of salvation effects in determining the pore structure of the template products. The salvation of both the polar head groups and the apolar tail of the surfactant is temperature and solvent dependent. Consequently, the packing parameter and templating properties of the surfactant also depend on temperature and solvent polarity.

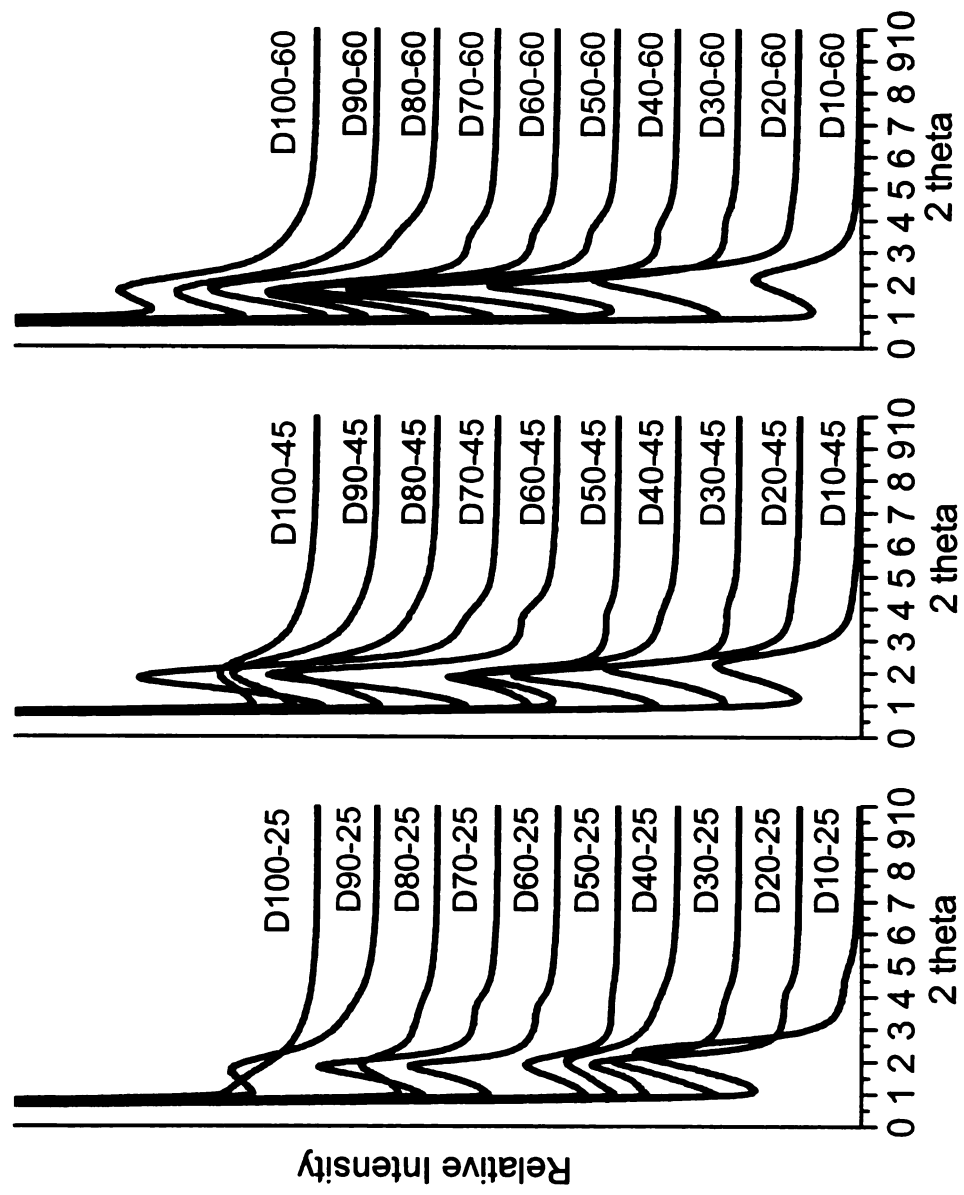


Figure 2.8 Powder x-ray diffraction of mesostructured silica products synthesized from Duomeen O (oleyl-NH(CH₂)₃NH₂) at 25, 45, and 60°C. The labeling scheme is described in the text.

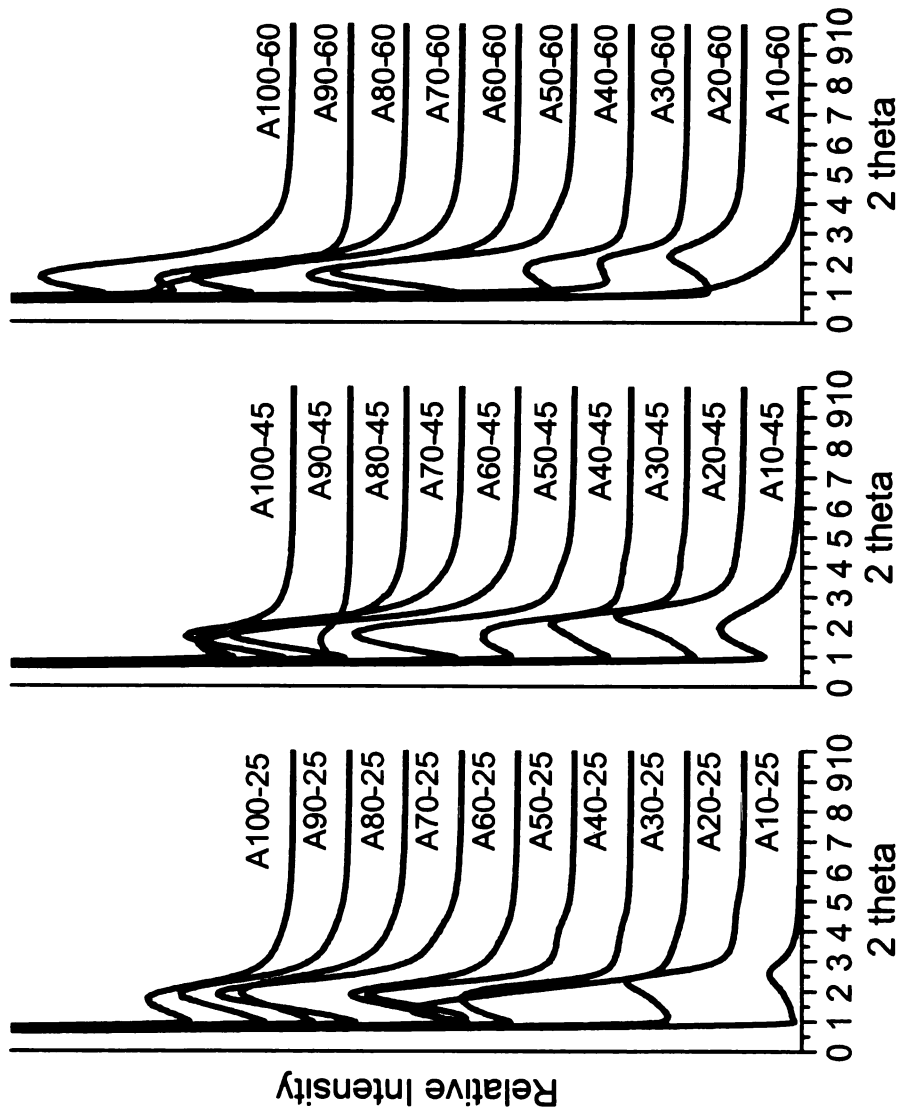


Figure 2.9 Powder x-ray diffraction of mesostructured silica products synthesized from Armeen OLD (oleyl-NH₂) in reaction medium containing 10% to 100% H₂O at 25, 45, and 60 °C. The labeling scheme for each sample is described in the text

The nitrogen adsorption isotherms confirm mesoporosity and usually, reveal more information on pore size than the power x-ray diffraction. The nitrogen adsorption isotherms and BJH pore distributions for the materials synthesized at 25°C using Duomeen O are presented on Figures 2.10 and 2.11, respectively. At first glance, the isotherms confirm the presence of mesopores. It is normally expected for interparticle textural porosity to appear when the water fraction during the synthesis becomes high, because high solvent polarity normally favors small particles. However as can be seen from the isotherms, there is little or no nitrogen uptake of nitrogen at high partial pressure ($P/P_0 > 90$) indicating the absence of significant textural porosity and the presence of large particles. As shown in the TEM images in Figure 2.12, most solvent compositions give large particles. Moreover, there is a decrease in the volume of adsorbed nitrogen at very low solvent polarity. This can be explained by the amount of surfactant in micellar form. As the solvent polarity decreases, the surfactant template becomes more soluble in monomeric form and fewer go to form micelles. This results in a decrease in porosity.

Another feature of the isotherm is the shifting of the adsorption step corresponding to framework mesopore filling. In the process of nitrogen adsorption, nitrogen first forms a monolayer of molecules on the surface of the pores. From this information the surface area is calculated. As the partial pressure of nitrogen is increased, the gaseous nitrogen that is adsorbed begins to form multi-layers and these multi-layers of nitrogen begin to condense and behaves like

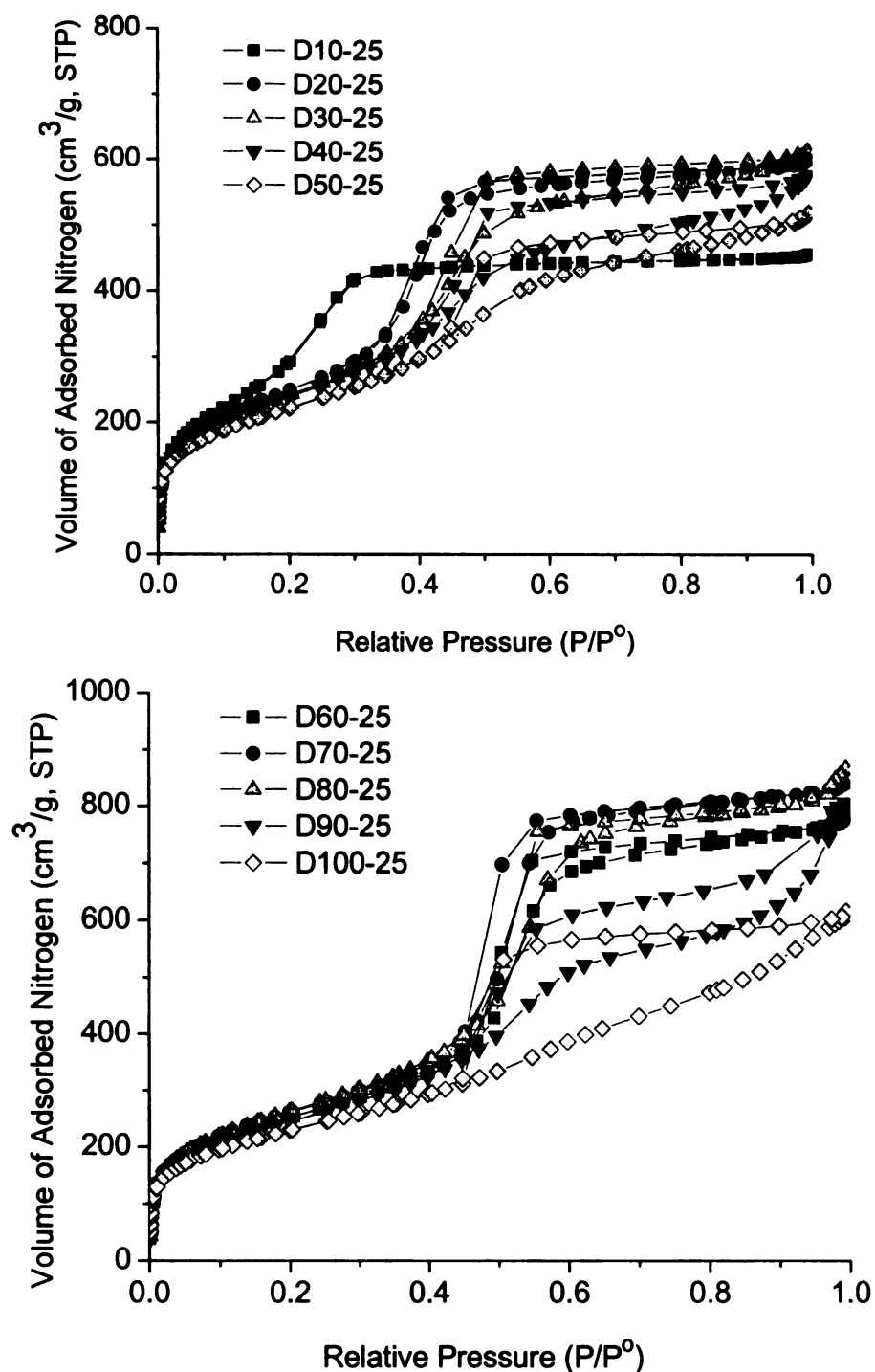


Figure 2.10 Nitrogen adsorption isotherms of mesostructured silica synthesized from Duomeen O at 25 °C with varying water fraction (Top) 10-50%, (Bottom) 60-100%

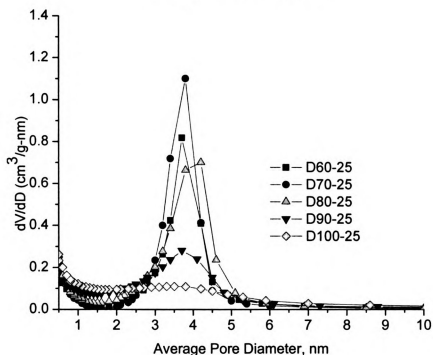
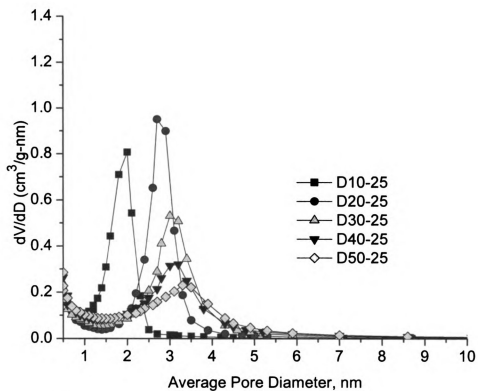


Figure 2.11 BJH pore size distribution of mesostructured silica synthesized from Duomeen O at 25 °C with varying water fraction (Top) 10-50% (Bottom) 60-100%

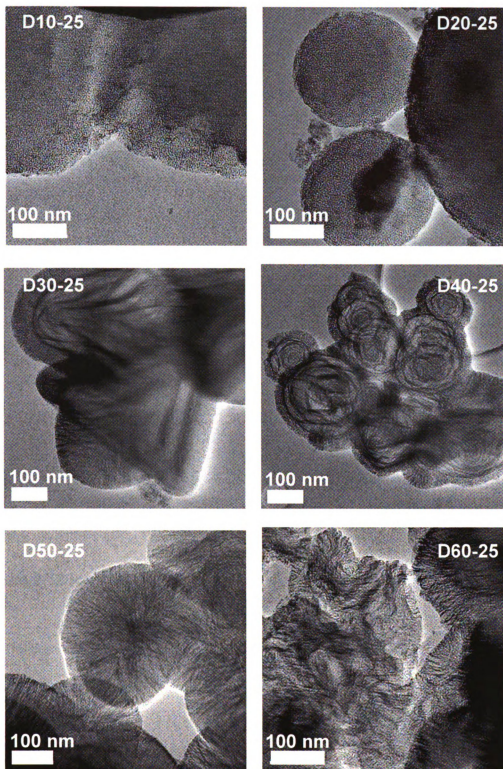


Figure 2.12 TEM images of mesostructured silica synthesized from Duomeen O at 25 °C with varying solvent polarity a liquid.

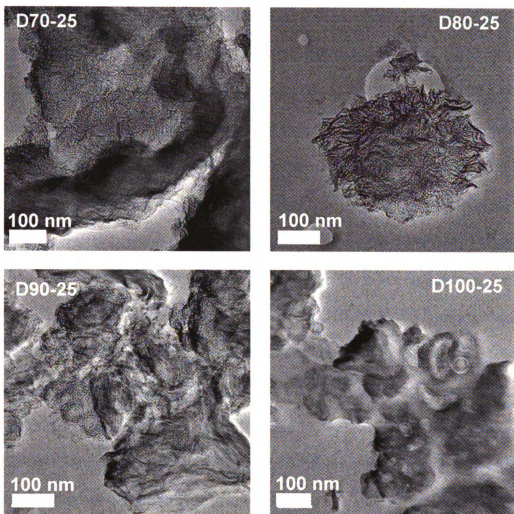


Figure 2.12 (cont'd)

This has been described as capillary condensation which is represented by a step in the nitrogen adsorption isotherm when the mesopore are uniform in size. During this stage, the mesopores are being filled. For the templated products made at 25°C, there is a shift in the partial pressure for framework adsorption as the water content is increased over the range of 10 to 50 % H₂O. This shift signals a change in the pore diameter. The changes in pore diameters with respect to increasing solvent polarity are best seen by the BJH pore distribution plot shown in Figure 2.11. From these plots, it can be seen clearly that the pore diameters increases from ~2.0 nm for sample D10-25 to ~3.5 nm for sample D50-25 and remains more or less constant there after. To the best of our knowledge, this ability to change framework pore structure from 2.0 nm to 3.5 nm by changing solvent polarity is unprecedented.

The TEM images shown in Figure 2.12 confirm the suspected presence of layered structures, particularly as shown by products D30-25 to product D90-25. Fiber-like morphologies in conjunction with the wormhole structure also are observed. The presence of lamellar structures is in agreement with the XRD results.

Mesostructure synthesis at 45° and 60°C was also done to observe the temperature behavior of the templating agent. At higher temperature the surfactant becomes more soluble in water but the H-bonding interaction also is weakened. Figure 2.13 and 2.14 shows the nitrogen isotherms of products synthesized at 45°C and 60°C respectively, and Figure 2.15 and 2.16 and Figure 2.17 and 2.18 provide the respective pore size distributions and TEM images for

the products. As was observed for the materials synthesized at room temperature, there is a shift to higher partial pressures for the mesopore adsorption step as the solvent polarity was increased under both temperature conditions. The shift to higher partial pressure continues until the water fraction is 50% (D50-x). Moreover, little or no textural porosity is observed up to 50% water media but products D80-45 and D80-60 exhibit substantial textural porosity. From these results, only at 80% water and at elevated temperature provide products with high textural porosity.

The mesopore adsorption step shift to higher partial pressure represents an increase in pore diameter which is better seen on the BJH pore distribution plots on Figure 2.15 and 2.16. Figure 2.17 and 2.18 shows the TEM images of the materials. The materials still exhibited wormhole pore structure but there are still parts where fiber like morphologies (e.g. products D40-45, D60-45, D50-60, D70-60) and lamellar vesicle-like particles are observed (D100-45, D20-60 and D60-60).

Figure 2.19 shows the nitrogen adsorption isotherms for materials synthesized at 25°C with Armeen OLD. These templated products exhibit properties similar to those synthesized with Duomeen O. The mesopore adsorption step shifted to higher partial pressure as solvent polarity is increased. There is little or no textural porosity for the products made at room temperature.

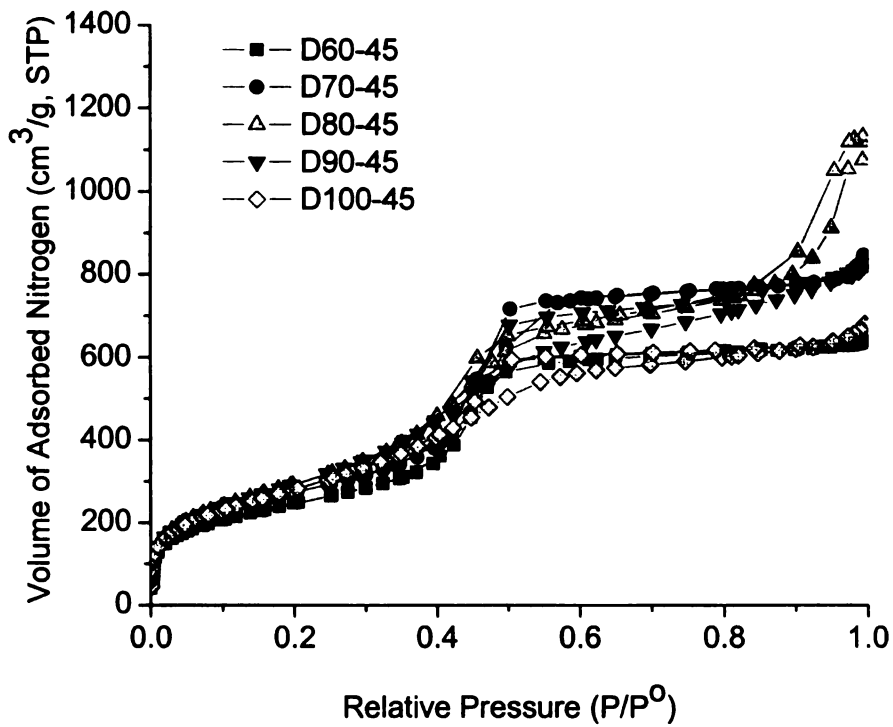
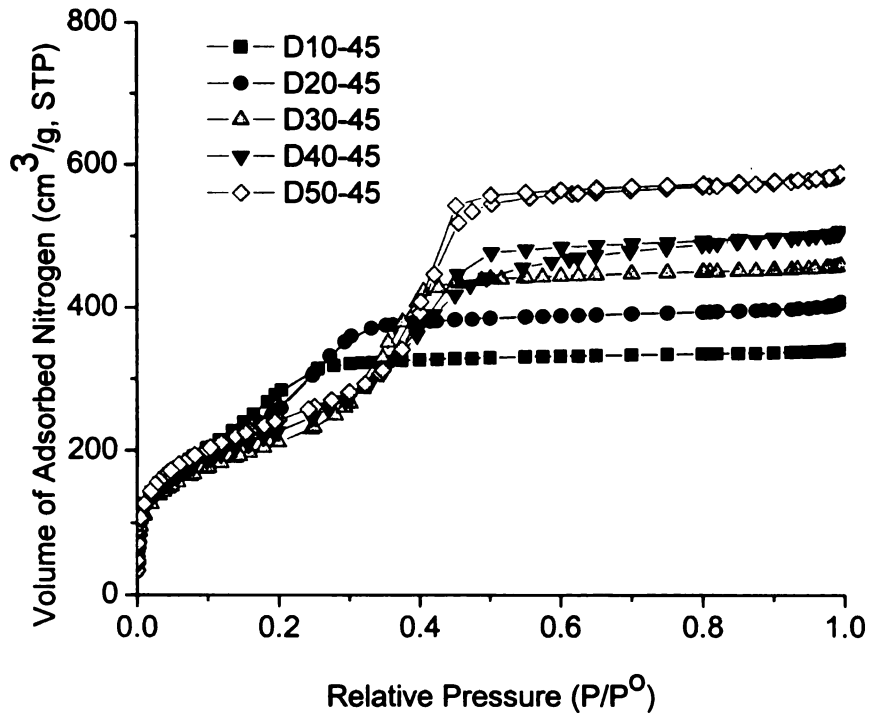


Figure 2.13 Nitrogen adsorption isotherms of mesostructured silica synthesized from Duomeen O at 45 °C with varying water fraction (Top) 10-50% (Bottom) 60-100%.

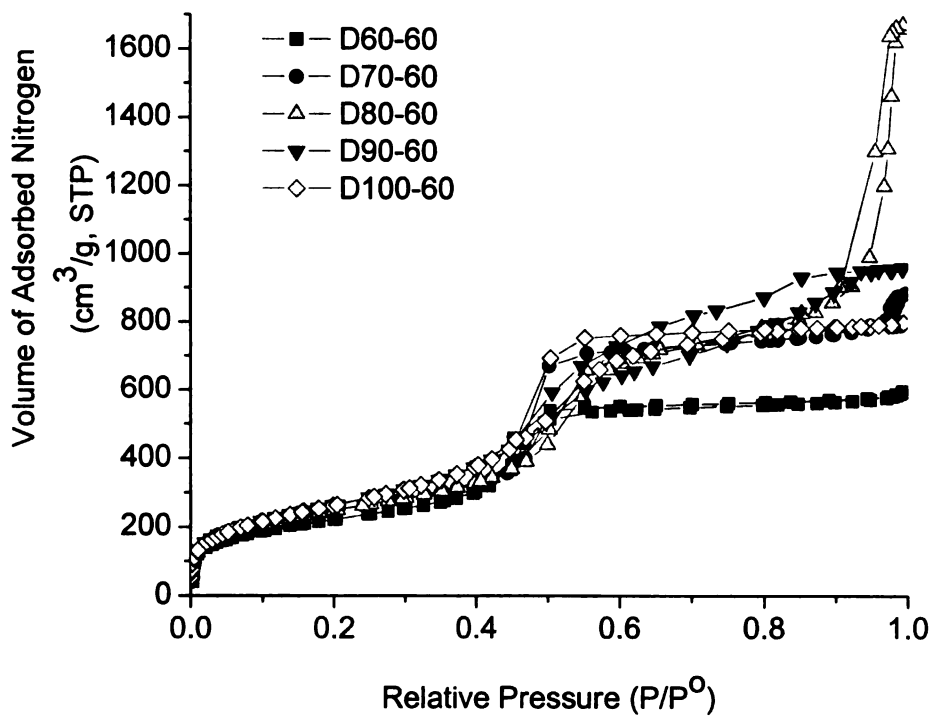
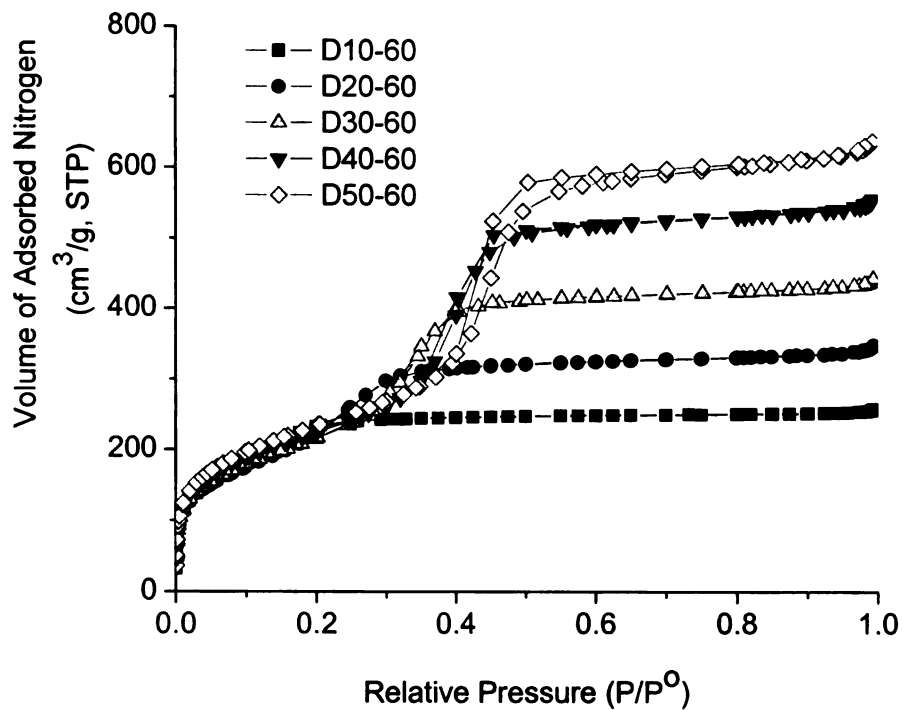


Figure 2.14 Nitrogen adsorption isotherms of mesostructured silica synthesized from Duomeen O at 60 °C with varying water fraction (Top) 10-50% (Bottom) 60-100%.

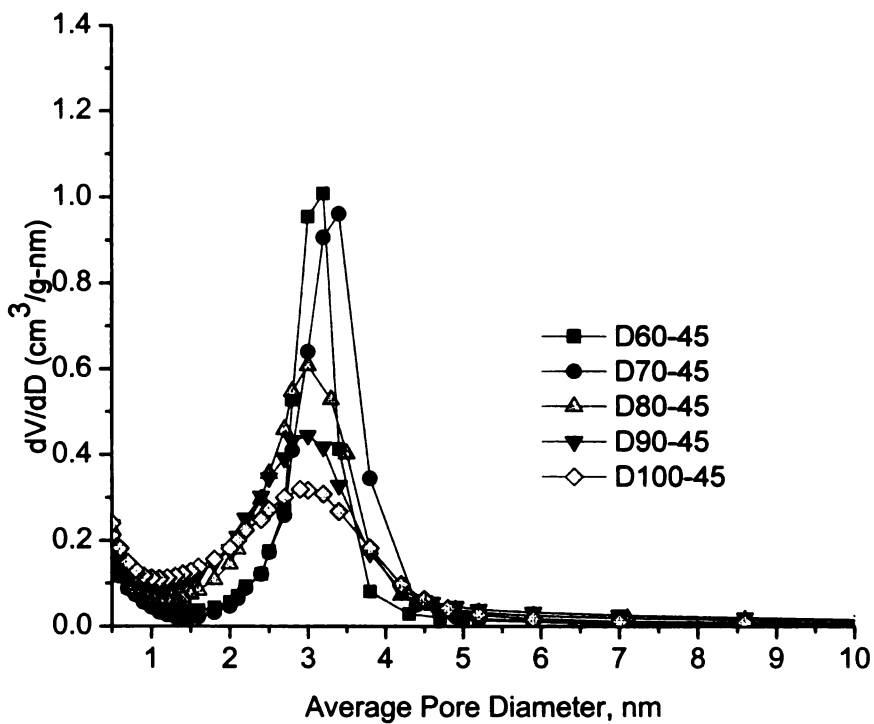
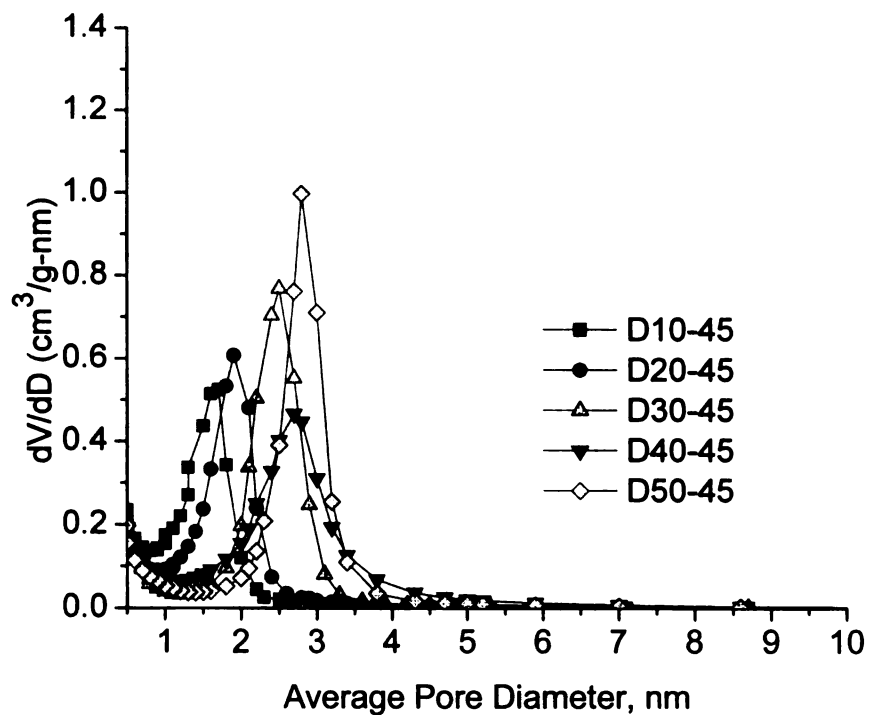


Figure 2.15 BJH pore size distribution of mesostructured silica synthesized from Duomeen O at 45 °C with varying water fraction (Top) 10-50% (Bottom) 60-100%.

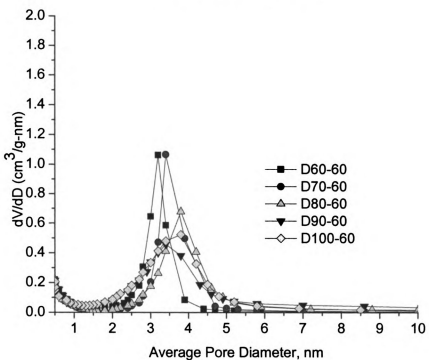
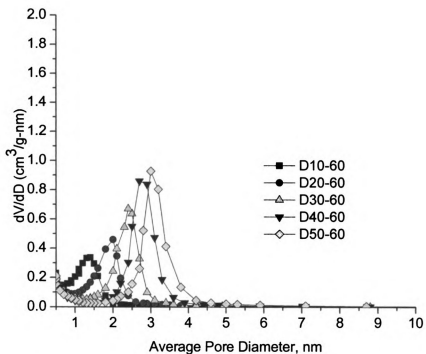


Figure 2.16 BJH pore size distribution of mesostructured silica synthesized from Duomeen O at 60 °C with varying water fractions of (Top) 10-50% and (Bottom) 60-100%.

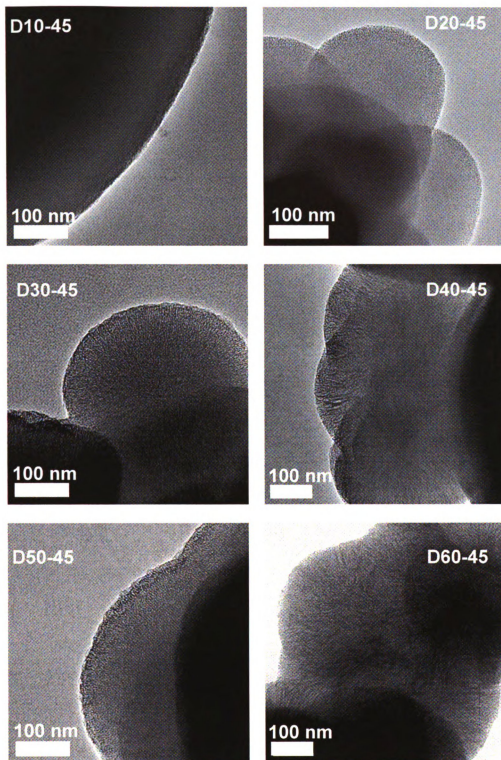


Figure 2.17 TEM images of mesostructured silica synthesized from Duomeen O at 45 °C with varying solvent polarity.

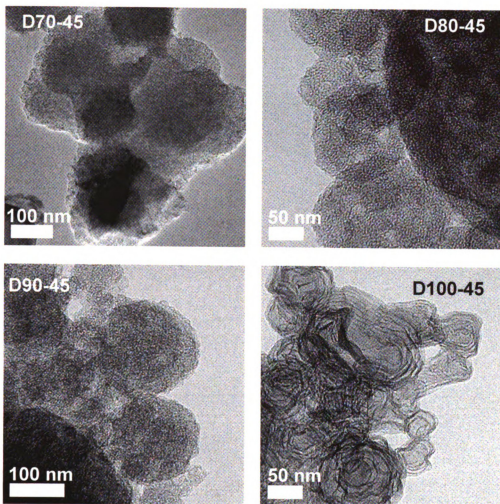


Figure 2.17 (cont'd)

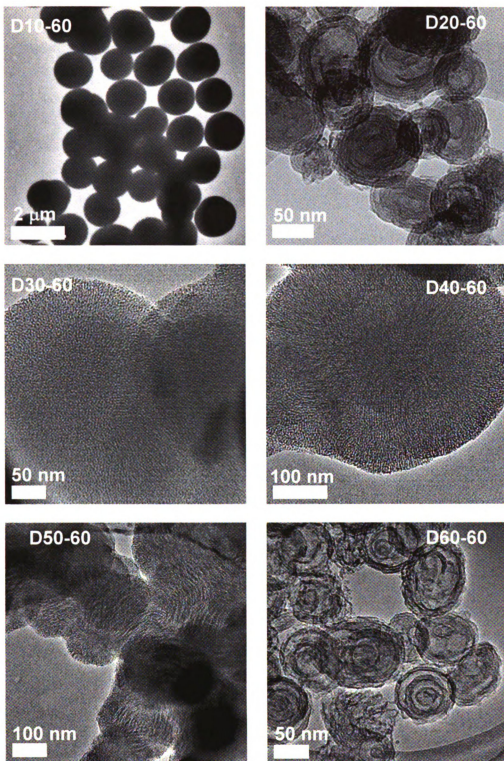


Figure 2.18 TEM images of mesostructured materials synthesized from Duomeen O at 60 °C with varying solvent polarity.

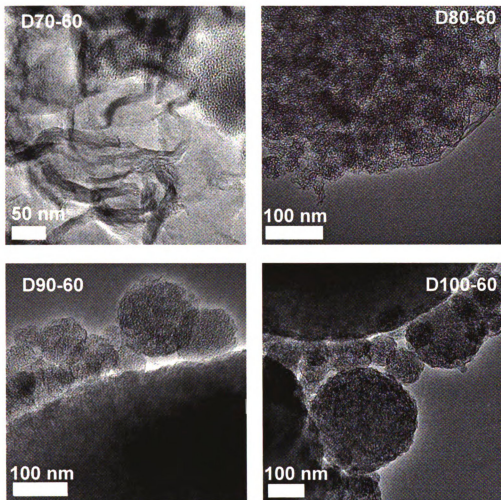


Figure 2.18 (cont'd)

Figure 2.20 and 2.21 provide the corresponding BJH pore distributions and TEM images for these template products. The BJH pore size for products A10-25 and A20-25 are in the supermicroporous range. As the water fraction (> 30 volume % water) is increased, the pore size increases to about 3.1 nm where it remains more or less constant for all silica products template for Armeen OLD. The TEM images show the dominant wormhole framework morphology.

At 45°C, the increase in temperature is enough to disrupt the hydrogen bonding interactions between the template and the silica precursor that the mesostructure that is formed is not as well defined as the others, resulting in a product with high textural porosity as revealed by the uptake of nitrogen at high P/P₀ for the products made in media containing 60-100 volume % water. This observation is confirmed by the isotherm in Figure 2.22, the pore size distribution in Figure 2.23 and the TEM images on Figure 2.24. As with the other templated products, increasing the water fraction from 20-50% results in increased pore diameter (Figure 2.26) with the formation of high texture porosity materials above 50% water fraction. The nitrogen isotherms of the products A20-45 to A50-45 showed a steady increase in the volume of adsorbed nitrogen. This is indicative of how much surfactant is in micellar form. As the percentage of water is increased, more surfactant aggregates to template the mesostructure.

At 60 °C, Armeen OLD a non structured product is formed in 10% water medium. As the water fraction is increased to 40%, the products produced are without textural porosity and from 50% to 100% water, the isotherms and pore

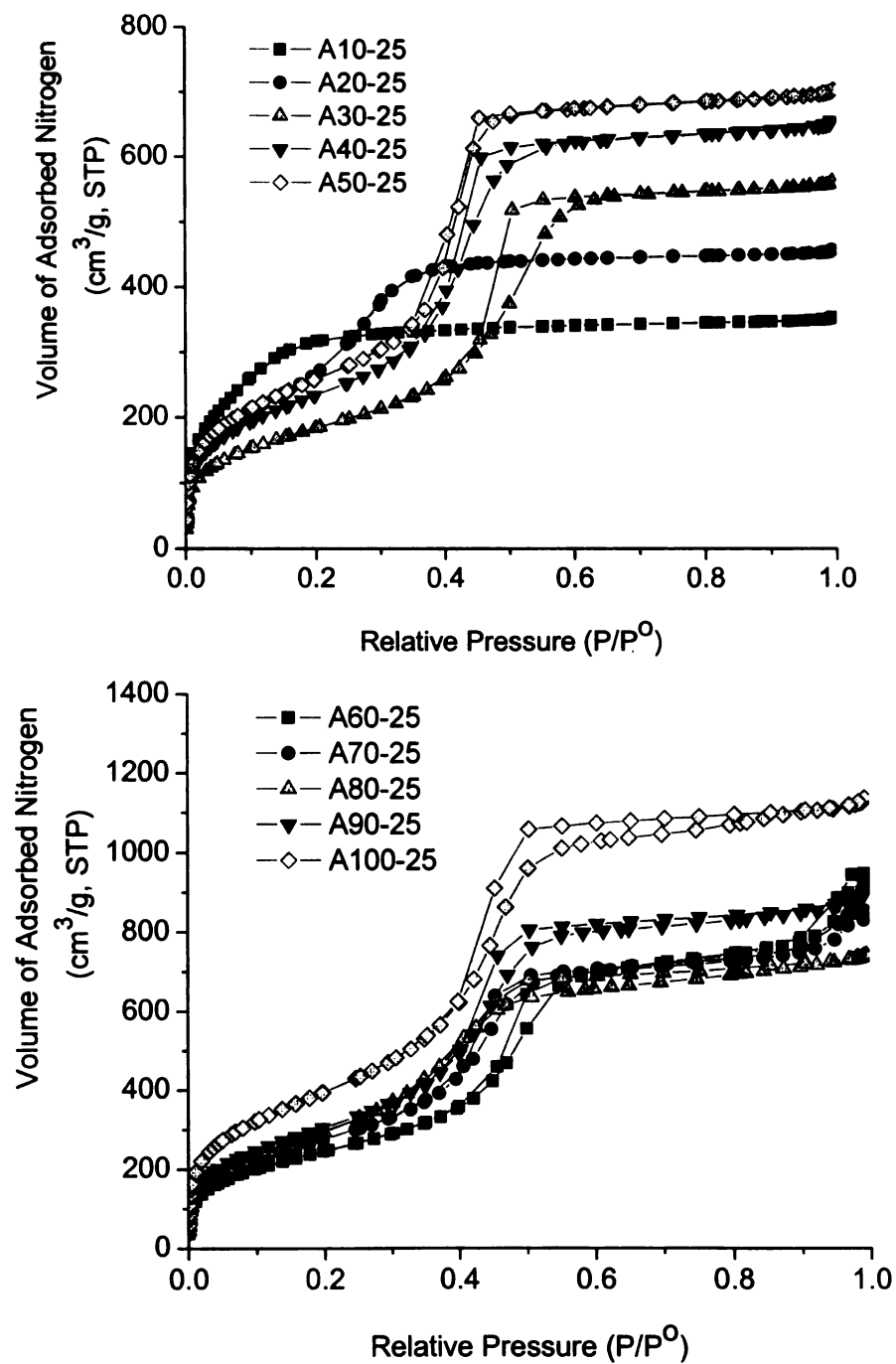


Figure 2.19 Nitrogen adsorption isotherms of mesostructured silica synthesized from Armeen OLD at 25 °C with varying water fraction (Top) 10-50% (Bottom) 60-100%.

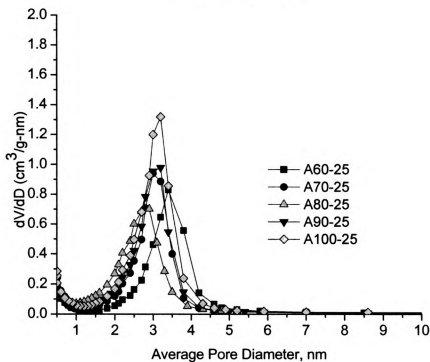
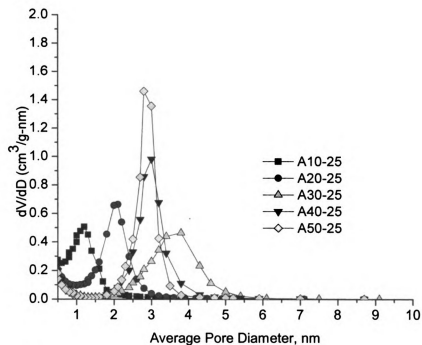


Figure 2.20 BJH pore size distribution of mesostructured silica synthesized from Armeen OLD at 25°C with varying water fraction (Top) 10-50% (Bottom) 60-100%.

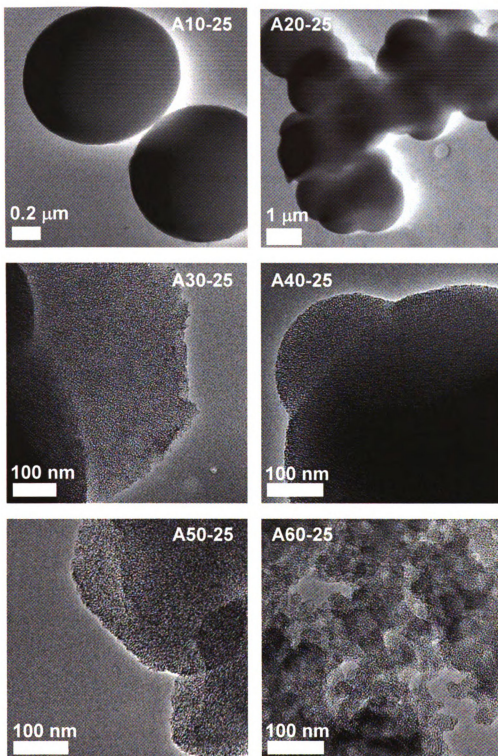


Figure 2.21 TEM images of mesostructured materials synthesized from Armeen OLD at 25 °C with varying solvent polarity.

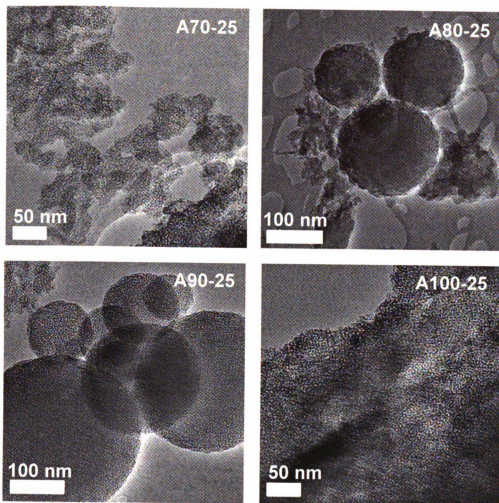


Figure 2.21 (cont'd)

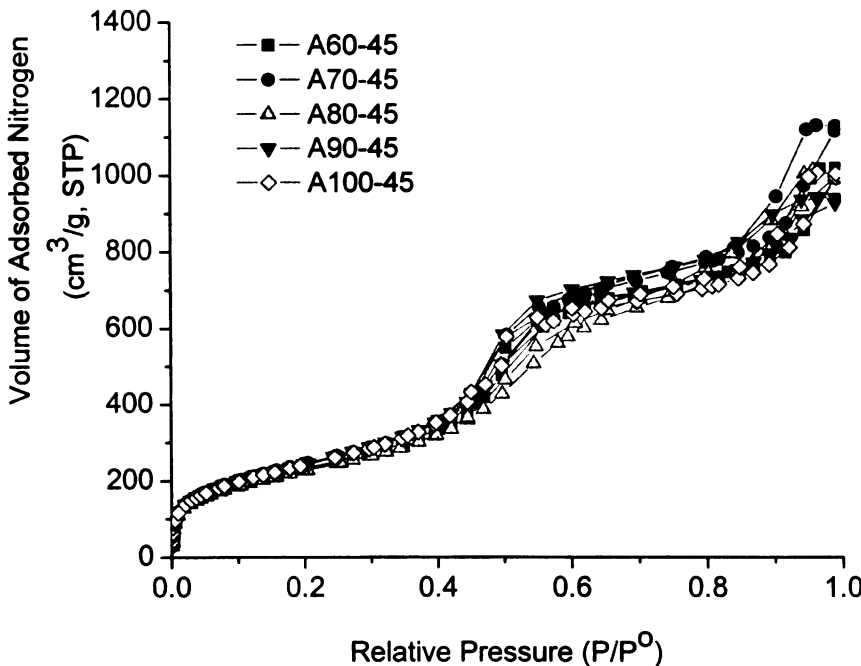
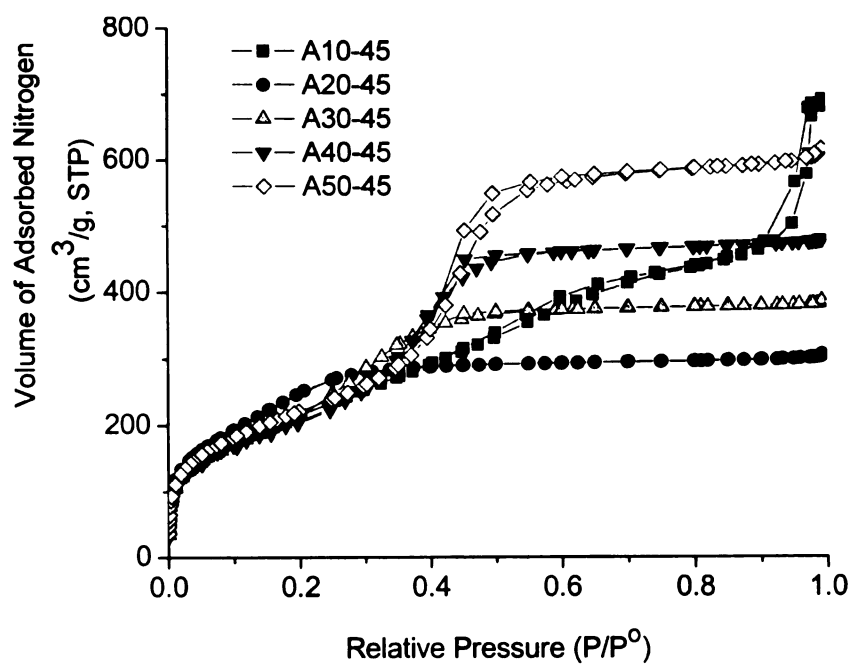


Figure 2.22 Nitrogen adsorption isotherms of mesostructured silica synthesized from Armeen OLD at 25 °C with varying water fraction (Top) 10-50% (Bottom) 60-100%.

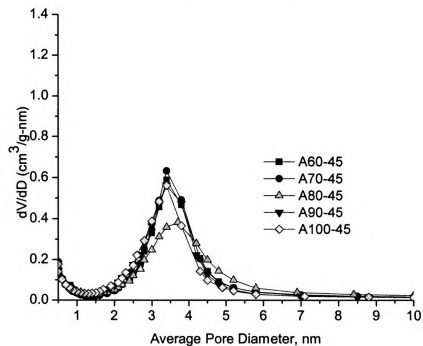
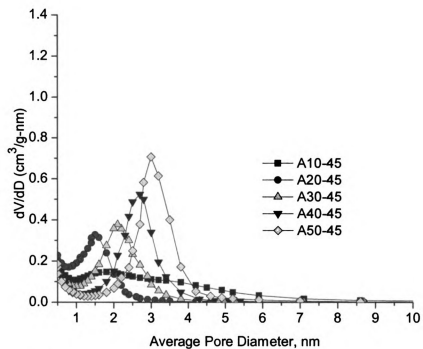


Figure 2.23 BJH pore size distribution of mesostructured silica synthesized from Duomeen O at 25 °C with varying water fraction (Top) 10-50% (Bottom) 60-100%.

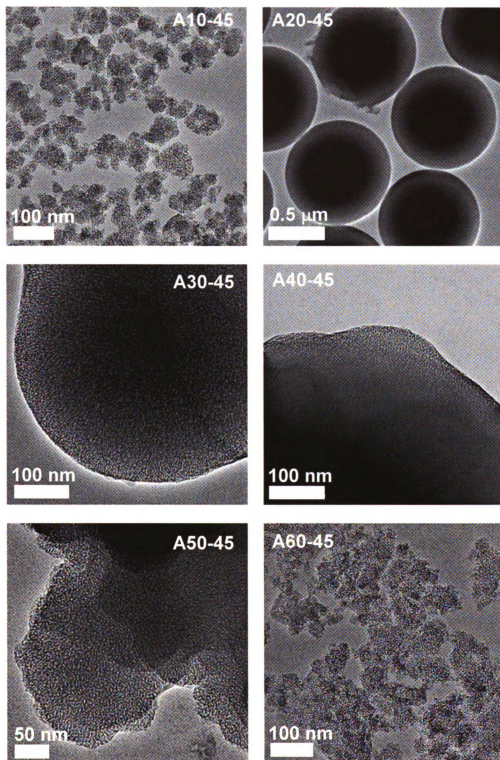


Figure 2.24 TEM images of mesostructured materials synthesized from Armeen OLD at 45 °C with varying solvent polarity.

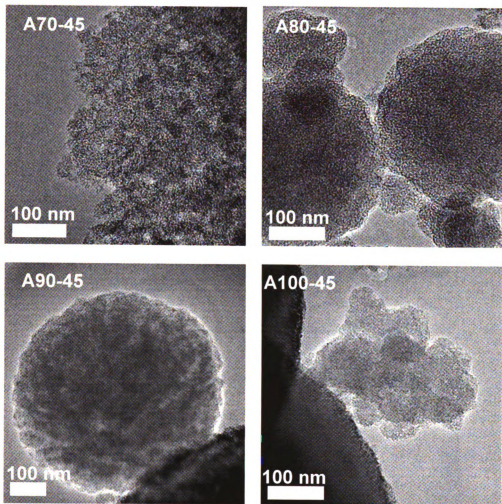


Figure 2.24 (cont'd)

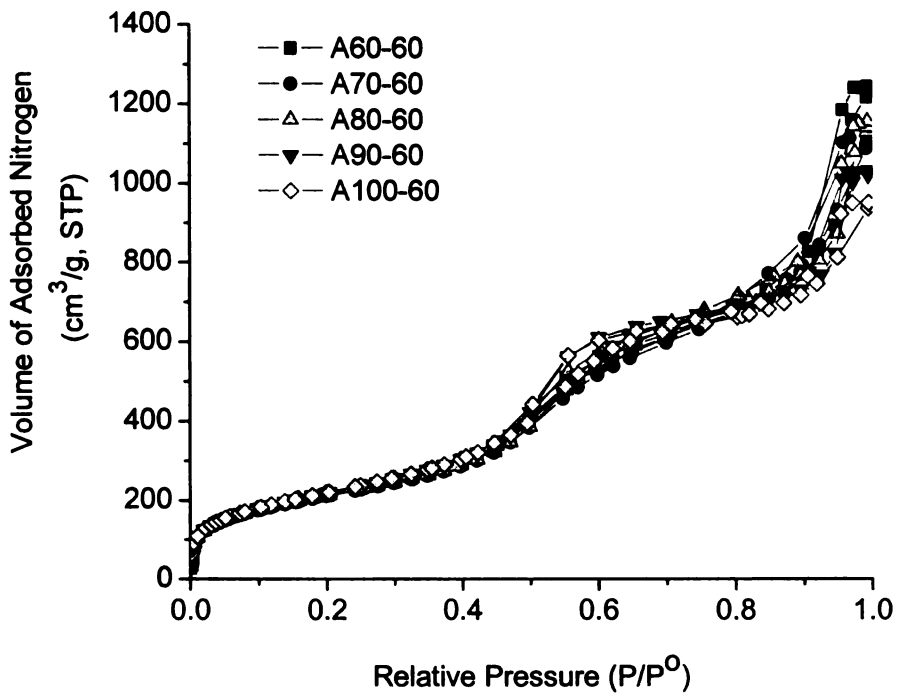
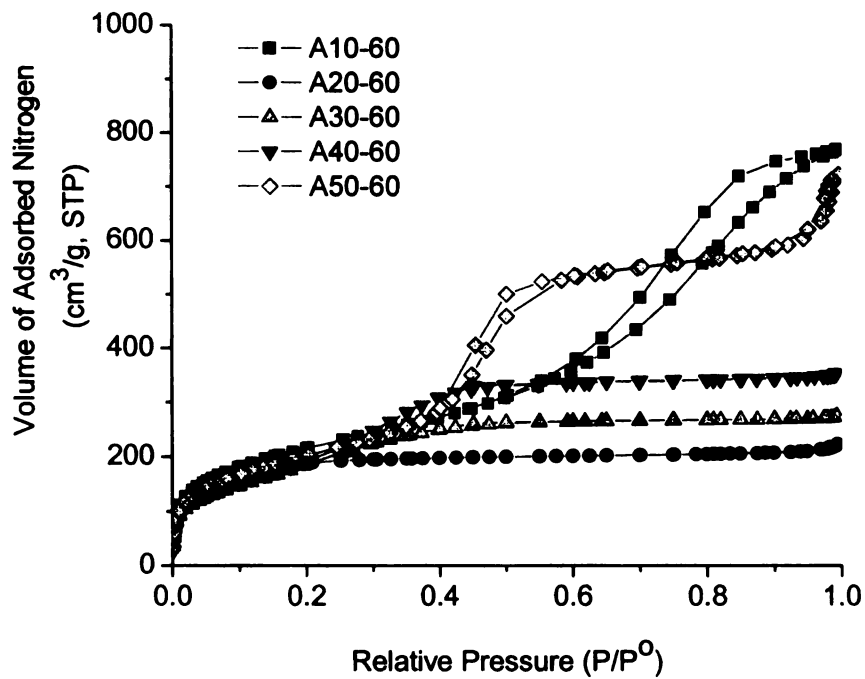


Figure 2.25 Nitrogen adsorption isotherms of mesostructured silica synthesized from Armeen OLD at 25 °C with varying water fraction (Top) 10-50% (Bottom) 60-100%.

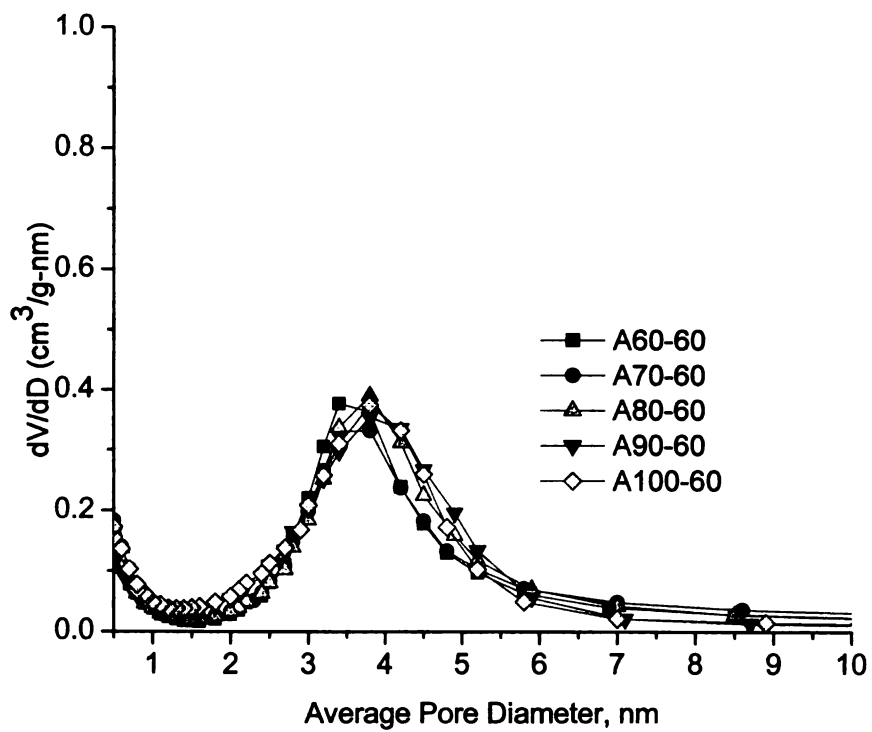
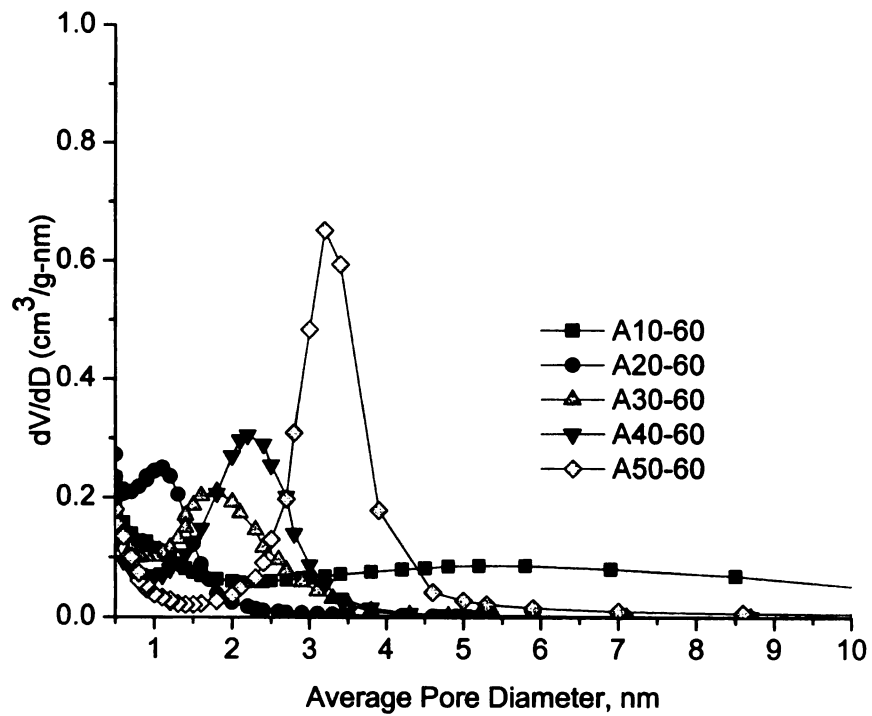


Figure 2.26 BJH pore size distribution of mesostructured silica synthesized from Duomeen O at 25 °C with varying water fraction (Top) 10-50% (Bottom) 60-100%.

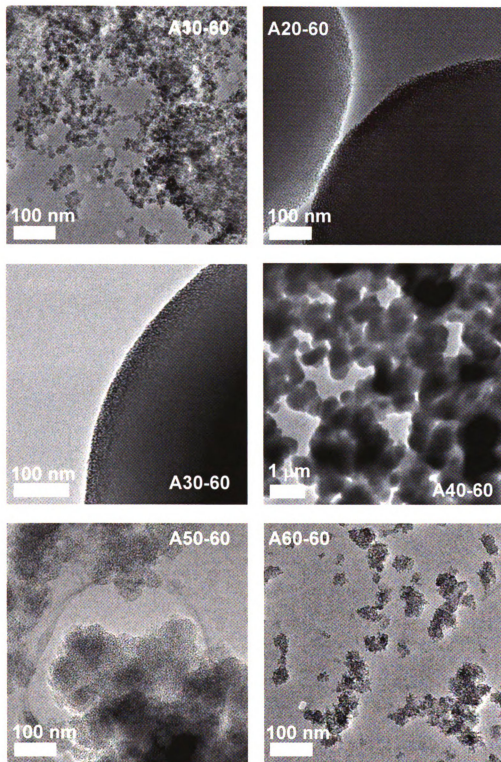


Figure 2.27 TEM images of mesostructured materials synthesized from Armeen OLD at 60 °C with varying solvent polarity.

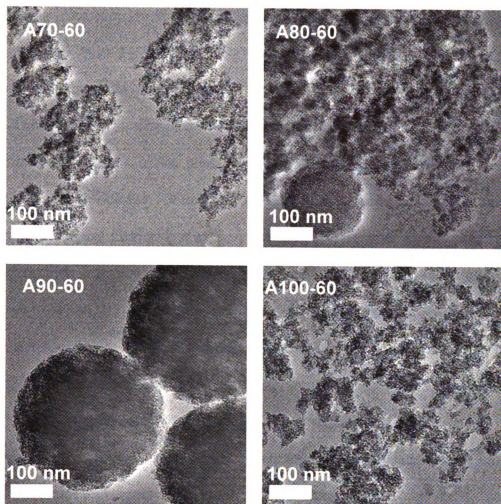


Figure 2.27 (cont'd)

distributions for the products are similar as shown in Figures 2.25 and 2.26. The TEM images (Figure 2.27) confirm the formation of high texture porosity products with wormhole framework structure.

Table 2.4-2.5 summarizes the pore properties for the products. Overall the most remarkable result of the study was the ability to control the pore diameter through simple mediation of solvent polarity and assembly temperature. For assembly reactions carried out at very low solvent polarity, the mesostructured silica products are super-microporous. Super-microporous silicas have pore diameter between 1-2 nm and bridge the gap between the microporous zeolites and the mesoporous silica. Relatively few studies have been reported for the synthesis of supermicroporous silicas. It has been suggested that they offer more selectivity towards size and shape-selective separation or catalysis. These materials are not easily synthesized. Even though their synthesis is based on supra-molecular assembly using surfactant templates, finding a suitable surfactant to produce the desired 1-2 nm diameter pores is not easy because solvated surfactant micelle typically are larger than 2 nm in diameter. Making the hydrophobe of the surfactant template shorter compromises the amphiphilic property of the surfactant. Typical surfactants, such as alkylammonium ions and block co-polymers used for mesostructured silica synthesis produce micelles that are >2 nm in diameter. When the surfactant hydrophobe becomes too short, it does not form a micelle anymore, instead, it becomes soluble in monomer form. The oleyl surfactants which have 18 carbons on its hydrophobic tail are expected

Table 2.5 Summary of the pore properties of mesoporous silica products assembled using Duomeen O as a templating agent under varying assembly temperature and varying water composition.

Material	Calcined d-spacing, nm	Average Pore Diameter, nm	Wall Thickness, nm	BET Surface Area, m ² /g	Framework Pore Volume, mL/g (taken @ P/P ₀ = 0.75)
25°C					
D10-25	3.9	2.0	1.9	1263.5	0.691
D20-25	4.4	2.7	2.0	923.7	0.888
D30-25	4.7	3.0	1.7	871.9	0.861
D40-25	4.5	3.2	1.3	855.0	0.766
D50-25	4.6	3.4	1.2	786.2	0.720
D60-25	4.7	3.7	1.0	892.1	1.124
D70-25	4.9	3.8	1.1	928.6	1.237
D80-25	4.6	4.2	0.4	941.3	1.200
D90-25	5.4	3.7	1.7	872.2	0.874
D100-25	-	3.4	-	801.6	0.698
45°C					
D10-45	3.9	1.6	1.4	990.9	0.519 (0.75)
D20-45	4.2	1.9	2.3	1098.1	0.609(0.75)
D30-45	4.6	2.5	2.1	862.9	0.670 (0.8)
D40-45	4.6	2.7	1.9	865.4	0.760 (0.8)
D50-45	4.8	2.8	2.0	883.6	0.880 (0.75)
D60-45	4.7	3.1	1.6	884.0	0.942 (0.75)
D70-45	4.8	3.3	1.5	986.1	1.176 (0.75)
D80-45	4.3	3.0	1.5	1106.1	1.146 (0.8)
D90-45	4.5	3.1	1.4	1114.2	1.094 (0.8)
D100-45	4.5	3.0	1.5	1048.0	0.931 (0.8)
60°C					
D10-60	4.2	1.4	2.8	738.4	0.387 (0.75)
D20-60	4.2	1.9	2.3	909.8	0.510 (0.75)
D30-60	4.6	2.4	2.2	880.0	0.658 (0.8)
D40-60	4.9	2.8	2.1	826.4	0.822 (0.8)
D50-60	5.0	3.1	1.9	834.3	0.932 (0.8)
D60-60	5.0	3.3	1.7	785.3	0.854 (0.75)
D70-60	5.1	3.4	1.7	876.5	1.141 (0.75)
D80-60	4.9	3.8	1.1	884.3	1.210 (0.8)
D90-60	5.1	3.5	1.6	967.7	1.486 (1.0)
D100-60	5.1	3.7	1.4	969.9	1.189 (0.8)

Table 2.6 Summary of the pore properties of mesoporous silica products assembled using Armeen OLD as a templating agent under varying assembly temperature and varying water composition.

Material	Calcined d-spacing, nm	Average Pore Diameter, nm	Wall Thickness, nm	BET Surface Area, m ² /g	Framework Pore Volume, mL/g (taken @ P/P ₀ = 0.75)
25°C					
A10-25	3.4	1.2	2.2	1003.8	0.533
A20-25	3.8	2.1	1.7	1179.4	0.693
A30-25	6.7	3.8	2.9	666.4	0.845
A40-25	5.2	3.0	2.2	868.4	0.980
A50-25	4.7	2.9	1.8	683.1	1.485
A60-25	4.7	3.4	1.3	910.4	1.132
A70-25	4.7	3.0	1.7	1050.9	1.115
A80-25	4.6	2.9	1.7	1183.5	1.057
A90-25	4.5	3.2	1.3	1175.2	1.272
A100-25	5.0	3.2	1.8	1506.8	1.637
45°C					
A10-45	4.6	1.9 (broad)	2.7	794.8	0.676 (0.8)
A20-45	3.7	1.6	2.1	859.7	0.458
A30-45	5.2	2.1	3.0	902.1	0.587
A40-45	5.3	2.7	2.6	820.4	0.725 (0.8)
A50-45	5.0	3.1	1.9	820.2	0.910 (0.8)
A60-45	5.3	3.5	1.8	853.3	1.117 (0.8)
A70-45	5.3	3.5	1.8	900.5	1.192 (0.8)
A80-45	6.1	3.6	2.5	832.1	1.099 (0.8)
A90-45	6.1	3.5	2.6	908.0	1.124 (0.8)
A100-45	6.0	3.4	2.6	896.3	1.132 (0.8)
60°C					
A10-60	-	6.0 (broad)	-	1.191	1.191 (1.0)
A20-60	4.0	1.0	3.0	586.8	0.316
A30-60	4.7	1.8	2.9	698.4	0.413
A40-60	5.1	2.3	2.8	784.3	0.524
A50-60	5.1	3.3	1.8	730.2	0.873 (0.8)
A60-60	5.7	3.5	2.2	767.8	1.192 (0.9)
A70-60	6.0	3.6	2.4	761.6	1.041 (0.8)
A80-60	6.2	3.7	2.5	770.3	1.069 (0.8)
A90-60	-	3.9	-	803.2	1.052 (0.8)
A100-60	5.8	3.9	1.9	804.5	1.026 (0.8)

to produce micelles with diameter about 3-3.5 nm but instead at the proper solvent polarity it is able to produce micelles with diameters within the super-microporous range. This flexibility arises is due to the double bond present on the oleyl chain. This double bond provides a kink that gives the hydrophobe the propensity to fold in a hair pin conformation thus decreasing the chain length and consequently the micelle diameter. This is thought to happen at low solvent polarity (i.e. high EtOH fraction). As illustrated in Figure 2.28, when there is inadequate water to solvate the head groups of a micelle with fully extended hydrophobic chains. This results to a more fully hydrated but smaller micelle. As the water concentration is increase, there is enough water to hydrate the micelle being formed thus the hydrophobe is able to extend completely to its maximum size. This interpretation is supported by the observed increase in pore diameters as the water fraction is increased up to a volume fraction where the hydrophobe segment is fully extended. Beyond that point, further increase in the volume fraction of water does not result in an increase in templating micelle size.

To further explore this hypothesis, a parallel experiment was done using a saturated amine surfactant template, namely, hydrogenated tallow amine (abbreviated TA). The hydrophobic tails of this surfactant contains primarily 18 carbon atoms with a minority of the tails containing 14 or 16 carbon atoms. The template silica products were synthesized the same way as the oleyl-templated silicas. The nitrogen isotherms and BJH pore size distribution of the products synthesized at room temperature are presented in Figure 2.29. The isotherms exhibit qualitatively similar step shaped (Type IV) isotherms, indicating the

presence of mesopores with diameters >2 nm, regardless of the solvent polarity. The BJH pore size distributions indicate the absence of pores below the mesopore region of (< 2 nm). The smallest average pore size was obtained at 10% water (TA10-25) which is about 2.5 nm. Thus, the effect of solvent polarity on the average pore size of TA templated silica is much more limited and confined entirely to smaller variations in the small mesopore range. The lack of double bond in the hydrophobic tail limits the hairpin folding thus limiting the effect of solvent polarity on the template mesopore size of the silica.

Figure 2.30 presents the plot of pore sizes of mesoporous silica products assembled using Armeen OLD. In the studies conducted by Pauly²⁶ regarding the effect of assembly temperature on the BJH pore size distribution of wormhole silica, an increase in assembly temperature corresponds to an increase in pore diameter. In their experiment, they maintained the water to ethanol volume ratio to 90/10 while varying the assembly temperature. In the experiments done, mesoporous silica products assembled at 90 volume % water showed a similar behavior where an increase in assembly temperature results in the increase in pore diameter. However, since the synthesis using oleylamine surfactants covered most of the possible water/ethanol ratios, the results gave a bigger picture on how the surfactant aggregates at different temperatures and water/ethanol ratios. For silica products assembled using Armeen OLD, the expected increase in pore diameter is observed from 50 – 100 % water fractions. When the water fraction decreases to 40 to 10 percent, an increase in temperature has an opposite effect where the smaller pore diameters are

observed at higher temperature. This result can be attributed to the greater solubility of the surfactant at elevated temperature. The high ethanol fractions already make the surfactant more soluble in the dispersing medium thus less surfactant molecules aggregates to form micelles. Moreover, the increase in temperature also increases the movement of molecules thus disrupting the H-bonding interaction of the H₂O molecules solvating the micelle. The presence of water solvating the micelle increases the diameter of the micelle but at elevated temperatures, some of these water molecules are lost.

Figure 2.31 presents the variation of pore sizes with respect to temperature as a function of water to ethanol ratio. The plot shows a different trend as opposed to oleyl-NH₂. In all cases except for A100-60 (100 volume % water at 60°C using Armeen OLD), silica products obtained at room temperature have bigger pores than the products obtained at 45° and 60°C. For materials assembled at 60°C, all have bigger pore sizes except for A10-60 (10 volume % water at 60°C using Armeen OLD) as opposed to silica products assembled at 45°C. Compared to oleyl-NH₂, the results did not show a shift in the trend for pore sizes. This suggests that more factors come into play for the assembled mesoporous silica using Duomeen O. The diamino functionality of the surfactant gives it greater stability with regards to the micelle that is produced. The presence of the diamino functionality gives more sites for H-bonding thus making the micelle less prone H-bonding disruptions due to an increase in temperature. Moreover, the headgroup of the surfactant also increases the amount of H₂O hydrating the micelle thus increasing its apparent size. This also might explain

why at elevated temperature, the templated silica products have smaller pore sizes since it will be expected that there will be less water of hydration around the micelle.

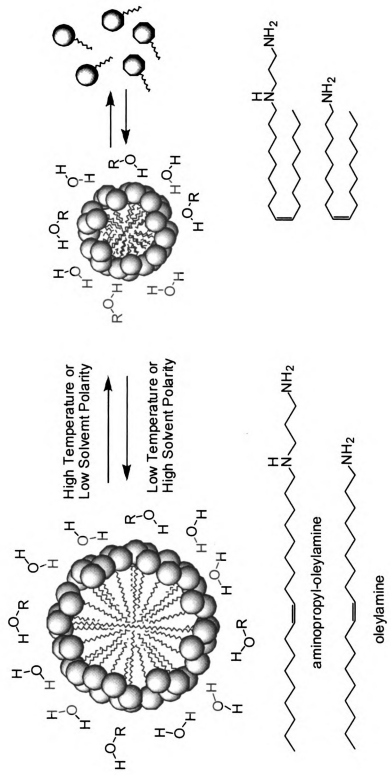


Figure 2.28 Schematic illustration on how the oleyl surfactant decreases their hydrophobe chain length.

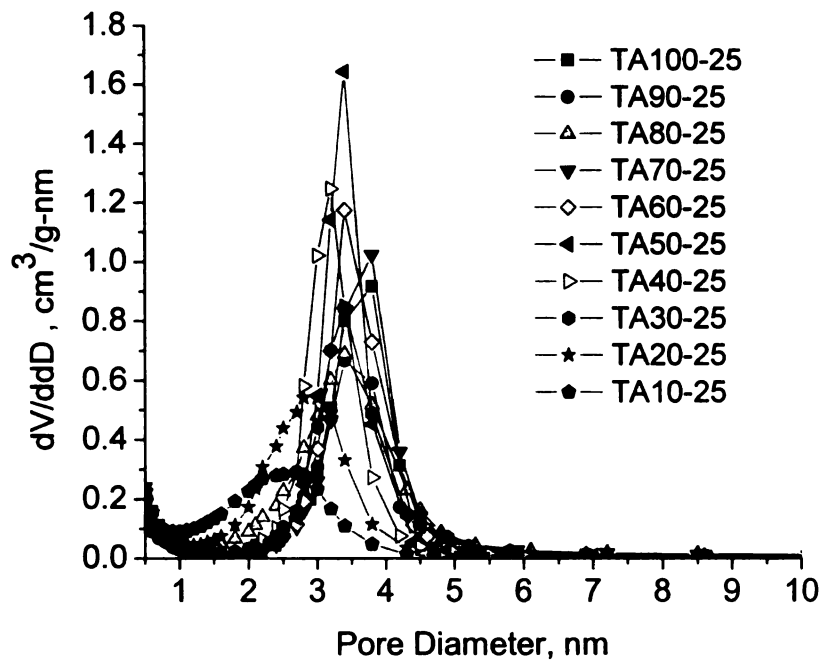
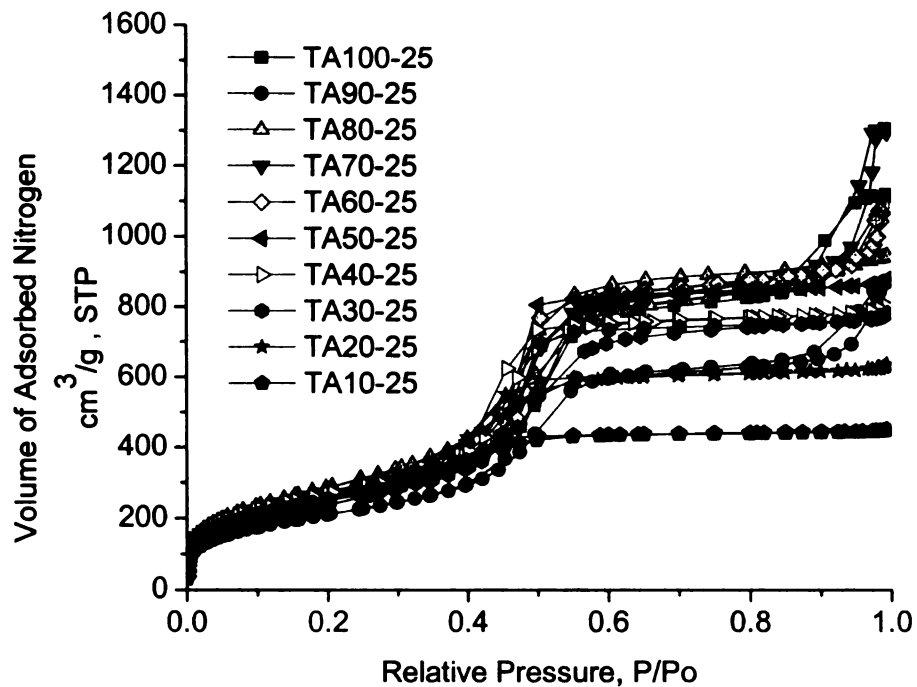


Figure 2.29 Nitrogen isotherms (top) and BJH pore size distributions (bottom) of mesostructured silicas synthesized from tallow amine (TA) at 25 °C under varying water fractions (10-100%).

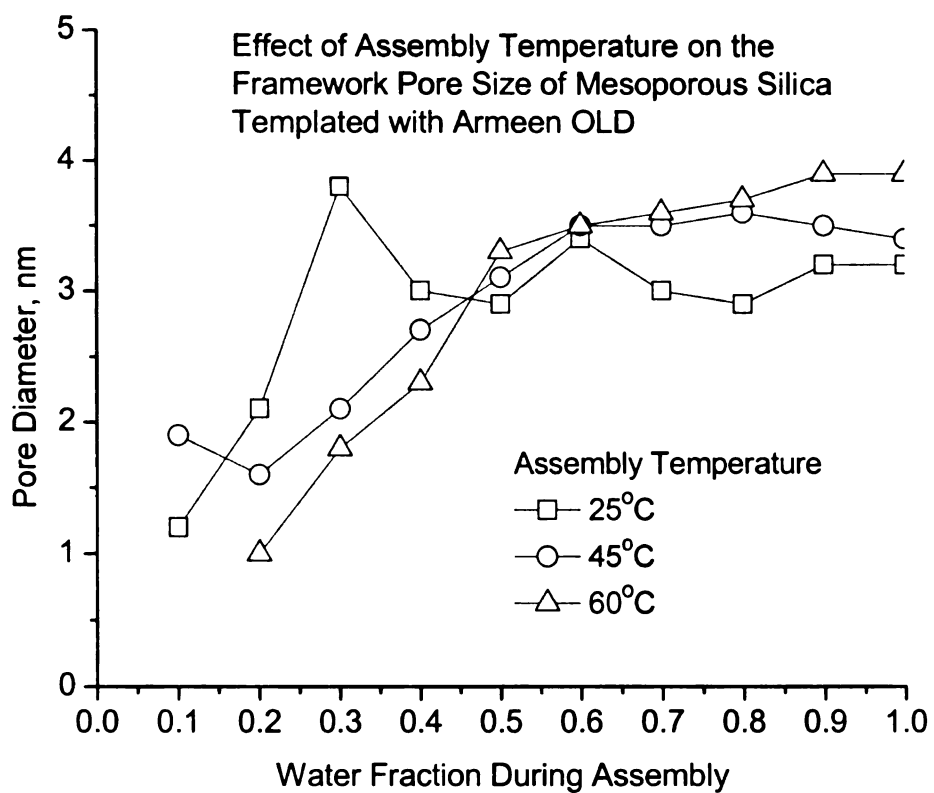


Figure 2.30 Pore size variations of mesoporous silicas assembled under varying water fractions using Armeen OLD (oleyl-NH₂) with respect to temperature variations. (Note: A10-60 (10 volume % water) was not included in the plot since it did not produced a mesostructured silica.)

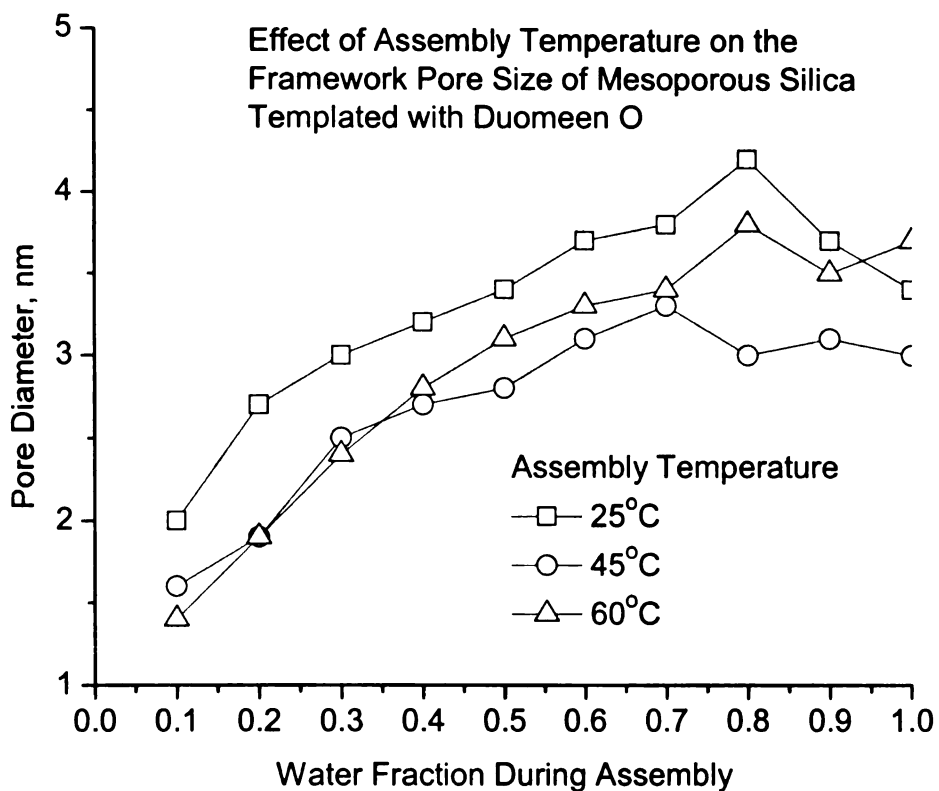


Figure 2.31 Pore size variations of mesoporous silicas assembled under varying water fractions using Duomeen O (oleyl-NH(CH₂)₃NH₂) with respect to temperature variations.

2.5 Conclusions

Among the oleylamine surfactants that were investigated on their ability to template a mesostructured silica, Ethomeen (oleyl-N(CH₂CH₂OH)₂) did not produce a mesoporous silica with well defined pores on both water-rich and ethanol-rich media. This conclusion is based on the results obtained from the powder x-ray diffraction where the product obtained using Ethomeen showed no low angle diffraction peak typical of mesostructured wormhole structures and the lack of mesoporous adsorption step in nitrogen adsorption isotherms.

The attempted synthesis of well ordered hexagonal mesoporous silica similar to MCM 41 using Ethoquad (oleyl-N⁺(CH₂CH₂OH)₂CH₃) was not successful as evidenced by the lack of the characteristic peaks in the low angle powder x-ray diffraction.

Ethomeen (oleyl-(CH₂CH₂OH)₂) and Ethoquad (oleyl-(CH₂CH₂OH)₂CH₃) did not produce mesostructures but instead produce high surface area silica gels at 25°C regardless of the polarity of the reaction medium. This result was attributed to the hydroxyl ethyl group present on the head group of the surfactant. The relatively bulky hydroxyl ethyl group poses steric hindrance on the H-bonding interactions for the case of Ethomeen and electrostatic interaction for the case Ethoquad.

Armeen DMOD (oleyl-N(CH₃)₂) did not produce a good mesostructured silica. This is evidenced by the weak diffraction peak on the powder XRD and very weak mesopore adsorption step on its nitrogen adsorption isotherm. This result is attributed to the weakened H-bonding interaction due to the presence of

the methyl groups on the nitrogen. Replacing the H atoms of Armeen OLD (oleyl-NH₂) with methyl groups reduces the sites for possible H-bonding interactions between the surfactant and oxygen atoms of the silica framework.

Among the five surfactants surveyed for the assembly of mesoporous wormhole silicas, oleyl-NH₂ and oleyl-NH(CH₂)₃NH₂ are judged to be the best among the oleylamine surfactant template. Both surfactants produced better mesostructured wormhole silica as compared to dodecylamine (DDA) template products when the synthesis is done under water-rich (70 volume %) media as evidenced by the volume of adsorbed nitrogen and the framework pore volume. The powder x-ray diffraction peaks also suggest the presence of lamellar structures on the products obtained. Although mesoporous silica products of both surfactants are superior to DDA in water-rich media, under ethanol-rich media, both produced silica with lower framework pore volume as opposed to DDA. The templating properties of the latter two surfactants was used on the succeeding steps of the study in an effort to determine the effects of solvent polarity and assembly temperature on framework structure and pore size.

Mesostructured silica templated by Duomeen O and Armeen OLD under varying solvent polarities and temperatures were successfully synthesized. TEM images revealed that the silica products have a wormhole pore network with some fractions having a lamellar morphology. The mesostructured mesoporous silicas synthesized from these two templates have pore structures that extend into the super-microporous range. Also, the two surfactants are able to produce mesostructured silica over the entire super-microporous range of 1-2 nm by

merely modifying the solvent polarity. This capability of the surfactant is attributed to the double bond present on the hydrophobe. This double bond provides a kink for the surfactant tail to fold into a hairpin structure that assembles into micelles of smaller diameters. At higher solvent polarity the surfactant favor the elongated conformation that results to larger pore diameters. Parallel studies of mesoporous silica products assembled using tallow amine template showed that the double bond on the hydrophobic tail plays a key role in the supramolecular assembly of supermicroporous silica. At high ethanol volume fractions (10-20 volume % ethanol), the tallow amine surfactant did not template silica products with pore sizes below 2 nm.

The effect of temperature on the products also was observed. The effect of temperature on silica products templated using Armeen OLD and Duomeen O showed very different trends. For Armeen OLD (oleyl-NH₂), high water fraction (50-100 volume % water) synthesis along with elevated temperature results to increased pore size while low fractions (< 30 volume % EtOH) results in a decrease in pore size. As for silicas assembled using Duomeen O, it is observed that the pore size of the materials assembled at room temperature are bigger than those silicas assembled at elevated temperature. It is hypothesized, that there are more water hydrating the Duomeen O micelle because of the two amino groups on the hydrophilic tail thus results to a bigger micelle diameter. At elevated temperature, the H-bonding interactions get disrupted and the amount of water molecules solvating the micelles are less thus the smaller micelles.

Overall, the assembly of mesostructured silica material using Armeen OLD for all water/ethanol ratios is best carried out under a 45°C temperature. This temperature provides more control over the morphology and pore dimensions of the mesoporous silica products because at this temperature where one can assemble silicas with low and high textural porosities with similar pore size distribution. As for Duomeen O, the best assembly temperature would be at 60°C. The diamino functionality of surfactant template gives it more sites for H-bonding thus giving it the flexibility for elevated temperature assembly. The 60°C, the silica products have better pore size fidelity as evidenced by the nitrogen adsorption isotherms and the BJH pore size distribution.

2.6 References

1. Beck, J. S. Vartuli, J. C., Roth, W. J., Leonowicz, M.E., Kresge, C.T. Schmitt, K. D., Chu, C.T-W., Olsom, D.H., Sheppard, E.W., McCullen, B., Higgins, J.B., Schlenker, J.L. *J. Am. Chem. Soc.* **1992**, *114*, 10834
2. Kresge, C.T., Leonowicz, M.E., Roth, W. J., Vartuli, J.C., Beck, J.C. *Nature* **1992**, *359*, 710
3. Hou, Q.S., Margolese, D.I., Stucky, G.D. *Chem Mater.* **1996**, *8*, 1147
4. Wan, Y. and Zhao, D. *Chemical Reviews* **2007** *107*, 7 2821-2860
5. Beck, J.S., Vartuli, J.C., Kennedy, G.J., Kresge, C.T., Roth, W.J., Schramm, S.E. *Chem. Mater.* **1994** *6*, 1816-1821
6. Zhao, D.Y., Feng, J.L., Huo, Q.S. Melosh, N. Fredrickson, G.H., Chmelka, B.F., Stucky, G.D. *Science* **1998**, *279*, 548-552
7. Zhao, X.S., Lu, G.Q. *J. Phys. Chem. B* **1998**, *102*, 1556-1561
8. Zhao, D.Y.Q., Huo, Feng, J.L. Chmelka, B.F., Stucky, G.D. *J. Am. Chem. Soc.* **1998**, *120*, 6024-6036
9. Tanev, P.T.; Pinnavaia, T.J. *Science* **1995**, *267*, 865-867
10. Pauly, T.R.; Pinnavaia, T.J. *Chem. Mater.* **2001**, *13*, 987
11. Bagshaw, S.A., Prouzet, E. Pinnavaia, T.J. *Science* **1995**, *269*, 1242-1244
12. Bagshaw, S.A. and Pinnavaia, T.J. *Angew. Chem-Int. Edit. Engl.* **1996**, *35*, 1102-1105
13. Cheng, C.F., Zhou, W., Klinowski, J. *Chem. Phys. Lett.* **1996**, *263*, 247
14. Corma, A., Kan, Q., Navarro, M.T., Perez-Pariente, J., Rey, F. *Chem. Mater.* **1997**, *9*, 2123
15. Khushalani, D.; Kuperman, A., Ozin, G.A., Tanaka, K.; Garces, J.; Olken, M.M.; Coombs, N. *Adv. Mater.* **1995**, *7*, 842
16. Sayari, A., Liu, P. Kruk, M. Jaroniec, M. *Chem Mater.* **1997**, *9*, 2499
17. Sayari, A., Kruk, M. Jaroniec, M. Moudrakovski, I. *Adv. Mater.* **1998**, *10*, 16, 1376
18. Sayari, A., Liu, P., Kruk, M., Jaroniec, M. *J. Phys. Chem B* **1999** *103*, 4590
19. Sayari, A. *Angew. Chem. Int. Ed.* **2000** *39*, 2920

20. Lettow, J.S., Han, Y.J., Schmidt-Winkel, P., Yang, P.D., Zhao, D.Y., Stucky, G.D., Ying, J.Y. *Langmuir*, **2000**, 16, 8291
21. Blin, J.L., Su, B.L. *Langmuir*, **2002**, 18, 5303
22. Jana, S.K., Nishida, R., Shindo, K., Kugita, T., Namba, S. *Microporous Mesoporous Mater.* **2004**, 68, 133
23. Park, B.G., Guo, W.P., Cui, X.G., Park, J.Y., Ha, C.S. *Microporous Mesoporous Mater.* **2004**, 68, 133
24. Hanrahan, J.P. Copley, M.P., Ryan, K.M., Spalding, T.R., Morris, M.A., Holmes, J.D. *Chem. Mater.* **2004** 16, 424
25. Prouzet, E., Pinnavaia, T.J. *Angew. Chem. Int. Ed. Engl.* **1997**, 35, 5, 516
26. Pauly, T.R., Pinnavaia, T.J. *Chem Mater.* **2001**, 13, 987-993
27. Patarin, J., Lebeau, B. Zana, R. *Curr. Opin. Colloid Interface Sci.* **2002**, 7, 107
28. Chen, X.Y., Huang, L.M. Li, Q.Z. *J. Phys. Chem. B.* **1997**, 101, 8460
29. Di Renzo, R., Testa, F., Chen, J.D., Cambon, H., Galarnau, A. Plee, D., Fajula, F. *Microporous Mesoporous Mater.* **1999**, 121, 8835
30. *Nanoparticles and Nanostructured Films* (Ed: J.H. Fendler), Wiley-VCH, Weinheim, **1998**
31. Park, M., Harrison, C., Chaikin, P.M. Register, R.A., Adamson, D.H. *Science*, **1997**, 276, 1401
32. *Metal Nanoparticles* (Eds: Feldheim, P.M., Foss, C.A. Jr. Marcel Dekker, New York **2002**
33. Cheng, J.Y., Ross, C.A., Chan, V.Z.H., Thomas, E.L. Lammertink, R.G.H. Vancso, G.J. *Adv. Mater.* **2001**, 13, 1147
34. Spatz, J.P., Chan, V.Z.H., Mobmer, S. Moller, M. Herzog, T., Krieger, M., Boyen, H.G., Ziemann, P. *Langmuir*, **2000**, 14, 407
35. Spatz, J.P., Chan, V.H.Z., Mobmer, S., Kamm, F.M., Plettl, A., Ziemann, P., Moller, M. *Adv. Mater.* **2002**, 14, 1827
36. Zhou, Y., Antonietti, M. *Adv. Mater.* **2003**, 15, 17, 1452-1455
37. Bagshaw, S.A., Hayman, A.R. *Chem. Commun.* **2000** 533
38. Bagshaw, S.A., Hayman, A.R. *Adv. Mater.* **2001**, 13, 1011-1013

39. Sun, T. Wong, M.S., Ying, J.T. *Chem Commun.* **2000**, 2057
40. Yuan, Z.Y., Zhou, W., Peng, L.M. *Chem. Lett.* **2000**, 1150
41. Zhou, Y., Antonietti, M. *Chem. Mater.* **2004**, 16, 544-550
42. White, J., Edler *Chem. Mater.* **1997**, 9, 1226
43. Pauly, T.R., Liu, Y., Pinnavaia, T.J., Billinge, S.J.L., Rieker, T.P. *J. Am. Chem. Soc.* **1999**, 121, 8835-8842
44. Iler, R.K. *The Chemistry of Silica.* **1979**. John Wiley & Sons. New York

Chapter 3. Encapsulation of Polymeric Neutral Amine Surfactant on Mesoporous Silica

3.1 Introduction to Mesoporous Silica Functionalization

The advent of mesoporous materials opened new possibilities for the catalysis of compounds that large for processing over traditional zeolite catalysts. In order to expand the usefulness of high surface area mesoporous silica, organic functionality must be introduced. Catalysis and environmental remediation are two areas where functionalized mesostructures are employed. The incorporation of the appropriate functional group on the pore walls tunes the mesoporous silica for a particular application. For instance, the introduction of amine functionality into the mesoporous framework pores can allow for arsenate adsorption^{1,2} or as a basic catalyst.^{3,4} Thiol functionalization makes the mesoporous silica suitable for mercury adsorption.^{5,6} In addition, the fields of protein immobilization,⁷⁻⁹ drug delivery systems¹⁰⁻¹² and chiral catalysis¹³⁻¹⁴ also are probable applications for functionalized mesoporous silica materials. Aside from their inherently large pores, mesoporous silicas have the advantage of greater catalytic activity and stability than modified silica gels.¹⁵ The two most common methods of introducing functionality into mesoporous silica are post-synthesis grafting and direct assembly (co-condensation)

3.1.1 Post-Synthesis Grafting Technique

Post-synthesis grafting is a method of functionalizing silica where in the organic moieties are anchored through coupling to the hydroxyl groups on the surface of the incompletely condensed silica. Figure 3.1 illustrates the post-synthesis grafting technique. Beck and co-workers were the first to employ this technique using chloromethylsilane as a coupling agent.¹⁶ Since then, this approach has been used to add a variety of organic functionalities to MCM-41,⁶ SBA-15¹⁷ and HMS² wormhole silicas. Mesoporous cellular foams (MCF) are attractive for the immobilization of bulky molecules such as enzymes and the separation of proteins. The large pore size in the 30 nm range enables the accommodation of bulky functional groups for separation and reactions of large molecules. MCF's have been functionalized by a two-step grafting approach for protein separation and the immobilization enzymes like chloroperoxidase.^{18,19}

Post-synthesis grafting method has several drawbacks. The lack of control over the distribution of silanol groups on the surface of the silica can yield islands of functional groups that lead to limited loading.⁶ Also for calcined silicas, the silica has to be rehydrated to regenerate the surface silanol groups that have been lost during the calcinations process. This adds another step to the process. This grafting method also is limited by the possibility of the organofunctionalized silica condensing onto itself which can lead to pore blockage.²⁰ Furthermore, the surface area and the framework pore volume can be compromised upon organic modification by post-synthesis grafting.^{1,21-23} Concomitantly, as the organic loading is increased, the more pronounced is the decrease in surface area and

framework pore volume. Also, the accessibility of the grafted derivatives typically is less than that of derivatives made by directly assembled material.

3.1.2 Direct Assembly / Co-Condensation

As shown in Figure 3.2, direct Assembly is a method of functionalizing mesoporous silica wherein the organosilane co-condense with the inorganic silica precursor in the initial reaction mixture. The resulting products have the anhydrous formula $(\text{SiO}_2)_{1-x} (\text{LSiO}_{1.5})_x$, where L is the organic moiety and x is the fraction of the framework silicon centers that is functionalized. Thus the organic moiety is covalently bonded within the structure through the non-hydrolyzable Si-C bond. The advantage of this approach in comparison to the grafting method is that it affords greater loading for the organic functional group, fewer steps in the overall synthesis and a more homogeneous distribution of the organic functional groups. Until recently, direct-assembly method has been limited by the miscibility of the organosilanes and TEOS. This process has been extended to the use of sodium silicate as the inorganic silica source.²⁴⁻²⁵ Functionalities such as mercaptopropyl, aminopropyl, cyanopropyl and calyx[8]arene moiety have been incorporated into mesoporous silica using direct assembly approach.^{26,27}

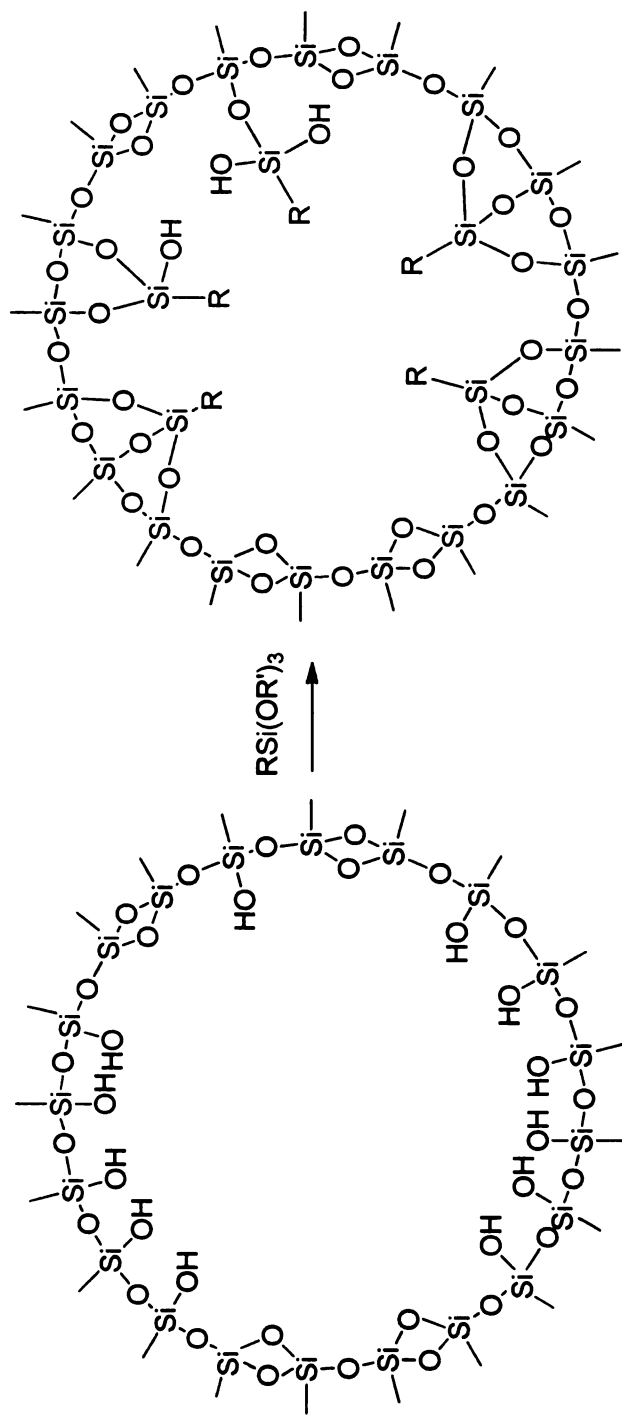


Figure 3.1 Schematic representation of the post-synthesis grafting technique for introducing organic functionality in the pore walls of mesoporous silica.

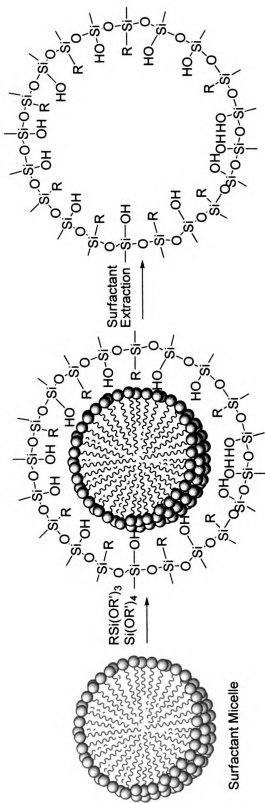


Figure 3.2 Schematic representation of direct assembly or co-condensation technique of introducing organic functionality in mesoporous silica.

The most commonly seen challenge in using the direct-assembly approach is the incorporation of the organic functional group into the wall so that the organogroup is oriented toward the pore surface and not on the pore wall making it inaccessible. Overall, direct assembly is the preferred method for organic incorporation, except for amines. The difficulty of incorporating amines using this approach is its reactivity. Under acidic conditions, the amine gets protonated and can interact with the silanol groups thus disrupting the interaction of the silane with the surfactant. Another problem with the basic nature of amines is that they can contribute to local hydrolysis that can result to the collapse of the mesostructure.

Stein and co-workers²¹ examined the stability and reactivity of vinyl group incorporated by direct assembly as opposed to grafting onto MCM-41. The use of the grafting technique afforded products with greater hydrothermal stability but the distribution of vinyl groups was not uniform. The grafting process allowed the hexagonal long range order of the material to be retained but directly assembled materials generally lose their long range order above 20% loading of the functionalized silane.

Mercier and Pinnavaia²⁸ also compared various organo-functionalized mesoporous wormhole silica prepared by direct assembly and grafting. Mesoporous wormhole silicas prepared by direct assembly method exhibited higher surface area and pore volumes. It was also observed that the directly assembled products displayed a more uniform distribution of functional groups in the pore channels as opposed to grafted mesoporous wormhole silica, as judged

by the narrower pore distributions from the Horvath-Kawazoe method of pore distribution.

3.1.3 Polymerization of Surfactants

Although Freedman and co-workers²⁹ synthesized potassium styryl undecanoate and studied the 'poly soap' properties of its copolymers in 1958, the first premeditated and attempted micellar polymerization of an amphiphilic monomer reported in open literature appears to be the work of Hyde and Robb.³⁰ In their work, they synthesized undecenyltrimethylammonium bromide and undecenyl sulfate and polymerized these and sodium oleate above their critical micelle concentration (CMC) in order to produce stabilized micelles. Larrabee and Sprague³¹ in 1979 reported micelle polymerization using γ -irradiated aqueous micelles of sodium 10-undecanoate. They confirmed their observation by the disappearance of the vinyl signals in the ¹H-NMR spectrum. Further studies on the polymerization of sodium 10-undecenoate were done by Paleos and co-workers,³² wherein they demonstrated using electrical conductivity measurements that the 'polymerized micelle' exhibited a CMC equal to zero.

The polymerization of allyldimethyldodecylammonium bromide under bulk and micellar conditions has been reported by Paleos and co-workers.^{33,34} Photochemical and thermal polymerization in quantitative yield was reported, but this result was not reproduced by the groups of Rodriguez³⁵ and McGrath.³⁶ In all of these reports, the polymerization has been carried out above the CMC.

Emulsion polymerization is an area where polymerizable surfactants or surfmers (surfactant monomers) are used. Studies have shown that incorporating a polar group such as a surfactant molecule on the surface of the latex particle adds stability to the emulsion and helps prevent the coagulation of the emulsion upon aging. Polymerization of alkyl methacrylate,⁴¹⁻⁴³ acrylate⁴³ and maleate⁴⁴⁻⁴⁶ surfactants has also been studied. Surfmers have been used to make polymeric⁴⁷ and barium sulfate⁴⁸ nanoparticles and as a possible drug delivery system.⁴⁹

Sherrington published several papers describing the synthesis and characterization of mono and divalent quaternary cationic surfmers.³⁷⁻⁴⁰ He questioned the report of 'polymerized micelles' by Paleos, saying that the term insinuates topochemical polymerization, that is, the linking the monomers in such manner that the final polymer mirrors the parent micelle. He argued that micellar systems are dynamic systems. There exists a rapid exchange of surfactant molecules between micelles that occurs in the time scale range of 10^{-5} - 10^{-9} s and the complete breaking and reforming of the micelle occurs on the average every 10^{-3} - 10^{-2} s. Because the average rate of chain propagation during polymerization is 10^{-6} - 10^{-2} s, the rate of surfactant exchange between micelles should be faster than polymerization, leading to the belief that topochemical polymerization is extremely unlikely.^{38, 50-52} Instead, he proposed a more accurate model based on the formation of oligomeric species that exhibit micellar properties,³⁸ as shown in Figure 3.3.

The influence of monomer reactivity and the position of the polymerizable group within the surfactant on the nature of the polymerized species has been emphasized. Surfmers can be classified as T-type if the polymerizable group is located at the hydrophobic tail or H-type if the polymerizable group is located on the hydrophilic end of the surfactant. ⁵¹

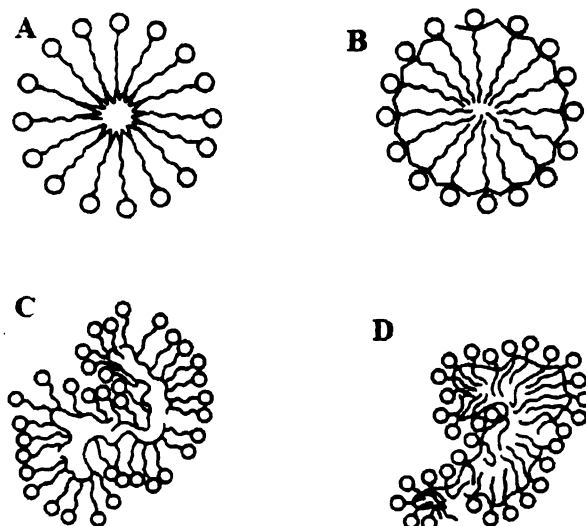


Figure 3.3 Two dimensional, highly idealized polymeric micelle with polymerizable group on the hydrophobic tail (A) and on the hydrophilic head (B); C-D: Sherrington's concept of a polymerized micelle with polymerizable group on the hydrophobic tail (C) and on the hydrophilic head (D).

It also was observed that polymerization for T-type surfmers was faster than for H-type surfmers. This observation was readily explained by the higher concentration of the methacrylate groups in the interior of the micelle for a T-type surfmer and by the electrostatic repulsions between adjacent headgroups which retards the propagation rate of the H-type surfmer.

3.1.4 Polymerization In Mesoporous Silica

Several studies have been reported regarding the encapsulation of organic polymers inside mesoporous silica materials. Polyaniline polymerization inside MCM-41 has been reported by Bein and co-workers.¹⁷ Such systems, wherein conjugated polymers with mobile charge carriers are confined within nanometer-size galleries, can be considered a significant step toward designing nanoscale electronic devices.

Moler and co-workers studied the polymerization of methyl methacrylate inside microporous and mesoporous silica⁵³. It was observed that the resulting polymer has distinct properties compared with the bulk polymer. Tolbert and co-workers⁵⁴ showed that semiconducting polymers aligned inside mesopores exhibit unique energy transfer and photophysical properties that can be used for developing electronic and optoelectronic devices. Dendrimers⁵⁵ and polystyrene nanofibers^{27,28} have also been synthesized in the pores of mesoporous silica. In all these reports, the polymer completely fills the mesopores, resulting in a non-porous material.

In a recent paper by Ryoo and co-workers⁵⁶ a new way a new way was shown for functionalizing mesoporous silica. This involved polymerizing poly(chloromethylstyrene) in SBA-15 while keeping the mesopores open. It was noted that the micropores of SBA-15 play a crucial role in restricting the polymer layer to the mesopore surface and in stabilizing the entire polymer network. The poly(chloromethylstyrene) polymer inside the mesoporous is a good starting

material for transformation into other functional groups suited for ion exchange, catalysis and protein immobilization.

3.1.5 Heavy Metal Trapping Using Mesoporous Silica

Heavy metals in water can be harmful to ones health. This has been enough for researchers to engage in extensive research for trapping metals from water. Traditional methods of trapping metals include the use of activated carbon, zeolites, silica gel, sulfide precipitates, ion exchange resins and clays.⁵⁸ The low loading capacity and poor selectivity have impeded the use of these materials for remediation purposes. Mesoporous materials overcome these factors, which makes them a very good candidates for trapping metals. The metals that were previously studied were arsenic,⁵⁸ copper,⁵⁹ zinc,⁵⁹ mercury,^{6,58} palladium,^{60,61} platinum,^{60,61} cadmium⁶¹ and nickel.⁶¹ The amine functional groups were the best for trapping copper ions. The thiol functional group has a high affinity for trapping mercury in aqueous media. Radioactive element trapping has also been demonstrated for mesoporous silica. One ligand that is known to bind with an actinide cation is carbamoylphosphine oxide (CMPO). The CMPO MCM-41 have been shown by Fryxell et al to be highly efficient and selective in binding plutonium⁶²

3.2 Objectives

In Chapter 2, two oleyl surfactants, namely oleyl-NH₂ (Armeen OLD) and oleyl-NH(CH₂)₃NH₂ (Duomeen O) were identified as potential candidates for trapping lead. But since Duomeen O is capable of chelating metal ions, the efforts were concentrated on using this templating agent for the synthesis of mesoporous silica for lead trapping. The extra amino group suggests greater trapping capacity and the formation of a more stable coordination compound due to chelate effect.

For this part of the study, mesoporous silica derivatives are prepared using the Duomeen O surfactant and divinyl benzene (DVB) as a cross-linking agent. An effort was made to incorporate the maximum amount of polymeric complexant inside the framework structure in order to optimize the trapping capacity. The amount of the encapsulated complexant was determined quantitatively, as well as its resistance to leaching. Finally, the cross-linked products were evaluated for their ability to trap lead ions in solution.

3.3 Experimental

3.3.1 Co-Polymerization of the Templating Agent Inside HMS Wormhole Mesostructures with Divinylbenzene as the Cross-linker

Initial attempts to polymerize Duomeen O using azobisisobutyronitrile (AIBN) as initiator showed no success. The internal double bond in the oleylamine chain is sterically hindered and its polymerization by a radical

pathway is limited. This was circumvented by adding a crosslinking agent, divinyl benzene to facilitate the polymerization process.

Initial polymerization attempts were done by varying the mole ratio of oleylamine surfactant to divinylbenzene, DVB over the range of 1.0:0.1 to 1.0:0.5). The highest yield of copolymer was obtained at the ratio of 1:0.5. Thus, this ratio was used for polymerization within the framework walls of the mesostructure. The addition of DVB also raised the question if the surfactant will still be capable of templating mesostructured silica. This was addressed by the hypothesis that DVB will behave like trimethylbenzene (TMB) as a co-surfactant when added to the reaction mixture. TMB still permit the formation of mesostructures although with expanded pores.

The incorporation of a polymeric templating agent inside the framework pores of mesostructured silica can be approached in two ways. As can be seen on Figure 3.4, the template can be polymerized prior to the formation of mesostructure (pre-assembly polymerization) or the mesostructure can first be assembled and the template polymerized later (post-assembly polymerization).

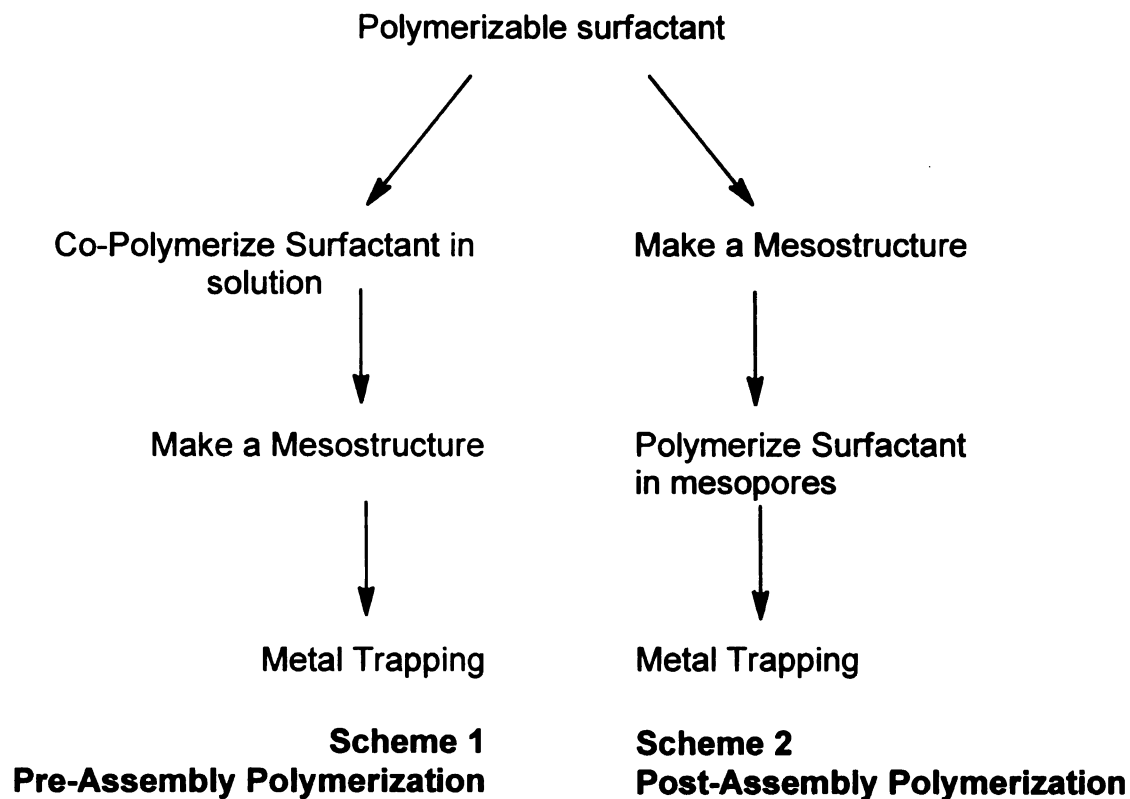


Figure 3.4 Two possible schemes on incorporating a polymeric complexant inside mesoporous silica materials.

Scheme 1 Pre-Assembly Polymerization

The oleylamine surfactant (0.013mol) was added the desired mixture of ethanol and water (see to Table 3.1) in a round bottom flask. Then the divinyl benzene (DVB, 0.87g, 0.007mol) was added followed by the addition of the initiator. This reaction mixture was stirred until all the AIBN (0.034g, 0.0002mol) was completely dispersed. The mixture was then heated to 90°C for 3 hours. After the polymerization, the resulting product was cooled to room temperature. TEOS was then added and the reaction mixture was stirred for 15 hours. The reaction products were separated from the mother liquor by filtration followed by washing with copious amount of deionized water. The mesoporous silica

products were then air dried. Some of the sample was calcined at 620°C for 4 hours for TEM analysis.

Scheme 2 Post-Assembly Polymerization

The oleylamine surfactant (0.013mol) was added into a mixture of ethanol and water (see to Table 3.1) in a polypropylene bottle. Then the divinyl benzene (DVB, 0.87g, 0.007mol) was added, followed by the addition of the initiator. This reaction mixture was stirred until all the AIBN (0.034g, 0.0002mol) was completely dispersed. TEOS was then added and the reaction mixture was stirred for 15 hours at room temperature. The reaction products were separated from the mother liquor by filtration. The DVB was expected to reside inside the micelle template of the as-made mesostructure. Copolymerization with the surfactant was achieved by placing the freshly filtered product in a 90°C oven for 2 hours.

Table 3.1. Wormhole Silica Products Synthesized in 60 volume % Ethanol Media.

	<i>Mass of Surfactant</i>	<i>Mass of DVB</i>	<i>Mass of Initiator</i>	<i>Volume of H₂O</i>	<i>Volume of Ethanol</i>
Oleyl-NH(CH ₂) ₃ NH ₂	4.36g	0.87g	0.034g	22.4mL	33.6mL

Mole Ratio: 1 SiO₂ : 0.27 Surfactant : 0.135 DVB
 Initiator: AIBN @ 1mol % of Surfactant + DVB

3.3.2 Leaching Studies

One of the goals of this study is to synthesize a mesoporous silica material with an entrapped polymeric complexant that also serve as a structure-directing agent for mesoporous silica. The polymeric complexant has to be resistant to leaching from the framework pores. The use of the interconnected framework pores of a wormhole structure is considered to be a good approach to preventing the polymeric complexant from leaching since a polymer can get entangled within the 3D framework pore network.

To examine whether the polymer inside the mesoporous wormhole resists leaching, the material was subjected to two types of extraction experiments using ethanol and water as solvents for extraction. For the water extraction experiment, 0.4 g of the as-made mesoporous silica-copolymerized surfactant composite was added to 200 mL of deionized water was added. This mixture then was stirred overnight. The composite was separated from water through filtration and air-dried. The pore volumes of the products before and after water extraction were compared by thermal gravimetric analysis.

For the ethanol extraction experiments, 1.0 g of the mesoporous silica was measured into a 350 mL round bottom flask. Absolute ethanol (150 mL) was added and this mixture was refluxed for 15 hours. The silica was separated from ethanol by filtration and air-dried. The pore volumes of the products before and after ethanol extractions were compared by nitrogen adsorption isotherms.

3.3.3 Lead (II) Trapping by Batch Studies

Preparation of Standards

A 500 ppm, 1 L lead stock solution was prepared by dissolving 0.64 g of $\text{Pb}(\text{NO}_3)_2$ (99.999 %) in water. From this solution, aliquots of Pb(II) were taken to prepare the standards for the calibration curve for the analysis through atomic absorption spectroscopy. Standard solutions were prepared with lead concentrations in the range of 1-100 ppm Pb(II).

Trapping Pb(II) in Water using Mesoporous Silica with Encapsulated Polymeric Complexant

Approximately 0.1g mesoporous silica composite was measured into 250mL polypropylene bottles. Then, a 100mL of a 100 ppm aliquot of Pb(II) solution was added. This mixture was then allowed to equilibrate with stirring at room temperature for 15 hours. The mesoporous silica was separated from solution by filtration and the filtrate was analyzed by atomic absorption spectroscopy.

3.3.4 Characterization

The products were characterized using powder X-ray diffraction (XRD) and nitrogen adsorption-desorption isotherms. The powder X-ray diffraction (XRD) patterns were obtained using a Rigaku Rotaflex Diffractometer with $\text{CuK}\alpha$ radiation ($\lambda = 0.154\text{nm}$). Counts were accumulated every 0.02 degree (2θ) at a scan speed 0.5 degree per minute.

N₂ adsorption-desorption isotherms were obtained at -196°C on a Micromeritics Tristar 3000 sorptometer. Samples were outgassed under vacuum at 100°C for 16 hours. BET surface areas were calculated from the linear part of the BET plot according to IUPAC recommendations.

Transmission electron microscopy (TEM) images were obtained on a JEOL 2200FS with an accelerating voltage of 200kV. Samples were prepared by sonicating powdered samples in ethanol for 15 minutes and evaporating two drops of the suspension onto a carbon coated film supported on a 3 mm, 300 mesh copper grid.

Atomic absorption spectroscopy was employed to determine the lead trapped in mesoporous silica by determining the concentration of Pb(II) left in the filtrate. The difference in the initial and final concentration of Pb(II) in the filtrate provided the amount of Pb(II) trapped. Pb(II) was analyzed using a Varian Spectra AA 200 Model in flame absorption mode at 283.3 nm wavelength.

Thermal gravimetric analysis was done using a thermobalance (TGA 7, Perkin-Elmer) coupled with a thermal analysis controller (TAC 7/DX, Perkin-Elmer) was employed. The instrument was calibrated with “alumel” alloy and nickel for temperature settings and with a 100-mg standard for weight accuracy. Approximately 5 mg of each sample were added to a tared aluminum balance pan. The pan was then placed in the furnace at room temperature, and the exact sample weight was determined. The temperature was then increased to 100 °C at the rate of 10 °C min⁻¹, and the sample was held at this temperature for 15 min to remove any residual water. Thereafter, the sample was heated to 800 °C

at the rate of 10 °C min⁻¹. Air was chosen as the sample purge gas (flow of 50 cm³ min⁻¹), whereas N₂ was used as balance purge gas at the flow rate of 75 cm³ min⁻¹.

3.4 Results and Discussions

Synthesis and Leaching Studies

As mentioned earlier, the neat oleylamine surfactant does not polymerize due to steric limitations. The addition DVB as a crosslinker solved this problem, but it also raised the issue of whether the surfactant will still be able to template a mesostructured silica. The initial goal was to evaluate the mesoporous silica templated by the crosslinked surfactant. Another goal was to attempt the crosslinking of the surfactant in the as-made mesostructure.

Figure 3.5 shows the low angle powder x-ray diffraction of a mesostructured silica obtained by pre- and post-assembly crosslinking of the oleyl surfactant. The diffraction peaks show the pore-pore correlation typically seen for a mesostructure with a wormhole framework structure. The product obtained by post-assembly crosslinking shows a diffraction peak typical of wormhole pore structure. On the otherhand, the material obtained through pre-assembly surfactant cross-linking suggests the presence of layered structure based on the sharpness of the diffraction peak. TEM images (Figure 3.6 and 3.7) show the pore structures of the two products. The TEM images also revealed the suspected layered structure of the materials. The structure of the silica products

synthesized is a combination of wormhole and layered structure similar to the previously synthesized silica without DVB.

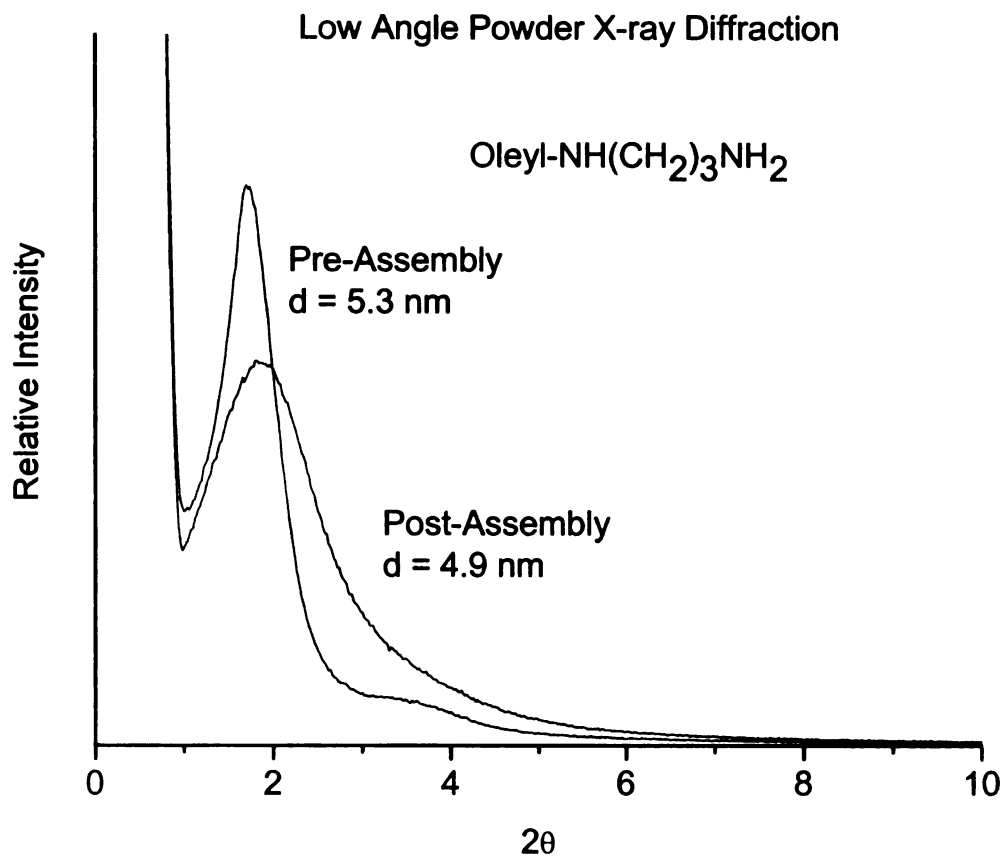


Figure 3.5 Low angle powder x-ray diffraction pattern of crosslinked oleyl surfactant in mesostructured silicas made by pre-assembly and post-assembly crosslinking of the surfactant porogen.

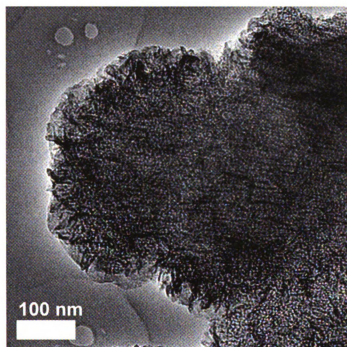
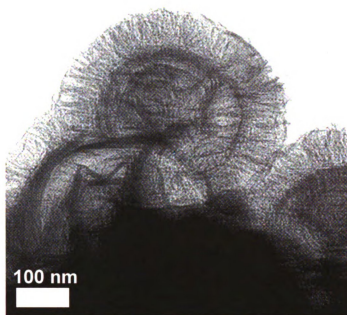


Figure 3.6 Representative TEM images mesostructured silica assembled in the presence of oleyl surfactant cross-linked by divinylbenzene prior to the addition of TEOS (pre-assembly crosslinking).

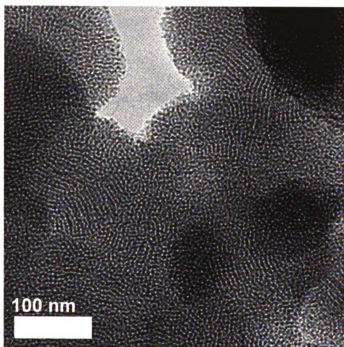
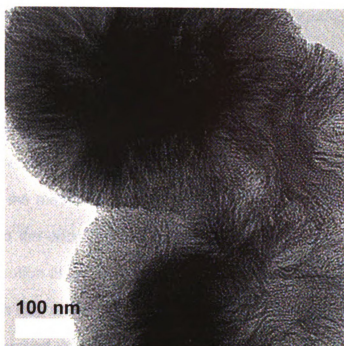


Figure 3.7 Representative TEM images calcined mesostructured silica assembled in the presence of oleylamine surfactant followed by crosslinking of the surfactant by divinylbenzene.

The formation of mesostructured silica from a divinylbenzene crosslinked oleyl surfactant is a bit counterintuitive. Sherrington described a polymerized micelle as being irregularly shaped. For a surfactant template to give rise to a narrow and uniform pore distribution, the surfactant micelle should be regularly shaped. The representative nitrogen adsorption isotherms and BJH pore distributions for the mesoporous silica assembled by polymerizing the surfactant template prior to the addition of TEOS are shown on Figure 3.8. Based on the BJH pore distribution plots, the narrow pore size distribution suggest a template that is uniform in size and shape. This suggests that the DVB crosslinked micelle must have preserved the topology of the micelle before polymerization. The kinetics of radical polymerization and micelle formation suggests that the polymerized micelle could not have preserved the spherical shape or its initial micellar shape. But the presence of the hydrating solvent may forced the micelle to adapt a shape other than the irregularly shape polymer that will minimize energy and maximize entropy in the mixture. It is plausible that the crosslinked micelle re-adapts a spherical or its original micellar shape to minimize its energy and maximize the entropy. This in turn permits the crosslinked surfactant to template a mesostructured silica with a very uniform pore distribution.

After evaluating the fidelity of the mesostructure silica produced, we step evaluated whether the crosslinked template could be leached out of the framework pores by ethanol extraction. This is best evaluated by examining the nitrogen adsorption isotherms in Figure 3.8 and 3.9.

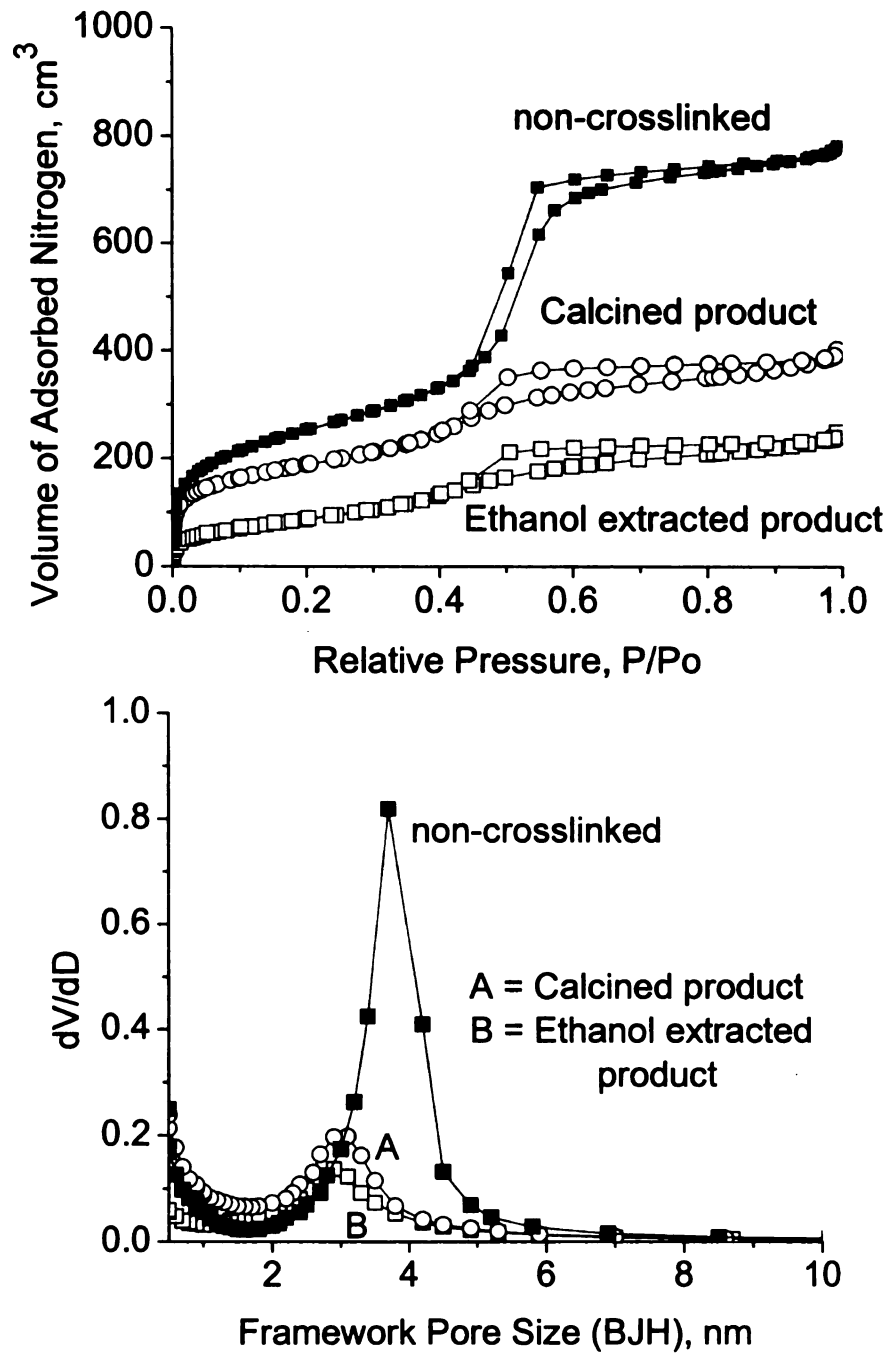


Figure 3.8 (Top) Nitrogen adsorption isotherms and (Bottom) BJH pore size distributions for non-crosslinked, calcined and ethanol extracted silicas made by pre-assembly DVB crosslinking of the surfactant.

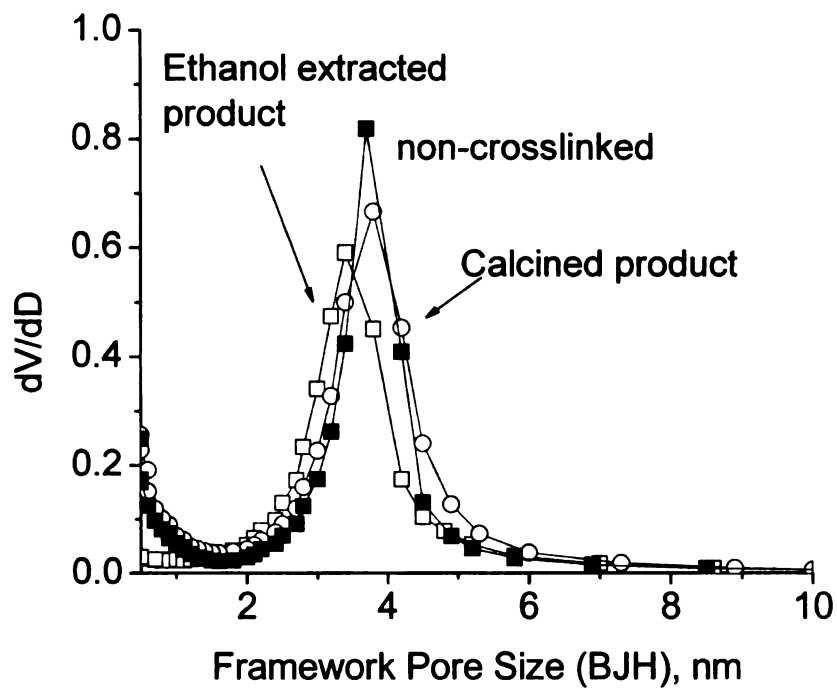
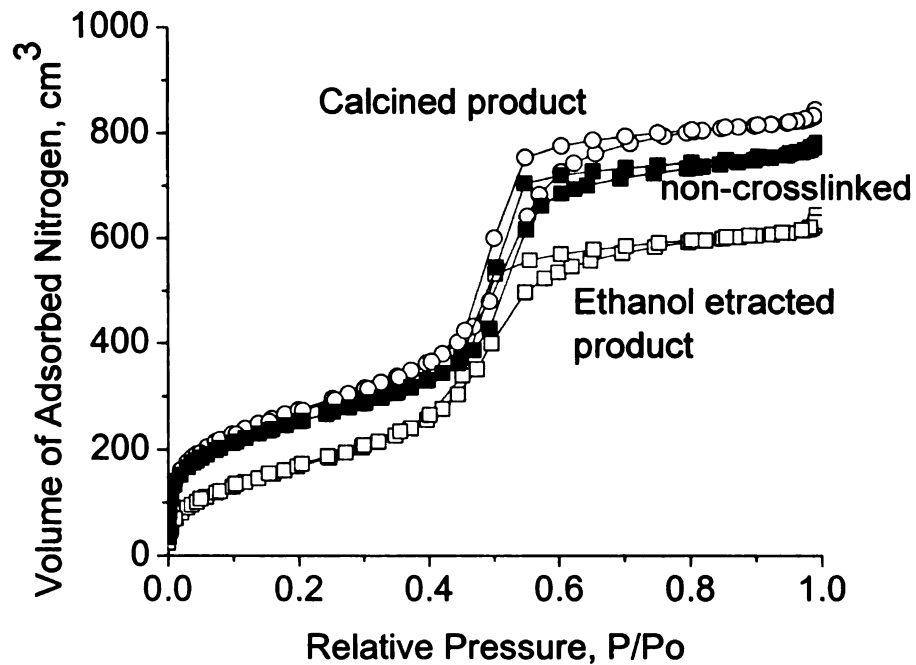


Figure 3.9 (Top) Nitrogen adsorption isotherms and (Bottom) BJH pore distributions for non-crosslinked, calcined and ethanol extracted silicas made by post-assembly DVB crosslinking of the surfactant.

Table 3.2 Summary of pore properties of calcined and extracted silica products assembled with crosslinked surfactant templates

Material	Calcined d-spacing, nm	Average Pore Diameter, nm	Wall Thickness, nm	BET Surface Area, m ² /g	Framework Pore Volume, mL/g (taken @ P/Po = 0.75)
Non-polymerized Duomeen O template	4.7	3.7	1.0	892.1	1.12
Calcined Pre-Assembly Crosslinked	5.3	3.1	2.2	642.3	0.58
Extracted Pre-Assembly Crosslinked	5.3	3.0	1.6	198.5	0.31
Calcined Post-Assembly Crosslinked	4.9	3.3	1.6	948.1	1.20
Extracted Post-Assembly Crosslinked	4.9	3.2	1.7	671.2	0.70

Ideally, non-porous materials are desired after ethanol extraction of the as-made products because this would mean that the polymerized surfactant resisted the leeching process. The nitrogen adsorption isotherms show that the ethanol extracted products are porous which means that a substantial fraction of the crosslinked surfactant leached out. On the basis of comparison of the nitrogen adsorption isotherms for the calcined and ethanol extracted materials synthesized by post-assembly crosslinking (Figure 3.8), there is a significant decrease in the volume of adsorbed nitrogen for the extracted sample compared to the calcined sample. Moreover, the partial pressure for mesopore adsorption occurs is about the same partial pressure for both products. This suggests that both products have about the same framework pore diameters. This also means

that the leaching process does not occur uniformly throughout the mesostructure. The crosslinked surfactant near the periphery of the mesoporous silica particle is extracted first and the crosslinked surfactant within the inner parts of the particle is retained. This explains why the partial pressure for the mesopore filling is not shifted after ethanol extraction.

Figure 3.9 also showed the same trend. Typically, an ethanol extracted mesophase would exhibit the same adsorption isotherm as with the calcined material. A single ethanol extraction is sufficient enough to remove most of the templating agent. The fact that the synthesized material with the polymerized template partially resisted complete extraction proves that the crosslinking of the surfactant template was successful. The partial extraction in ethanol more likely is due to the solubility of the polymerized surfactant in ethanol. The pore and surface area analysis are summarized in Table 3.2.

Comparing the nitrogen isotherms for the silicas with non-crosslinked surfactant template with the silicas with crosslinked templates, the silicas whose surfactant template was cross-linked after assembly (post-assembly crosslinking), the N_2 isotherm resembles that of the non-crosslinked product with a slightly higher framework pore volume as evidenced by the slightly volume of adsorbed nitrogen. This is explained by the expansion of the pores when DVB is added. The silicas whose surfactant template was crosslinked prior to the addition of TEOS (pre-assembly crosslinking) presented a different adsorption curve. This tells us that the micellar aggregates that templated the mesostructure is different from the non-crosslinked aggregates.

The extent of surfactant extraction using water was evaluated using TGA. The results for this experiment are shown in Figure 3.10. From the TGA plots, the as-made silica assembled from unpolymerized surfactant (A) contains about 55% organic surfactant. The extent of extraction by water is shown by curve B where the organic content of the water extracted product is about 10%, indicating that more than 80% of the surfactant template is extracted by water. C and D in Figure 10 represent the TGA plots for silica made by the pre-assembly crosslinking of the surfactant. The plots show that the material did not lose a significant amount of the weight and the TGA results reveal that there is about 10% increase in the organic composition of the material after water extraction. This slight increase in the percentage of organic component can be explained by the slight dissolution of some of the silica when the water extraction was conducted. This also demonstrates that the polymerized surfactant is not soluble in water.

Batch Studies of Pb(II) Uptake from Water

Lead exposure is hazardous to health. The EPA has set the levels for drinking water at zero mg/L though the maximum contaminant level for treatment technique was set at 0.015 mg/L (15ppb). Prolonged exposure to lead among infants can cause delays in physical or mental development and among children it can cause deficits in attention span and learning disabilities. Among adults,

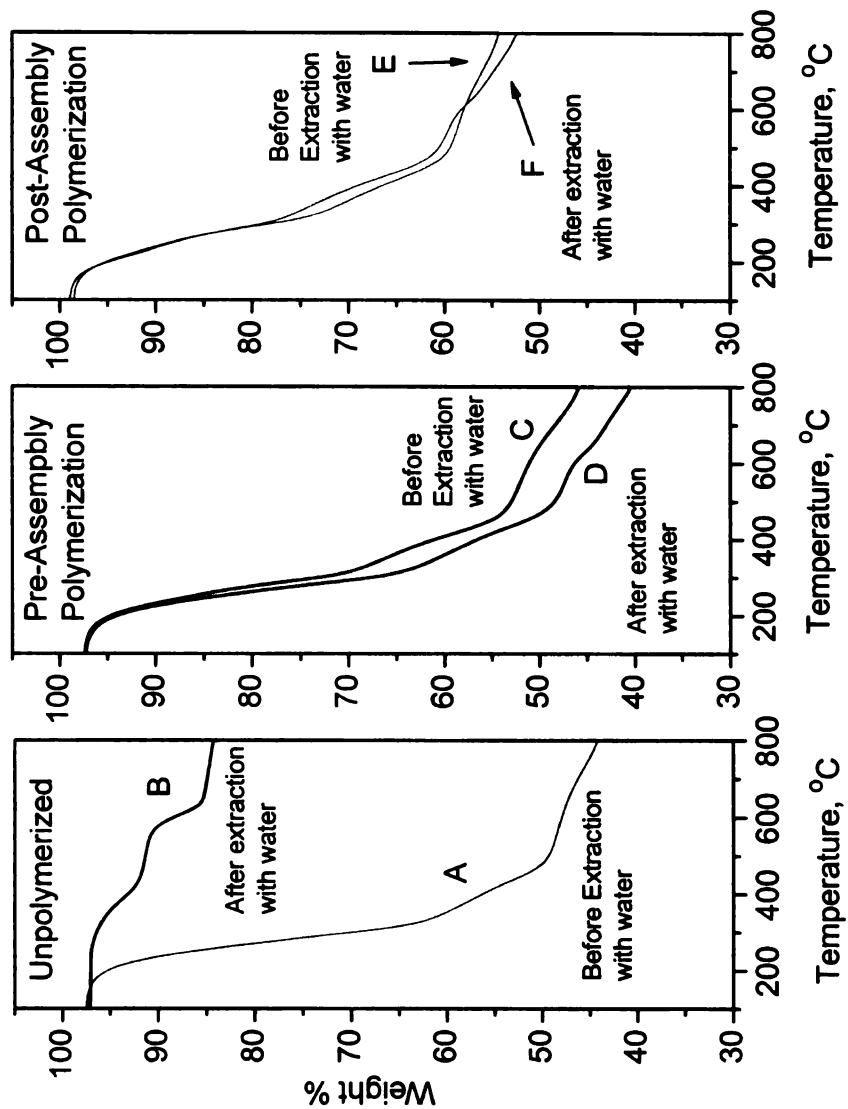


Figure 3.10 Thermal gravimetric analysis plots for: Left panel: A. As-made mesostructured silica templated with unpolymerized oleyl amine surfactant, B. Mesostructured silica from A after water extraction; Central Panel: C. Mesostructured silica whose surfactant template was crosslinked with DVB before supramolecular assembly(post-assembly crosslinking), D. Mesostructured silica C after water extraction; Right panel: E. Water extracted mesostructured silica material whose surfactant template was crosslinked after supramolecular assembly, F. Material E after water extraction.

Pb^{2+} can cause kidney problems and high blood pressure. Figure 3.11 shows the pH dependence of lead species in water at a concentration of 0.01M. From the species distribution, it is inferred that lead adsorption experiments should be done at pH below 8 where most of the lead is in cationic form and suitable for complexation.

Table 3.3 presents representative results for Pb(II) trapping by crosslinked oleyl amine surfactants encapsulated in mesoporous silicas. As-made and ethanol extracted mesoporous silica products with pre- and post-assembly crosslinked surfactant reduced the concentration of 100 ppm Pb(II) in water. The silica with post-assembly crosslinked template trapped the most Pb(II) with capacity of 0.4 mmol Pb(II)/g of as-made material while the silica with pre-assembly crosslinked template gave a lower amount of Pb(II) trapping capacity of 0.36 mmol Pb(II)/g of as-made product. The equilibrium N:Pb ratio revealed that the post-assembly crosslinked product was more efficient in trapping lead with ratio of N:Pb ratio of about 6.00 while the pre-assembly polymerized product has a N:Pb ratio of 7.54. The extracted counterparts of the as-made silica products gave lower trapping capacity which is expected since both have less surfactant content.

Figure 3.12 presents the curves for the uptake of Pb(II) under batch equilibrium conditions. The uptakes curves show that the as-made silica product containing pre-assembly crosslinked template has a capacity of trapped Pb(II) about 0.75 mmol per gram as-made silica with a N:Pb ratio of 3.63. The post-assembly polymerized silica has a lower uptake of about 0.55 mmol Pb(II) per

gram as-made silica with a N:Pb ratio of 3.73. Overall the difference in terms of the stoichiometry of the N:Pb is not significant for both material. The reason why there is a difference in the uptake capacity toward Pb(II) is due to the amount of encapsulated polymerized template. Pre-assembly crosslinking is slightly more effective in maximizing the polymeric complexant loading of the mesoporous silica. A possible explanation of this result lies in the assembly process. For the pre-assembly crosslinking approach, the template is already crosslinked after the condensation of the silica. Thus, washing the as-made sample with water after the removal of the mother liquor does not extract the surfactant template. On the other hand, in the post-assembly polymerization approach, the as-made silica products are washed with water after separating them from the mother liquor and in this step, there is a chance that some of the non-crosslinked surfactant template is extracted thus decreasing the amount of surfactant template available for the succeeding crosslinking step.

3.5 Conclusions

The synthesis of mesoporous silica with crosslinked oleyl diamine template was accomplished. The surfactant template is crosslinked with the use of DVB. Because internal double bond in the hydrophobic tail of the oleyl surfactant is sterically hindered, it is difficult for the surfactant to polymerize in neat. The use of DVB as a cross-linking agent circumvents this limitation. A 1:0.5 mole ratio of surfactant to DVB was found to be best for the synthesis of mesoporous silica with encapsulated polymeric complexant. The incorporation of

DVB in the as-made mesophase under post assembly crosslinking conditions occurs through adsorption inside the hydrophobic interior of the micelle.

Two approaches were used for the encapsulation of the surfactant complexant inside mesostructured silica, namely pre-assembly crosslinking by DVB and post-assembly DVB crosslinking. The low angle powder x-ray diffraction showed a single diffraction peak typical of wormhole to lamellar framework pores for the products obtained using both approaches. The nitrogen isotherms and the BJH pore size distributions showed well defined framework pores of ~3.0 nm. TEM images also revealed the wormhole and lamellar morphology of the mesoporous silica is similar to the silica products assembled without DVB. Of the two approaches both are effective in preventing the surfactant template from leaching from of the framework pores during the metal absorption process. The unpolymerized template of an as-made silica product is readily leached out into solution as shown by the TGA. The silica product obtained by pre-assembly polymerization has a slightly higher loading of polymeric complexant than the other silica product but it provides a much lower mesopore volume. This slight difference is attributed to the loss of surfactant during the washing of the as-made product before polymerization. The Pb(II) trapping studies have shown that the capacity of the silica product is dependent amount of complexant present as the ratio of N:Pb(II) for both silica products is about the same.

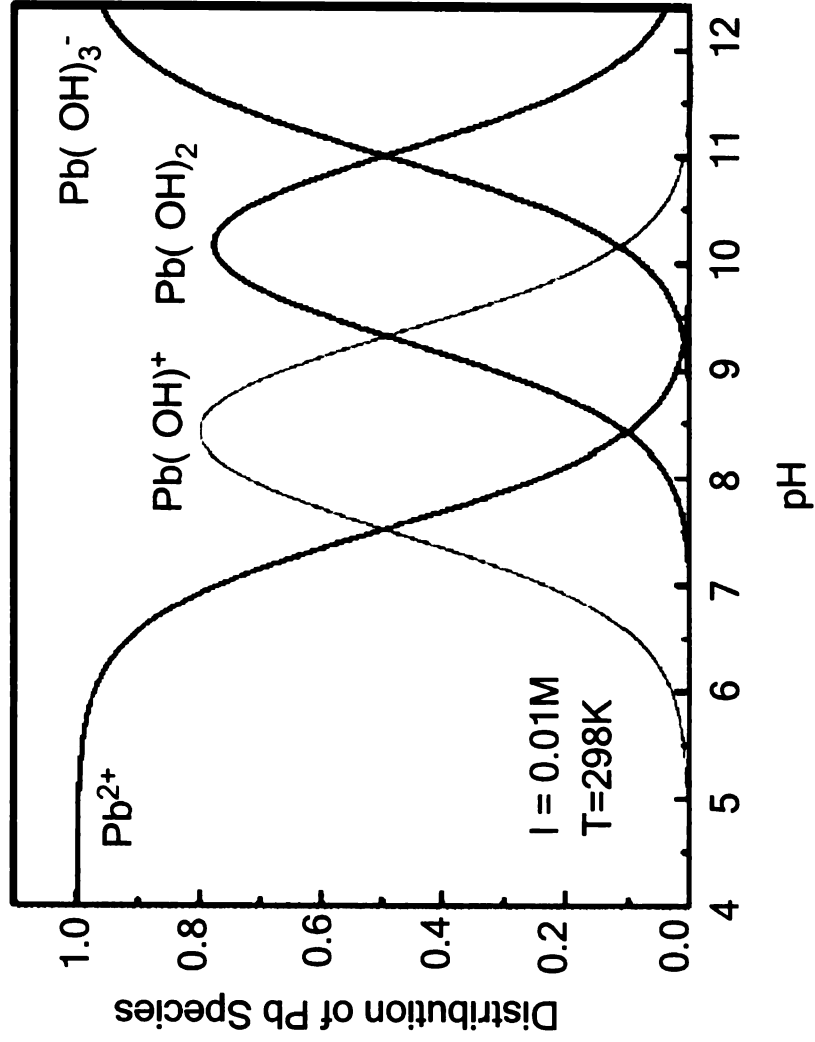


Figure 3.11 Distribution of Pb(II) species as a function of pH based on the equilibrium constants.

Table 3.3 Pb(II) uptake of mesoporous materials by crosslinked oleylamine surfactant encapsulated in mesoporous silica.

Material	Initial Pb(II), ppm	Free Pb(II), ppm	Pb(II) Removed, ppm	mmol Pb(II)/g	mmol N/g	N:Pb
Pre-Assembly, As-Made	100	24.83	75.17	0.361	2.72	7.54
Post Assembly, As-Made	100	10.21	89.79	0.405	2.42	5.99
Pre-Assembly, Ethanol Extracted	100	57.46	42.54	0.199	0.73	3.66
Post Assembly, Ethanol Extracted	100	54.73	45.27	0.204	0.83	4.07

Uptake experiments were carried out at ambient temperature under batch equilibrium conditions (equilibration time is 16 hours).

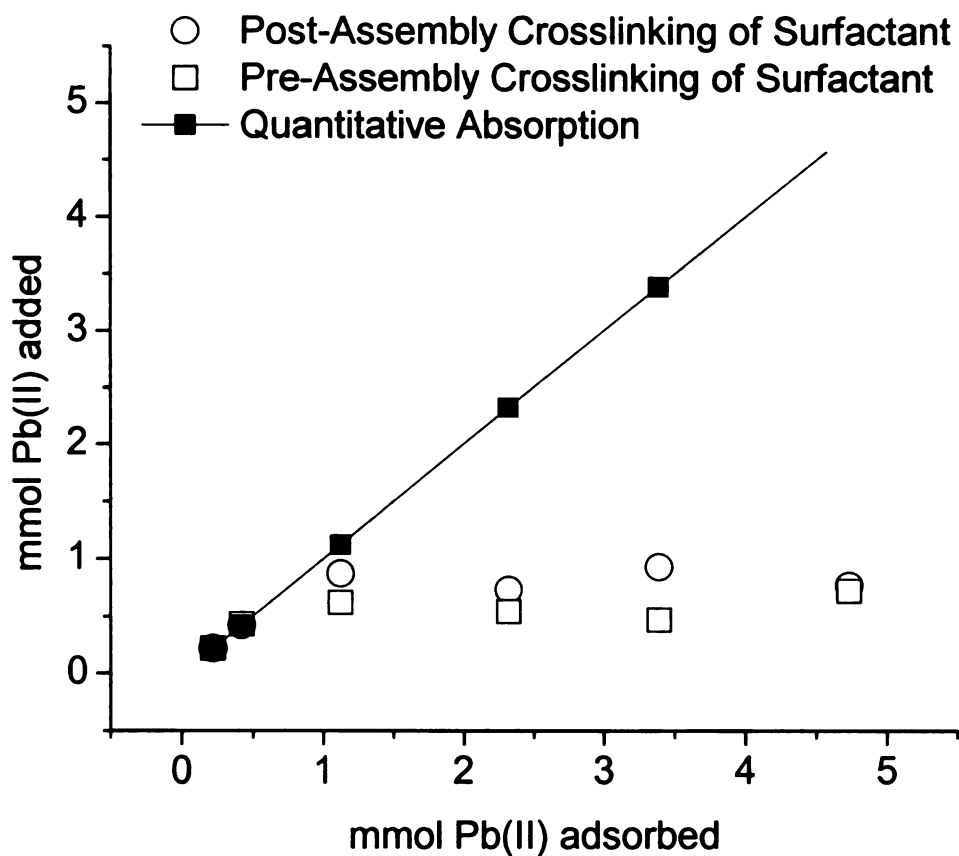


Figure 3.12 Pb(II) uptake by mesoporous silica with encapsulated crosslinked oleylamine surfactant as a complexant. The amount of Pb(II) added varied from 0.22 to 4.73 mmole Pb(II) per gram as-made material. The ratio of N : Pb for pre- and post-assembly polymerization are 3.63 and 3.73 respectively.

3.6 References

1. Fryxell, G.E., Liu, J., Hauser, T.A., Nie, Z.M., Ferris, K.F., Mattigod, S., Gong, M.L., Hallen, R.T. *Chem. Mater.* **1999**, 11, 2148-2154
2. Yoshitake, H., Yokoi, T., Tatsumi, T., *Chem. Mater.* **2002**, 14, 4603-4610
3. Mdoe, J.E.G., Clark, J.H., Macquarrie, D.J. *Synlett.* **1998**, 625-627
4. Rao, Y.V.S., De Vos, D.E., Jacobs, P.A. *Angew. Chem., Int. Ed. Engl.* **1997**, 36, 2661-2663
5. Mercier, L., Pinnavaia, T.J. *Adv. Mater.* **1997**, 9, 500
6. Feng, X., Fryxell, G.E., Wang, L.Q., Kim, A.Y., Liu, J., Kemmer, K.M. *Science*, **1997**, 276, 923-926
7. Takahashi, H., Inagaki, S., Kajino, T., Usuki, A., Li, B. *In Eur. Pat. Appl. (Kabushiki Kaisha Toyota Chuo Kenkyuso, Japan)*, Ep. **1999**, p 18
8. Yiu, H.H.P., Wright, P.A., Botting, N.P. *J. Mol. Catal. B. Enzym.* **2001**, 15, 81-92
9. Lei, C., Shin, Y., Liu, J., Ackerman, E.J. *J. Am. Chem. Soc.* **2002**, 124, 11242-11243
10. Kulak, A., Hall, S.R., Mann, S. *Chem. Commun.* **2004**, 576-577
11. Lai, C.Y., Trewyn, B.G., Jeftinja, D.M., Jeftinja, K., Xu, S., Jeftina, S., Lin, V.S.Y., *J. Am. Chem. Soc.* **2003**, 125, 4451-4459
12. Lin, V.S.Y., Lai, C.Y., Trewyn, B.G., *Abstracts of Papers, 225th ACS National Meeting, New Orleans, LA, United States, March 23-27, 2003* MTLS-029
13. Bellocq, N., Abramson, S., Lasperas, M., Brunel, D., Moreau, P. *Tetrahedron-Asymmetry* **1999**, 10 3229-3241
14. Johnson, B.F.G., Raynor, S.A., Shephard, D.S., Mashmeyer, T., Thomas, J.M., Sankar, G., Bromley, S., Oldroyd, R., Gladden, L., Mantle, M.D. *Chem. Commun.* **1999**, 1167-1168
15. Macquarrie, D.J. *Philos. Trans. R. Soc. London, Ser. A.* **2000**, 358, 419-430

16. Beck, J.S., Vartuli, J.C., Roth, W.J., Leonowicz, M.E., Kresge, C.T., Schmitt, K.D., Chu, C.T.W., Olson, D.H., Sheppard, E.W., McCullen, S.B., Higgins, J.B., Schlenker, J.L., *J. Am. Chem. Soc.* **1992**, 114, 10834-10843
17. Morey, M.S., O'Brien, S., Schwarz, S., Stucky, G.D. *Chem. Mater.* **2000**, 12, 898-911
18. Han, Y.J., Watson, J.T., Stucky, G.D., Butler, A. *J. Mol. Catal. B: Enzym.* **2002**, 17, 1-8
19. Schmidt-Winkel, P., Lukens, W.W., Zhao, D.Y., Yang, P.D., Chmelka, B.F., Stucky, G.D., *J. Am. Chem. Soc.* **1999**, 121, 254-255
20. Walcarius, A., Etienne, M., Lebeau, B., *Chem. Mater.* **2003**, 15, 261-2173
21. Pauly, T.R., Liu, Y., Pinnavaia, T.J., Billinge, S.J.L., Rieker, T.P. *J. Am. Chem. Soc.* **1999**, 121, 8835-8842
22. Lim, M.H., Stein, A. *Chem. Mater.* **1999**, 11, 3285-3295
23. Yokoi, T., Yoshitake, H., Tatsumi, T. *J. Mater. Chem.* **2004**, 14, 951-957
24. Shah, J., Kim, S.S., Pinnavaia, T.J., *Chem. Commun.* **2004**, 572-573
25. Yu, N. Gong, Y., Wu, D., Sun, Y., Luo, Q., Liu, W., Deng, F. *Microporous and Mesoporous Mater.* **2004**, 72, 25-32
26. Liu, C., Naismith, N., Fu, L., Economy, J. *Chem. Commun.* **2003**, 2472-2473
27. Liu, C., Lambert, J.B. *Polym. Mater. Sci. Eng.* **2003**, 88, 433-434
28. Mercier, L., Pinnavaia, T.J., *Chem. Mater.*, **2000**, 12, 188-196
29. Freedman, H.H.; Mason, J.P.; Medalia, A.I. *J. Org. Chem.* **1958**, 23, 76
30. Hyde, A.J.; Robb, D.J.M.; *J. Phys. Chem.* **1963**, 67, 2089
31. Larrabee, C.E. Jr.; Sprague, E.D. *J. Polym. Sci. Polym. Lett. Ed.* **1979**, 17, 749-751
32. Paleos, C.M.; Stassinopoulou, C.I.; Milliaris, A. *J. Phys. Chem.* **1983**, 87, 251-254
33. Paleos, C.M.; Dais, P. *Rec. Adv. Liq. Cryst. Polym.* **1985**, 6, 1985
34. Paleos, C.M.; Babilis, D. *J. Polym. Sci. Part A: Polym. Chem.* **1988**, 26, 2141-2156

35. Rodriguez, J.L.; Soltero, J.F.A.; Puig, J.E.; Schulz, P.C.; Espinoza-Martinez, M.L.; Pieroni, O. *Colloid Polym. Sci.* **1999**, *277*, 1215-1219
36. McGrath, K.M. Drummond, C.J. *Colloid Polym. Sci.* **1996**, *274*, 316
37. Sherrington, D.C. ; Hamid, S.M.; *Polymer*, **1987**, *28*, 325
38. Sherrington, D.C. ; Hamid, S.M.; *Polymer*, **1987**, *28*, 332
39. Joynes, D.; Sherrington, D.C. *Polymer*, **1996**, *8*, 1453
40. Joynes, D.; Sherrington, D.C. *Polymer*, **1997**, *38*, 1427-1438
41. Eastoe, J.; Summers, M. *Chem. Mater.* **2000**, *12*, 3533-3537
42. Summers, M.; Eastoe, J.; Davis, S.; Du, Z. Richardson, R.M.; Heenan, R.K.; Steytler, D.; Grillo, I. *Langmuir* **2001**, *17*, 5388-5397
43. Eastoe, J.; Summers, M. *Langmuir* **2003**, *19*, 6357-6362
44. Guyot, A.; Goux, A. *J. Appl. Polym. Sci.* **1997**, *65*, 2289-2296
45. Zicmanis, A.; Hamaide, T.; Graillat, C. Monnet, C.; Abele, S.; Guyot, A. *Colloid Polym. Sci.* **1997**, *275*, 1-8
46. Montoya, A.; Sherrington, D.C. *Polymer* **1999**, *40* 1067-1079
47. Herold, M.; Brunner, H.; Tovar, G.E.M. *Macromol. Chem. Phys.* **2004**, *204*, 770-778
48. Summers, M.; Eastoe, J.; Davis, S. *Langmuir*, **2002**, *18*, 5023-5026
49. Scholz, C. Iijima, M.; Nagasaki, Y.; Kataoka, K. *Polym. Adv. Technol.* **1998**, *9*, 768-776
50. Hamid, S.; Sherrington, D. *J. Chem Soc., Chem. Commun.* **1986**, 936-938
51. Eastoe, J.; Summers, M. *Adv. Coll. Interf. Sci.* **2003**, *100-102*, 137-152
52. Tajima, K.; Aida, T. *Chem. Commun.* **2000**, 2399-2412
53. Moller, K.; Bein, T.; Fischer, R.X. *Chem. Mater.* **1998**, *10*, 1841-1852
54. Acosta, E.J.; Carr, C.S.; Simanek, E.E.; Shantz, D.F. *Adv. Mater.* **2004**, *15*, 985

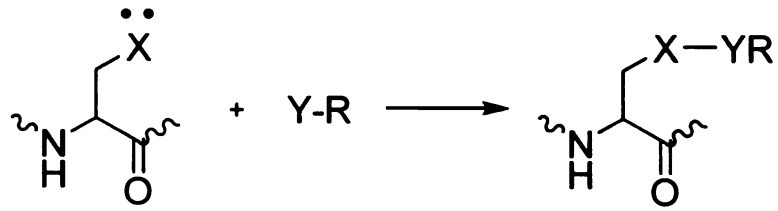
55. Choi, M.; Kleitz, F.; Liu, D.; Lee, H.Y. Ahn, W.S, Ryoo, R. *J. Am. Chem. Soc.* **2005**, *127*, 1924-1932
56. Dais, P.; Paleos, C.M.; Nika, G.; Milliaris, A. *Makromol. Chem.* **1993**, *194*, 445-450
57. McKimmy, Emily Jane. Supramolecular Assembly of Organofunctional Mesostructures: Synthesis, Characterization and Application in Environmental Remediation. *Unpublished Dissertation. Department of Chemistry. Michigan State University.* (2005)
58. Dai, S., Burleigh, M.C., Ju, Y.H., Gao, H.J., Lin, J.S., Pennycook, S.J., Barnes, C.E. & Xue, Z.L. *J. Am. Chem. Soc.* **2000**. *122*, 992-993
59. Kang, T.; Park, Y.; Yi, J. *Ind. Eng. Chem. Res.* **2004**, *43*, 1478-1484
60. Kang, T. Park, Y. Choi, K. Lee, J.S & Yi, J. *J. Mater. Chem.* **2004** .*14*, 1043-1049
61. Birnbaum, J.C.; Busche, B.; Lin, Y.; Shaw, W.J. Fryxell, G.E. *Chem. Commun.* **2002**, 1374-1375

Chapter 4. Phosphoprotein Enrichment Using Grid Supported Mesoporous Metal Oxide Thin Films

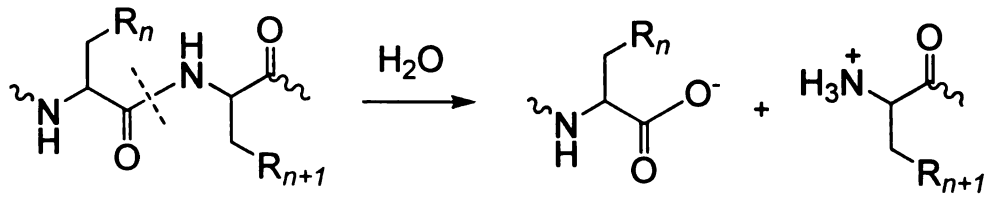
4.1 Introduction to Post-translational Modification

The proteome is the inventory of all the proteins in a cell or organism. There are two major mechanisms in which the proteome is expanded beyond that what can be predicted by the genes in eukaryotic organisms. The first route for diversifying proteins occurs at the transcriptional level through mRNA splicing including the tissue specific alternate splicing which is the central topic in RNA metabolism in eukaryotic biology.^{1,2} The second route for proteome diversification and expansion is through covalent post-translational modification (PTM). These covalent modifications occur after the DNA has been transcribed into RNA and translated into proteins.³ Hundreds of enzymes are dedicated to such protein modifications. In general, post-translational modification can occur either through the covalent addition of a chemical group or by the cleavage of a protein backbone. (See Figure 4.1)

PTM achieved through covalent addition reaction includes phosphorylation, acylation, alkylation, glycosylation and oxidation. The resulting modified proteins comprise the phosphoproteome, acyl proteome, alkyl proteome, glycoproteome and the oxidized proteome subsets. (See Figure 4.2)



Covalent modification



Cleavage of Protein Backbone

Figure 4.1 The two general schemes for post-translational modification: covalent modification and covalent cleavage.

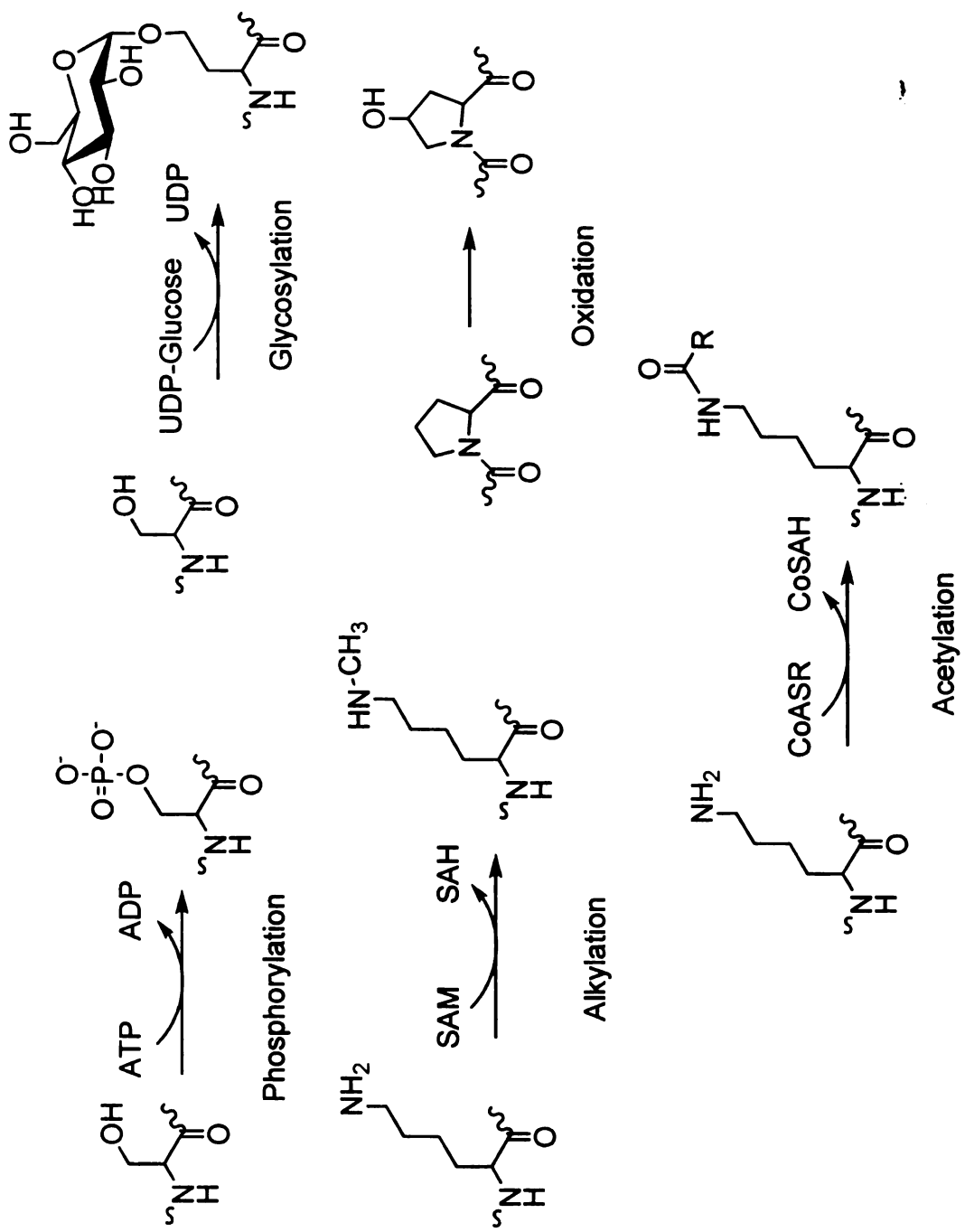


Figure 4.2 The five major types of covalent additions to protein side chains.



17

18

Directed post-translational modifications enable the expansion of distinct covalent forms of proteins beyond that is predicated by DNA encoding. Presently, the phosphorylation of proteins is the most studied and best understood pathway among PTMs. It is also the most ubiquitous among the PTMs.

4.1.1 Background on Protein Phosphorylation

Beginning with the isolation of phosphoserine of Levene and Lipmann, protein phosphorylation has turned out to be one of the most biologically relevant and ubiquitous post translational protein modifications.^{5,6} Phosphorylation is a reversible modification process effecting both the folding and function of proteins and regulating essential functions such as cell division, signal transduction, enzymatic activity, cell cycle, cell proliferation and differentiation.^{6, 7} It has been estimated that about 30-50% of proteins are phosphorylated at some point ⁸ and about 2-3% of the genes in the entire eukaryotic genome are involved in the phosphorylation process.⁹ It is further estimated that one-third of all cellular functions are directly or indirectly affected by protein phosphorylation.¹¹ Among the amino acids that can be phosphorylated, the ortho-phosphates are the most abundant, mostly attached to serine, threonine and tyrosine residues. Phosphorylation of serine and threonine residues is more frequent than on tyrosine with an approximate ratio of 1800:200:1 for pSer/pThr/pTyr respectively. Phosphoramidates of arginine, histidine and lysine also occur, as do acyl derivatives of aspartic and glutamic acid, but they are less abundant.^{12,13} (See Figure 4.3)

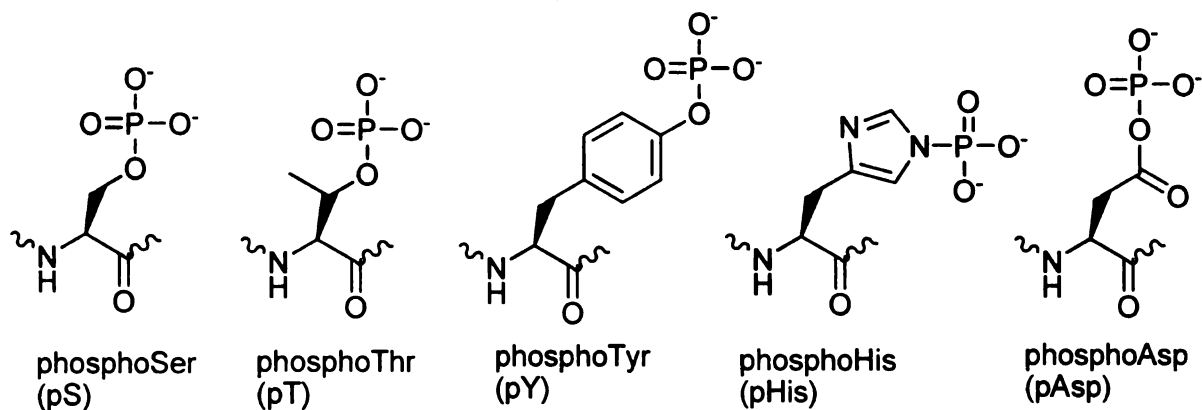


Figure 4.3 The phosphorylated amine residues.

The disruption of the phosphorylation and dephosphorylation events involved in signal transduction pathways has been implicated in diseases such as cancer,^{14,15} type II diabetes,^{16,17} cystic fibrosis¹⁸ and Alzheimer's disease.^{19,20}

Given the importance of protein phosphorylation in cell function, one must conclude that the characterization of the phosphoproteome will be the key to understanding the mechanism of cellular processes and in identifying targets for therapeutic intervention.¹⁰ The great interest in acquiring a complete knowledge of phosphorylation mechanisms also is due to the fact that more than a hundred different protein kinases have been implicated in human cancer.²¹ It is therefore not surprising that protein kinases have emerged as the most studied class of new drug targets in oncology and other disease areas.²² Approximately 100,000 potential phosphorylation sites are present in the human proteome and currently very little is known about them. This emphasizes the need for sensitive, high-throughput methods to identify, characterize and monitor new sites of protein phosphorylation.¹³

Traditional methods have been long employed in studying and detecting phosphopeptides such as gel electrophoresis and radiolabeling of phosphopeptides or proteins.^{23,24,26-29} The use of these methods is well documented but they do require a large initial amount of protein samples. The advancement of technology in mass spectrometry has greatly improved the study of the phosphoproteome. Mass spectrometry when combined with phosphoprotein enrichment methods is the analytical tool of choice given its speed and sensitivity.^{6,23,25}

Even with the development of mass spectrometry, proteomic techniques relevant to the elucidation of signal transduction have lagged in development when compared to genomic technologies. The challenge is due to the complexity of cellular samples and the low stoichiometry of the phosphoproteins when compared to the non-phosphorylated counterparts. This makes it necessary to develop efficient enrichment technologies for studying the phosphoproteome at the cellular level. Through enrichment technologies, the complexity of cellular samples is reduced.

Phosphoproteomics focuses on the analysis of protein phosphorylation and makes use of mass spectrometry (MS) and specific methods to purify phosphorylated proteins and peptides.³⁰⁻⁴³ However, the use of mass spectrometry in analyzing the phosphoproteome is far from becoming a routine. Aside from the inherent problem of substoichiometric phosphorylation, three other reasons as to why phosphorylation analysis is so problematic are often quoted, including increased hydrophilicity of the phosphopeptide with a

concomitant loss during the loading onto reversed-phase columns, selective suppression of their ionization/detection efficiencies in the presence of large amounts of unphosphorylated peptides, and lower detection efficiencies of phosphopeptides as compared with their unphosphorylated cognates.

Phosphopeptides are often lost during loading onto the reversed-phase columns because the addition of anionic/acidic phosphate groups increase the hydrophilicity resulting in reduce retention. This is one reason why LC/MS failed. Steen and co-workers³⁶ hypothesized that phosphorylation indeed increases hydrophilicity. However if the peptide contains basic amino acid residues that are positively charged under standard LC/MS conditions, the increase in hydrophilicity can be overcompensated by charge neutralization. The presence of a phosphate group decreases hydrophilicity thus increasing the LC retention time as long as the positive net charge decreases but once the phosphate groups exceeds the number of basic residues, the hydrophilicity increases again. The same group also tested the notion of phosphorylated species being selectively suppressed in the presence of unmodified peptides. They found that there is no significant change in the signal intensity of the phosphorylated peptide in the presence of a 100-fold excess of non-phosphorylated peptides. To test further peptide/phosphopeptide pairs, samples were spiked with 1000-fold excess of tryptic bovine serum albumin (BSA) digest. As expected, the signal intensity of the peptides and phosphopeptides were significantly reduced but no selective suppression was observed. The common belief that phosphopeptides showed lower ionization/detection efficiencies that their non-phosphorylated

cognates could not be substantiated as a general fact. When testing the peptide/phosphopeptide pairs using liquid chromatography in combination with electro spray ionization – mass spectrometry (LC/ESI-MS), the majority of the phosphopeptides tested actually showed better ionization/detection than their unmodified cognates. This indicates that LC combined with ESI-MS is a good choice for routine phosphorylation analyses.

Despite the recent advancements in mass spectrometry, lability of the phosphate group under mass spectrometry conditions can lead to dominant neutral losses of H_3PO_4 (98 Da) and HPO_3 (80 Da) in MS and MS/MS analyses makes peptide sequencing and phosphorylation site assignment more difficult.^{40,41}

4.1.2 Enrichment of Phosphoproteins

The major challenge for the application of phosphoproteomics lies within successfully isolating phosphoproteins from the whole cell lysate with a focus on identification of low abundant phosphoproteins. To date, several strategies have been developed to enrich samples for phosphopeptides and to remove non-phosphorylated acidic peptides.

Immunoprecipitation

Immunoprecipitation utilizes antibodies specific to phosphorylated residues.^{44,45} Antibodies specific to phosphorylated residues are used to immunoprecipitate total protein rather than phosphopeptides.⁴⁶ The

immunoprecipitation of phosphotyrosine containing proteins is more frequent than immunoprecipitation using phosphoserine or phosphothreonine specific antibodies as the former is more reliable than the antibodies of the latter. This is due to the fact that at present, antibodies specific for phosphoserine and phosphothreonine suitable for immunoprecipitation are not known.⁴⁶⁻⁴⁹ The success of this approach is due to the high-quality antiphosphotyrosine antibodies that have little crossreactivity with other phosphorylated or non-phosphorylated residues. However, in practice, the immunoprecipitation of phosphoproteins usually requires an expensive mixture of different antibodies. Therefore, there have only been a limited number of reports that used this approach.

Chemical Modification of Phosphate Groups

In chemical modification approach, the phosphorylated peptides are chemically altered to an affinity tag to selectively fish them out of the pool of non-modified peptides. Most of these approaches exploit the β -elimination chemistry of the phosphate esters of serine and threonine under basic conditions.^{50,51} This β -elimination is accompanied by the formation of α,β -unsaturated double bonds as illustrated in Figure 4.4.

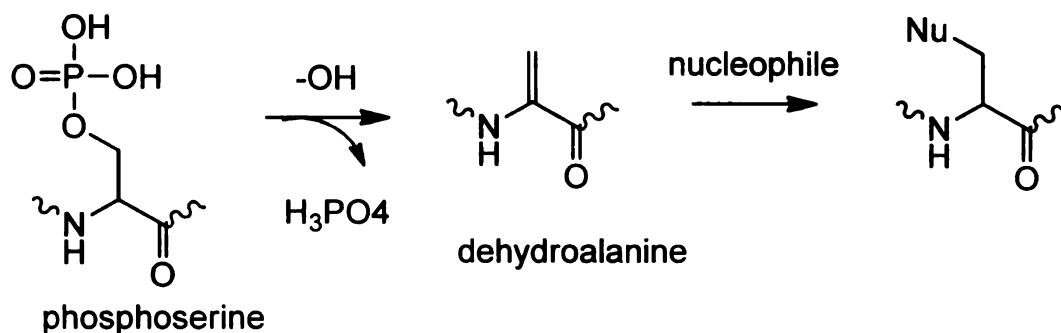


Figure 4.4 General scheme for the modification for phosphoserine by β -elimination.

This intermediate species reacts readily with a thiol reagent thus providing a way to introduce an affinity group. Oda and co-workers have demonstrated that it is possible to isolate phosphorylated peptide or protein on an Avidin matrix via the Michael addition of ethanedithiol, followed by the attachment of biotin (See Figure 4.5).⁵² Mclachlin and co-workers introduced a thiol tag as the ligand for affinity purification via disulfide linkage exchange with an activated thiol resin (See Figure 4.6).⁵³ Apart from minor degree of side reaction in which the non-phosphorylated peptides were also modified, this strategy has shown to be effective.

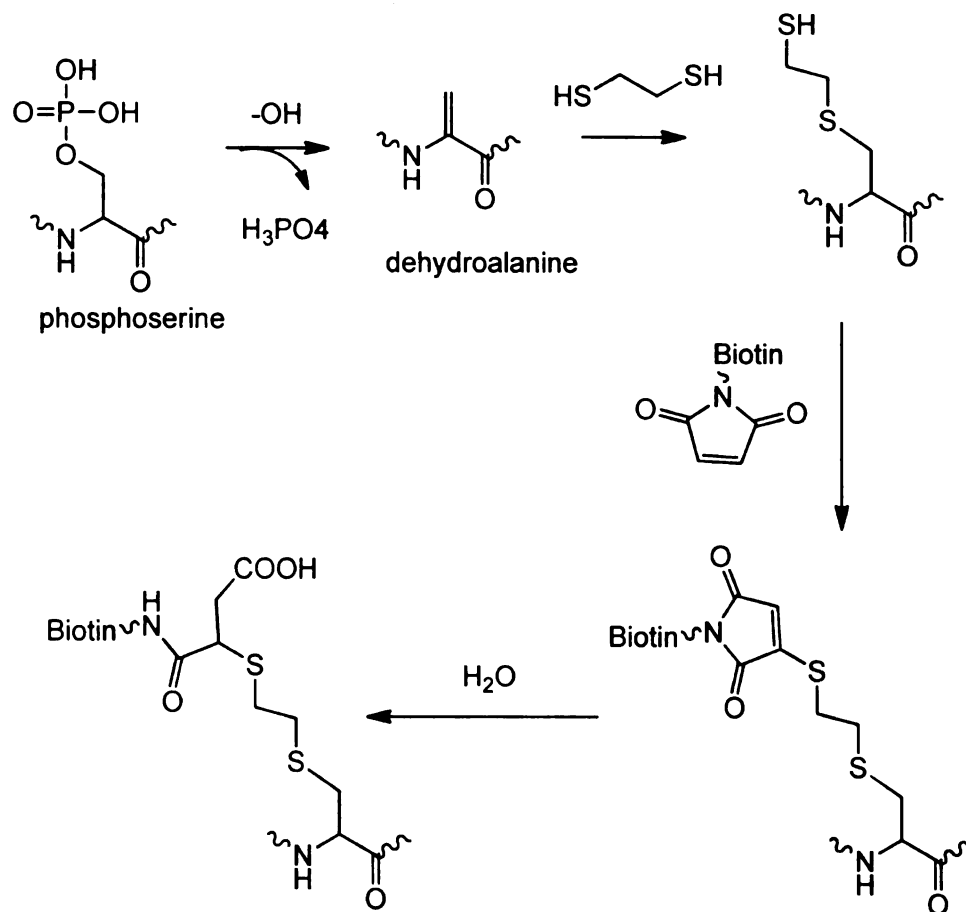


Figure 4.5 Enrichment of a modified phosphopeptide coupled with a biotin affinity tag.

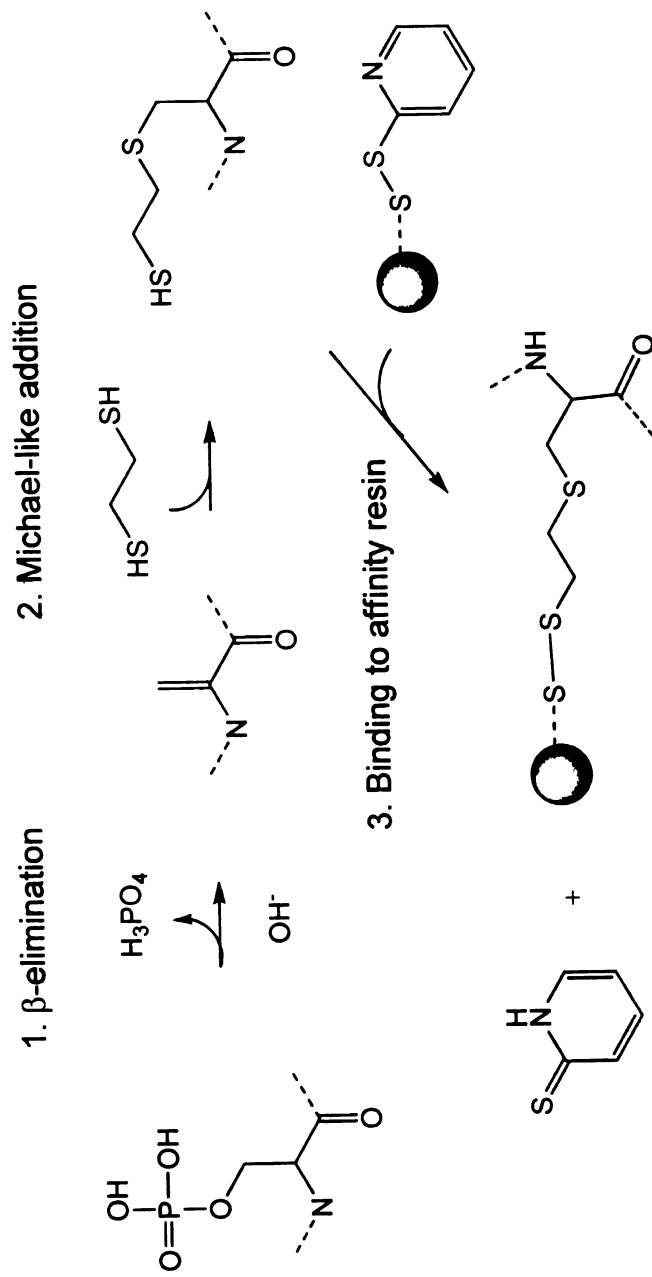


Figure 4.6 Modified phosphopeptide enrichment via direct attachment to a solid support.

Moreover, phosphotyrosine does not β -eliminate, making this approach specific for phosphorylated serine and threonine residues. Also, deglycosylation of the sample appears to be a prerequisite since o-glycosylated peptides also β -eliminate producing a modified peptide indistinguishable from the modified phosphorylated peptides.

Zhou and co-workers employed carbodiimide catalyzed cysteamine addition of free phosphate groups as a phosphospecific chemical modification strategy. The cysteamine is first reduced then the phosphorylated peptides are immobilized onto an iodoacetyl matrix. The procedure requires several chemical reactions and purification steps that lead to sample loss.⁵⁴

Recently, Tao and co-workers introduced another approach of enriching phosphoprotein through single step covalent coupling to a synthetic polyamine dendrimer.⁵⁵ The phosphopeptides are recovered via acid hydrolysis and can be subsequently analyzed by mass spectrometry.

Immobilized Metal-Ion Affinity Chromatography (IMAC)

The isolation of phosphoproteins through their natural affinity to metal cations has been explored over the years. In 1975, Porath and co-workers originally proposed this approach in purifying histidine-tagged proteins.⁵⁶ Back then, it was called 'metal chelating affinity chromatography. Subsequent studies revealed that phosphorylated amino acids also bind to the iron(III) charged species coordinated to agarose bound iminodiacetic acid that later became what is known as immobilized metal affinity chromatography (IMAC).⁵⁷

IMAC is currently the most popular method for phosphopeptide enrichment for MS-based phosphoproteome studies. It is based on the formation of reversible coordination complexes between the amino acid side chains and the positively charged metals bound to chelating groups such as nitrilotriacetic acid (NTA) or iminodiacetic acid (IDA) immobilized on a support. Immobilized metal ions of Fe^{3+} , Ga^{3+} , Al^{3+} and recently Zr^{4+} have shown very high selectivity toward phosphopeptides.⁵⁸⁻⁶⁰ IMAC materials are synthesized by the addition of metal ions to chelating agents such as iminodiacetic acid (IDA) or nitrilotriacetic acid that are immobilized on a resin, bead, glass chip or membrane. The metal-IDA and the NTA complex result to coordinatively unsaturated metal centers with three and two sites available for coordination, respectively (See Figure 4.7). These coordination sites are apparently only available to the phosphate at a pH range between 2.0-3.5. Thus, in order to develop an IMAC material that can be used at a physiological pH, phos-tag, an alkoxide-bridged di-nuclear Zn (II) was developed.⁶¹

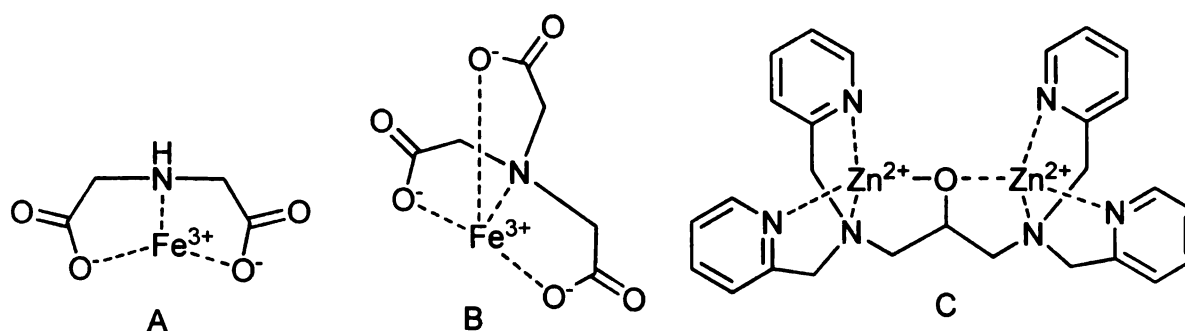


Figure 4.7 Structures of A. Fe(III) iminodiacetic acid complex B. Fe(III) nitrilotriacetic acid complex C. phos-tag.

Enrichment using IMAC is typically carried out by the introduction of a protein digest or cellular extract onto a column or surface that contains the immobilized cations. The phosphate functional group forms a coordination

complex with the metal thereby allowing the removal of unbound non-phosphorylated peptides. The bound phosphopeptides are released from the affinity material through washing the column with an alkaline solution or by the addition of excess ligand such as a phosphate buffer. The eluted phosphopeptides are typically analyzed directly either by matrix assisted laser desorption/ionization mass spectrometry (MALDI-MS) or electrospray ionization mass spectrometry (ESI-MS) to obtain the peptide sequence and to determine to phosphorylation site. IMAC procedures have become very popular due to its good compatibility with subsequent separation and detection techniques such as ESI-MS and MALDI-MS. Moreover, the main advantage of this technique is that it has been proven to be useful in large scale analysis. IMAC based techniques have been reported to recover up to 70-90% of the total phosphoprotein samples for whole cell extracts based on ^{32}P or ^{33}P radioactivity.

However, there are several drawbacks with this technique. The first challenge is the recovery of multiply phosphorylated peptides that has stronger affinity to the immobilized support, resulting in poor elution and requiring harsher conditions to liberate the phosphopeptides.^{39,62} Another challenge is the non-specific binding of phosphorylated peptides through the carboxylate groups of aspartic and glutamic acid residues and the strong binding of the multiply phosphorylated peptides.³⁹ The non-specific binding of the acidic peptides is diminished by esterification of the carboxylic acids to methyl esters using HCl-saturated in dried methanol. Reaction conditions have to be chosen carefully to avoid both the incomplete esterification of carboxylate group and side reactions

because they increase sample complexity. Despite following an apparently simple common scheme (binding-washing-eluting), IMAC experiment conditions are very variable and care should be taken as small variations in the experiment conditions such as pH, ionic strength and organic composition of the solvents could drastically affect the selectivity of the IMAC stationary phase.

Strong Ion Exchange Chromatography

In addition to IMAC, strong cation exchange chromatography (SCX)^{63,64} has been used for the enrichment of phosphorylated peptides. This procedure is based on the fact that under acidic conditions (pH 2.7), tryptic phosphorylated peptides are singly positively charged and amenable to further separation from non-phosphorylated tryptic peptides that usually have a net charge of 2+ at same pH. Although this technique does not have high specificity and the fractions enriched in phosphopeptides also contain a high percentage of contaminant, SCX enrichment have been used for massive phosphoprotein proofing mainly due to the fact that the tryptic mixtures can be analyzed directly.

Metal Oxide Affinity Chromatography

Metal oxides have emerged as alternatives to the use of IMAC.⁶⁵⁻⁶⁷ Pinkse and co-workers⁵⁹ first described the use of titania as a possible alternative for IMAC for the enrichment of phosphorylated peptides. This approach is based on the selective interaction of water soluble phosphates with porous titania microspheres via a bidentate binding on the titania surface. In this

technique the phosphopeptides are trapped on the surface of titania precolumn under acidic conditions and are desorbed under alkaline conditions. As with IMAC, non-specific binding of acidic non-phosphorylated peptides also is encountered with titania but this problem also can be minimized by methyl esterification. Larsen and co-workers also have demonstrated that the inclusion of 2,5-dihydroxybenzoic acid (DHB) in the loading buffer enhances the selectivity towards phosphopeptides while retaining high binding affinity.⁶⁸ The exact mechanism on how DHB improves selectivity is not clearly understood but it appears that DHB competes with the acidic nonphosphorylated proteins for binding sites on the titania surface. This hypothesis was confirmed by studies of the coordination of substituted aromatic carboxylic acids with the surface of titania. Spectroscopic studies have revealed that substituted aromatic carboxylic acids (such as DHB) coordinate more strongly with titania as compared to monofunctional carboxylic acids (such as benzoic acid).⁶⁹

Metal oxides of zirconium,⁶⁶ aluminum,⁷⁰ gallium,⁷¹ tin⁷² and niobium⁷³ also have been reported to be very selective for phosphopeptide enrichment. Overall, the metal oxide affinity chromatography technique offers fast, straightforward enrichment since it can easily be coupled with ESI-MS or MALDI-MS. Moreover, the metal oxide materials are robust and chemically inert. One drawback however, is that desorption process can be considerably slower.

The discovery of mesostructured metal oxides such as titania, alumina and zirconia are of particular interest for applications in catalysis, catalyst supports and molecular separations because of their large pore size and high

specific surface area. The high specific surface area of mesoporous metal oxides together with reports of metal oxides being good materials for enriching phosphoprotein make mesoporous metal oxides good candidates for phosphoproteomic applications. The inherent high surface area will give the material higher enrichment capacity.

4.2 Objectives

There is no single technique that can be considered the 'holy grail' for phosphoprotein enrichment. In this study modified metal oxide affinity chromatography approach for enriching phosphorylated proteins is introduced. This approach serves as an alternative to the use of IMAC and metal oxide pre-columns. The general objective of the study is to further simplify the phosphopeptide enrichment process with a technique that will allow high throughput without sacrificing high selectivity and capacity toward phosphopeptides. This will be accomplished by utilizing mesoporous metal oxide thin films of titania, alumina and zirconia. These metal oxides have high selectivity towards phosphorylated proteins and peptides. Thus, it is expected that the high surface area would translate to high capacity. Specifically, this study fabricates mesoporous thin films of titania, alumina and zirconia on supports that permits easier enrichment procedures. Metal TEM grids will be used as support for the thin films. The metal TEM grids are very well suited for this application since they have small enough dimensions to carry out the enrichment

procedures. Moreover the physical properties of the mesoporous metal oxide thin films also were elucidated. Ultimately, the end goal would be to successfully enrich model phosphoproteins at the femtomolar level and to develop a protocol for phosphoprotein enrichment using grid supported mesoporous metal oxide thin films.

4.3 Experimental

4.3.1 Materials

Copper, nickel, gold, molybdenum, titanium and aluminum TEM grids were purchased from Ted Pella. Silver and stainless steel grids were procured from SPI Supplies. All grids have a 400 mesh size except for stainless steel, aluminum and titanium where they have 100, 200 and 300 mesh sizes respectively. All of the grids were used as received. Titanium chloride, zirconium tetrabutoxide and aluminum isopropoxide were procured from Aldrich.

4.3.2 Precursor Solution Preparation

Preparation of Alumina Precursor Solution

Aluminum tri-sec-butoxide (0.1 mol) was dissolved in 100 mL water. This initial mixture was then mixed with 10 ml of 0.1 M HNO₃ solution. The resulting solution was allowed to incubate overnight at 100°C. The mixture was then mixed with 9.0 g of Tergitol 15-S-9 surfactant. Finally, the resulting mixture was diluted with 100 mL ethanol.⁷⁴

Preparation of Titania Precursor Solution

A precursor mixture with a composition of 1 TiCl₄ : 22 EtOH : 0.004 F127 was prepared by first adding TiCl₄ to absolute ethanol under vigorous stirring. This was followed by the addition of the Pluronic F127 (EO₁₀₆PO₇₀EO₁₀₆) porogen dissolved in ethanol.

Preparation of Zirconia Precursor Solution

Zirconium propoxide (Zr(PrO)₄), 70% wt. solution in n-propanol and non-ionic triblock copolymer Pluronic F127 (EO₁₀₆PO₇₀EO₁₀₆) were used as the inorganic source and the structure directing agent, respectively. A precursor solution has a molar composition of 1.0 Zr(PrO)₄ : 0.0075 F127 : 2.4 HCl : 35.2 EtOH and 2.4 n-propanol.

The solution was prepared by mixing the Zr(PrO)₄ and half the required volume of ethanol together. In a second vessel, Pluronic F127 was dissolved using the remaining volume of ethanol together with concentrated HCl. The two solutions were then mixed together to produce a homogeneous solution. The solution was kept in the fridge when not in use and was brought back to room temperature for the casting of grid supported thin films.⁷⁵

4.3.3 Preparation of Thin Films

Gold grids were dipped into the mesoporous metal oxide precursor solution were allowed to dry to form the surfactant intercalated metal oxide thin

film on the grid.. The films were allowed to incubate in a 100% humidity chamber for at least 48 hours. The films were then calcined at the appropriate temperature to obtain the metal oxide form for the phosphoprotein enrichment. In the case of mesoporous alumina thin films, the grids were calcined at 500°C for 2 hours at a heating rate of 2 degrees per minute.

4.3.4 Characterization of Mesoporous Metal Oxide Thin Films

Powder x-ray diffraction patterns were measured using Cu K α radiation ($\lambda = 1.542 \text{ \AA}$) and a Rigaku Rotaflex diffractometer equipped with a rotating anode operated at 45 kV and 100 mA. Counts were accumulated every 0.02 degree 2 theta at a scan speed of 0.5 degree per minute. Thin films specimen for X-ray diffraction analysis were prepared by dropping the precursor solution onto a glass slide and allowing it dry. The films were then calcined at the appropriate temperature before they were analyzed.

Transmission electron microscopy (TEM) images were obtained on a JEOL 2200FS with an accelerating voltage of 200kV. TEM specimen were prepared by dip-coating bare grids (3 mm, 400 mesh gold grid) into a metal oxide precursor solution. These grids were dried and subsequently calcined at the appropriate temperature to obtain the grid supported mesoporous metal oxide thin films.

Scanning electron microscopy (SEM) images were obtained on a 6400 SEM with an accelerating voltage of 220 kV. Samples were coated with gold prior to recording images.

4.3.5 Protein Digestion

The protein digests were obtained from Bruening's and Reid's group. The digestion procedures are described below.

β -casein and chicken ovalbumin were dissolved in 6M urea containing 50 mM Tris-HCl to form solutions containing 50 μ g protein / μ L. The disulfide bonds of the ovalbumin were cleaved by adding 5 μ L, 10mM 1,4-dithio-DL-threitol (DDT) to 20 μ L of protein solution prior to heating in a water bath at 70°C for 1 hour. Though β -casein does not contain disulfide bonds, the same procedure also was employed for preparing β -casein digest for consistency. A 160 μ L aliquot of 50mM ammonium bicarbonate and a 10 μ L aliquot of 100 mM was added to the solutions at room temperature and then the solutions were placed in the dark for 1 hour. Next, trypsin (10 μ L, 0.5 μ g/ μ L) was added and the solutions were incubated for about 16 hours at 37°C. The digestion was quenched by adding enough glacial acetic acid to make a 5% solution. The digests were stored in a -70°C freezer until use.

4.3.6 Phosphoprotein Enrichment

Effects of incubation time

Figure 4.8 schematically illustrates the enrichment process. Initially, individual TEM grids are placed inside 1.5mL Eppendorf tubes using self closing tweezers. Then, 10 μ L of tryptic protein digest is carefully added to the tube to ensure that the TEM grid was submerged in the protein digest. Special care also

is made so that the grid does not fold and the digest has no bubbles or air pockets. To determine the optimum incubation time, the grids together with the protein digest are allowed to incubate for 1-5 hours with samples being analyzed at 1 hour intervals. After incubation, the TEM grid is separated from the protein digest by simply picking it out using a tweezer. Then, the grid is immediately placed in a new Eppendorf tube so that the grid did not dry out. Next, 10 μL of the first washing solution of 2,5-dihydroxybenzoic acid in acetonitrile is added and allowed to equilibrate for 10 minutes. After 10 minutes, the grid is again picked out from the washing solution and placed in a new Eppendorf tube for the second washing with 10 μL of the washing solution was added and was allowed to equilibrate for another 10 minutes. The second washing solution this time was composed of trifluoroacetic acid in acetonitrile solution. Both washing steps were employed to remove nonphosphorylated peptides adsorbed onto the grid. After 10 minutes, the grid was again removed and placed in an Eppendorf tube for a final wash with distilled water. The washed grid was then mounted on a stainless steel MALDI plate using conducting carbon cement. Once the carbon cement was dried, the phosphopeptides were desorbed or eluted from the grid by the addition of 3 μL of ammonium hydroxide solution onto the top of the grid. (See Figure 4.9). The ammonium hydroxide solution was allowed to dry completely and then 3 μL of the DHB matrix solution was dropped onto the grid and dried before the MALDI spectrum was obtained.

Mass Spectrum Analysis

The MALDI mass spectrum shown were representative of many similar spectra as each experiment was replicated three times using different TEM grids. All mass spectra were obtained using a MALDI linear ion trap mass spectrometer (Thermo vMALDI LTQ XL)

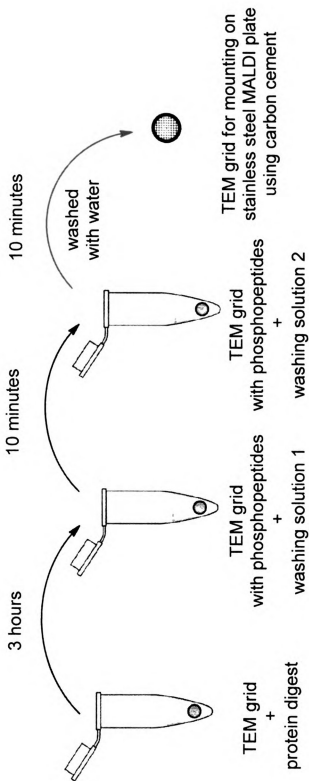


Figure 4.8 Schematic illustration of the phosphopeptide enrichment process using grid supported mesoporous metal oxide thin films. Washing solution 1 is 2,5-dihydroxybenzoic acid in acetonitrile. Washing solution 2 is trifluoroacetic acid in acetonitrile.

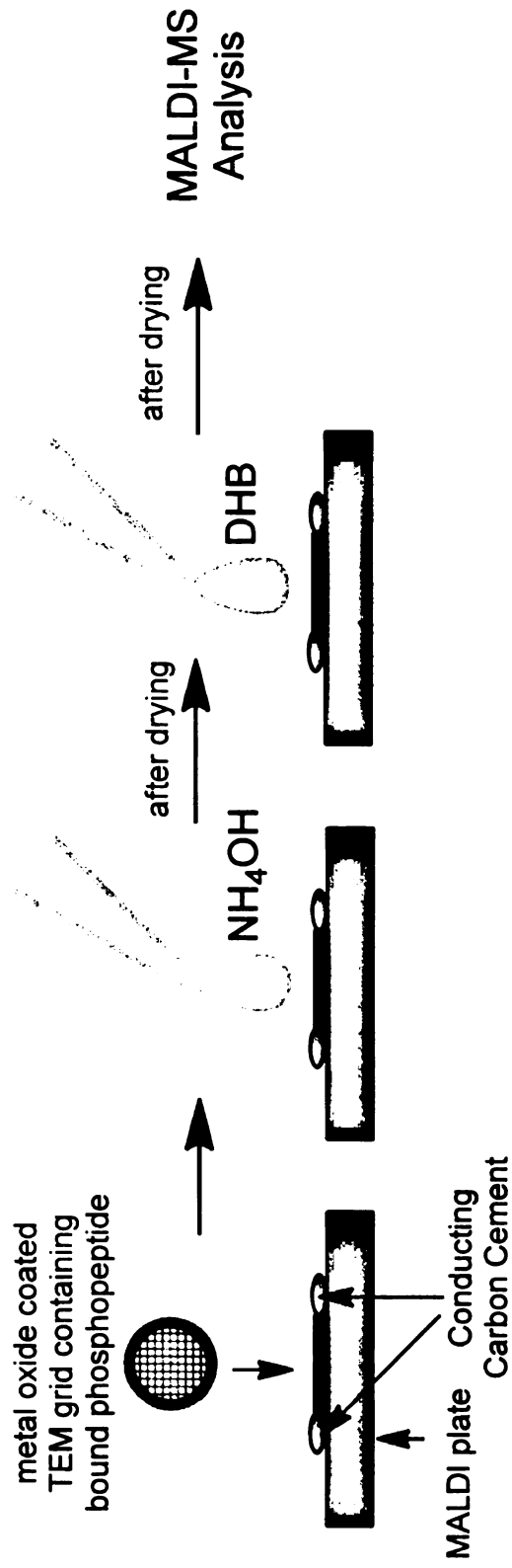


Figure 4.9 Schematic representation of grid-supported mesoporous metal oxide thin film containing bound phosphopeptide being mounted on a MALDI plate and the subsequent release of the bound phosphopeptide for MALDI mass spec analysis.

4.4 Results and Discussions

4.4.1 Fabrication of Grid Supported Mesoporous Metal Oxide Thin Films

In this study, three mesoporous metal oxides of titania, alumina and zirconia were used for phosphoprotein enrichment. The approach involved the fabrication and characterization of TEM grid supported mesoporous metal oxide thin film. A TEM grid is a circular shaped metal usually 3mm in diameter that is use to mount samples for Transmission Electron Microscopy (TEM). These grids can be segmented in many ways like square mesh, hexagonal and diamond mesh, slots and holes, parallel, folding and tabbed. (See Figure 4.10)

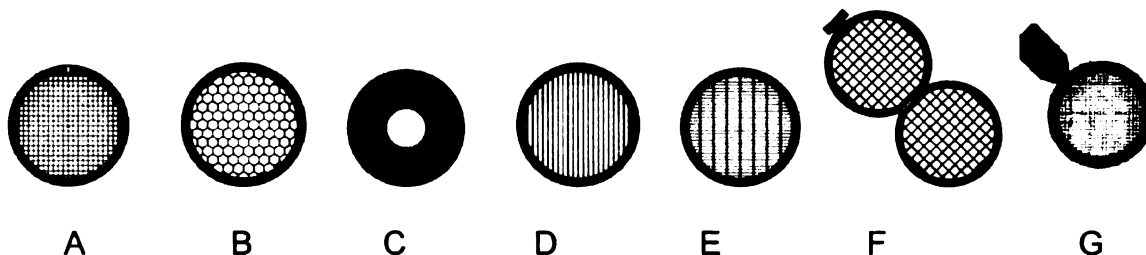


Figure 4.10 Different types of grids. A square mesh B. hexagonal mesh C. slots D. parallel E. combination of parallel and mesh F. folding and G. tabbed.

Grids are usually made from copper, nickel, gold but other metals and materials are also used like beryllium, molybdenum, aluminum, titanium. Grids are also described by their mesh size and the most popular mesh sizes are 200, 300 and 400 mesh. Aside from mesh sizes, grids can vary based on the size of the hole and the bar (See Figure 4.11). Sometimes pitch is also used to describe TEM grids, which is the sum of the bar and the hole.

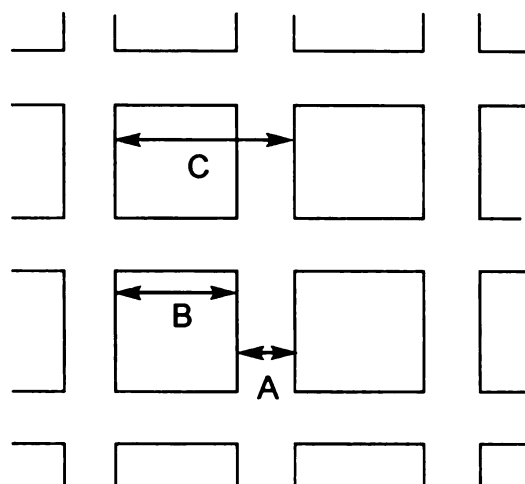


Figure 4.11 A. Bar B. Hole C. Pitch

The use of TEM grids as supports for mesoporous metal oxide offers the advantage of very high throughput because more samples can be processed at the same time. Moreover, the phosphoprotein can be separated from the digest by simply pulling out the grid from the digest and washing off the non-phosphorylated peptide off the grid. The TEM grid can also be use as received and MS analysis can be done on the grid itself. The only disadvantage seen on using TEM grids for phosphoprotein enrichment is that a steady hand is needed, because the grids since the TEM grids are very thin and are easy folded.

Figure 4.12 shows the x-ray diffraction patterns for the mesoporous titania, zirconia and alumina thin films. Based on the x-ray diffraction patterns, the alumina pattern is characteristic of the gamma form of alumina. The titania pattern is characteristic of anatase and the zirconia phase is cubic. Figure 4.13 and 4.14 also shows the electron diffraction patterns of titania and zirconia taken using selected area diffraction mode of the TEM microscope. The diffuse

diffraction rings indicate the nanocrystalline nature of the films. The diffuse reflections of the grid-supported aluminum films could not be resolved.

Figure 4.15 shows high resolution TEM images of a titania thin film. The image on the left shows contrast where in the lighter shades represents the pores of the mesoporous film. The image on the right shows a higher magnification of the image on the left. At this magnification, the fringes due to the crystalline nature of the material are visible. The different orientations of the fringes indicate the polycrystalline nature of the material.

Figure 4.16 shows TEM images of mesoporous zirconia thin film. The image on the left reveals the mesopores present in the film. The image on the right shows a higher magnification of the material where the crystal fringes are clearly seen. Figure 4.17 shows the TEM image of the mesoporous alumina film. The image shows the random stacking of the lathlike alumina nanocrystals that give rise to the pores of the materials.

Figure 4.18 shows the SEM image of a bare gold grid. The left image was taken from the matted side of the grid and the image on the right was taken from the glossy side of the bare gold TEM grid. These images were taken to ascertain whether a thin film was deposited by knowing the initial morphology of the bare grid. Figure 4.19 shows SEM image of the mesoporous titania supported by a gold TEM grid. As the film is calcined to form the anatase structure, the TiO_2 rearranged itself and in the process produce the broken glass-like morphology. On the other hand, the lath-like structure of alumina permitted the formation of a film that completely fills the holes of the TEM grid as shown in Figure 4.20.

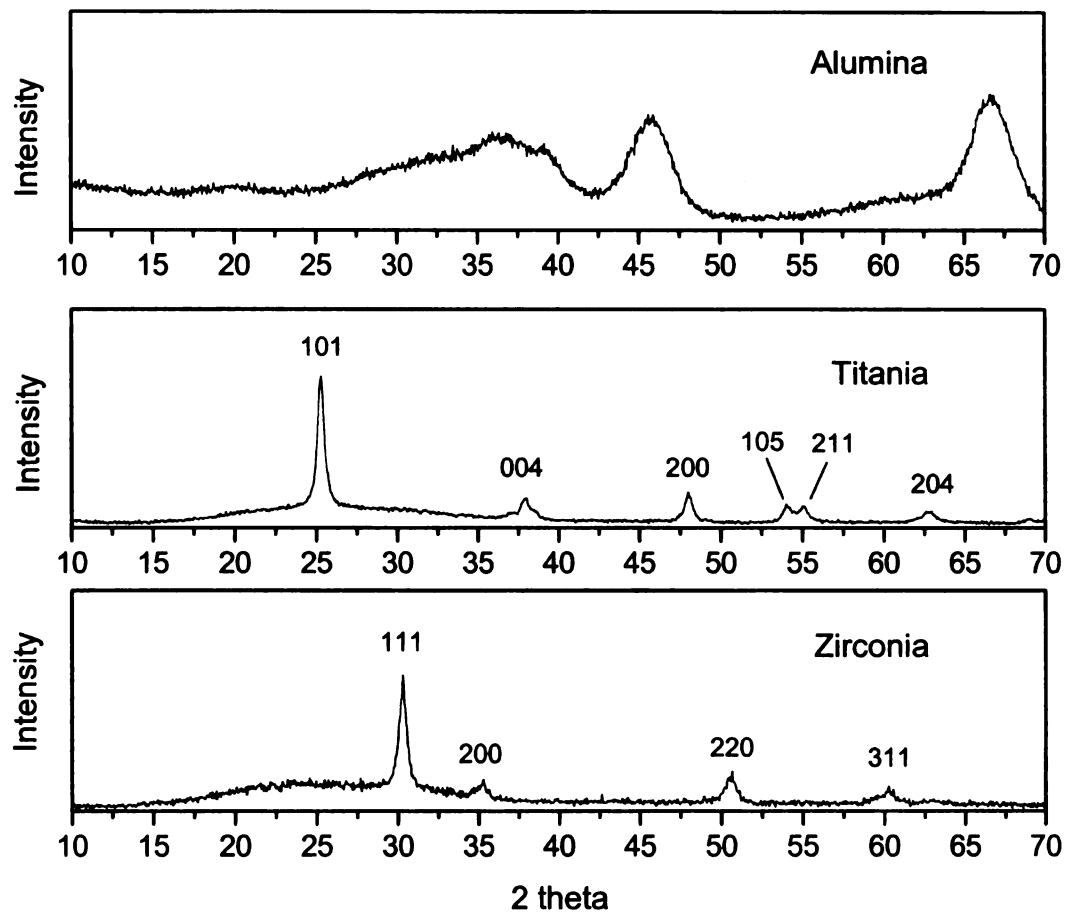


Figure 4.12 Wide angle x-ray diffraction of calcined alumina, titania and zirconia powders.

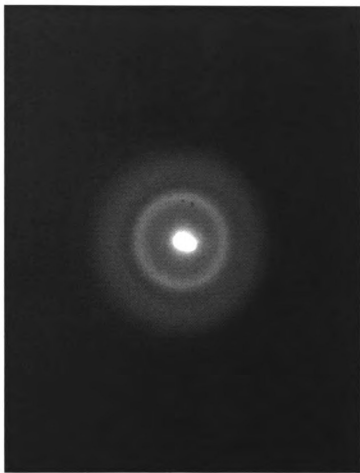


Figure 4.13 Electron diffraction of grid supported mesoporous zirconia thin films taken from TEM selected area diffraction mode showing several rings indicating a polycrystalline structure.

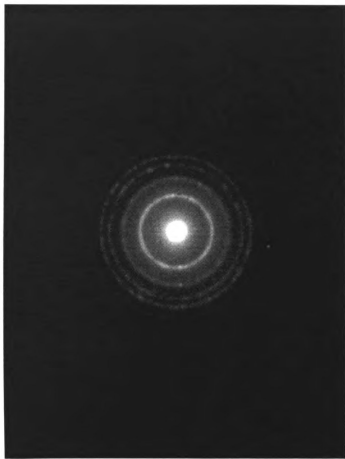


Figure 4.14 Electron diffraction of grid supported mesoporous titania thin film taken from TEM selected area diffraction mode showing several rings indicating a polycrystalline structure.

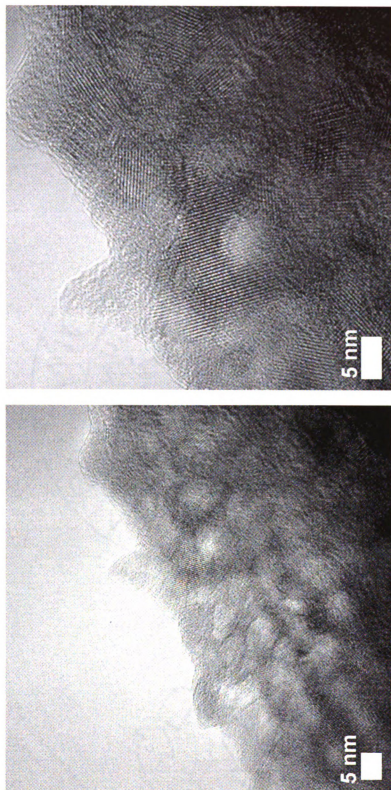


Figure 4.15 TEM images of mesoporous titania thin film supported on a gold TEM grid (400 mesh). (Left) The lighter shades on the image represent the mesopores. (Right) Variable orientations of lattice fringes indicate the polycrystalline nature of the film.

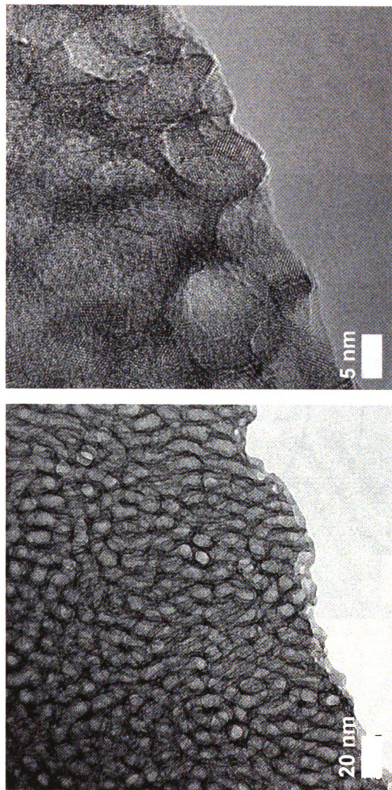


Figure 4.16 TEM images of mesoporous zirconia thin film supported on a gold TEM grid (400 mesh). (Left) The lighter shades on the image represent the pores. (Right) Lattice fringes on different directions indicate the polycrystalline nature of the material.

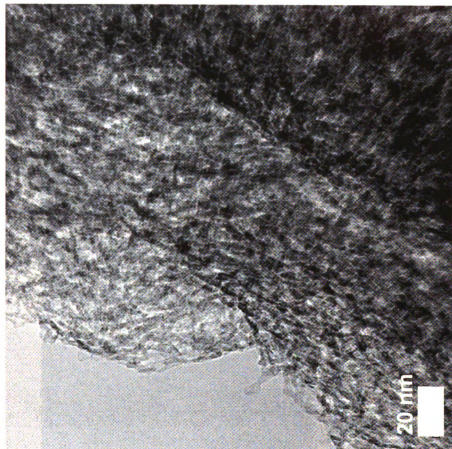


Figure 4.17 TEM image of mesoporous alumina thin film supported on a gold grid. The image shows the mesopores that arises from the stacking of lath-like nanocrystals of alumina.

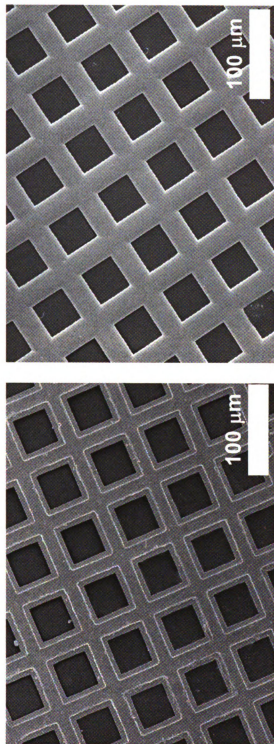


Figure 4.18 SEM images of bare gold grid. The left image was taken from the matted side of the grid and the right image was taken from the glossy side of the grid.

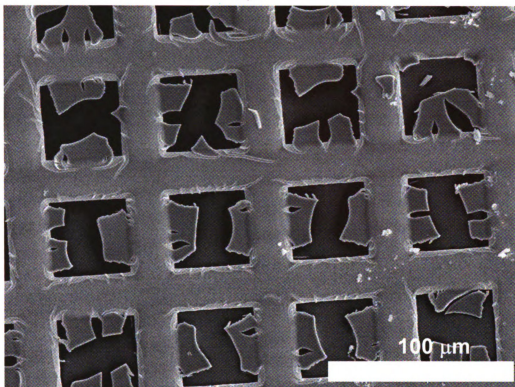


Figure 4.19 SEM image of a calcined mesoporous titania thin film supported on a gold grid. The crystalline anatase coats the bars of the grid and extends into the holes of the grid. The crystallization of the anatase phase during calcinations causes shrinkage which fragments the films.

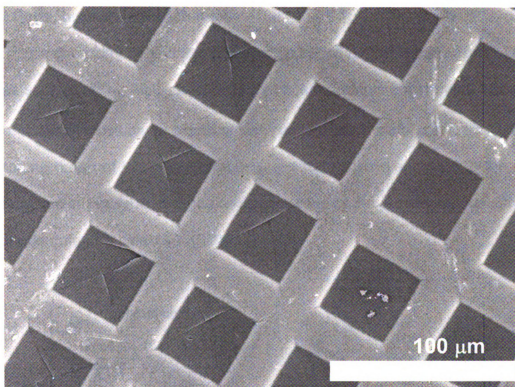


Figure 4.20 SEM image of a calcined mesoporous alumina thin film showing completely filled holes on the TEM grid as well as the coated bars of the grid.

4.4.2 Phosphoprotein Enrichment

The chemistry behind this approach is based on the reported use of metal oxides such as TiO_2 , Al_2O_3 and ZrO_2 for phosphoprotein enrichment. The metal oxide surface provides a coordinatively unsaturated metal center where the phosphate group of the phosphopeptide can form a covalent bond to the metal as illustrated in Figure 4.21. The phosphate group of the protein can act either as a monodentate or a bidentate ligand.

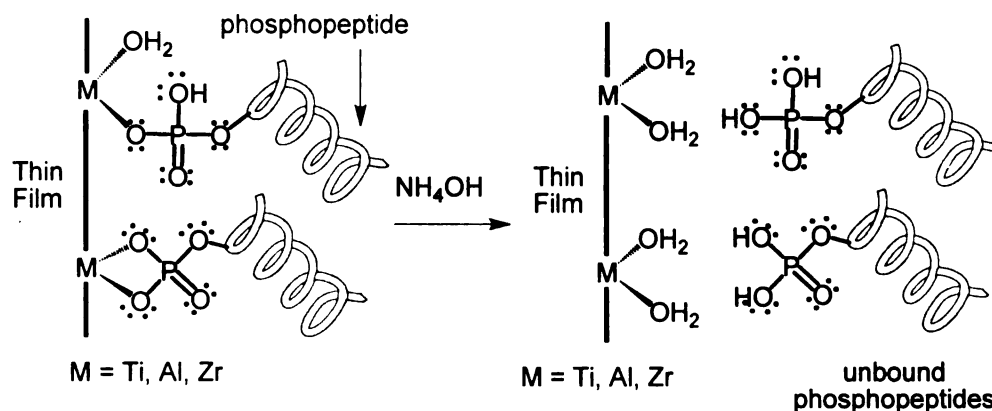


Figure 4.21 Schematic illustration of phosphopeptide binding to a metal oxide surface and the release of the protein by reaction with ammonium hydroxide.

β -Casein and ovalbumin were used to demonstrate the ability of TEM grid supported mesoporous metal oxide thin films to enrich phosphoproteins. β -casein represents 36% of bovine casein. It has a variety of functional properties which in some cases are similar to but mostly differ from, those of α_{s1} - and κ - caseins. The β -casein molecule is a single chain of known sequences with five phosphoserine residues and a molecular weight of 20,020 Da. Tryptic digestion of β -casein yields three phosphorylated peptides fragments – two

tetraphosphorylated peptides and one monophosphorylated peptide (See Table 4.1). Ovalbumin is the major protein in avian egg-white and was one of the first protein to be isolated in pure form.¹ Its availability in large quantities has led to the widespread use as a standard preparation studies of the structure and properties of proteins and in experimental models of allergies.² Ovalbumin is also a glycoprotein with a relative molecular mass of 45,000. The amino acid sequence of hen ovalbumin is comprised of 386 amino acids. This sequence was deduced from the mRNA sequence by McReynolds and co-workers.³ This result was also in agreement with the sequence of purified protein⁴ and the cloned DNA.⁵ It has two potential phosphorylation sites at serine 69 and 345.⁶ Trypsin cleaves on the carboxyl side of arginine and lysine residues. Tryptic digests of ovalbumin typically yields three phosphorylated peptides with the third fragment resulting from a miscleavage.⁷ The tryptic digest fragments for ovalbumin and β -casein are shown in Table 4.1.

Table 4.1. Phosphorylated peptides from tryptic digests of β -casein and ovalbumin.

	Peptide Sequence	m/z
β -Casein		
1P ₂₀₆₂	FQpSEEQQQTEDELQDK	2062
4P ₂₉₆₆	ELEELNVPGEIVEpSLpSpSpSEESITR	2966
4P ₃₁₂₂	RELEELNVPGEIVEpSLpSpSpSEESITR	3122
Ovalbumin		
1P ₂₀₈₈	EVVGpSAEAGVDAASVSEEFR	2088
1P ₂₅₁₁	LPGFGDpSIEAQCGTSVNVHSSLR	2511
1P ₂₉₀₁	FDKLPGFGDpSIEAQCGTSVNVHSSLR	2901

Effect of Incubation Time

The binding of phosphopeptide onto a metal oxide surface will be governed by equilibrium. In this case, the maximum amount of specific binding for the phosphopeptides is desired. But the specific binding of the phosphopeptide is difficult to achieve without the proper protocol, particularly with regard to the length of incubation time. Tryptic digest of β -casein yields phosphopeptide fragments composed of a monophosphorylated peptide (m/z = 2062) and two fragments both tetraphosphorylated with m/z values of 2966 and 3122. The non-specific binding of phosphopeptide is usually due to the presence of basic (i.e. $-\text{NH}_2$) and/or acidic ($-\text{COOH}$) donor groups in the peptide sequence. This problem is usually circumvented by adding trifluoroacetic acid (TFA) to protonate the amino side chain of basic amino acid residue as well as to keep the carboxylic acid side chain protonated. For the case of titania, it has been reported that 2,5-dihydroxybenzoic acid (DHB) was most effective in achieving this effect thus, DHB was used in the studies.

Figure 4.22 shows the MALDI spectrum of 100 fmol of β -casein tryptic digest without enrichment. From the spectrum, phosphorylated peptides are not visible. Figure 4.23 shows the enrichment studies of 100 fmol β -casein on grid supported mesoporous titania thin films. The figure shows MALDI spectrum after different incubation times in the presence of DHB. The results of this experiment were very interesting. Previously, it was thought that the longer the incubation time, the better the enrichment becomes until it reaches equilibrium where no

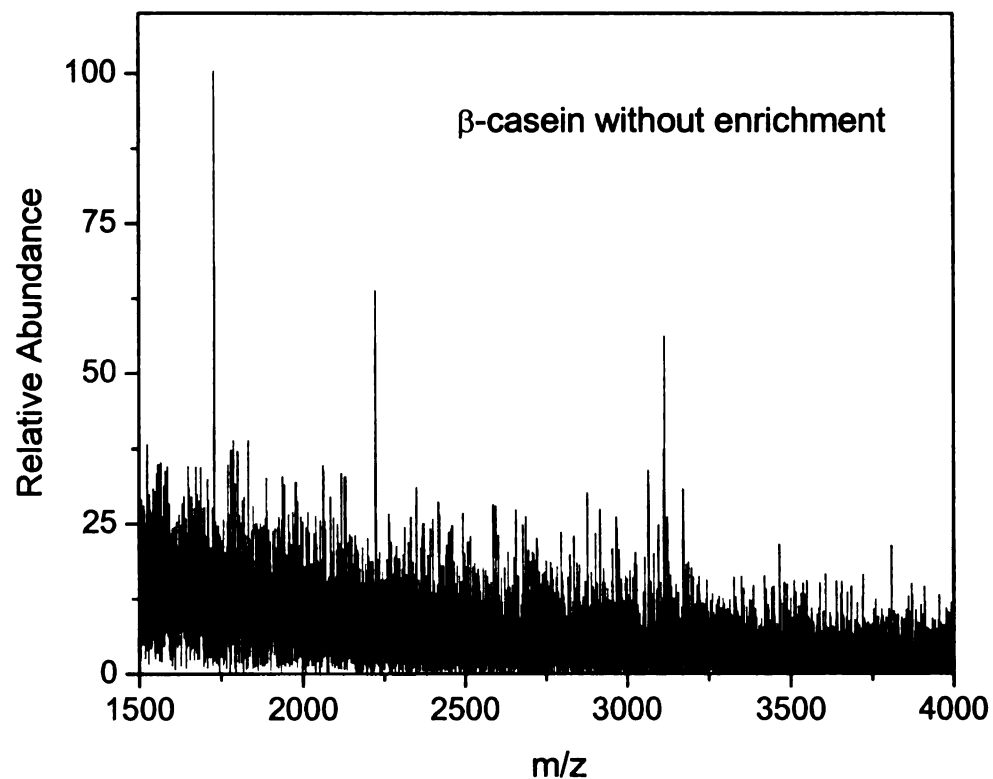


Figure 4.22 MALDI spectrum of un-enriched β -casein. The specimen was supported on a stainless steel MALDI plate.

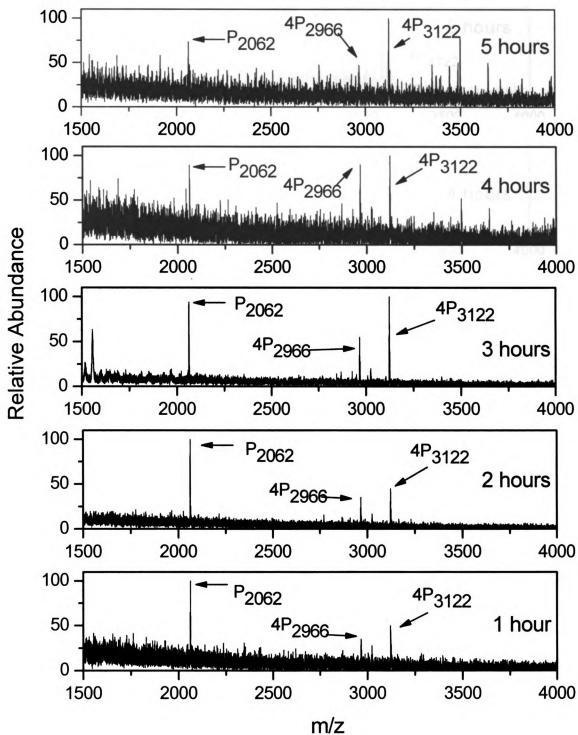


Figure 4.23 Incubation studies of 100 fmol β -casein on grid supported mesoporous titania (TiO₂) thin film.

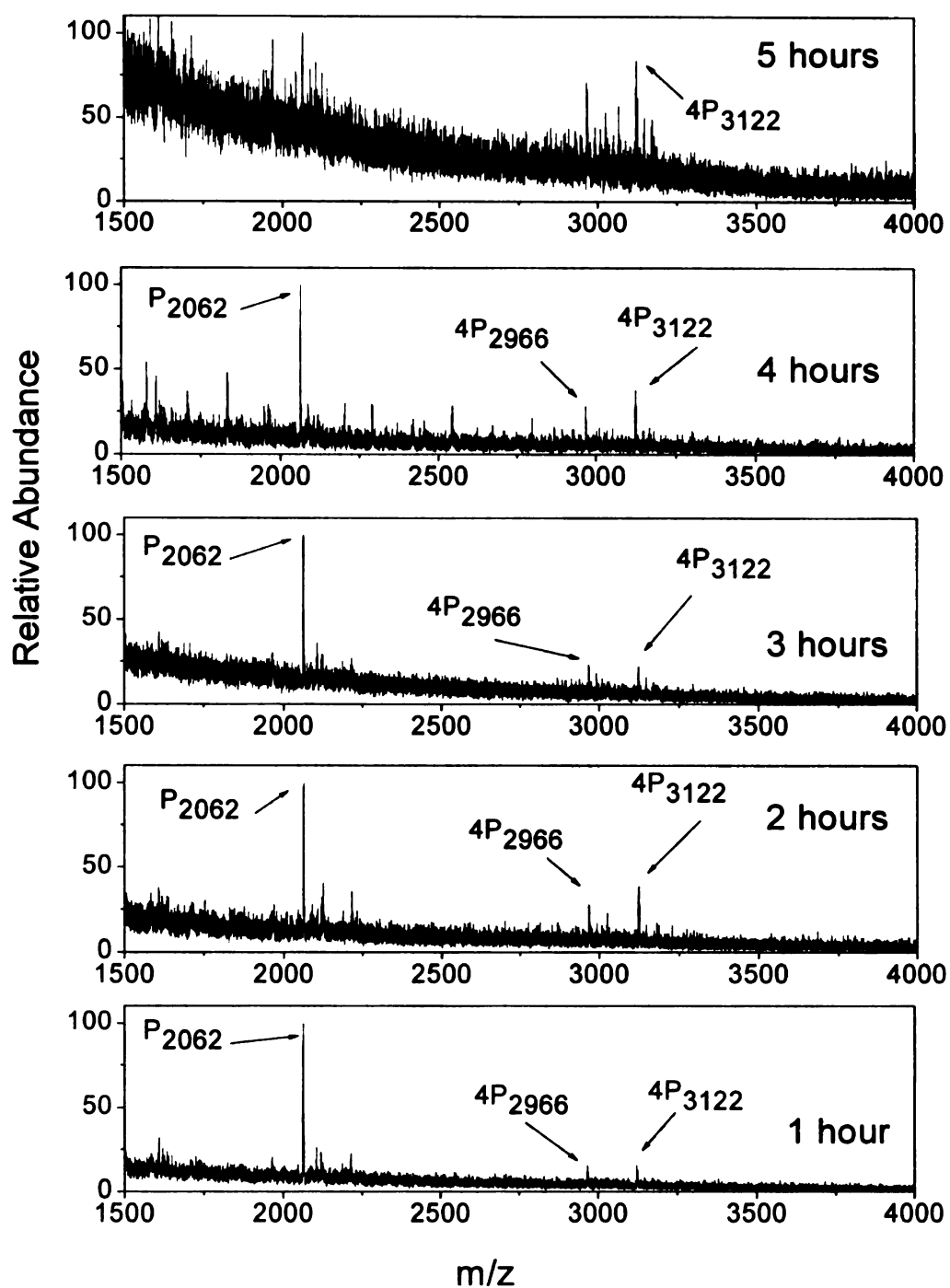


Figure 4.24 Incubation studies of 100 fmol β -casein on grid supported mesoporous alumina (Al_2O_3) thin film.

further improvement in enrichment is observed. Results showed that very good enrichment can be achieved at 1-3 hours of incubation. Good enrichment in this

case was defined as obtaining a MALDI spectrum very high signal to noise intensity and with high selectivity towards the phosphorylated peptides. MALDI spectra taken after 3 hours started to show non-specific binding and the signal to noise ratio decreased. It seems that the addition of DHB only delays the non-specific binding of the non-phosphorylated protein but doesn't stop it. DHB is said to compete with the carboxylic acid side chain of the peptide chain thus delaying non-specific binding. But as the system moves towards equilibrium, the carboxylic acid group side chain of the non-phosphorylated peptide will eventually compete with the phosphorylated peptide for binding sites on the metal oxide surface as shown on the MALDI spectra at 4 and 5 hours incubation.

Figure 4.24 shows the MALDI spectra for 100 fmol β -casein on grid supported mesoporous alumina thin film at different incubation times. As in the case of mesoporous titania thin films, highly specific binding was observed from 1-3 hours of DHB incubation time. Non-specific binding starts to appear in the spectra after 3 hours. From these two studies, it was decided that 3 hours is the incubation time needed to ensure optimum specific binding. Thus, three-hour incubation time was used for subsequent studies of both ovalbumin and β -casein.

Enrichment of β -casein

The results for this part of the study are shown in Figure 4.25 where 50 fmol of tryptic digest of β -casein was enriched using mesoporous zirconia, alumina and titania thin film. As previously reported in literature, the three metal oxides showed highly specific enrichment.

In all of the spectra, the monophosphorylated peak ($m/z = 2062$) was the most intense. The monophosphorylated peak was enriched at least 2600 times as shown by the peak intensities. Also, the tetraphosphorylated peaks were observed, though at very low intensity. Peaks corresponding to the lost of phosphate group/s were also observed.

The spectrum for the control sample where a bare gold grid is used for the enrichment process is shown in Figure 4.26. The results for this spectrum were remarkable and unprecedented in part because there has not been previous reports of gold surface being used for phosphopeptide enrichment and because the surface is highly selective for the enrichment of two tetraphosphorylated peptide of β -casein. This is a level of enrichment that the mesoporous metal oxide thin films failed to achieve. The spectrum for bare gold also showed peaks corresponding to the lost of the phosphate moieties. Another interesting observation is that the monophosphorylated peak is very weak to almost non-existent.

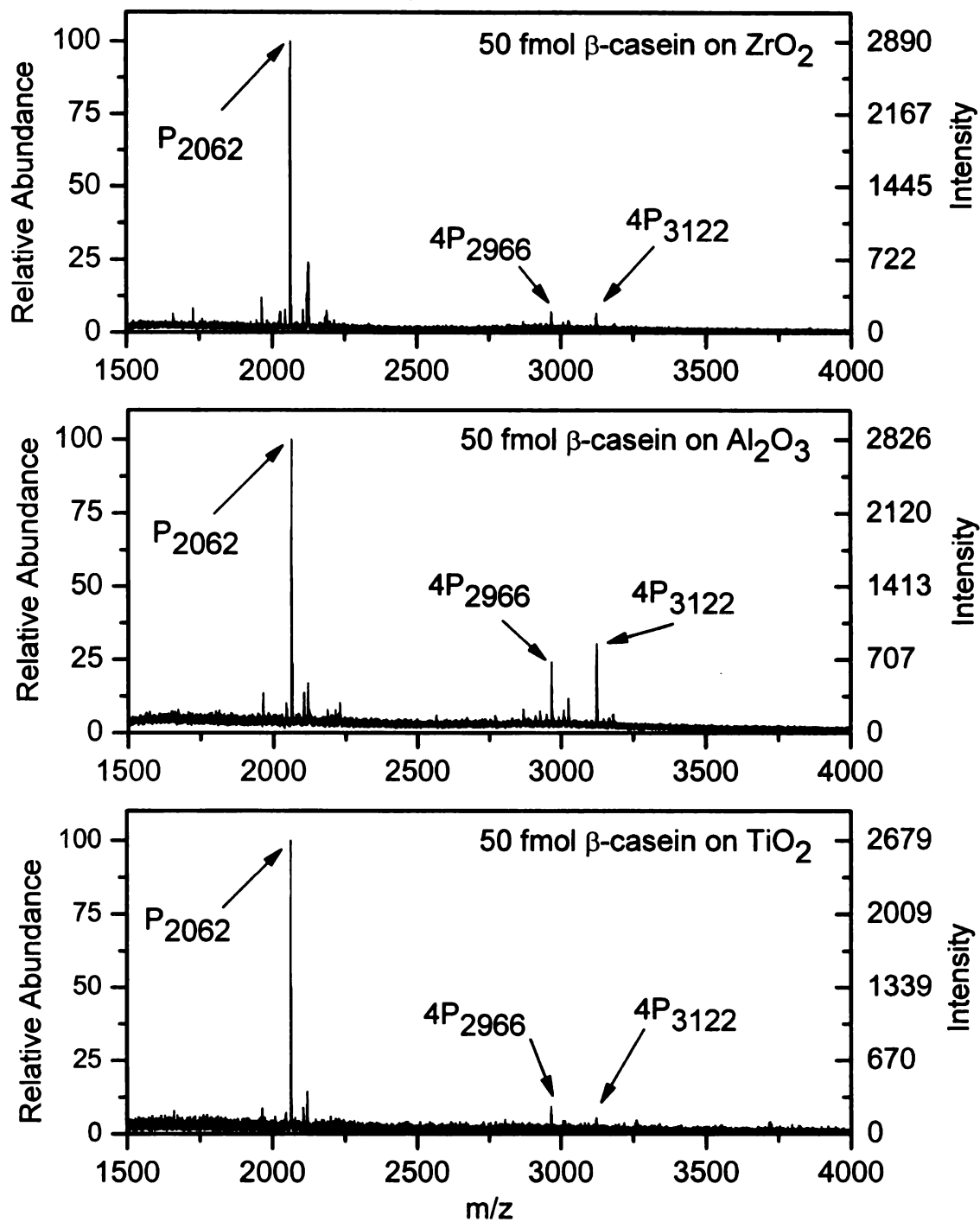


Figure 4.25 Enrichment of the monophosphorylated and tetraphosphorylated peptides in a tryptic digest of 50 fmol β -casein on TEM grid supported mesoporous zirconia (top), alumina (middle), and titania (bottom). A three-hour incubation time was used in obtaining each spectrum.

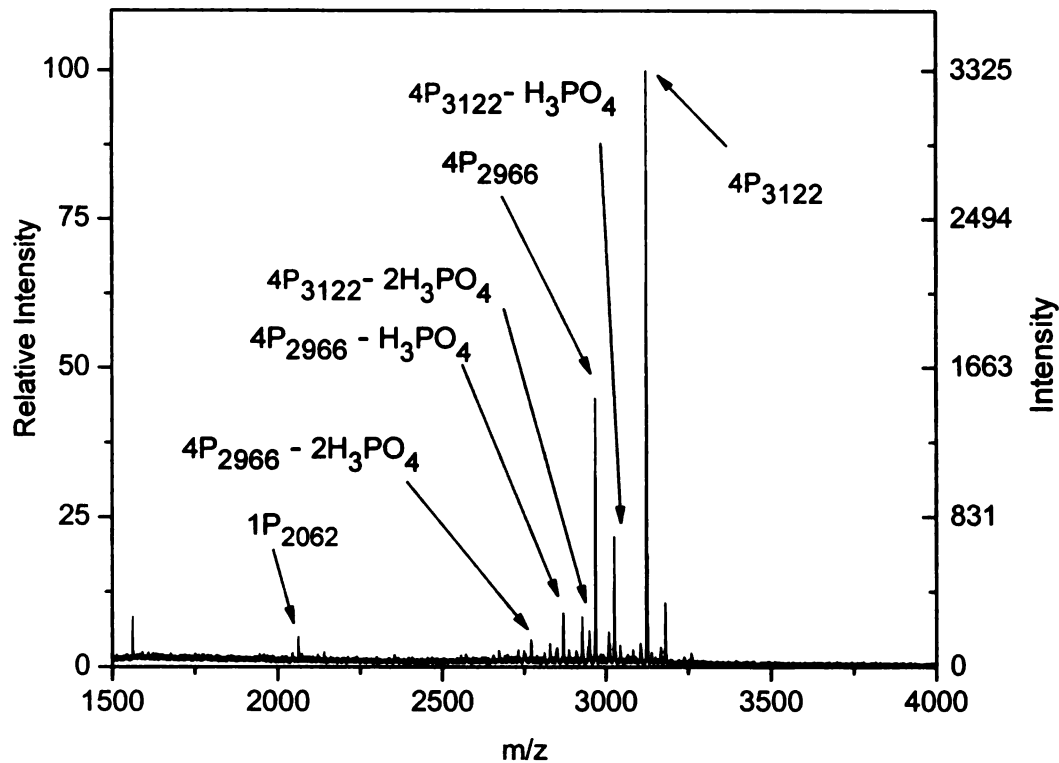


Figure 4.26 Enrichment of 50 fmol β -casein on gold TEM grid showing high selectivity towards tetraphosphorylated peptides – $4P_{2966}$ and $4P_{3122}$.

The above results prompted an investigation of other metallic TEM grids for potential use in enriching phosphopeptides. Among the metal grids tested were tested were molybdenum, aluminum, copper, nickel, titanium, silver and stainless steel. These metal TEM grids were tested using β -casein as the best model system, because it contains both mono and tetraphosphorylated peptide. Test results showed that molybdenum, nickel and copper showed did not show any evidence of enriching β -casein. On the other hand, silver and stainless steel showed some evidence of enrichment but they were not as good as the metal oxides or of gold.

Aluminum was expected to give very good enrichment results since as a metal, it is easily oxidize to form a thin Al_2O_3 layer. This is the same oxide as the

mesoporous alumina where enrichment can be performed. Unfortunately, the aluminum grid did not show any enrichment. This result was explained by the fact that Al_2O_3 is amphoteric and the enrichment conditions are highly acidic. Though the chemical composition of the aluminum surface oxide and the mesoporous alumina are the same, they have different structure. The aluminum oxide film on the metal surface is unstable towards acids and dissolves during the process of enrichment, thus the observed lack of enrichment. The test results for the titanium metal grid also are shown on Figure 4.27.

For the titanium grid, as in the case of the grid supported mesoporous titania, all three phosphorylated fragments are visible with the monophosphorylated fragment having the highest intensity. This was quite expected since just like other metals, titanium forms a thin layer of TiO_2 on its surface. This oxide is more stable thus it persists in acidic conditions and it is responsible for the enrichment process.

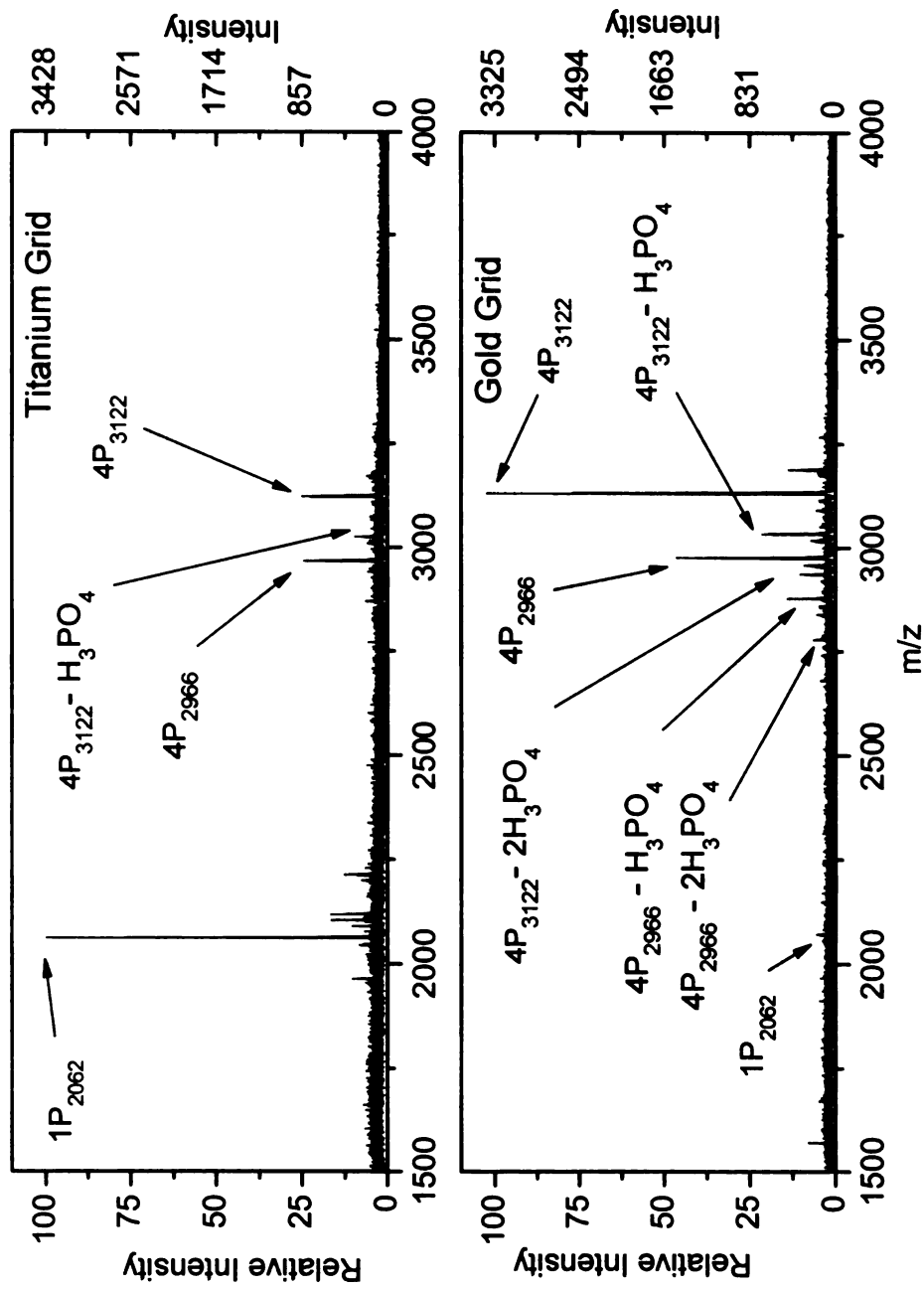


Figure 4.27 Enrichment of 50 fmol of β -casein tryptic digest on bare gold (bottom) and bare titanium (top) TEM grids.

The results for the bare gold and titanium complements each other. Titanium is very effective in enriching the monophosphorylated peptide of β -casein while gold is very effective in enriching the tetraphosphorylated peptides. Moreover, comparing the intensity of the MALDI spectrum for the bare grids and the mesoporous metal oxides, signal to noise the intensity for the bare metal grids was higher than for the mesoporous metal oxide thin films. This is explained by the presence of nooks and crannies on the mesoporous metal oxide thin film. It has been suggested that a high surface area material is needed for higher capacity material for enrichment. A high surface area material can have a very high capacity and will be very useful when enriching relatively large amounts of proteins but experimental data showed that it can also pose as a disadvantage when working on very low protein concentration (ie. femtomole concentration). If the phosphorylated peptide gets bound deep into the mesoporous film, the desorption of the peptide during MALDI analysis can be difficult because it would have to go through a more complicated path and it may even result to desorption failure. The non-porous and relatively flatter morphology of the bare metal grid does not have this problem. The bound phosphopeptide will be on its surface and would be easily desorbed during analysis. Though the bare metal grids might not have the surface area of the mesoporous metal oxide thin films, it seems that their surface area is enough in enriching phosphoprotein in the femtomole concentration range. They not only have the advantage of highly specific binding but they are commercially available and can be used without preliminary cleaning. This further simplifies the process of enriching phosphoproteins.

Enrichment of ovalbumin

Ovalbumin is a phosphoprotein whose tryptic digest yields three monophosphorylated fragments. Figure 4.28 shows the MALDI spectra of the enrichment of ovalbumin on grid supported mesoporous metal oxides and on a bare titanium grid. Gold was also tested but it gave no enrichment thus the spectrum was not included. This was quite expected from gold since from the results in β -casein, where it weakly enriched the monophosphorylated fragment in comparison to the tetraphosphorylated segments.

Mesoporous titania and alumina showed highly selective enrichment where the $m/z = 2088$ peak was the strongest. Titania also show some non-specific binding at $m/z = 1774$. This has been attributed to the residue that contains the histidine group. Alumina doesn't show this non-specific binding but the intensity of the 2088 peak was lower compared to titania. The absence of non-specific binding still can't be explained but the lower intensity of the 2088 peak could be due to the relatively more porous nature of alumina where the bound peptide have difficulties desorbing during MALDI analysis. Zirconia on the other hand

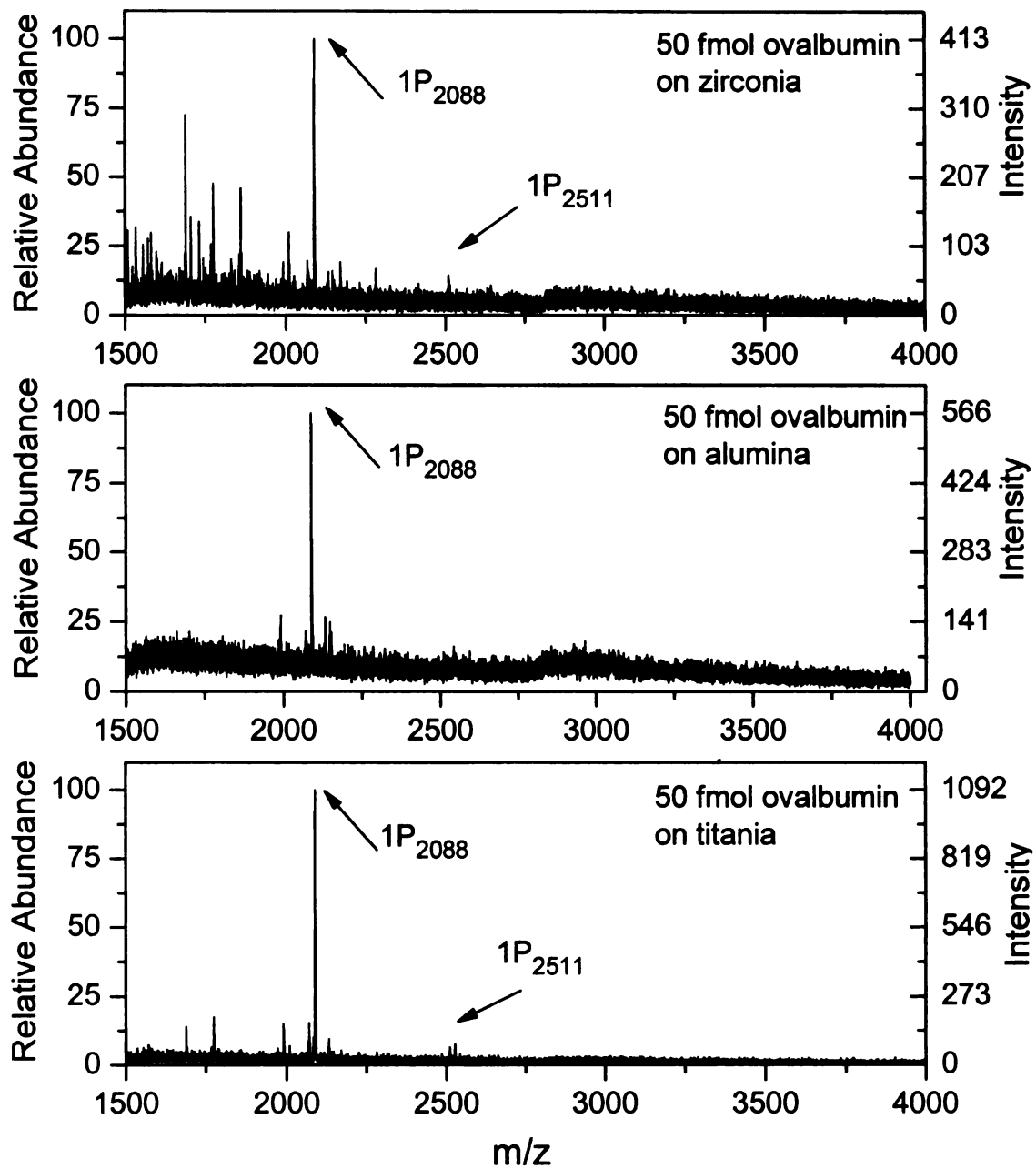


Figure 4.28 Enrichment of a 50 fmol tryptic digest ovalbumin on grid supported mesoporous zirconia, alumina, and titania.

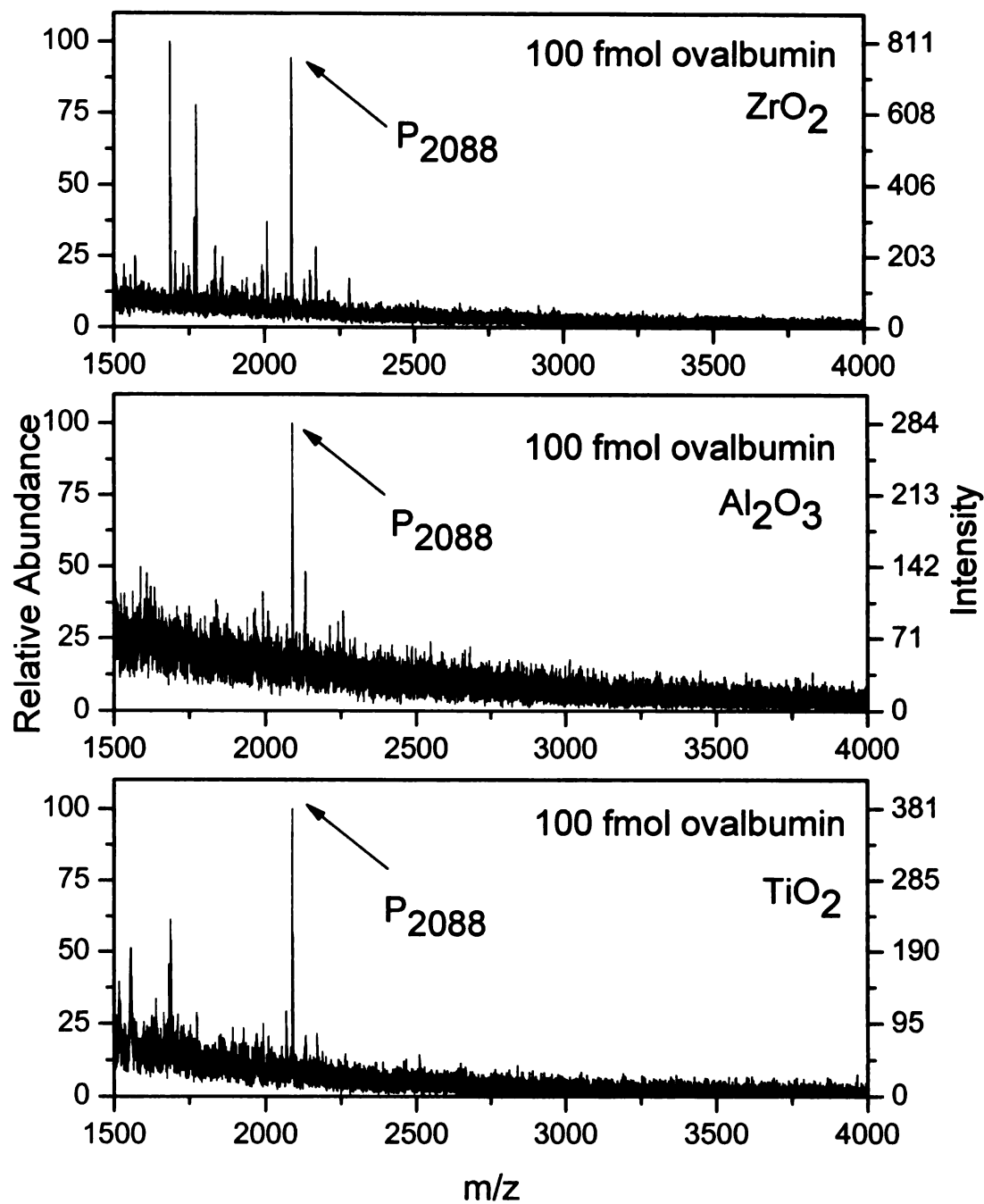


Figure 4.29 MALDI spectrum of 100 fmol ovalbumin tryptic digest enriched on grid supported mesoporous zirconia, alumina and titania thin films. Note the weak or absence of enrichment for 1P₂₅₁₁ and 1P₂₉₀₁ fragments.

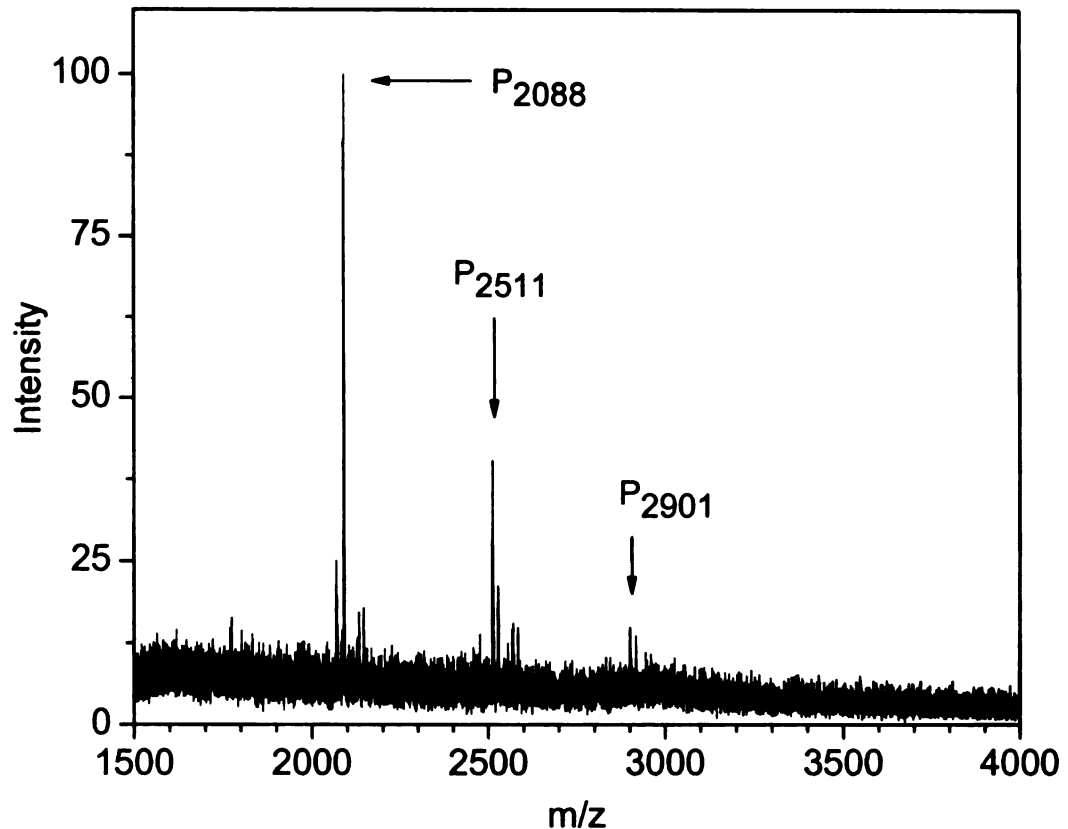


Figure 4.30 MALDI spectrum of the 50 fmol ovalbumin phosphorylated peptide enriched using titanium metal grid.

showed the monophosphorylated peaks at $m/z = 2088$ and 2511 but also showed more non-specific binding. The reason to why this happen on zirconia and not on alumina and titania is still yet to be investigated further. The results for the bare titanium grid are more promising. Compared to titania, the spectrum did not show non-specific binding. Titania showed two phosphorylated peptide peaks with $m/z = 2088$ and 2511 while all three monophosphorylated peptides $m/z = 2088$, 2511 and 2901 are all visible for the case of the bare titanium grid.

4.5 Conclusions

Gold grid supported mesoporous metal oxide thin films were successfully fabricated. Ideally, the holes of the grid should be filled with the metal oxide thin film. Of the three metal oxides produced, only alumina was able to completely fill the holes of the TEM grids as revealed by the SEM and TEM images. The lath-like nature of alumina helped the thin film that was produced to be relative more flexible than that of the films from titania or zirconia where the film doesn't completely fill the hole. In principle, the holes on the TEM grid can be filled by adjusting the concentration of the precursor solution such that enough material can be deposited during the dip-coating process. It was reasoned out that at this point of the study that it is more important first to concentrate efforts on exploring the properties of the material towards phosphoprotein enrichment. Results also showed that there seems to be enough metal oxide surface area on the as supplied grid. On the basis of x-ray diffractions patterns the alumina that as produced was gamma alumina, titania as anatase and zirconia as the cubic polymorph. TEM imaging also revealed that the thin films were indeed mesoporous.

From these results, the feasibility of using grid supported mesoporous metal oxide thin films for phosphorylated protein enrichment has been demonstrated. This approach simplifies the enrichment process as well as increasing sample throughput because multiple grid samples can be processed simultaneously.

DHB incubation studies have shown that for highly selective enrichment, one hour incubation time is enough and this can be extended to no more than three hours. Beyond three hours, non-specific binding starts to appear on the MALDI spectrum.

For the mesoporous metal oxide thin films tested, titania, alumina and zirconia, all were very effective in enriching the mono- and tetraphosphorylated segments of β -casein. For the enrichment of ovalbumin, mesoporous alumina was the best among the mesoporous thin films tested since non-specific binding was not observed. The next best material was mesoporous titania showing some non-specific binding. The worst was zirconia because of very large amounts of non-specific binding.

The results with the bare TEM grids of gold and titanium were the biggest breakthrough in this study. There have not been reports of using bare gold and bare titanium metal for enriching phosphoproteins. The capability of gold and titanium complement each other. Gold is very selective on tetraphosphorylated peptides. Titanium is capable of enriching both tetra- and monophosphorylated peptides but it is more selective towards the monophosphorylated peptide fragments. These results together with the protocol that was developed in enriching these model proteins will help make the study of phosphoproteomics easier because of the simplicity of the protocol and the relatively cheap TEM grids.

4.6 References

1. Black, D. L. *Annu. Rev. Biochem.* **2003**, 72 291-336
2. Maniatis, T., Tasic, B. *Nature* **2002**, 418, 236-243
3. Walsh, C. *Post Translational Modifications of Proteins: Expanding Nature's Inventory*, B.Roberts, Colorado **2005**
4. Walsh, C. T.; Garneau-Tsodikova, S.; Gato, G. *J. Angevandte Chemie – International Edition* **2005**, 44, (44), 7342-7372
5. Lipmann, F.A., Levene, P.A. *The Journal of Biological Chemistry* **1932**, 109-114
6. Paradela, A., Albar, J.P., *Journal of Proteome Research.* **2008**, 7, 1809-1818
7. Schmidt, S.R. Schweikart, F., Anderson, M.E., *J. Chromatogr. B.* **2007** 849, 154-162
8. Kalume, D.E., Molina, H., Pandey, A. *Curr. Opin. Chem. Biol.* **2003** 7 1, 64-69
9. Hubbard, M. J and Cohen, P. *Trends Biochem.Sci.* **1993**, 18 (5) 172-177
10. Wehr, T. *LCGC North America* **2008** s6, 6, 550-559
11. Aebersold, R., Mann, M. *Mass Spectrometry-Based Proteomics. Nature.*, **2003** 422, 6928 198-207
12. Mann, M. Ong, S.E., Gronborg, M., Steen, H., Jensen, O.N., Pandey, A. *Trends Biotechnol.* **2002**, 20, 261-268
13. Bodenmiller, B. et al. *Nat. Methods* **2007**, 4 (3) 231-237
14. Sherr, C.J. *Science*, **1996** 274, 5293, 1672-1677
15. Klumpp, S., Krieglstein, J. *Current Opinion in Pharmacology* **2002**, 2, 4, 458-462
16. Debouis-Mouthon, C., Danan, C., Amselen, S., Eggelpoel, M.J.B.V. Serthlangeron, C., Gooseens, M., Besmond, C., Capeau, J., Caron, M. *Metabolism - Clinical and Experimental* **1996**, 45 12, 1493-1500
17. Saltiel, A.R. *American Journal of Physiology – Endocrinology and Metabolism*, **1996**, 33, 3, E375-E385
18. Gadsbym D.C., Nairn, A.C., *Ion Channel Regulation* **1999**, 33, 79-106

19. Goedert, M., Jakes, R., Spillatini, M.G., Crowther, R.A. Cohen, P., Vanmechelen, E. Probst, A., Gotz, J.,Burki, K., *Biochemical Society Transactions* **1995**, 23, 1, 80-85
20. Hanger, D.P., Balts, J.C., Loviny, T.L.F. Blackstock, W.P., Anderton, B.H., *Journal of Neurochemistry* **1998**, 71, 6, 2465-2476
21. Blume-Jensen, P. Hunter, T. *Nature* **2001**, 411 (6835) 355-365
22. Cohen, P. *Nat. Rev. Drug Discovery* **2002**. 1 (4), 309-315
23. Reiders, J., Sickmann, A., *Proteomics* **2005**, 5, 16, 4052-4061
24. Stasyk, T., Morandell, S., Bakry, R., Feuerstein, I., Huck, C.W., Stecher, G., Bonn, G.K., Huber, L.A. *Electrophoresis* **2005**, 26, 14, 2850-2854
25. Salih, E. *Mass Spectrometry Reviews*, **2005**, 24, 828-846
26. Rall, T.W., Sutherland, E.W., Wosilait, W.D., *Journal of Biological Chemistry*, **1956**, 218, 1, 486-495
27. Hunter, T. *Methods on Enzymology*, **1991** 200, 3-37
28. Setton, B.M., *Methods in Enzymology*, **1991**, 201, 245-251
29. Salih, E., Zhou, H.Y.,Glimcher, M.J., *Journals of Biological Chemistry*, **1996**, 271, 28, 16897-16905
30. Graves, J.D., Krebbs, E.G. *Pharmacol. Ther.* **1999** 82, 2-3 111-121
31. Gabor-Miklos, G.L., MAleszka, R. *Proteomics*, **2001**, 1, 30-41
32. Witse, E.S., Old, W.M. Resing, K.A. Ahn, N. *Nature Methods* 4, 10, 798-806
33. Smith, J.C., Figeys, D., *Biochem. Cell Biol.* **2008**, 86, 137-148
34. Schroeder, M.J. Shabanowitz, J., Schwastz, J.C. Hunt, D.F., Coon, J. *Anal. Chem.* **2004**, 76, 3590-3598
35. Bruce, C., Shitman, M.A., Miller, P., Gulcicek, E.E. *Anal Chem.* **2006**, 78, 4374-4382
36. Liu, S., Zhang, C., Campbell, J.L., Zhang, H., Yeung, K.K.C., Han, V.K.M., Lajoie, G.A., *Rapid Commun Mass Spectrom* **2005** 19, 2747-2756
37. Schmelzle, K., White, F.M., *Current Oppinion in Biotechnology*, **2006**, 17, 406-414

38. Garcia, B.A., Shabanowitz, J., Hunt, D.F., *Methods*, **2005**, 35, 256-564
39. Ficarro, S.B., McClelland, M.L., Stukenberg, P.T., Burke, D.J., Ross, M.M., Shabanowitz, J. Hunt, D.F., White, F.M., *Nature Biotechnology* **2002**, 20, 301-305
40. Tholey, A., Reed, J., Lehmann, W.D. *J. Mass Spectrom.* **1999**, 34, 117-123
41. Lee, J., Xu, Y., Chen, Y., Sprung, R., Kim, S.C., Xie, S., Zhao, Y. *Molecular and Cellular Proteomics* **2007**, 669-676
42. Palumbo, A.M., Tepe, J.T., Reid, G.E., *Journal of Proteome Research*, **2008**, 7, 771-779
43. Collins, M.O., Yu, L. Choudhary, J.S. *Proteomics* **2007**, 7, 2751-2768
44. Ross, A.H., Baltimore, D., Eisen, H.N., *Nature*, **1981** 294, 654
45. Mechtler, K. Bonn, G.K., Huber, L.A., *Proteomics*, **2006** 6 4047-4056
46. Delom, F. Chevet, E., *Proteome, Sci.* **2006**, 4, 15
47. Pandey, A., Podtelejnikov, V., Blagoev, B., Bustelo, X.R., Mann, M., Lodish, H.F., *Proc. Nat. Acad. Sci. USA.* **2000**, 97, 197-184
48. Zhang, G. Neubart, T.A., *Proteomics*, **2006**, 6, 571-578
49. Spek, E.J., Zhang, H., Zha, X.M. Polakiewicz, R.D., Comb, M.J. *Nat. Biotechnol.* **2005**. 23-94-101
50. Goshe, M.B., Conrads, T.P., Panisko, E.A., Angel, N.H., Veenstra, T.D., Smith, D., *Anal Chem* **2001**, 73, 2578-2586
51. Jaffe, H., Veerana, T. Pant, H.C., *Biochemistry* **1998**, 37, 16211-16224
52. Oda, Y., Nagasu, T., Chait, B.T. *Nature Biotechnology*, **2001**, 19 379-382
53. McLachlin, D.T. Chait, B.T., *Anal. Chem.* **2003**, 75, 6826-6836
54. Zhou, H., Watts, J.D., Aebersold, R., *Nat. Biotechnol.* **2001**, 19, 375-378
55. Tao, W.A., Wollscheid, B., O'Brien, R., Eng, J.K., Li, X., Bodenmiller, B., Watts, J.D., Hood, L., Aebersold, R., *Nature Methods*, **2005**, 2, 591-598
56. Porath, J., Carlson, J., Olsson, I., Belforge, G., *Nature* **1975**, 258, 5536, 598-599
57. Anderson, L. Porathc, *J. Analytical Biochemistry*, **1986**, 154, 1, 250-254

58. Kweon, H.K. and Hakansson, K. *Anal. Chem* **2006**, 78 (60), 1743-1749
59. Pinkse, M.W., et al. *Anal. Chem.* **2004**, 76 (14), 3935-3943
60. Larsen, M.R. et al. *Mol. Cell Proteomics* **2005**, 4 (7), 873-886
61. Kinoshita, E., Yamada, A., Takeda, H., Kinoshita-Kikuta, E., Koike, T. *Journal of Separation Science*, **2005**, 28, 2, 155-162
62. Jensen, S.S., Larsen, M.R., *Rapid Communications in Mass Spectrometry* **2007**, 21, 22, 3635-3645
63. Beausoleil, S.A., Jedrychowski, M. Schwartz, D., Elias, J.E., Villen, J. Li, J.X., Cohn, M.A., Cantley, L.C., Gygi, S.P., *Proceedings of the National Academy of Sciences of the United States of America*, **2004**. 101, 33, 12130-12135
64. Balif, B.A., Villen, J., Beausoleil, S.A., Schwartz, D., Gygi, S.P., *Molecular and Cellular Proteomics*, **2004**, 3, 11, 1093-1101
65. Pinkse, M.R., Mohammed, Gouw, J.W., van Breukelen, B., VOs, H.R., Heck, A.J.R. *J. Proteome Res.* **2008**, 7, 687-697
66. Kweon, H.K. and Hakansson, K. *Anal. Chem* **2006**, 78 (60), 1743-1749
67. Wang, Y., Chen, W., Wu, J., Guo, Y., Xia, X., *J. Am. Soc. Mass Spectrom.* **2007**, 18, 1387-1395
68. Larsen, M.R., Thingholm, T.E., Jensen, O.N., Roepstorff, P., Jorgensen, T.J.D., *Molecular and Cellular Proteomics*, **2005**, 4, 7, 873-886
69. Dobson, K.D., McQuillan, A.J., *Spectrochimica Acta Part A. Molecular and Biomolecular Spectroscopy*, **2000**, 56, 3, 557-565
70. Li, Y., Liu, Y., Tang, J., Lin, H., Yao, N., Shen, X., Deng, C., Yang, P., Zhang, X., *Journals of Chromatography A* **2007**, 1172 1 57-71
71. Li, Y., Lin, H.Q., Deng, C.H., Yang, P.Y., Zhang, X.M., *Proteomics*, **2008**, 18, 16, 2381-2389
72. Sturn, M., Leitner, A., Smath, J.H., Linden, M., Lindner, W., *Adv. Functional Materilas*, **2008**, 18, 16, 2381-2389
73. Ficarro, S.B., Parikh, J.R., Blank, N.C. Marto, J.A., *Analytical Chemistry*, **2008**, 80, 12, 4606-4613
74. Zhangm Z. Pinnavaia, T.J. *J. Am. Chem. Soc.* **2002**, 124, 12294-12301

75. Wang K., et al. *Microporous and Mesoporous Materials* **2009** 117 161–164

MICHIGAN STATE UNIVERSITY LIBRARIES



3 1293 03063 5597